THE IDENTIFICATION AND CHARACTERISATION OF NOVEL INHIBITORS OF THE 17B-HSD10 ENZYME FOR THE TREATMENT OF ALZHEIMER'S DISEASE

Patrick Guest

A Thesis Submitted for the Degree of PhD
at the
University of St Andrews

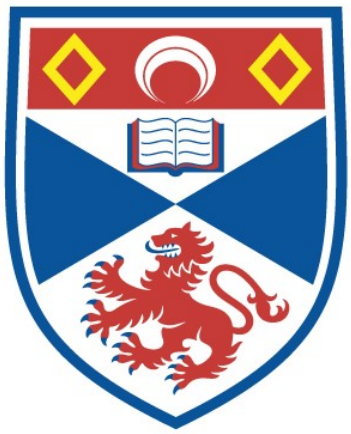

2016

The identification and characterisation of novel inhibitors of the 17β-HSD10 enzyme for the treatment of Alzheimer's disease

Patrick Guest, B.Sc., M.Res.

University of
St Andrews

This thesis is submitted in partial fulfilment for the degree of PhD
at the
University of St Andrews

Date of Submission: 23-09-2016

Declarations

1. Candidate's declarations:

I, Patrick Guest, hereby certify that this thesis, which is approximately 70,000 words in length, has been written by me, and that it is the record of work carried out by me, or principally by myself in collaboration with others as acknowledged, and that it has not been submitted in any previous application for a higher degree.

I was admitted as a research student in September, 2012 and as a candidate for the degree of PhD in September, 2012; the higher study for which this is a record was carried out in the University of St Andrews between 2012 and 2016.

(*If you received assistance in writing from anyone other than your supervisor/s*):

I, ….., received assistance in the writing of this thesis in respect of [language, grammar, spelling or syntax], which was provided by ……

Date …… signature of candidate ……

2. Supervisor's declaration:

I hereby certify that the candidate has fulfilled the conditions of the Resolution and Regulations appropriate for the degree of PhD in the University of St Andrews and that the candidate is qualified to submit this thesis in application for that degree.

Date …… signature of supervisor ……

3. Permission for publication: (*to be signed by both candidate and supervisor*)

In submitting this thesis to the University of St Andrews I understand that I am giving permission for it to be made available for use in accordance with the regulations of the University Library for the time being in force, subject to any copyright vested in the work not being affected thereby. I also understand that the title and the abstract will be published, and that a copy of the work may be made and supplied to any bona fide library or research worker, that my thesis will be electronically accessible for personal or research use unless exempt by award of an embargo as requested below, and that the library has the right to migrate my thesis into new electronic forms as required to ensure continued access to the thesis. I have obtained any third-party copyright permissions that may be required in order to allow such access and migration, or have requested the appropriate embargo below.

The following is an agreed request by candidate and supervisor regarding the publication of this thesis:

PRINTED COPY

~~a) No embargo on print copy~~

b) Embargo on all or part of print copy for a period of 2 years (maximum five) on the following ground(s):
    - Publication would be commercially damaging to the researcher, or to the supervisor, or the University
    - Publication would preclude future publication
    - ~~Publication would be in breach of laws or ethics~~

~~c) Permanent or longer term embargo on all or part of print copy for a period of … years (the request will be referred to the Pro-Provost and permission will be granted only in exceptional circumstances).~~

Supporting statement for printed embargo request if greater than 2 years:

ELECTRONIC COPY

~~a) No embargo on electronic copy~~

b) Embargo on all or part of electronic copy for a period of 2 years (maximum five) on the following ground(s):
    - Publication would be commercially damaging to the researcher, or to the supervisor, or the University
    - Publication would preclude future publication

- ~~Publication would be in breach of law or ethics~~

c) ~~Permanent or longer term embargo on all or part of electronic copy for a period of … years (the request will be referred to the Pro-Provost and permission will be granted only in exceptional circumstances).~~

Supporting statement for electronic embargo request if greater than 2 years:

ABSTRACT AND TITLE EMBARGOES

An embargo on the full text copy of your thesis in the electronic and printed formats will be granted automatically in the first instance. This embargo includes the abstract and title except that the title will be used in the graduation booklet.

If you have selected an embargo option indicate below if you wish to allow the thesis abstract and/or title to be published. If you do not complete the section below the title and abstract will remain embargoed along with the text of the thesis.

a)	I agree to the title and abstract being published	YES
b)	I require an embargo on abstract	NO
c)	I require an embargo on title	NO

Date …… signature of candidate …… signature of supervisor ……

Please note initial embargos can be requested for a maximum of five years. An embargo on a thesis submitted to the Faculty of Science or Medicine is rarely granted for more than two years in the first instance, without good justification. The Library will not lift an embargo before confirming with the student and supervisor that they do not intend to request a continuation. In the absence of an agreed response from both student and supervisor, the Head of School will be consulted. Please note that the total period of an embargo, including any continuation, is not expected to exceed ten years.

Where part of a thesis is to be embargoed, please specify the part and the reason.

Acknowledgements

I would like to extend a thank you to both of my supervisors, Professor Frank Gunn-Moore and Professor Terry Smith, for their continued advice, encouragement and support throughout the course of my PhD. For the motivational words when things were going badly, for pushing me onwards when things were going well and for the continuous stream of ideas and suggestions.

I would also like to extend a special thank you to Dr. Siavash Khazaipoul, for his advice and expertise in all things related to protein purification, for his humour and the helpful reminders that there is life outside of the PhD and other career options are available, for staying late on Friday afternoons and allowing me to borrow, and occasionally to break, his equipment. Without his assistance this project would not be at the stage it is now.

To the members of the Frank Gunn-Moore research group, both past and present; Zoe Allen, Dr. Laura Aitken, Dr. Eva Borger, Madhurima Dey, Frances Goff and Dr. Andrew Tilston-Lunel who made the lab a fun and productive place to be. In particular, a thank you goes to Dr. Andrew Tilston-Lunel, Dr. Laura Aitken and Dr. Eva Borger, for helping me to find my feet in the lab, for putting up with an endless stream of questions and for the never-ending science related discussions.

To our collaborators in the Czech Republic, particularly Professor Kamil Musilek, Ondrej Benek and Lukas Hroch, for synthesising our Frentizole derived compound series, which was fundamental to the work conducted herein.

To my friends and family for the continued support and for putting up with the constant ups and downs associated with life in the lab.

Finally, to the EastBio Doctoral Training Partnership, BBSRC, which funded this project.

Abstract

In 2015, an estimated 46.8 million people were living with dementia, a number predicted to increase to 74.7 million by 2030 and 131.5 million by 2050. Whilst there are numerous causes for the development of dementia, Alzheimer's disease is by far the most common, accounting for approximately 50-70% of all cases. Current therapeutic agents against Alzheimer's disease are palliative in nature, managing symptoms without addressing the underlying cause and thus disease progression and patient death remain a certainty. Whilst the main underlying cause for the development of Alzheimer's disease was originally thought to be an abnormal deposition of insoluble amyloid-β peptide derived plaques within the brain, the failure of several high-profile therapeutic agents, which were shown to reduce the plaque burden without improving cognition, has recently prompted a shift in focus to soluble oligomeric forms of amyloid-β peptide. Such soluble oligomers have been shown to be toxic in their own right and to precede plaque deposition. Soluble amyloid-β oligomers have been identified in various subcellular compartments, including the mitochondria, where they form a complex with the 17β-HSD10 enzyme resulting in cytotoxicity. Interestingly, hallmarks of this toxicity have been shown to be dependent on the catalytic activity of the 17β-HSD10 enzyme, suggesting two therapeutic approaches may hold merit in treating Alzheimer's disease: disrupting the interaction between the 17β-HSD10 enzyme and amyloid-β peptide, or directly inhibiting the catalytic activity of the 17β-HSD10 enzyme. In 2006, Frentizole was identified as a small molecule capable of disrupting the 17β-HSD10/amyloid interaction.

The work described herein details the generation of a robust screening assay allowing the catalytic activity of the 17β-HSD10 enzyme to be measured *in vitro*. This assay was subsequently employed for small molecule screening using two methodologies; first in a targeted approach using compounds derived from the Frentizole core scaffold, and second in an explorative manner using a diverse library of compounds supplied by the National Cancer Institute. As a result, a range of novel small molecule inhibitors of the 17β-HSD10 enzyme have been identified and the most promising characterised in terms of potency and mechanism of action. De-selection assays were developed to allow the efficient triage of hit compounds and work was begun on a cellular based assay which would allow the ability of compounds of interest to reverse a disease relevant phenotype to be assessed in a cellular environment.

As such, we now have a number of hit compounds which will form the basis for the generation of subsequent series of derivatives with improved potency and specificity, as well as the robust assays required to measure such criteria, potentially leading to the generation of novel therapeutic agents against Alzheimer's disease.

Table of Contents

Table of Contents

Table of Contents

Table of Contents

Table of Contents

Abbreviations

17β-HSD10 = 17β-Hydroxysteroid dehydrogenase type 10

17β-HSD14 = 17β-Hydroxysteroid dehydrogenase type 14

17β-HSD8 = 17β-Hydroxysteroid dehydrogenase type 8

4-HNE = 4-hydroxynoneal

ABAD = Amyloid-binding alcohol dehydrogenase

ABAD-DP = Amyloid-binding alcohol dehydrogenase decoy peptide

ABAD-RP = Amyloid-binding alcohol dehydrogenase reverse peptide

AChE = Acetylcholinesterase

AD = Alzheimer's disease

ADAS-cog = Alzheimer's Disease Assessment Scale - Cognitive Subscale

ADDL = Amyloid-beta derived diffusible ligands

ADSC-ADL = Alzheimer's Disease Cooperative Study - Activity of Daily Living Inventory

AICD = Amyloid intracellular domain

AMPA receptor = α-amino-3-hydroxy-5-methyl-4-isoxazolepropionic acid receptor

AMV Reverse Transcriptase = Avian myeloblastosis virus reverse transcriptase

Apo-E = Apolipoprotein E

APP = Amyloid precursor protein

APPswe = Swedish mutation of the amyloid precursor protein

Aβ = Amyloid beta-peptide

BCA Assay = Bicinchoninic acid assay

bp = Basepair

BSA = Bovine serum albumin

CAT = Choline acetyltransferase

cDNA = Complementary DNA

CNS = Central nervous system

COX8 = Cytochrome c oxidase subunit VIII

CSF = Cerebrospinal fluid

dCTP/dGTP = Deoxycytidine triphosphate/ deoxyguanosine triphosphate

DMSO = Dimethyl sulfoxide

DSF = Differential scanning fluorimetry

DTT = Dithiothreitol

Abbreviations

E. coli = *Escherichia coli*

ECM = Extracellular matrix

EDTA = Ethylenediaminetetraacetic acid

ELISA = Enzyme-linked immunosorbent assay

EOAD = Early-onset Alzheimer's disease

FAD = Familial Alzheimer's disease

FBS = Foetal bovine serum

FDA = Food and Drug Administration

GST-tag = Glutathione S-transferase-tag

HFIP = Hexafluoroisopropanol

His-tag = Histidine-tag

HSD10 = 17β-HSD10

HSD14 = 17β-HSD14

HSD8 = 17β-HSD8

IC_{50} = Concentration required for 50% inhibition of target

IPTG = Isopropyl β-D-1-thiogalactopyranoside

kb = Kilobase

kDa = Kilodalton

K_m = Substrate concentration for half-maximal rate of reaction

LDH = Lactate Dehydrogenase

LDL receptor = Low density lipoprotein receptor

LIC = Ligation independent cloning

LOAD = Late-onset Alzheimer's disease

LTD = Long-term depression

LTP = Long-term potentiation

mAPP = Mutant amyloid precursor protein (generating elevated Aβ)

MBP = Maltose-binding protein

MBP-HSD8 = 17β-HSD8-Maltose-Binding Protein Fusion

MHBD Deficiency = 2-methyl-3-hydroxybutyryl-CoA dehydrogenase deficiency

M-MLV Reverse Transcriptase = Moloney murine leukemia virus reverse transcriptase

MMSE = Mini-Mental State Examination

MRI = Magnetic resonance imaging

mRNA = Messenger RNA

Abbreviations

mtRNase P = Mitochondrial ribonuclease P

MTT = 3-(4,5-dimethythiazol-2-yl)-2,5-diphenyl tetrazolium bromide

MWCO = Molecular weight cut-off

NAD^+ = β-Nicotinamide adenine dinucleotide

NADH = β-Nicotinamide adenine dinucleotide, reduced

NCI = National Cancer Institute

NFDM = Non-fat dried milk

NMDA receptor = N-methyl-D-aspartate receptor

PCR = Polymerase chain reaction

PDAPP Mice = V717F mutation of the amyloid precursor protein

PEI = Polyethylenimine

PiB-PET = Pittsburgh compound B based positron emission tomography

PSEN = Presenilin

RCSB-PDB = Research Collaboratory for Structural Bioinformatics - Protein Data Bank

ROS = Reactive oxygen species

SDM = Site directed mutagenesis

SDR Family = Short-chain dehydrogenase/reductase family

SDS-PAGE = Sodium dodecyl sulfate polyacrylamide gel electrophoresis

SIB = Severe Impairment Battery

SOC = Super optimal broth with catabolite repression

TEV = Tobacco etch virus

Tg257APP Mice = Swedish mutation of the amyloid precursor protein

T_m = Protein denaturation temperature

pcDNA4/TO = Mammalian expression vector with tetracycline operator mediated control of expression

pcDNA6/TR = Mammalian expression vector harbouring the tetracycline repressor protein

tRNA = Transfer RNA

VLDL receptor = Very low density lipoprotein receptor

V_{max} = Maximum rate of reaction

Chapter 1: Introduction

1.1 Neuropathology of Alzheimer's Disease

With advancing age there is a well-recognised trend towards decreased cognitive function. In most individuals this decline is gradual and mild, however in others it is markedly more pronounced, interfering with the ability to perform everyday tasks, a condition termed senile dementia. Whilst numerous disorders can underlie the development of senile dementia, Alzheimer's disease (AD) is by far the most common accounting for 50-70% of all cases (Figure 1.01)[1,2].

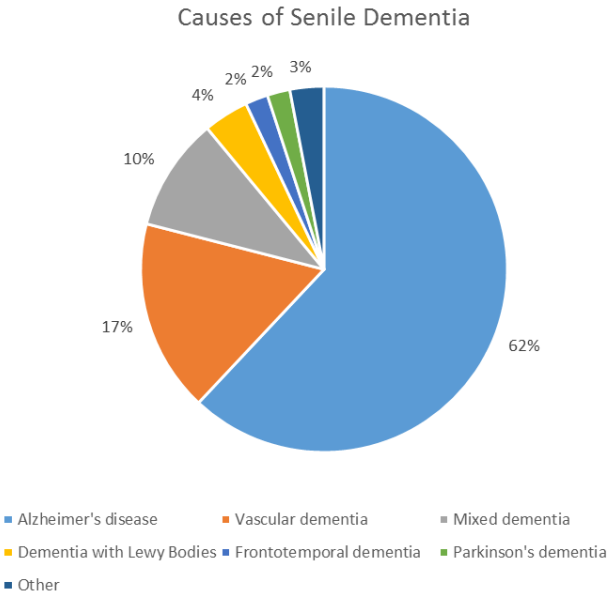

Figure 1.01 Prevalence of individual causes of senile dementia. Whilst numerous disorders can generate the clinical symptoms of dementia, Alzheimer's disease is by far the most common accounting for an estimated 62% of cases. Data taken from Alzheimer's Society, 2014 dementia infographic[1].

In 2015, there were an estimated 46.8 million people worldwide living with dementia, with an associated cost to the global economy of an estimated $818 billion[3]. With the global trend towards an aging population, the number of people with dementia is predicted to increase to 74.7 million by 2030 and 131.5 million by 2050[3]. When these facts are taken together, it is apparent that dementia and thus Alzheimer's disease, represent a global problem both financially and in terms of patient suffering, which is likely to get significantly worse in the near future. Current therapeutic agents against AD are palliative in nature; managing symptoms without addressing the underlying cause and thus patient deterioration and death remain a certainty. As such, there is a clear and present need for improved therapeutic agents to treat Alzheimer's disease.

In 1907, Alois Alzheimer undertook the histological examination of the brain of a 51-year-old patient presenting with an atypical dementia, leading to the identification of the disease which would subsequently bear his name[4]. Clinically, AD is characterised by a progressive neurodegenerative phenotype, with a marked impairment of episodic memory being the characteristic lesion associated with the disease[5]. Following disease progression, additional higher-order cognitive abilities are also perturbed

leading to executive dysfunction, apraxia and visuospatial dysgnosia[5]. Patient prognosis is variable, showing a strong age dependency, but death typically occurs within 8-10 years of diagnosis[6]. Following post-mortem examination, Alois Alzheimer reported a generalised atrophy of the brain and, using the Bielschowsky silver staining methodology, an abnormal accumulation of intracellular fibrillar structures alongside similar extracellular deposits, presumed to be the remains of degenerating neuronal cells, together termed neurofibrillary tangles (NFTs)[4]. Concomitantly, it was noted that distributed throughout the cortex were additional abnormal foci, later to be termed senile plaques. Subsequently, in 1968, Blessed *et al.* showed for the first time an association between plaque burden and cognitive impairment, indicating causation[7].

Senile plaques (Figure 1.02, a[8]) can be divided into two subtypes, termed diffuse plaques and dense-cored plaques. Diffuse plaques are amorphous in nature and are not stained by beta-sheet labelling dyes, Thioflavin-S or Congo Red, whereas dense-cored plaques stain positively with the aforementioned agents[5]. Diffuse plaques are not typically associated with dystrophic neurites, synaptic loss or activated microglia and are commonly observed in the brains of non-demented individuals indicating that they may not in of themselves be a toxic species[5,9]. Conversely, dense-cored plaques are associated with dystrophic neurites, neuronal loss, synaptic loss and an activation of the immune response in the form of activated microglia and astrocytes, indicating that this form of amyloid deposit may play a role in the pathogenesis of AD[5,10-13].

Similarly, NFT's (Figure 1.02, b[8]) can be subdivided into pre-NFT's, mature NFTs and ghost NFTs based upon their appearance following histological analysis[5]. Pre-NFTs appear as diffuse or punctate staining within the cytoplasm of otherwise healthy appearing neurons[5]. Mature-NFTs are larger and more pronounced in nature and are often seen to displace the nucleus of the cell to the outer edge of the cytoplasm and extend into abnormal appearing dendrites[5]. Ghost NFT's are extracellular deposits of hyperphosphorylated tau protein which are thought to represent the remnants of neurons which have previously been lost[5].

The temporal and spatial deposition of senile plaques and NFTs within the AD brain shows a characteristic pattern of distribution.

Thal staging describes the deposition of senile plaques within the AD brain and is composed of 5 phases[14,15] (summarised in Figure 1.02, e[8]) . In phase I, deposits are observed predominantly in the frontal, parietal, temporal or occipital neocortex[14,15]. Phase II is defined by the appearance of senile plaques in the allocortex, with deposits observed in the entorhinal cortex, hippocampal CA1 region, the insular cortex and, less frequently, the amygdala and cingulate gyrus[14,15]. Phase III involves additional subcortical regions including; the striatum, thalmus, hypothalamus and the basal forebrain[14,15]. In phase IV, plaque pathology is more pronounced in the midbrain and spread to the medulla oblongata becomes apparent[14,15]. Phase V is defined by the appearance of deposits in the pons and the molecular layer of the cerebellum[14,15]. These five distinct phases have subsequently been summarised in three by Serrano-Pozo

et al, with stage I showing isocortical involvement, stage II involving the allocortex and limbic systems and stage III defined by subcortical involvement[5].

Work conducted by Braak *et al.* in 1991 showed that the progression of NFT pathology within the AD brain also follows a distinct pattern[16] (summarised in Figure 1.02, f[8]). Initially, sparse deposits are observed in the transentorhinal cortex of mildly affected individuals (stage I), which increase in density and spread to the CA1 region of the hippocampus (stage II)[16]. Subsequently, NFTs are observed in the entorhinal region of the cortex and in the subiculum (Stage III)[16]. In stage IV, the intensity of NFTs in the transentorhinal and entorhinal regions is seen to increase, as does NFT burden in the CA1 region of the hippocampus, sparse deposits also begin to become apparent in the amygdala, thalamus and claustrum[16]. In the final stage, the intensity of NFT deposition in the aforementioned regions is seen to increase and pathology is found dispersed through the isocortex, first in the associative areas (stage V) followed by the primary sensory motor and visual regions (stage VI)[16].

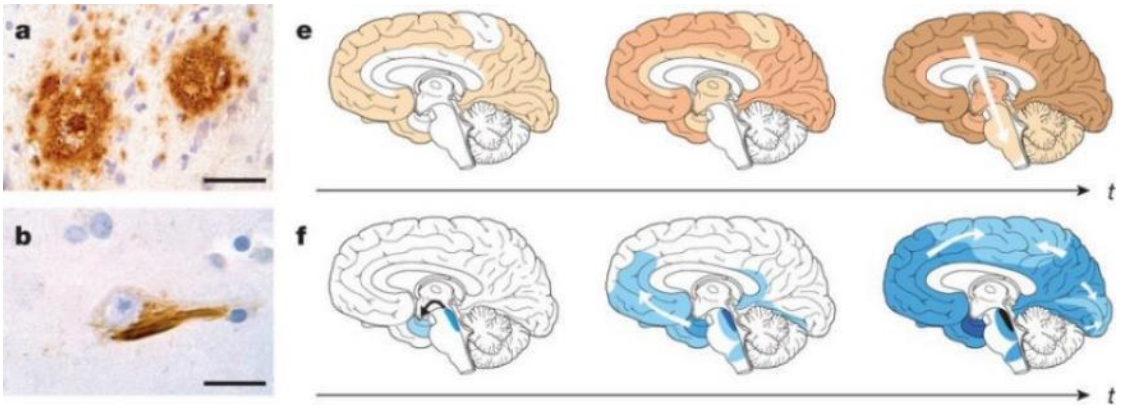

Figure 1.02. Deposition of senile plaques and neurofibrillary tangles in the AD brain. The spatiotemporal deposition of senile plaques and neurofibrillary tangles within the Alzheimer's diseased brain shows a characteristic pattern of distribution. a = senile plaques, b = Neurofibrillary tangle, e = Pattern of senile plaque deposition, f f= Pattern of neurofibrillary tangle deposition. Figure reproduced from Jucker & Walker[8].

The isolation and subsequent biochemical characterisation of senile plaques and neurofibrillary tangles led to the identification of amyloid-beta peptide (Aβ)[17-19] and the microtubule associated protein, tau, as their respective major components[20-22].

Amyloid Beta-Peptide:

Aβ is derived by the proteolytic cleavage of an integral transmembrane protein termed the amyloid precursor protein (APP), the gene for which was identified independently by four groups in 1987[23-26]. The *APP* gene is located on chromosome 21 (21q21.3), spans approximately 240 kilobases and contains 18 exons[27]. Alternate splicing of the *APP* gene results in three predominant isoforms, APP770, APP751 and APP695, the latter lacking exon 7 and exons 7 and 8 respectively[28]. APP has been shown to be expressed in all tissue types tested, with the highest expression reported in the CNS[29,30], particularly in the cerebral cortex and the hippocampus[31]. The tissue based distribution of APP expression is isoform specific, with

APP695 the predominant form seen in the CNS[32,33] whilst APP770 and APP751 are expressed in the periphery. Within the CNS, APP expression is also cell-type specific, with APP695 shown to be the predominant isoform expressed in neuronal cells[29] whilst APP770 and APP751 are preferentially expressed by astrocytes[29].

The APP protein consists of two large extracellular domains, E1 and E2, linked via a flexible acidic region, a transmembrane domain and an intracellular domain[34]. The longer APP770 isoform incorporates a Kunitz-type protease inhibitor (KPI) domain and an OX-2 antigen domain, the latter of which is absent in the APP751 isoform, whilst the APP695 variant lacks both features[35]. Due to structural flexibility, a complete crystal structure of the APP protein has not been generated, however subdomains of the protein have been successfully crystallised allowing a putative structure to be assembled (Figure 1.03[36]).

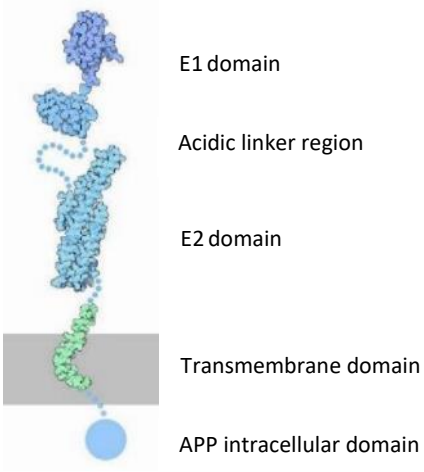

Figure 1.03. Putative Structure of the APP Protein. A complete crystal structure of the APP protein has not been generated, however subdomains have been successfully crystallised allowing a hypothetical model to the generated (PDB: 1MWP, 1OWT, 3NYL and 1IYT). Figure reproduced from[36].

The APP protein can be sequentially processed by an α-secretase and then a γ-secretase or a β-secretase and then a γ-secretase, termed the non-amyloidogenic and amyloidogenic pathways, respectively (reviewed in[37-39]). Cleavage by α-secretase occurs within the region encoding Aβ, precluding its production[37]. sAPP-α is released into the extracellular space whilst the membrane bound CTF-83 is subsequently cleaved by γ-secretase releasing the amyloid-intracellular domain (AICD) and P3 fragments (Figure 1.04, non-amyloidogenic)[37]. Cleavage by β-secretase produces sAPP-β and the membrane bound CTF-99, which is subsequently cleaved by γ-secretase producing the AICD and Aβ (Figure 1.04, amyloidogenic)[37]. Cleavage by γ-secretase, results in Aβ molecules of 38-43 amino acids in length, of which $A\beta_{1-40}$ is the most common, and $A\beta_{1-42}$ the most aggregation prone[40]. $A\beta_{1-42}$ is therefore the predominant isoform seen in senile plaques and has classically been considered the main pathogenic isoform.

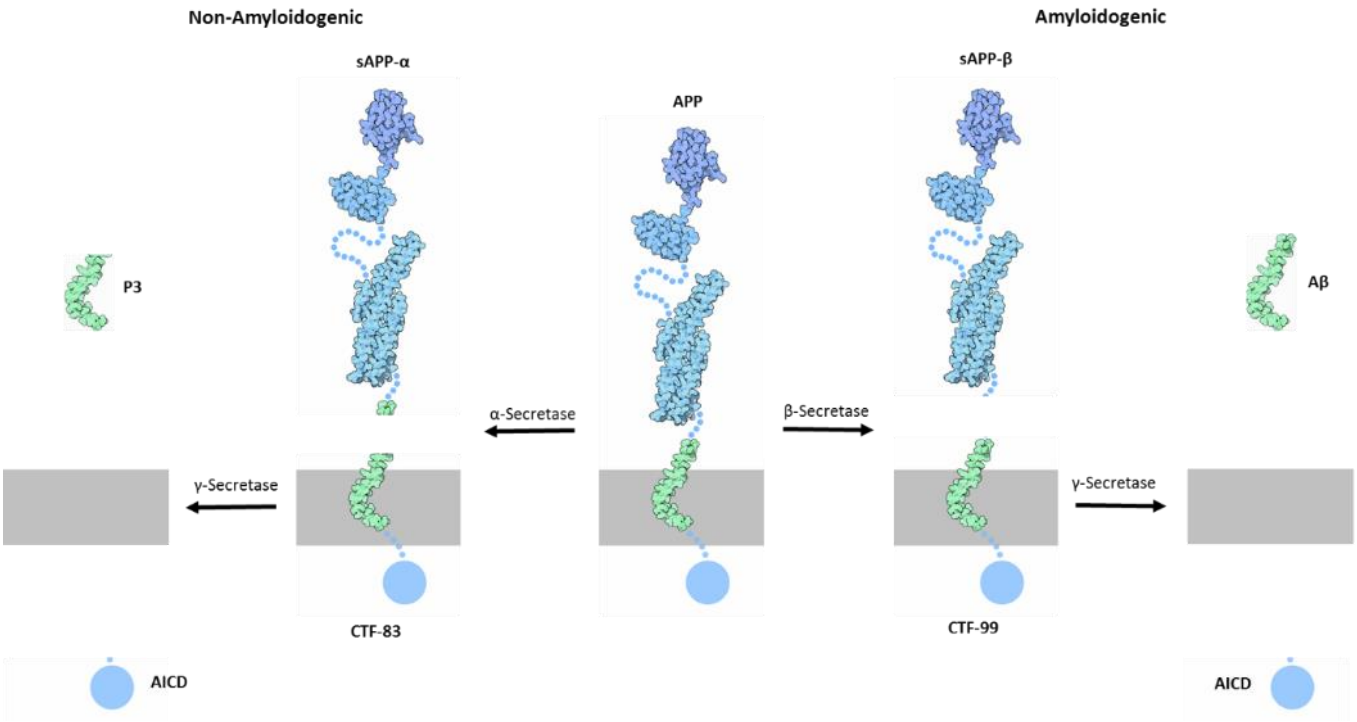

Figure 1.04. Amyloidogenic and non-amyloidogenic processing of APP. APP can be sequentially cleaved by α-secretase and γ-secretase producing the AICD and P3 fragments (non-amyloidogenic) or by β-secretase and γ-secretase producing Aβ and AICD (amyloidogenic). Figure adapted from[36,39].

The normal physiological roles of APP and the AD associated cleavage product, Aβ, are poorly defined. The ectodomain of APP is known to be capable of binding to heparan sulfate proteoglycans[41-43], type I collagen[44] and laminin[45], components of the extracellular matrix, and the APP protein colocalises with integrins in cultured hippocampal neurons[46] indicating a role in cell-ECM adhesion. Such interactions have been shown to stimulate neurite outgrowth, suggesting APP acts as a neurotrophic factor[44,45,47-50]. Additionally, APP has also been shown to be involved in intracellular adhesion via the formation of dimers at the cell surface, mediated by heparin binding via the E1 and E2 domains of the protein[51,52]. In concordance with these findings, an siRNA mediated knockdown of APP in neuronal cell lines has been shown to reduce cell division, cell adhesion and neurite outgrowth[53-56], with similar effects observed in primary hippocampal neuronal cultures derived from APP knockout mice[57]. The temporal and spatial expression of APP has been shown to peak in areas of the brain associated with synapse formation during rat embryonic and post-natal development, suggestive of a role for APP in synaptogenesis[58,59]. In addition, the expression of APP in both the pre and post synaptic termini has been shown to be required for neuromuscular synapse formation and the expression of APP in HEK293 cells was found to promote synapse formation in contacting co-cultured primary neurons providing further evidence for the role of APP in synapse formation[60]. The E1 domain of the APP protein has been shown to be capable of binding metal ions, most notably zinc[61] and copper[62]. The binding of the latter inducing a translocation of the APP protein to the cellular surface[63] and resulting in the reduction of Cu^{2+} to Cu^{+}, suggested to result in the generation of reactive oxygen species and indicative of a role for APP in the homeostasis of such ions[64].

Using primary neuronal cultures from transgenic mice, a homozygous knockout of APP has been shown to protect against copper induced toxicity, thus providing further evidence for the role of APP in copper homeostasis[65]. A homozygous knockout of APP in mice results in viable and fertile animals with reduced grip strength[66], decreased locomotor activity[66], reduced growth, a reduction in brain mass, defects in copper homeostasis[67] and impaired LTP resulting in learning defects[68-71], supporting the aforementioned putative functions of the APP protein derived from *in vitro* studies. The phenotypic abnormalities resulting from a homozygous APP knockout in murine models have been shown to be ameliorated or entirely reversed by the reintroduction of the sAPP-α domain of the APP protein, suggesting sAPP-α is critical for normal APP functionality[72].

The normal function of the AD relevant APP cleavage product, Aβ, is similarly poorly defined. The production of Aβ has been shown to be required for the viability of primary neuronal cultures and SH-SY5Y cells, with the administration of γ-secretase (2-naphthoyl-VF-CHO/γ-secretase inhibitor IX) or β-secretase (βSI/ βSII) inhibitors seen to induce a decrease in mitochondrial function, as measured using the MTT assay[73]. This effect was found to be neuron specific and was seen to be ameliorated upon treatment with exogenous Aβ at concentrations as low as 10 pM, indicating an Aβ specific mechanism[73]. The generation of Aβ has been shown to be dependent on neuronal activity[74]. In the presence of stimulatory or inhibitory compounds (tetrodotoxin, high magnesium, flunitrazepam/picrotoxin) a concomitant increase or decrease in the levels of soluble $A\beta_{1-40}$ and $A\beta_{1-42}$ generated by organotypic hippocampal sections derived from transgenic mice (APP Swedish mutation) was detected, an effect attributed to altered β-secretase activity[74]. The overexpression of APP was seen to induce a significant depression of excitatory synaptic responses, an effect which was dependent upon the proteolytic activities of both β-secretase and γ-secretase, indicating that Aβ is the causative species[74]. It therefore appears that neuronal activity enhances Aβ production, and Aβ inhibits neuronal activity, suggesting Aβ may act in a negative feedback loop preventing excessive neuronal stimulation and possibly excitotoxicity[74]. The *in vivo* sequestration of Aβ using a monoclonal antibody based approach has been shown to inhibit both short-term and long-term memory formation, an effect which was reduced in magnitude with the concomitant administration of purified $A\beta_{1-42}$ at a physiologically relevant dose (100 pM)[75]. Similar results were reported by Puzzo *et al.* where the administration of low pM concentrations of $A\beta_{1-42}$ to mice enhanced LTP and memory formation, whilst a scrambled peptide did not[76]. Both antibody mediated sequestration of $A\beta_{1-42}$ and siRNA mediated knockdown of APP were found to result in defects in LTP and memory formation which was rescued by the addition of picomolar concentrations of exogenous $A\beta_{1-42}$[77]. Thus it seems at low, picomolar concentrations, Aβ exerts positive neurological effects, enhancing neuronal viability, LTP and memory formation.

In the healthy brain, Aβ is rapidly turned over with an estimated rate of production and clearance from the CNS of ~7.6% and ~8.3% of total Aβ per hour[78]. A range of processes are thought to be involved in the clearance of Aβ including; draining via the interstitial fluid[79], astrocytic or microglial phagocytosis and degradation[80], transport across the blood-brain barrier into the circulation[79,81,82] and enzymatic

degradation[83]. It has been hypothesised that a defect in one or more of the Aβ production or clearance pathways induces an abnormal accumulation of Aβ within the brain, giving rise to the characteristic neuropathology and clinical symptoms associated with AD[84].

Tau Protein:

The NFT associated tau protein is encoded by the microtubule-associated protein tau gene (*MAPT*) which consists of 16 exons and maps to chromosome 17[85,86]. Six predominant isoforms of the tau protein are expressed within the adult brain, generated through alternate splicing of exons 2, 3 and 10 and resulting in isoforms harbouring either 3 or 4 carboxy-terminal repeat domains (3R/4R)[86]. The tau protein localises to the neuronal axon where it interacts with the microtubule assembly, via the carboxy-terminal repeat domains, acting to stabilise its structure and altering the dynamics of assembly and disassembly of the cytoskeleton, critical for both neuronal development and maintenance[87]. The tau protein is also thought to influence axonal transport by competing with the molecular motor proteins, dynein and kinesin, for the microtubule assembly, retarding both anterograde and retrograde transport along the microtubule[88,89].

Whilst the native tau protein harbours an intrinsically disordered structure with low propensity for aggregation[90], in the AD brain tau forms NFTs, composed of paired helical filaments[91]. Tau is subject to a range of post-translational modifications (reviewed in[86]), but most notably phosphorylation with around 45 experimentally verified phosphorylation sites[92]. The tau protein shows a development associated phosphorylation profile, with approximately 7 phosphate groups per molecule during foetal development and approximately two per molecule in the adult[86]. However, in the AD brain, the tau protein is known to become hyperphosphorylated, with approximately 8 phosphate groups per tau molecule (although it has been suggested that due to post-mortem delay this may be an underestimation)[93]. Whether hyperphosphorylation of tau is sufficient in of itself to promote aggregation is not entirely understood. Hyperphosphorylated tau extracted from the brains of human AD patients has been shown to be capable of self-assembly into tangles *in vitro*, an effect which was prevented by dephosphorylation[94]. However, certain phosphorylation sites on the tau protein have been shown to inhibit tangle formation[95] and reversible AD like hyperphosphorylation of the tau protein has been shown to occur during hibernation, using the European ground squirrel as a model, with no evidence of tangle formation[96]. In addition, transgenic mouse models have shown that neuronal loss does not correlate with tangle formation, with cells dying in the absence of observable pathology[97] and it has been suggested that cells bearing NFTs can remain viable for up to 20 years[98]. Thus, the mechanism by which tau forms NFTs, and the mechanistic link between NFT formation and neuronal loss *in vivo* remains unknown, and indeed there is now evidence that soluble forms of tau may be the true neurotoxic tau species as opposed to NFTs, although there are conflicting reports regarding this topic (discussed in[86]).

1.2 The Genetics of Alzheimer's Disease

Cases of AD are commonly divided into two classes on the basis of the age of onset. When clinical symptoms become apparent prior to the age of 65, the case is classed as early-onset AD (EOAD) and conversely, when symptoms become apparent after the age of 65, the case is classed as late-onset AD (LOAD). Whilst these brackets are somewhat arbitrary in nature, being based around the typical age of retirement, the distinction provided proves useful. For cases of EOAD there is typically an underlying causative genetic abnormality, predisposing to disease development and thus giving rise to the comparatively early onset of clinical symptoms. Such genetic perturbations are often heritable, leading to the term familial AD (FAD), and if inherited in an autosomal dominant fashion, autosomal dominant AD (ADAD). No deterministic mutations are known to cause LOAD, rather a number of genetic variations, alongside environmental factors, are thought to increase the risk of disease development and thus such cases are also referred to as sporadic AD. In terms of prevalence, the vast majority of cases of AD, 94.5%, present over the age of 65 and thus fall under the LOAD bracket with the remainder being classified as EOAD[99].

Early-Onset Alzheimer's Disease (EOAD)

In the majority of EOAD cases, the disease shows an autosomal dominant mechanism of inheritance with complete penetrance. The clinical symptoms of such patients mirror those with LOAD but present comparatively early[100].

The observation that patients with Trisomy 21 (Down's Syndrome) often present with AD like symptoms at a comparatively young age and, at autopsy, frequently exhibit AD like lesions within the brain, led to the hypothesis that a causative mutation may lie on chromosome 21[26]. The subsequent genetic appraisal of four families with FAD via genetic linkage analysis provided support for such a theory with linkage observed to chromosome 21[101]. In 1991, the first EOAD causing mutation was identified as a valine to isoleucine missense mutation at position 717 within the gene encoding the amyloid-precursor protein (*APP*), located on chromosome 21[102]. As a result of subsequent linkage studies, two additional loci were identified on chromosome 14 (14q24.3)[103-106] and chromosome 1 (1q31.42)[107] with causative mutations later identified in presenilin 1 (*PSEN1)*[108] and presenilin 2 (*PSEN2*)[109,110] respectively, components of the APP processing γ-secretase complex. At the time of writing, 58 causative mutations have been identified in the *APP* gene, 243 in *PSEN1* and 48 in *PSEN2* (for an up to date list, see Alzforum[111]).

EOAD mutations in the *APP* gene cluster around the cleavage sites for the β-secretase and γ-secretase enzymes, components of the amyloidogenic APP processing pathway. The Swedish mutation (KM670/671NL) is the only mutation known to increase the efficiency of β-secretase mediated cleavage of APP[112,113], leading to increased flux through the amyloidogenic pathway and a corresponding increase in total Aβ generation[114-116]. The remaining mutations cluster around the γ-secretase cleavage site and, whilst not increasing total Aβ levels, consistently alter the ratio of $A\beta_{1\text{-}40}$ and $A\beta_{1\text{-}42,}$ in favour of the latter more aggregation prone and thus more pathogenic isoform[117,118].

The γ-secretase complex is formed by nicastrin (*Nct*), presenilin (*PSEN1*, *PSEN2*), aph-1 and pen-2, with presenilin forming the catalytic core of the enzyme (Figure 1.05)[119]. Whilst a range of EOAD associated mutations have been identified in both *PSEN1* and *PSEN2*, a mechanistic appraisal of their affects has revealed a consistent alteration in the ratio of $A\beta_{1-40}$ and $A\beta_{1-42}$ in favour of the aggregation prone $A\beta_{1-42}$ isoform[120]. Although this increase in $A\beta_{1-42}$ was initially attributed to a gain of function, thereby increasing production of $A\beta_{1-42}$, subsequent experiments have indicated that the increase in $A\beta_{1-42}$ was more likely due to a defect in the generation of $A\beta_{1-40}$ resulting in increased production of $A\beta_{1-42}$ at the expense of $A\beta_{1-40}$[121-126].

Figure 1.05. Crystal structure of the γ-secretase complex. γ-secretase complex formed by Nicastrin (green), Presnilin 1 (blue), PEN-2 (yellow) and Aph-1 (pink) (PDB: 5A63).

Also of note is the protective Icelandic mutation of *APP* (A673T)[127]. Located adjacent to the β-secretase cleavage site, A673T reduces the efficiency of β-secretase cleavage and thus reduces the production of Aβ by approximately 40%[128]. Simultaneously, this mutation also appears to reduce the propensity of Aβ to aggregate, protecting against the development of AD[129-131].

Thus, all known EOAD causing mutations affect various facets of Aβ processing, promoting the formation of disease causing isoforms of Aβ. Additional autosomal dominant forms of AD have been reported for which no causative mutation could be identified in the *APP*, *PSEN1* or *PSEN2* genes, suggesting additional, as of yet unknown, genes are also involved[132].

Late-Onset Alzheimer's Disease (LOAD)

The vast majority of AD cases, 94.5%, are classified as late-onset due to clinical presentation occurring after the age of 65[99]. In contrast to familial forms of EOAD, no deterministic mutations are known to cause LOAD, rather a number of risk-associated genetic variants have been identified which, alongside environmental factors, are thought to predispose to the diseased state. The most well documented genetic risk factor for the development of LOAD is the ε4 allele of apolipoprotein-E (apo-E).

Apo-E is a 299 amino acid protein expressed in various tissues throughout the body, including the liver, brain, kidney and spleen[133] (Figure 1.06).

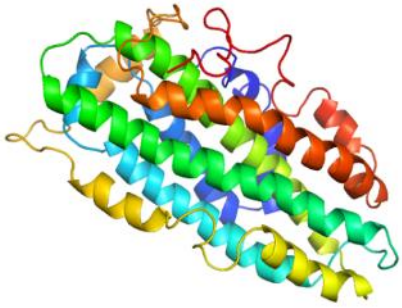

Figure 1.06. Structure of apoE-ε3. The apoE-ε3 structure was solved using NMR in 2010 (PDB: 2L7B).

In the plasma, the apo-E protein is found associated with lipoproteins, such as intermediate density lipoproteins, very low density lipoproteins, chylomicrons, chylomicron remnants and some forms of high density lipoproteins, together responsible for lipid transport[134]. Apo-E acts as a ligand, primarily for the low-density lipoprotein (LDL) receptor but also LDL receptor related-protein and the VLDL receptor and therefore mediates the transport of lipids between the tissues of the body, fulfilling a similar role within the brain[134].

In 1991, a linkage based study, performed by Pericak-Vance *et al,* identified a region of chromosome 19 as being associated with late-onset cases of AD[135]. Two years later, apo-E was shown to co-localise with neurological lesions characteristic of AD, namely senile plaques, cerebral amyloid angiopathy and neurofibrillary tangles[136] and, as apo-E is located on chromosome 19 (19q13.2), it was proposed as a candidate gene accounting for the previously described genetic linkage[136]. The ε4 allele of apo-E was subsequently found to be over represented in familial forms of LOAD, suggesting a causal link[136,137], a finding which has since been replicated using genome wide association studies, providing further evidence for such an association[138,139]. The apo-E protein has three alleles, ε2, ε3 and ε4, which differ at two amino acids; ε2 (Cys112, Cys158), ε3 (Cys112, Arg158) and ε4 (Arg112, Arg158)[140], giving rise to 6 potential genotypes (ε2/ε2, ε3/ε3, ε4/ε4, ε2/ε3, ε2/ε4, ε3/ε4)[141]. The relative frequencies of each allele within the normal population are; 8.4%, 77.9% and 13.7% for ε2, ε3 and ε4 respectively[142]. However, in LOAD cases the relative frequency of the ε4 allele has been shown to be increased to 36.7% (Caucasian population)[142]. The ε2 allele is thought to be protective, ε3 neutral, whilst the ε4 allele is thought to increase the risk of disease in a dose dependent manner with ε2/ε4 heterozygotes having an odds ratio for disease development of 2.6, ε3/ε4 an odds ratio of 3.2 and ε4 homozygotes an odds ratio of 14.9[142].

The molecular mechanism through which the ε4 allele of apo-E exerts its effect is not fully understood and likely involves a number of effects. Carriers of the apo-E ε4 allele have been shown to have increased deposition of senile plaques within the brain, with no corresponding increase in NFTs, suggestive of an amyloid mediated mechanism[143-145]. The identification of apo-E as a component of neuritic plaques prompted the hypothesis that apo-E may bind to and thereby promote the aggregation of Aβ[146]. Although

investigations into the relative ability of the three isoforms of apo-E to bind to Aβ *in vitro* have generated conflicting results[147-151], it is now generally accepted that apoE-ε2 shows highest affinity, followed by ε3 and finally ε4[152]. *In vitro* apoE-ε4 has been shown to enhance the rate of $A\beta_{1-42}$ fibril formation 10-20 fold whilst the effect of the ε3 variant was found to be less pronounced, followed by that of ε2[153]. Thus, it seems that the apoE protein is capable of interacting with Aβ, and in doing so can speed the formation of fibrillary assemblies in an isoform dependent manner[154], an effect which correlates with the aforementioned allelic disease association (ε4> ε3> ε2).

In vivo, using the PDAPP (APP V717F mutation) and Tg2576APP (APP Swedish mutation) mouse models, a knockout of the murine equivalent of apo-E was found to delay the appearance of Aβ pathology and prevent the formation of neuritic plaques, although diffuse plaques were apparent[155,156]. In the absence of APP, the introduction of human apoE-ε4 allele into knockout mice induced cognitive defects, as measured using the radial water arm maze, which were not apparent with ε3[157]. The introduction of human apoE-ε4 into transgenic mice overexpressing human APP resulted in markedly higher levels of fibrillar Aβ as compared to apoE-ε3[156,158,159], consistent with *in vitro* results and suggesting the ε4 variant speeds Aβ fibrillization *in vivo*.

A decrease in the level of $A\beta_{1-42}$ in the CSF has been established as a reliable marker for cerebral amyloid accumulation[160,161] and, interestingly, in a cohort of cognitively normal individuals, a correlation has been shown between apo-E allelic genotype and the abundance of $A\beta_{1-42}$ in the CSF. Higher levels of $A\beta_{1-42}$ were observed in the CSF of patients with the ε2 allele and lower levels observed with the ε4 allele, indicating protection from and exacerbation of cerebral amyloid deposition[162], an effect which was subsequently confirmed via PiB-PET scanning[162]. Consistent with the previously described AD association, the ε3 allele was found to give rise to an intermediate phenotype (cerebral amyloid deposition: ε4> ε3> ε2). This effect was seen to translate to decreased clearance of soluble forms of Aβ from within the brains of aged transgenic PDAPP mice (APP-V717F), and a corresponding increase in plaque burden in an apo-E isoform dependent manner, suggesting apo-E may play a role in the clearance of Aβ from the brain[162].

With the advent of genome-wide association studies and next generation sequencing, a number of additional risk associated loci have been identified, each with varying levels of molecular characterisation. A detailed discussion of these putative disease associated genetic variations is outside the scope of this introduction, but is reviewed comprehensively by Karch & Goate (Figure 1.07)[163].

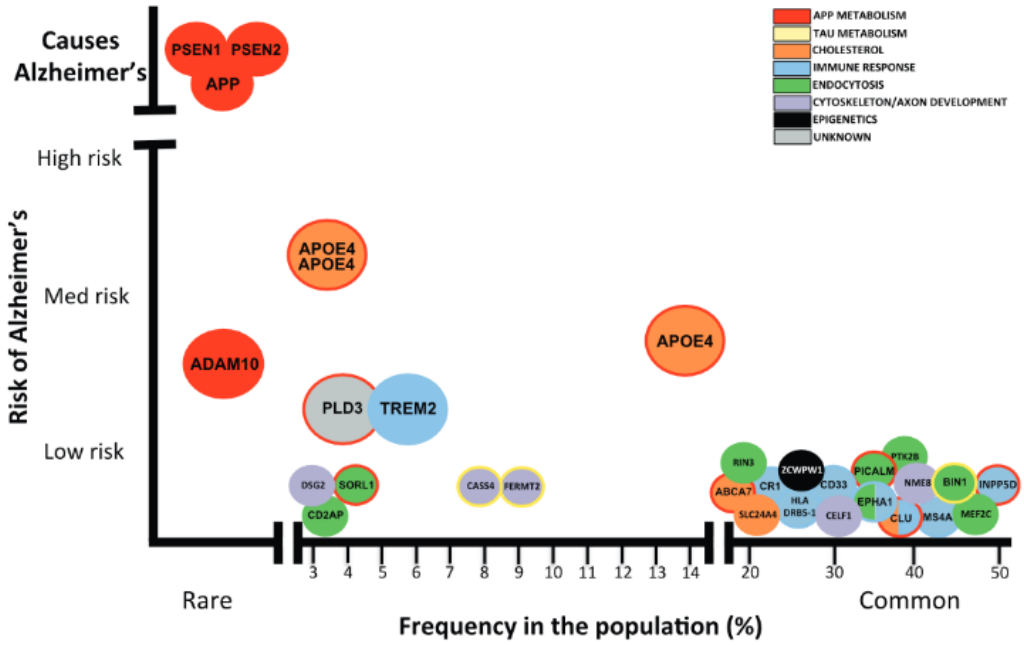

Figure 1.07. Alzheimer's disease associated genes. A number of genes have been suggested to increase the risk of AD development each with a range of potential mechanisms and varying penetrance. Figure reproduced from[163].

1.3 The Amyloid Cascade Hypothesis and Therapeutic Intervention

The amyloid cascade hypothesis was proposed by Hardy and Higgins in 1992 and posits that the abnormal deposition of Aβ plaques within the brain is the main causative factor for the development of AD, resulting in the characteristic neuronal loss associated with the disease[164-166]. Such a theory is supported by both histology, as evidenced by the deposition of abnormal aggregates of Aβ in the brains of AD patients (Section 1.1), and genetic association, with mutations in *APP*, *PSEN1* and *PSEN2* giving rise to autosomal dominant forms of AD (Section 1.2). Whilst there are a number of alternative hypotheses related to the underlying cause of AD, predominantly related to the tau protein[167] the amyloid cascade hypothesis has arguably become the most widely accepted theory within the AD field and will form the basis for the subsequent discussion of AD directed therapeutic agents.

Approved therapeutic agents against AD are at best palliative, treating symptoms but failing to address the underlying cause and as such disease progression and patient death remain a certainty. Therapeutic agents can be placed into two categories, namely NMDA receptor antagonists, such as memantine (Ebixa), and acetylcholinesterase inhibitors, such as donepezil (Aricept), rivastigmine (Exelon) and galantamine (Reminyl). Alongside these approved molecules are a number of experimental therapeutic agents at varying stages of development, targeting various facets of Aβ production and clearance.

In order to correctly diagnose AD, to monitor disease progression and crucially to measure the efficacy of potential therapeutic agents, a convenient and accurate clinical grading scale is necessary. Several such scales have been described, and a brief overview of those relevant to the subsequent discussion of therapeutic agents; the Mini Mental State Examination (MMSE)[168], the Alzheimer's Disease Assessment Scale- Cognitive Subscale (ADAS-cog)[169], the Alzheimer's Disease Cooperative Study Activities of Daily Living Inventory (ADCS-ADL)[170] and the Severe Impairment Battery (SIB)[171], is provided herein.

The MMSE often forms the basis for patient inclusion criteria for clinical trials of novel therapeutics, as well as being used to measure efficacy of therapeutic agents. The MMSE is composed of 11 questions assessing attention, memory and spatial orientation, the ability to follow commands, both verbal and written, to name common objects, creatively write a sentence and to copy a complex image[172]. Following assessment, a numerical score on a range of 0-30 is generated, with lower values indicating a higher degree of impairment[173]. On the basis of the generated score, patients are typically segregated into the following groups; cognitively normal (MMSE= 30-24), mildly-cognitively impaired (MMSE= 23-20), moderately impaired (MMSE= 19-10) and severely impaired (MMSE= 9-0)[173]. The MMSE examination has been shown to be insensitive to patients with mild cognitive impairment due to “ceiling effects”, ie. some subtests are deemed too easy, masking the early signs of dementia, and also insensitive to the deterioration of severely demented patients, attributed to “floor effects”[173,174]. The ADAS-cog consists of 11 subtests designed to examine memory, language and motor coordination and is commonly used alongside the MMSE during clinical trials to examine the efficacy of therapeutic agents[169]. A score on a range of 0-70 is generated, with higher values indicating greater impairment. As with the MMSE, the

ADAS-cog is most sensitive to patients with moderate AD, again suffering from floor and ceiling effects[175]. The Alzheimer's Disease Cooperative Study, conducted in 1997, sought to identify a series of everyday activities, such as the ability to dress and feed oneself, which would be of prognostic use in monitoring the progression of dementia and would complement cognitive performance directed metrics[170]. 45 such activities were examined, identifying 27 which were deemed to be of use and leading to the generation of two scales; the ADCS-ADL_{19} consisting predominantly of core skills and providing a measure of severe AD, and the ADCS-ADL_{23} used for monitoring mild-moderate AD[175]. A score out of 78 is generated, with lower scores indicating a higher degree of impairment. The SIB was designed with the express intent of being able to evaluate patients with advanced dementia, a task to which the MMSE and ADAS-cog metrics are poorly suited[171,175]. The SIB examination tests memory, spatial orientation, language, response to name, attentiveness, social interaction, motor coordination and visuospatial abilities[175], a score out of 100 is generated with lower values indicating a higher degree of impairment.

1.31 Approved Therapeutic Agents:

NMDA Receptor Antagonists:

Memantine was developed by Eli-Lilly in 1963 for the treatment of diabetes but was found to be ineffective for this purpose[176]. In the 1980s, memantine was subsequently found to act as an NMDA receptor antagonist, exhibiting a favourable pharmacological profile as compared to similar molecules[177]. Memantine has been shown to act via an uncompetitive mechanism, binding explicitly to the open conformation of the NMDA receptor, and consequently blocking the flow of Na^+ and Ca^{2+} ions into the cell and K^+ out of the cell[177-179].

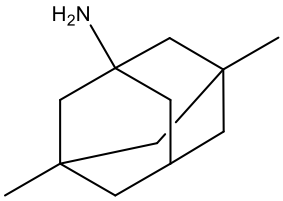

Memantine

Figure 1.08. Memantine Molecular Structure. Memantine is an NMDA receptor antagonist used for the treatment of moderate to severe AD.

The NMDA receptor is one of three classes of ligand gated ion channel which respond to L-glutamate, the others being the AMPA and Kainate classes of receptors[180]. Glutamate is the major excitatory neurotransmitter within the brain, with an estimated 70% of all excitatory synapses responding to this molecule[181]. Stimulation via the NMDA receptor is known to be key for learning and memory, a function attributed to NMDA mediated synaptic modulation resulting in long-term potentiation[182-186] and long-term depression[187-189]. The NMDA receptor forms a heterotetramer composed of four subunits (Figure 1.09). To date, a total of seven distinct subunit types have been identified; GluN1, GluN2 (A, B, C, D) and GluN3 (A, B), giving rise to a range of NMDA receptor of varying composition and with varying distribution and biophysical properties[180].

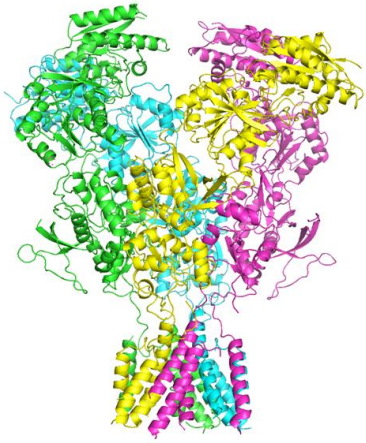

Figure 1.09. Crystal Structure of the NMDA Receptor. The NMDA receptor is a heterotetramer composed of four varying subunits. The structure shown is composed of two dimers of GluN1/GluN2B (PDB: 4PE5).

Following stimulation, L-glutamate is released from the pre-synaptic terminal and binds to NMDA receptors on the post-synaptic membrane, permitting the channel to open. At normal resting membrane potential (-70 mV), Mg^{2+} ions bind to the NMDA receptor blocking the flow of additional ions through the channel[190,191]. In the presence of a concomitant depolarisation of the postsynaptic membrane, Mg^{2+} is displaced allowing Ca^{2+} to flow from the extracellular compartment to within the neuronal cell[180], triggering intracellular calcium dependent signalling cascades, a process critical for both learning and memory via long-term potentiation and long-term depression[192]. However, hyperstimulation can result in an excess of intracellular calcium, causing neuronal cell death, a process termed excitotoxicity[193,194]. The mechanism through which NMDA receptor mediated excitotoxicity exerts its affect in the AD brain is not fully understood. It has been hypothesised that a generalised metabolic dysfunction within the cell may result in a deficit of ATP and a partial depolarisation of the plasma membrane, releasing bound Mg^{2+} ions from the NMDA receptor channel and resulting in chronic, pathological levels of intracellular calcium[195]. However, additional Aβ mediated mechanisms are also likely involved; such as an Aβ-mediated augmentation of glutamate release and reuptake (reviewed in[196]).

It is thought that the primary mechanism by which memantine exerts its neuroprotective effect is based around its higher affinity for the NMDA receptor as compared to Mg^{2+}, helping to prevent chronic, low level activation following of the NMDA receptor due to a partial depolarisation of the plasma membrane[197]. However, following a true depolarising event, memantine is released allowing the normal function of the NMDA receptor to be maintained, likely explaining its favourable toxicity profile as compared to other NMDA receptor antagonists[197] (reviewed in[197]).

The effects of memantine have been extensively examined in a number of clinical trials, two of which are outlined here (see ClinicalTrials.gov for a complete overview). In the first, 252 patients with moderate to severe AD were randomly allocated to placebo or memantine treatment and therapy maintained for a period of 28 weeks during which cognition was assessed using the Alzheimer's Disease Cooperative Study Activities of Daily Living Inventory (ADCS-ADL) and the Severe Impairment Battery (SIB), measuring various aspects of cognitive performance including; attention, orientation, language, memory and visuospatial ability[198]. Patients treated with memantine (NAMENDA) were found to have a significantly reduced rate of decline as compared to those treated with placebo, as assessed using the ADCS-ADL scale (Figure 1.10), and the SIB scale[199].

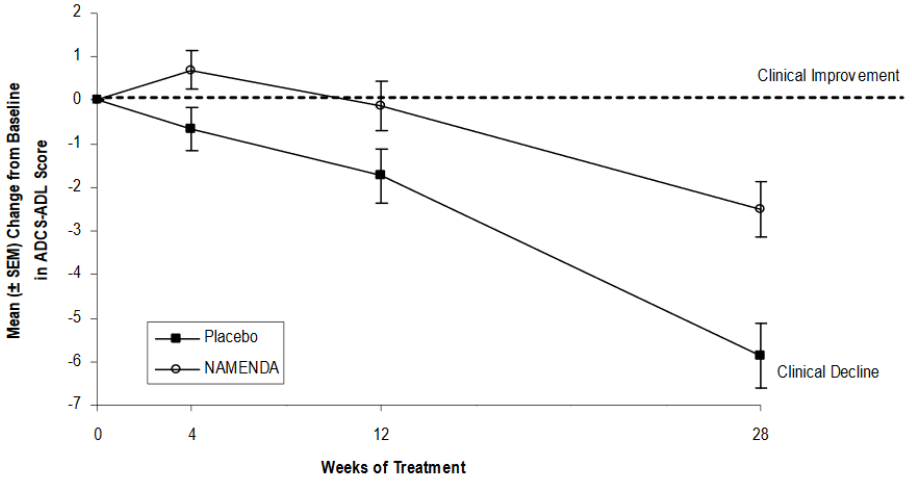

Figure 1.10. Efficacy of Memantine in Treating Moderate to Severe AD. Patients were treated with memantine (NAMENDA) or placebo for a period of 28 weeks during which cognitive performance was assessed using the ADCS-ADL scale. Patients treated with memantine were found to have a significantly reduced rate of cognitive decline. Figure reproduced from[199].

A second study investigated the effects of memantine in combination with the acetylcholinesterase inhibitor, donepezil. 404 patients with moderate to severe AD were randomly assigned to placebo treated and memantine treated groups. Following 24 weeks of treatment, cognitive ability was again assessed using the ADCL-ADL and SIB methodologies. Patients treated with a combination of memantine and donepezil were again found to exhibit a significantly reduced rate of clinical decline (Figure 1.11)[199].

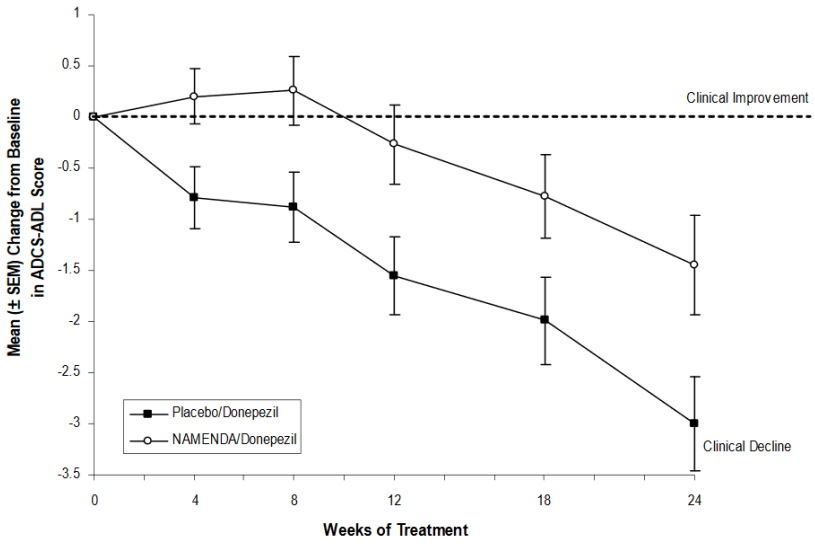

Figure 1.11 Efficacy of Memantine in combination with donepzil in treating moderate to severe AD. Patients were treated with either Donepezil alone, or Donepezil in combination with memantine (NAMENDA) for a period of 24 weeks during which cognitive performance was assessed using the ADCS-ADL scale. Patients treated with donepezil in combination with memantine were found to have a significantly reduced rate of cognitive decline. Figure reproduced from[199].

Acetylcholinesterase Inhibitors:

The second class of approved therapeutic agents for the treatment of AD are collectively known as acetylcholinesterase inhibitors. Acetylcholine acts as a neurotransmitter in the peripheral nervous system, particularly at the neuromuscular junction and in autonomic ganglia[200] and a neuromodulator in the central nervous system, altering axonal excitability[201-203], the release of neurotransmitters[204-208], coordinating groups of neurons to fire in unison and influencing synaptic plasticity[209-211]. Signalling occurs through two receptor subtypes; metabotropic muscarinic receptors, located on both the pre and post-synaptic membranes, and ionotropic nicotinic receptors, dispersed on the neuronal cell surface[200]. Acetylcholine is thought to act in a localised manner at the synapse and also at sites distant from the point of release, termed "volume effects", supported by the disjointed anatomical distribution of sites of acetylcholine release and cholinergic receptors[200]. Within the synaptic cleft, acetylcholinesterase (AChE) degrades released acetylcholine, terminating stimulation and producing acetate and choline, the latter of which is taken up by the presynaptic neuron and converted back to acetylcholine via choline acetyl-transferase (CAT) and acetyl-CoA[212] (Figure 1.12 and Figure 1.13).

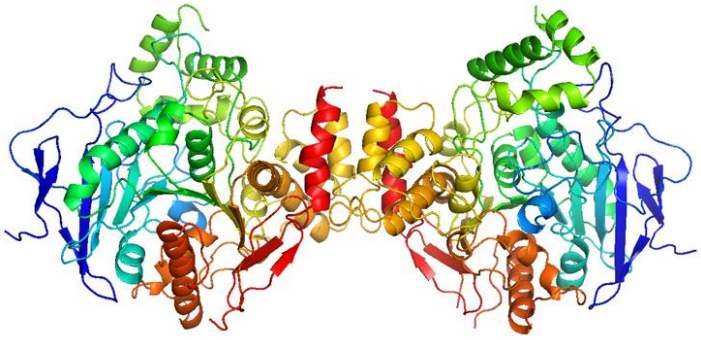

Figure 1.12. Crystal structure of acetylcholinsterase (AChE). AChE, a homodimer, catabolises the neurotransmitter acetylcholine within the synaptic cleft (PDB: 4EY7).

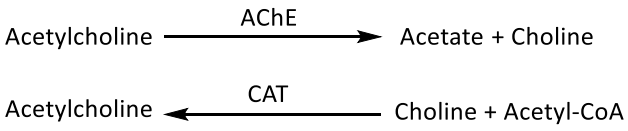

Figure 1.13. Catabolism and synthesis of acetylcholine. Acetylcholinesterase (AChE) catabolises acetylcholine, producing acetate and choline. Choline acetyltransferase (CAT) synthesises acetylcholine using choline and acetyl-CoA.

As a consequence of AD, there is a selective loss of cholinergic neurons in the basal forebrain[213] a substantial decrease in the activity of choline acetyltransferase[214,215], a decrease in the synaptic release of acetylcholine[216] and also in the subsequent re-uptake of choline, post AChE catabolism[217]. Thus, on the basis of the observed evidence, the cholinergic hypothesis was formulated, postulating that a generalised dysfunction of acetylcholine mediated neurotransmission plays a key role in the cognitive impairment associated with AD[218].

On the basis of the cholinergic hypothesis, AChE inhibitors were developed with the aim of slowing the catabolism of acetylcholine within the synaptic cleft, prolonging its retention time with the aim of maximising the activity of the reduced levels of acetylcholine observed in the diseased state[212]. AChE inhibitors can be subdivided into molecules which act via either an irreversible or reversible mechanism, the latter being the predominant form employed therapeutically due to their more favourable toxicity profiles[212]. The three most commonly prescribed AChE inhibitors are donepezil, rivastigmine, and galantamine (Figure 1.14).

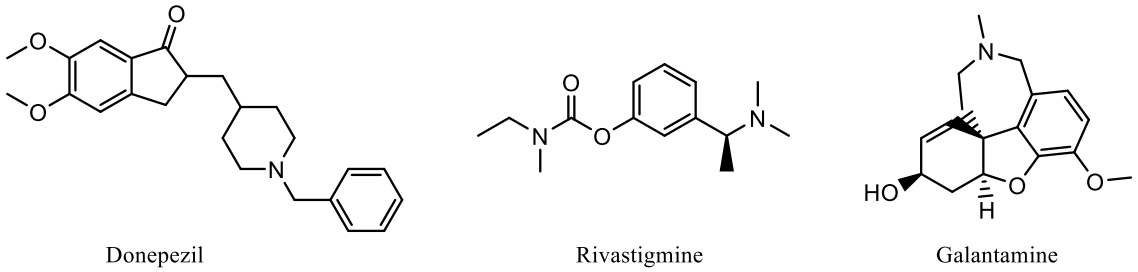

Figure 1.14. Molecular structure of donepezil, rivastigmine and galantamine. Donepezil, Rrivastigmine and galantamine are acetylcholine esterase inhibitors used for the treatment of AD.

All three drug molecules have been shown to induce a comparable, modest, improvment in cognition in patients with AD[219-222]. An illustrative example is provided using data derived from a 2002 clinical trial[223], testing the efficacy of donepezil in treating patients wih mild AD over a period of 24 weeks (5 mg/day for 6 weeks, 10 mg/day thereafter), indicating an improvement in cognition as measured using the ADAS-cog (Figure 1.15) and MMSE metrics (Figure 1.16).

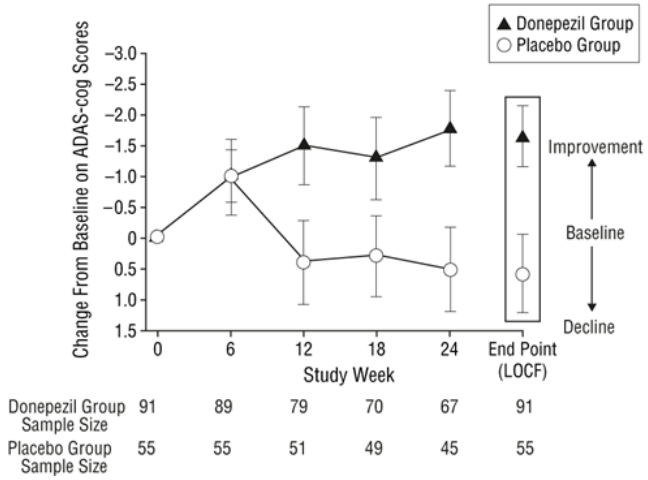

Figure 1.15. Efficacy of donepezil in treating mild-AD. The administration of donepezil was found to elicit an improvement in the cognitive performance of patients with mild AD, as measured using the ADAS-cog metric. Figure reproduced from[223].

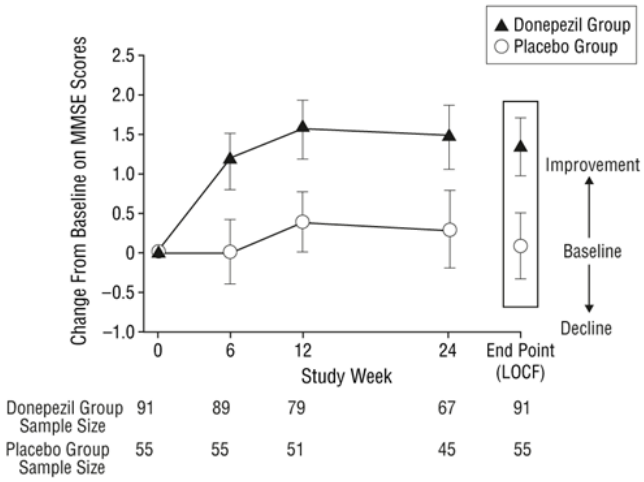

Figure 1.16. Efficacy of donepezil in treating mild-AD. The administration of donepezil was found to elicit an improvement in the cognitive performance of patients with mild AD, as measured using the MMSE metric. Figure from[223].

Whilst inducing an improvement in cognitive performance, the positive impact of both NMDA receptor antagonists and acetylcholinesterase inhibitors is modest in nature. In addition, neither class of molecule is capable of arresting disease progression, meaning that patient deterioration and eventual death remain a certainty and thus prompting the search for true disease modifying treatments, primarily targeting Aβ production and clearance, as per the amyloid cascade hypothesis[164]. Several such agents have been trialled, with varying levels of success, whilst others are still in development. Here, a focus is placed on therapeutic agents furthest through the development process (for a more complete overview see[224]).

1.32 Non-approved Therapeutic Agents

β-secretase and γ-secretase Inhibitors

On the basis of the amyloid cascade hypothesis[164], the direct inhibition of the amyloidogenic processing of APP via the therapeutic targeting of either β-secretase or γ-secretase,should serve to ameliorate the production of the pathogenic isoforms of Aβ ($A\beta_{1-40}$ and $A\beta_{1-42}$), hopefully arresting disease progression. A number of such compounds are in development by several large pharmaceutical organisations.

The compound E2609, a novel β-secretase inhibitor has been jointly developed by Eisai and Biogen (structure not published). At the time of writing, 8 phase I clinical trials have been performed using E2609, showing the compound to be well tolerated and to induce a dose dependent decrease in Aβ production, as measured in blood plasma[225]. Compound E2609 entered phase II clinical trials in 2014, the results of which are anticipated in January 2018[226]. MK-8931 (Figure 1.17, right), a second inhibitor of β-secretase developed by Merck, successfully passed phase I clinical trials in 2012 showing good tolerability and efficacy, measured via a decrease in CSF levels of Aβ. Compound MK-8931 is currently undergoing phase II/III trials for the treatment of mild to moderate AD, the results of which are an expected in July 2019[227,228]. LY2886721, is a third β-secretase inhibitor, in this instance developed by Eli Lilly (Figure 1.17, left). LY2886721 showed early promise, inducing a dose dependent decrease in $A\beta_{1-40}$ and $A\beta_{1-42}$, initially in cell culture, in mouse and dog models of AD and in human trials[229]. However, a phase II trial of LY2886721 was terminated prematurely as a result of a subset of patients displaying abnormal liver biochemical test results[230].

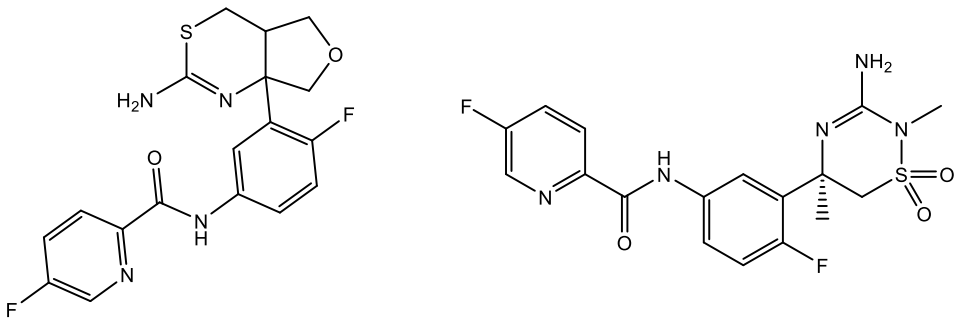

LY2886721 MK-8931

Figure 1.17. Structure LY2886721 and MK-8931. Molecular structure of β-secretase inhibitors LY2886721 and MK-8931 (E2609 not published).

Semagacestat (LY450139) is a γ-secretase inhibitor developed by Eli-Lilly (Figure 1.18, left) which was shown to decrease the production of $A\beta_{1-40}$ and $A\beta_{1-42}$ in CSF samples in a phase I clinical trial[231]. However, phase II trials raised potential issues. Following Semagacestat treatment, plasma levels of Aβ were found to be significantly reduced but with no corresponding decrease within the CSF[232,233]. In addition, a number of patients reported adverse reactions including drug induced rashes and alternations in hair pigmentation[232]. A large scale phase III trial of Semagacestat was halted prematurely when it was

recognised that the treatment group were exhibiting comparatively worse cognitive performance as compared to controls, measured by the ADAS-cog and ADCS-ADL metrics, and in addition, were exhibiting a significantly increased incidence of skin cancer and infection[234]. Subsequent work has shown Semagacestat preferentially inhibits Notch processing (IC_{50} = 24.62 nM, 95% CI = 15.74-38.51 nM) as compared to APP (IC_{50} = 257.8 nM, 95% CI = 190.2-349.5 nM) possibly explaining the aforementioned toxicity[235].

Avagacestat is a γ-secretase inhibitor developed by Bristol-Myers Squib (Figure 1.18, right). Avagacestat was initially reported to be 193-fold more specific for APP cleavage as compared to Notch[236], although this specificity index has subsequently been reported as only 3-fold[237]. Phase I trials were successful, but the compound subsequently failed phase II due to unacceptable side effects, including elevated rates of skin cancer, diarrhoea, nausea and rash and, as was seen previously with Semagacestat, a trend towards a worsening of cognition following drug treatment[238].

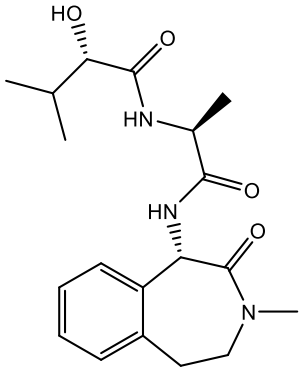

Semagacestat

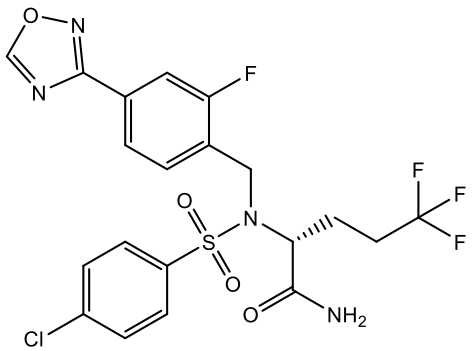

Avagacestat

Figure 1.18. Structure Semagacestat and Avagacestat. Molecular structure of γ-secretase inhibitors Semagacestat and Avagacestat.

Aβ Aggregation Inhibitors

An alternative therapeutic approach relates to the use of small molecules to perturb Aβ aggregation, curtailing plaque formation and, in theory, the associated cellular damage and neuronal loss. Alzhemed, (3APS, Tramiprosate) is one such aggregation inhibiting compound (Figure 1.19).

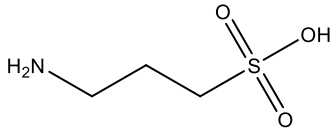

Alzhemed

Figure 1.19. Structure Alzhemed. Molecular structure of Aβ aggregation inhibitor Alzhemed (Tramprosate, 3-APS).

In 2007, Alzhemed was shown to be capable of binding $A\beta_{1-40}$ and $A\beta_{1-42}$ and to maintain $A\beta_{1-40}$ in a soluble, non-oligomerised form[239]. This effect was seen to translate into protection against $A\beta_{1-42}$ induced cell death using both rat primary cortical neurons and the neuroblastoma SH-SY5Y cell line[239]. A reduction in the deposition of Aβ plaques in a mouse model of the disease and in plasma and cerebral levels of $A\beta_{1-40}$ and $A\beta_{1-42}$ was also observed post Alzhemed treatment[239]. During a phase II clinical trial, Alzhemed was found to induce a decrease in CSF $A\beta_{1-42}$, but with no associated improvement in cognition[240], results mirrored in a subsequent large scale phase III trial[241]. Development of Alzhemed has subsequently ceased.

Additional small molecule inhibitors of Aβ aggregation include; Colostrinin[242,243], *scyllo*-inositol (ELND005)[244], PBT1 (clinoquinol)[245] and PBT2[246], each at varying levels of development.

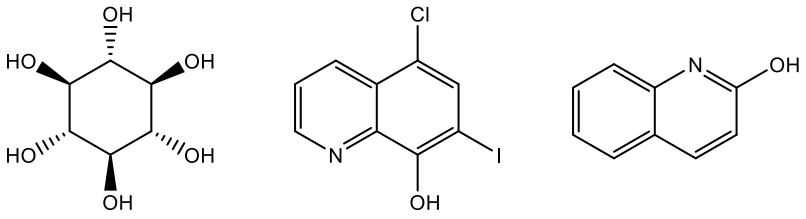

scyllo-inositol PBT1 PBT2

Figure 1.20. Small molecule inhibitors of Aβ aggregation. *Scyllo*-inositol, PBT1 and PBT2 have been identified as compounds capable of perturbing the aggregation of Aβ.

Aβ Directed Immunotherapy

An antibody based approach has also been employed with the aim of clearing amyloid plaques post deposition. Monoclonal antibodies directed against the N-terminus of Aβ (residues 1-28) have been shown to be capable of disrupting pre-formed fibrillar assemblies of synthetic Aβ[247], an effect which was subsequently shown to protect neuronal PC12 cells from Aβ induced neurotoxicity *in vitro*[247].

Following on from this work, a mouse model of AD (PDAPP, harbouring the V717F APP mutation) was immunized using $A\beta_{1-42}$, eliciting an active immune response, both prior to and after the onset of neuropathological symptoms. Immunisation prior to the onset of symptoms effectively prevented amyloid plaque deposition and hallmarks of plaque induced toxicity, namely the presence of dystrophic neurites and astrogliosis[248], whilst immunisation later in the disease course was found to dramatically reduce the plaque burden as compared to controls[248]. Such immunisation has subsequently been shown to protect against Aβ mediated cognitive deficits using various metrics and a range of mouse models of the disease[249-252].

The promising results observed in mouse models led to an initial human trial, conducted by ELAN Pharmaceuticals, in which patients with mild to moderate AD were treated with an aggregated form of $A\beta_{1-42}$, termed AN1792, on four occasions (weeks 0, 4, 12 and 24) inducing an active immune response[253]. AN1792 passed phase I clinical trials with no notable adverse effects, but was subsequently halted during phase II when 6% of patients developed acute meningoencephalitis[254]. Despite failing phase II clinical trials, the subsequent histological analysis of the brains of patients from within the trial suggested a marked clearance of Aβ plaques had indeed occurred whilst NFTs and cerebral amyloid angiopathy were still apparent[255-258]. Although a marked decrease in Aβ plaque abundance was seen in patients treated with AN1792, no difference in cognitive performance was observed between treated and control patients using a range of assessments including the ADAS-cog and MMSE scales[259]. A follow-up study has since confirmed that patients treated with AN1792, and who exhibited a significantly reduced plaque burden, still proceeded to a severe end-stage dementia with no significant difference in survival or time to dementia[260].

Also of note are the monoclonal antibody based therapeutic agents; Bapineuzumab, developed jointly by Janssen and Pfizer, and Solanezumab, by Eli-Lilly. As opposed to previous trials in which aggregated $A\beta_{1-42}$ (AN1792) was used to induce an active immune response, Bapineuzumab, and Solanezumab are instead administered as a passive immune therapy. The failure of AN1792 has been attributed to a T-cell mediated pro-inflammatory response giving rise to the observed meningoencephalitis[261], an effect which should not be seen with passive immunisation.

In phase II trials, Bapineuzumab was administered as 6 infusions over 78 weeks to 124 patients with mild to moderate AD (assessed via MMSE score) alongside 110 patients who were given a placebo. The primary measure of cognitive performance was the ADAS-cog metric with assessments performed prior to treatment, following each infusion and at termination at 78 weeks. No significant differences in cognitive

performance, CSF levels of Aβ, total-tau or phospho-tau, or brain volume (via MRI) were observed following treatment with Bapineuzumab[262]. A number of adverse effects were however observed, most notably vascular-edema, with a two-fold high prevalence in Bapineuzumab treated patients as compared to controls[262]. Phase III trials were conducted using patients with mild to moderate AD and subdivided into apoE-ε4 carriers (673 Bapineuzumab treated, 448 placebo) and non-carriers (807 Bapineuzumab treated, 524 placebo)[263]. Bapineuzumab was administered every 13 weeks for a total of 6 treatments. The primary measure of efficacy was the ADAS-cog metric, performed prior to treatment and following each infusion (a total of 6 over 78 weeks). PET scanning using the Pittsburgh compound B (PiB), giving a measure of cerebral amyloid load, was also employed prior to treatment and at weeks 45 and 71. As was seen during phase II trials, no significant differences in cognitive performance were observed between patients treated with Bapineuzumab or placebo and similarly, no brain volumetric changes were observed between untreated and treated groups, indicating disease progression[263]. As was seen during phase II trials, the most notable adverse effect following Bapineuzumab was an elevated incidence of vascular-edema[263]. On the basis of these findings, all subsequent trials of Bapineuzumab were halted.

Solanezumab is a humanized IgG1 monoclonal antibody targeted against the central domain of the Aβ molecule[264]. In mouse models, peripheral administration of m266, the murine antibody from which Solaneuzamab is derived, to PDAPP mice (harbouring the human V171F APP mutation), resulted in almost complete sequestration of plasma Aβ and interestingly, the total levels of plasma Aβ were found to be increased approximately 1000-fold following treatment, suggesting m266 was acting as an Aβ-sink and altering the equilibrium between peripheral and CNS localised Aβ[264,265]. Following treatment with m266, the levels of Aβ within the CSF were found to be rapidly increased, supporting such a theory and suggesting mobilisation of Aβ from within the CNS to the CSF and periphery[264]. This effect was seen to translate into a decrease in Aβ derived plaques within the brains of m266 treated mice[264].

Phase I trials mirrored the findings seen previously using PDAPP mice, with a marked increase in CSF and plasma levels of Aβ following administration of Solanezumab to patients with mild to moderate AD, with no evidence of adverse effects[266]. At phase II, 52 patients with mild to moderate AD were treated with Solanezumab once weekly for a total of 12 weeks[267]. Plasma and CSF levels of Aβ were assessed using an ELISA based assay, and cognitive performance measured using the ADAS-cog test. Treatment with Solanezumab was again seen to dramatically increase plasma and CSF levels of $A\beta_{1\text{-}40}$ and $A\beta_{1\text{-}42}$. However, no significant difference in cognitive ability was observed[267].

Solanezumab subsequently entered two different phase III clinical trials, termed EXPEDITION1 and EXPEDITION2. Patients with mild to moderate AD were allocated to Solanezumab or placebo treatment groups and Solanezumab administered once every 4 weeks over an 18-month period[268]. Cognitive performance was primarily assessed using the ADAS-cog and ADCS-ADL metrics. EXPEDITION1 employed 506 patients in each treatment group, Solanezumab or placebo, whilst EXPEDITION2 designated 521 to Solanezumab and 519 to placebo. In both studies, plasma levels of $A\beta_{1\text{-}40}$ and $A\beta_{1\text{-}42}$ were seen to

significantly increase following Solanezumab treatment, as were total levels of $A\beta_{1-40}$ and $A\beta_{1-42}$ in the CSF[268]. However, no differences in brain amyloid deposition was observed using ^{18}F-florbetapir-PET imaging and hippocampal and whole-brain volume was seen to decrease comparably between groups, indicative of disease progression[268]. Critically, no consistent significant difference in cognitive performance was observed in either study between patients treated with Solanezumab as compared to placebo[268]. A subsequent analysis of the data, specifically looking at a subset of early stage AD patients suggested that Solanezumab treatment may have been beneficial to this patient cohort, slowing cognitive decline[269].

Eli-Lilly is now conducting a third clinical trial using Solanezumab, termed EXPEDITION3, expected to end in October 2016. The Dominantly Inherited Alzheimer's Network is also running a phase II/III trial testing Solanezumab and Gantenerumab, a monoclonal antibody therapy developed by Roche, targeting familial forms of AD.

Therefore, whilst there is evidence that memantine and AChE inhibitors offer symptomatic improvement in patients with AD, the effects are slight and often transient. Bapineuzumab, an antibody based therapy targeting Aβ plaques, failed to meet any of its primary endpoints in large scale phase III clinical trials, inducing no significant improvement in cognition, and whilst there is evidence that Solanezumab, a second antibody mediated therapeutic agent, may induce a modest slowing of the disease process in patients with mild forms of AD, this effect has yet to be confirmed and again appears modest in nature. AN1792 was found to significantly reduce the plaque burden in patients with AD, with no associated improvement in cognition, no delay in the time to dementia, or in time to death, again calling into question the validity of targeting insoluble plaques of Aβ for the treatment of AD. Compounds targeting γ-secretase appear to have inherent issues of specificity, resulting in marked side effects, an effect most likely attributed to a simultaneous inhibition of Notch processing, whilst the efficacy of β-secretase inhibitors remains to be seen (results expected in 2018 and 2019).

Despite the myriad of approaches trialled, no single therapeutic agent has been shown to arrest, or markedly slow the progression of AD, nor to induce a marked improvement in cognition. Whether this failure is due the therapeutic intervention being made too late in the disease process, or whether the amyloid cascade hypothesis as it was originally formulated fails to accurately describe the AD process remains to be seen. In recent years, there has been a shift in focus from insoluble extracellular plaques of Aβ to soluble intracellular forms, which may be key in driving early disease progression and thus an attractive target for therapeutic intervention.

1.4 Soluble Aβ and 17β-Hydroxysteroid Dehydrogenase Type 10

1.41 Soluble Aβ

Despite being the most influential hypothesis regarding the cause of Alzheimer's disease, there are a number of issues related to the amyloid cascade hypothesis as it was originally formulated[164]. The deposition of Aβ plaques was posited as being the main disease causing lesion associated with the development of Alzheimer's disease[164], however plaque burden has been shown to correlate poorly with disease progression in both murine models and AD patients. In transgenic mouse models expressing ADAD associated mutations of the APP protein, markers of cognitive decline have been reported prior to plaque deposition; most notably a decrease in the level of synaptophysin and synaptic electrophysiological abnormalities, indicating a loss of functional synapses[270-272]. A similar lack of correlation between plaque burden and disease severity has been reported in AD patients, with the best correlate instead reported as synaptic loss[273,274], and indeed amyloid deposition has been reported to plateau whilst cognitive decline is seen to continue[275]. In addition, an estimated 20-40% of elderly individuals show sufficient Aβ plaque deposition to meet AD diagnostic criteria, despite being cognitively normal[276-280]. Together these observations suggest that plaque formation may not be the key disease driving event in the AD brain. Whilst early reports have suggested that Aβ requires assembly into fibrillary structures before toxicity becomes apparent[281-283] subsequent work has reported that soluble oligomeric forms of Aβ (Figure 1.23, right), referred to as Aβ-derived diffusible ligands (ADDLs), are a potent neurotoxic species in their own right and exhibit enhanced toxicity as compared to the aforementioned fibrillar assemblies[284].

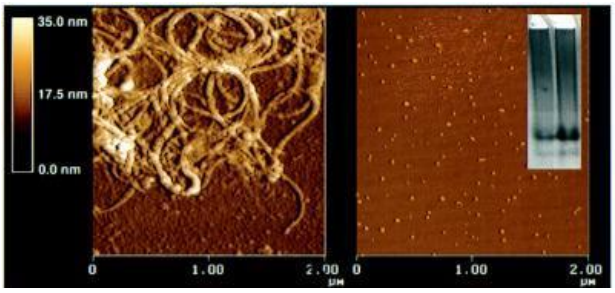

Figure 1.21. Aβ Oligomerisation. Aβ has been shown to be capable of forming large fibrils (left panel) or small diffusible oligomers (ADDLS, right panel) depending on the conditions utilised. Figure reproduced from[284].

The toxicity of soluble oligomeric forms of Aβ has been shown to be selective in nature, inducing cell death in the CA1 region of the hippocampus and the entorhinal cortex of organotypic mouse brain slice cultures at low nanomolar concentrations, whilst sparing neurons derived from the cerebellum, a pattern which matches that observed in the AD brain and is not observed with fibrillar assemblies of Aβ[285]. Such species also induced a deficit in long-term potentiation in rat hippocampal slices, correlating with observations made in mouse models of AD, prior to plaque deposition[284]. The production of such oligomeric Aβ species has been shown to increase in cell lines expressing wild-type APP or ADAD associated APP mutants[286,287], in transgenic mouse models of AD[288,289] and in the brains of AD patients but not in non-diseased

controls[290,291]. As previously mentioned, a decrease in synaptic density has been shown to be the strongest correlate for the neurological decline associated with AD[274] and the levels of soluble Aβ have since been shown to correlate strongly with both synaptic loss and disease severity in both mouse models and patients with AD[285,292,293]. Thus, it appears that soluble forms of Aβ may be the true toxic species in AD, responsible for the neuronal loss and disrupted synaptic function observed in the diseased state and independent of plaque formation.

Soluble forms of Aβ have been identified in various intracellular compartments, including the endoplasmic reticulum[294-296], the trans-golgi apparatus[294,296,297], the cytosol[298-300] and lysosomal compartments[301]. In addition, Aβ has also been identified in the mitochondria[302-307]. Within the mitochondria, Aβ has been hypothesised to interact with mitochondrial proteins, disrupting normal function and inducing cell death[308]. The 17β-HSD10 enzyme has been identified as one such mitochondrial Aβ binding protein.

1.42 17β-HSD10

The 17β-HSD10 enzyme, (also known as amyloid-binding alcohol dehydrogenase (ABAD), endoplasmic reticulum-associated amyloid beta-peptide binding protein (ERAB), HADH2, SCHAD, MRRP2, SDR5C1) is a member of the short-chain dehydrogenase/reductase (SDR) and 17β-hydroxysteroid dehydrogenase families. The monomeric 17β-HSD10 enzyme is 27 kDa in size, consists of 261 amino acids and localises to the mitochondrial matrix[309-311], the only enzyme within the 17β-hydroxysteroid family known to do so[312]. The enzyme forms a 108 kDa homotetramer (Figure 1.22) and is known to catalyse the conversion of a range of substrates, participating in the degradation of isoleucine, the β-oxidation of fatty acids and in the metabolism of steroidal hormones[313].

Figure 1.22. 17β-HSD10 Homotetramer. The 17β-HSD10 enzyme has been shown to form a 108 kDa homotetramer in solution. (PDB: 1U7T).

The tissue based distribution of the 17β-HSD10 enzyme has been characterised via immunoblotting, with highest levels observed in the liver, kidney, heart, brain and gonads[309]. The gene encoding the 17β-HSD10 enzyme has been shown to be evolutionarily conserved and its expression necessary for survival[314]. The *Drosophila* homologue of the 17β-HSD10 enzyme, *scully,* shows 61% sequence identity with the human

protein[315] and has been shown to have broadly similar catalytic activities[311]. *Scully* is however localised to the cytoplasm of the cell, as opposed to the mitochondria, likely due to a truncation of the N-terminus of the *Drosophila* protein resulting in a non-functional or absent mitochondrial targeting sequence[311]. Four mutations within the *scully* gene have been shown to be lethal during development; scu^{174} *and* scu^{152} inducing single amino acid substitutions, L33Q and F120I respectively, whilst scu^{3127} and scu^{4058} generate truncated isoforms of the protein, the former harbouring only 86 N-terminal amino acids out of the full 255 and thus lacking the majority of functional domains, whilst the latter lacks a C-terminal portion of the protein, thought to confer substrate specificity[315]. In male flies, all four mutants were found to impart a dramatic reduction in teste size, a decrease in the abundance of mitochondria and an increase in the deposition of intracellular lipid vesicles within testes cells, a phenotypic abnormality attributed to a defect in the β-oxidation of fatty acids[315].

In humans, inactivating mutations within the gene encoding the 17β-HSD10 enzyme have been associated with an X-linked neurodegenerative disorder termed 2-methyl-3-hydroxybutyryl-CoA dehydrogenase (MHBD) deficiency. The first case of MHBD deficiency was reported in 2000 by Zschocke *et al.* with the patient presenting on the second day of life with Kussmaul respiration associated with metabolic acidosis with hypoglycaemia, elevated lactate, hyperammonemia and ketonuria and subsequently recovering following glucose administration[316]. The patient showed normal early development of motor coordination, with head control achieved at 4 months of age, the ability to sit supported at 8 months and at 13 months the ability to move via rolling, sit unaided and stand with support[316]. Mental and language development were however delayed[316]. At 14 months of age, the patient began to exhibit regression, losing acquired skills, most notably the ability to sit and to stand[316]. In addition, restlessness and involuntary movements developed and by 24 months of age, severe retardation was apparent[316]. Isoleucine challenge was found to result in a marked increase in plasma isoleucine levels within 30 minutes of administration (780 µmol/L, normal range, 28–95 µmol/L) which remained outside of the normal range over 4 hours (230 µmol/L), suggestive of a defect in isoleucine degradation[316]. Enzyme assays performed using patient fibroblasts revealed an almost complete absence of 17β-HSD10 activity, measured as 0.02 $nmol/min^{-1}mg^{-1}$ (controls, 1.48 ± 0.12 $nmol/min^{-1}mg^{-1}$). During the catabolism of isoleucine, 17β-HSD10 catalyses the penultimate step, involving the conversion 2-methyl-3-hydroxybutyryl-CoA to 2-methylacetoacetyl-CoA which is subsequently cleaved by β-ketothiolase, producing propionyl-CoA and acetyl-CoA (Figure 1.23)[317,318].

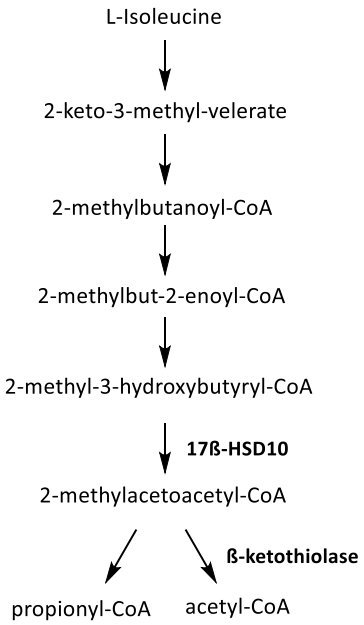

Figure 1.23 Isoleucine degradation pathway. The 17β-HSD10 enzyme is known to play a role in the catabolism of isoleucine, catalysing the conversion of 2-methy-3-hydroxybutyryl-CoA to 2-methacetoacetyl-CoA (Figure redrawn from[316]).

The administration of an isoleucine restricted diet was seen to arrest neurological decline over the following 7 months[316]. However, the patient has subsequently been reported deceased, although it is not known if this was disease related, and the efficacy of isoleucine restriction reported as limited in other instances[319,320]. It has also been noted that the progression of MHBD deficiency is atypical for a defect in the isoleucine degradation pathway, rather mirroring that of a mitochondrial disease[319]. β-ketothiolase deficiency represents a similar defect in isoleucine degradation, with β-ketothiolase responsible for the step immediately following that of 17β-HSD10, and presents with an almost identical metabolic profile[321]. β-ketothiolase deficiency results in periods of ketoacidosis with associated severe vomiting which, if not appropriately managed, may progress to coma and death. The administration of an isoleucine restricted diet treats β-ketothiolase effectively and when combined with the appropriate treatment of periods ketoacidosis, normal development is observed in the majority of patients (23 out of 26 sampled)[322,323]. Neurological degeneration is not a characteristic feature of the disease, although psychomotor degeneration may occur following severe periods of ketoacidosis suggesting an additional mechanism may be at work in the case of MHBD deficiency[319,323,324]. A number of additional cases of MHBD deficiency have since been reported[325-329], with symptoms varying depending on the nature of the causative mutation. Mutations N247S, R226Q and D86G give rise to a severe "neonatal form" of the disease characterised by little neurological development, cardiomyopathy and early death[330]. R130C, L122V and P210S represent the most common mutations associated with MHBD deficiency and generate an "infantile form" of the disease, with normal early development followed by a progressive

neurodegenerative phenotype[330], whilst Q165H is known to generate an "atypical form" of MHBD deficiency with normal development[330].

Due to the failure of an isoleucine restricted diet to effectively treat MHBD deficiency, an alternative explanation was proposed relating to the role of the 17β-HSD10 enzyme in the metabolism of neuroactive steroids, most notably the oxidation and thus inactivation of estrogen and allopregenalone[331], positing that a loss or indeed a gain of 17β-HSD10 activity would perturb the homeostasis of such molecules resulting in the neurological deficits associated with the disease[332]. However, the subsequent characterisation of a number of clinically relevant disease causing mutations demonstrated that the severity of MHBD deficiency does not correlate with the residual level of enzymatic activity, suggesting another facet of 17β-HSD10 mediated dysfunction is responsible[320].

Using *Xenopus* as a model organism and morpholino oligonucleotides, the 17β-HSD10 homologue (xHSD10) was selectively knocked down, resulting in abnormal mitochondrial morphology, as indicated by a marked depletion of cristae (Figure 1.24), and a concomitant increase in the number of apoptotic cells, as measured by DNA fragmentation[320]. Again using *Xenopus*, the selective knockdown of xHSD10 was also found to induce defects in both neural and eye development, a phenotype rescued by the introduction of human 17β-HSD10[320].

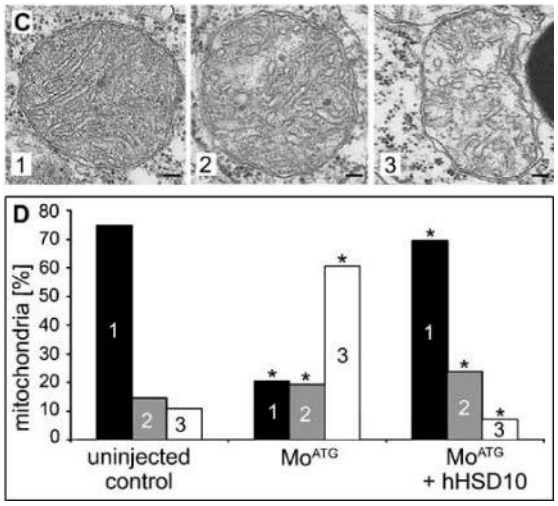

Figure 1.24. *Xenopus* xHSD10 knockdown. A knockdown of the *Xenopus* 17β-HSD10 homologue (xHSD10) was found to induce mitochondrial morphological abnormalities. On the basis of morphological appearance, mitochondria were classified as dense, dark (C1), loosely packed (C2) and with depleted cristae (C3) with corresponding quantification of each (D). Figure reproduced from[320].

Subsequently, two mouse models were produced using the Cre-Lox system, allowing the conditional knockout of the 17β-HSD10 enzyme (homozygous knockout reported as lethal)[320]. When 17β-HSD10 expression was selectively prevented in endothelial cells and cells of the immune system, the resultant mice were found to be viable and fertile but to die at around week 25[320]. In the second model, the expression of the 17β-HSD10 enzyme was selectively eliminated from noradrenergic neurons, causing death at occur at around week 26[320]. The subsequent analysis of mitochondrial integrity, via electron

microscopy, revealed a similar pattern of dysfunction to that seen with *Xenopus* models (Figure 1.26), with an elevation in the number of mitochondria harbouring loose, swollen or depleted cristae in the locus coeruleus (17β-HSD10 knockout) as compared to the cerebellum (control region) (Figure 1.25)[320].

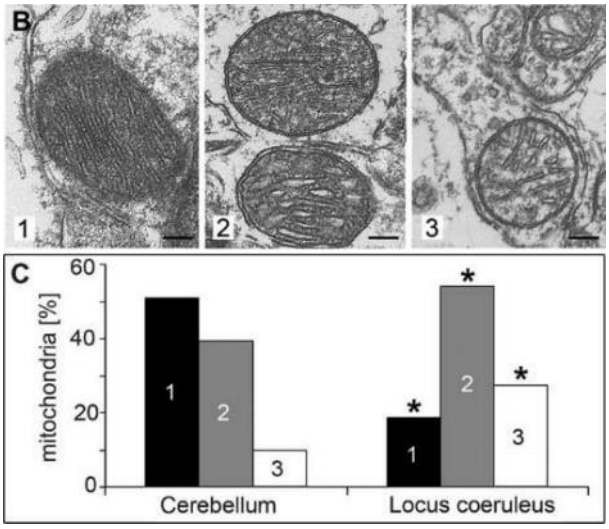

Figure 1.25. Murine 17β-HSD10 conditional knockout. A knockout of the 17β-HSD10 protein from noradrenergic neurons, present in the locus coeruleus, was found to induce mitochondrial morphological abnormalities. On the basis of morphological appearance mitochondria were classified as dense, dark (B1), loosely packed (B2) and with depleted cristae (B3) with corresponding quantification of each (C). Figure reproduced from[320].

Using recombinant protein, three clinically relevant mutants of the 17β-HSD10 enzyme; R130C, D86G and Q165H, were characterised in terms of residual levels of enzymatic activity, with 64%, 28% and 0% observed respectively, as compared to the wild-type enzyme[320]. Whilst showing the highest levels of residual activity, the R130C mutation was found to destabilise the enzyme, indicated by a time-dependent decrease in activity following incubation at room temperature, and a decrease in the level of detectable protein in lysates taken from patient fibroblasts[320]. All three mutants were confirmed to localise to the mitochondrial matrix, precluding the possibility of improper subcellular localisation influencing results[320]. Despite having no residual enzymatic activity, patients harbouring the Q165H mutation are known to display normal neurological development, whilst those with the D86G and R130C mutations present with a more severe phenotype[320]. In cultured fibroblasts the aforementioned mutations of the 17β-HSD10 enzyme were found to induce abnormalities in mitochondrial morphology as compared to non-diseased controls. Those taken from patients harbouring the R130C and D86G mutations showed aberrant morphology characterised by swollen or depleted cristae, whilst fibroblasts from patients with the Q165H mutation were found to display an intermediate phenotype[320].

Interestingly, using a *Xenopus* model, the catalytically inactive Q165H mutant was found to be capable of partially rescuing the enhanced levels of apoptosis observed following 17β-HSD10 knockdown, an effect not seen with the R130C and D86G mutants (Figure. 1.26)[320].

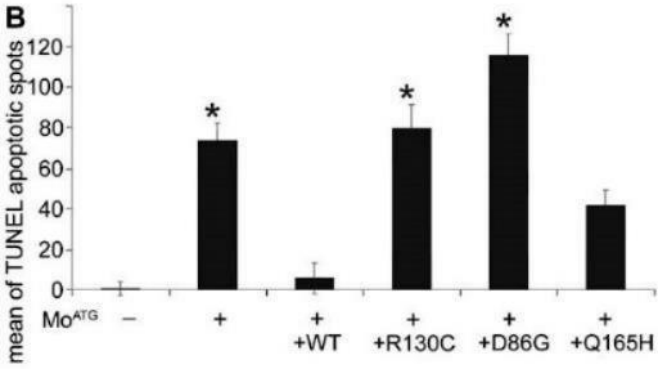

Figure 1.26. Rescue of 17β-HSD10 knockdown induced apoptosis by MHBD causing 17β-HSD10 mutations. The knockdown of the *Xenopus* 17β-HSD10 homologue (xHSD10) was found to induce a marked increase in apoptosis. Reintroduction of the 17β-HSD10 enzyme harbouring known MHBD disease causing mutations revealed a partial phenotypic rescue using the Q165H mutant but not with R130C or D86G. Figure reproduced from[320].

It therefore appears that the 17β-HSD10 enzyme plays a key role in maintaining mitochondrial integrity, with a loss of expression resulting in mitochondrial morphological abnormalities. The fact that this effect does not correlate with the residual level of enzyme activity indicates that the 17β-HSD10 enzyme performs an additional role outside of its catalytic activities, which becomes perturbed in the diseased state.

Subsequent work has shown the 17β-HSD10 enzyme (MRRP2) to be involved in the formation of the mitochondrial ribonuclease P complex (mtRNase P), along with tRNA methyltransferase 10C (TRMT10C/MRRP1) and proteinaceous RNase P (PRORP/MRRP3)[333]. Mitochondrial transfer RNA (tRNA) molecules are synthesised in an immature form often requiring extensive modification before being rendered active[334]. The mtRNase P complex has been shown to be capable of performing two of these steps, namely the endonucleolytic removal of 5' nucleotide extensions and the N1-methylation of adenosine and guanosine, required for the correct folding of tRNA molecules[335]. The physical presence of both TRMT10C and 17β-HSD10 has been shown to be required for mtRNase P activity, however the dehydrogenase activity of the 17β-HSD10 enzyme has been shown to be entirely dispensable for both the endonucleolytic and methyltransferase activities of the complex[335]. The selective knockdown of 17β-HSD10 has been shown to cause a corresponding decrease in the level of TRMT10C protein, with no corresponding decrease at the mRNA level, suggesting the primary function of the 17β-HSD10 enzyme in the mtRNase P complex may be to bind to and stabilise the TRMT10C subunit (Figure 1.27)[330].

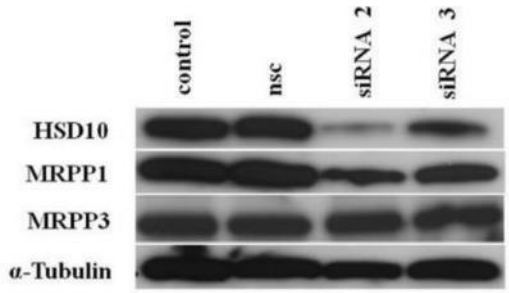

Figure 1.27. Effect of 17β-HSD10 knockdown on TRMT10C (MRPP1) and PRORP (MRRP3) protein levels. The knockdown of 17β-HSD10 using siRNA was found to induce a corresponding decrease in the level of expression of the TRMT10C protein, with no corresponding decrease at the mRNA level, suggesting 17β-HSD10 may bind to and thereby stabilise the TRMT10C subunit of the mtRNase P complex. MRRP3 expression was unaffected. Figure reproduced from[330].

When the levels of 17β-HSD10 and TRMT10C were assessed in fibroblasts taken from patients harbouring the R130C mutation (high dehydrogenase activity, severe phenotype) or the Q165H mutation (no dehydrogenase activity, mild phenotype) markedly lower levels of both proteins were observed with the R130C mutation, but less so with Q165H (Figure 1.28)[330].

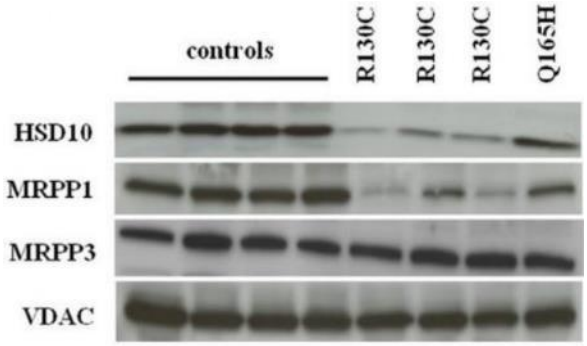

Figure 1.28. Expression of mtRNaseP components in MHBD patient fibroblasts. Patients harbouring the R130C mutation (high enzymatic activity, severe phenotype) were found to have significantly reduced expression of 17β-HSD10 and MRPP1 (TRMT10C) as compared to those with the Q165H mutation (no enzymatic activity, mild phenotype). Figure reproduced from[330].

In concordance with these findings, the knockdown of 17β-HSD10 in HeLa cells was found to induce a significant increase in unprocessed mitochondrial transcripts, possibly indicating an mtRNaseP defect, an effect which was mirrored by the R130C mutation, but not Q165H[330]. Thus, whilst the residual level of 17β-HSD10 catalytic activity does not correlate with MHBD disease severity, the absolute level of 17β-HSD10 protein, and its ability to stabilise the TRMT10C protein, appears to. Therefore, MHBD deficiency may primarily be due to a defect in mitochondrial tRNA processing, giving rise to a generalised mitochondrial dysfunction, as opposed to a direct loss of 17β-HSD10 enzymatic activity. In support of these conclusions, the subsequent assessment of 17β-HSD10 protein levels in an MHBD patient harbouring the N247S mutation revealed a decrease in expression, giving rise to a defect in mtRNase P activity and resulting in reduced assembly and activity of mitochondrial complexes I, III, IV and V[336].

In addition to its role in MHBD deficiency, the 17β-HSD10 enzyme has also been implicated in Alzheimer's disease. Using a yeast-two-hybrid system, the mitochondrial 17β-HSD10 enzyme has been shown to interact with Aβ in a highly potent manner[337]. Intriguingly, in cell culture, the 17β-HSD10/Aβ complex was found to be cytotoxic, resulting in enhanced levels of mitochondrial dysfunction and cell death, as measured by MTT reduction (Figure 1.29, left) and nuclear DNA fragmentation (Figure 1.29, right), compared to either species in isolation[337]. The disruption of this interaction was found to protect against these hallmarks of cellular stress, suggesting that the 17β-HSD10 enzyme may play a role in mediating the cytotoxic effects of Aβ and thus may offer a novel therapeutic target for treating AD[337].

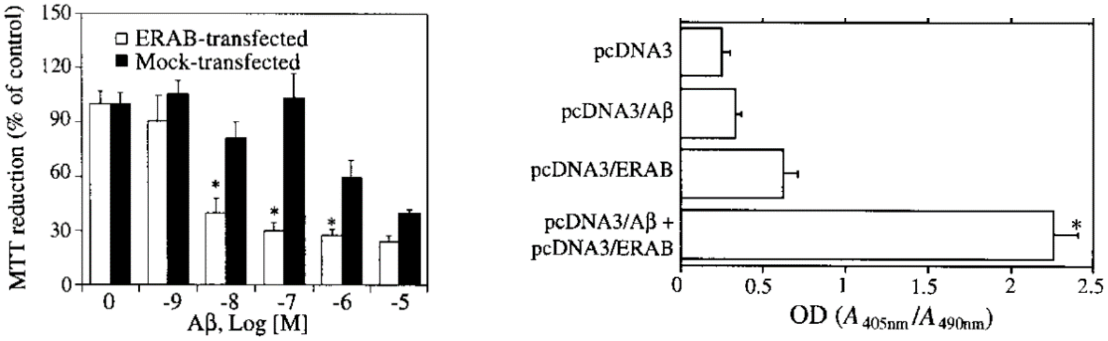

Figure 1.29. Cytotoxic effects induced by co-transfection of 17β-HSD10/Aβ. Transient transfection of COS-7 cells with both the 17β-HSD10 enzyme and Aβ was found to induce a marked increase in cellular stress as measured using the MTT assay (left) and DNA fragmentation (right) as compared to either species in isolation. Figures reproduced from[337].

Subsequent work further characterised the interaction of 17β-HSD10 with Aβ. Using radiolabelled ^{125}I-17β-HSD10, the interaction was confirmed to be of high affinity, with a K_D value of 40-70 nM, measured using both $Aβ_{1-40}$ and $Aβ_{1-42}$[338]. Although binding was observed in the low nanomolar range, an inhibition of the catalytic activity of the 17β-HSD10 enzyme was only apparent at markedly higher Aβ concentrations, with a Ki value of 1.6 ± 0.5 μM, as measured against the 17β-HSD10 conversion of acetoacetyl-CoA to L3-hydroxybutyryl-CoA, possibly indicating that oligomerised forms of Aβ are required to inhibit enzymatic activity[338]. As was shown previously (Figure 1.29), the simultaneous overexpression of wild-type 17β-HSD10 alongside $Aβ_{1-42}$ was again found to be toxic, resulting in oxidative stress and cell death, in this instance measured by 4-hydroxynoneal staining, a marker of oxidative damage (Figure 1.30, right) and DNA fragmentation (Figure 1.30, left)[338]. Site directed mutagenesis was used to introduce two missense mutations (Y168G/K172G) into the 17β-HSD10 cDNA sequence, altering conserved residues within the catalytic triad of the enzyme (S155, Y168, K172) and thereby rendering the enzyme inactive. The Y168G/K172G mutant (mutERAB) was confirmed to bind to $Aβ_{1-42}$ with comparable affinity to the wild-type enzyme, but when overexpressed alongside $Aβ_{1-42}$, no marked increase in oxidative damage or cell

death was apparent, suggesting the toxicity of the 17β-HSD10/Aβ interaction is dependent on the catalytic activity of enzyme (Figure 1.30)[338].

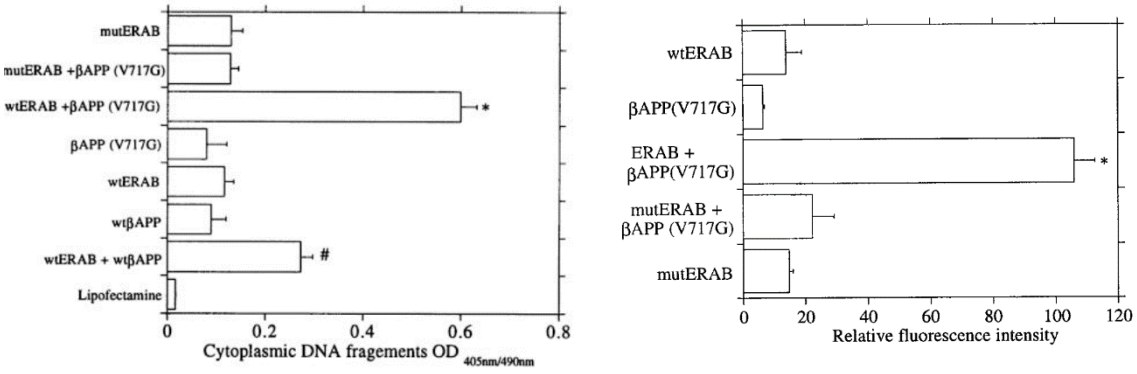

Figure 1.30. Effect of 17β-HSD10 catalytic activity on 17β-HSD10/Aβ cytotoxicity. Co-transfection of COS-7 cells with wild-type 17β-HSD10 (ERAB) and Aβ resulted in a marked increase in DNA fragmentation (left) and 4-hydroxynoneal levels (right) whilst a catalytically inactive mutant of the 17β-HSD10 enzyme (Y168G/K172G, mutERAB) with Aβ did not. Figures reproduced from[338].

In 2004, Lustbader *et al.* co-crystallised the 17β-HSD10 enzyme in the presence of molar excess of $Aβ_{1-40}$[303]. Although SDS-PAGE analysis of the produced crystals showed $Aβ_{1-40}$ was indeed present, no electron-density corresponding to $Aβ_{1-40}$ was observed, suggesting the region to which $Aβ_{1-40}$ is bound is highly disordered. The 17β-HSD10 enzyme harbours a unique insert, termed the loop D region, as compared to other members of the 17β-hydroxysteroid dehydrogenase family and as 17β-HSD10 is the only member reported to interact with Aβ, it was hypothesised that the loop D region may be the site to which Aβ binds[303]. Using site directed mutagenesis, this was confirmed to be the case, with two key regions found to be responsible for Aβ binding, S98-Y101 and T108-T101 (Figure 1.31)[303].

ABAD mutations	Aβ Binding
Experiments with ABAD truncations	
GST-ABAD (1–186)	+
GST-ABAD (1–158)	+
GST-ABAD (159–261)	–
Experiments with site-directed ABAD mutations	
G93A	+
S98A, K99A	+
S98A, K99A, T100A, Y101A	–
S98A, K99A, Y101A	–
N102A	+
N102A, L103A	+
T108A, H109A, T110A	–
V156A	+
Q162A	+

Figure 1.31. Effect of missense mutations on the ability of 17β-HSD10 to bind Aβ. The region of the 17β-HSD10 enzyme (ABAD) to which Aβ binds was identified as involving amino acids 1-158 and subsequently narrowed to amino acids S98A, K99A, T100A and Y101A. Figure reproduced from[303].

The region of the 17β-HSD10 enzyme encompassing the aforementioned residues (92-120) was cloned and fused to the human immunodeficiency virus-1 derived Tat protein, allowing cellular membrane penetration and generating a specific inhibitor of the 17β-HSD10/Aβ interaction, termed the ABAD-Decoy Peptide (ABAD-DP)[303]. Through the use of surface-plasmon resonance the ABAD-DP was found to be capable of disrupting the 17β-HSD10/Aβ interaction, with a Ki value of 1.72 ± 0.20 μM (Figure 1.32). A peptide harbouring the reversed amino acid sequence, termed ABAD-RP (residues 120-92) was found to have no effect, suggesting the ABAD-DP induced perturbation of the 17β-HSD10/Aβ interaction is specific in nature.

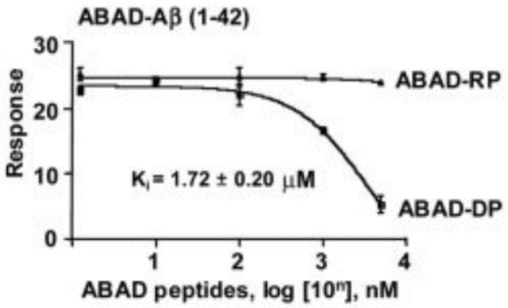

Figure 1.32. ABAD-DP mediated disruption of 17β-HSD10/Aβ interaction. Using surface plasmon-resonance, the ABAD-DP was found to be capable of disrupting the interaction between 17β-HSD10 (ABAD) and Aβ with a Ki value of 1.72 ± 0.20 μM. The reversed peptide sequence (ABAD-RP) had no effect. Figure reproduced from[303].

Transgenic mice were subsequently generated, harbouring mutant APP (mAPP), producing elevated levels of Aβ, neuronally expressed 17β-HSD10 or the two in combination[303]. Primary cortical neurons derived from 17β-HSD10 transgenic mice were found to display enhanced mobilisation of cytochrome c from the membrane fraction to the cytosol following $A\beta_{1-42}$ challenge, indicative of an induction of apoptosis, whilst neurons from dual transgenic animals expressing both 17β-HSD10 and mAPP showed spontaneous release of cytochrome c[303]. Pre-treatment with the ABAD-DP was found to protect against the observed mobilisation of cytochrome c, whilst no such effect was apparent with the ABAD-RP, suggesting disruption of this interaction is protective *in vitro* (Figure 1.33)[303].

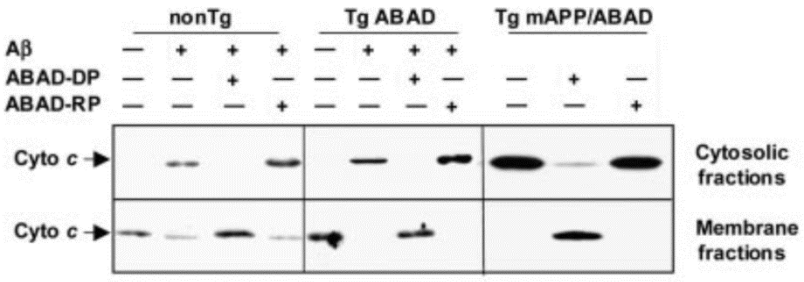

Figure 1.33. 17β-HSD10/Aβ induced apoptosis. Primary neuronal cultures were derived from transgenic mice overexpressing mutant APP, 17β-HSD10 (ABAD) or the two in combination. $A\beta_{1-42}$ challenge was seen to induce apoptosis in 17β-HSD10 expressing neurons, as measured by cytochrome c release, whilst neurons derived from dual transgenic animals showed spontaneous cytochrome c mobilisation. The ABAD-DP was found to protect against apoptosis, whilst the ABAD-RP did not. Figure reproduced from[303].

Subsequent work conducted by Yao *et al.* and Takuma *et al.* further characterised the protective effects of the ABAD-DP. Immunoprecipitation of Aβ from cortical mitochondria was performed using samples derived from transgenic mice expressing mutant APP, generating elevated levels of Aβ[339]. Samples were subsequently separated using SDS-PAGE and immunoblotting performed for the 17β-HSD10 enzyme. An enrichment of co-immunoprecipitated 17β-HSD10 was observed in mAPP expressing mice, indicative of elevated levels of the 17β-HSD10/Aβ complex[339]. The administration of the ABAD-DP intraperitoneally was found to reduce the level of co-immunoprecipitated 17β-HSD10, indicating that the ABAD-DP is capable of perturbing the 17β-HSD10/Aβ interaction *in vivo*, whilst no such effect was apparent with the ABAD-RP (Figure 1.34)[339].

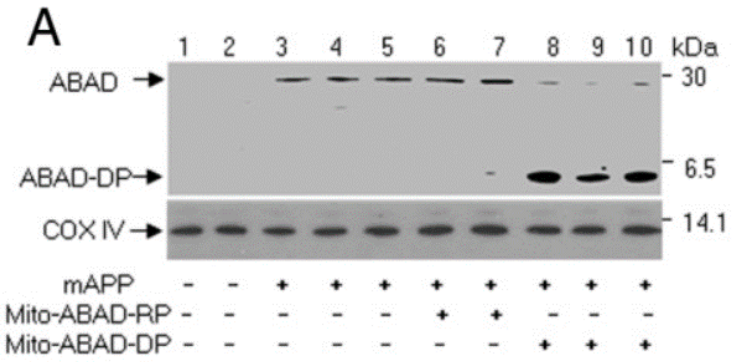

Figure 1.34. ABAD-DP mediated disruption of the 17β-HSD10/Aβ interaction *in vivo.* Following Aβ immunoprecipitation from purified mitochondria derived from mAPP transgenic mice, an increase in the level of 17β-HSD10 (ABAD) is apparent in mAPP expressing mice, indicating enhanced levels of 17β-HSD10/Aβ complex. Intraperitoneal administration of the ABAD-DP was found to perturb the 17β-HSD10/Aβ complex, whilst the ABAD-RP did not. Figure reproduced from[339].

Mitochondria from mAPP transgenic mice were found to exhibit significantly reduced levels of oxygen consumption and reduced activity of complex III and complex IV. In addition, immunocytochemistry revealed elevated levels of 4-HNE (a marker of oxidative stress) within the hippocampus in mAPP transgenic mice, effects which were reversed by the intraperitoneal administration of the ABAD-DP[339]. Using primary neuronal cultures from dual transgenic mice expressing both mAPP and 17β-HSD10, an elevation in reactive oxygen species leakage from the mitochondria was detected (hydrogen peroxide and superoxide) and was attributed to a defect in complex IV[340]. A reduced level of ATP was also seen in cultures derived from dual transgenic animals, again attributed to a defect in complex IV activity[340]. Following 6 days in culture, an increase in caspase-3 activity, DNA fragmentation and LDH release was observed in primary neuronal cultures derived from mAPP/17β-HSD10 dual transgenic mice, as compared neurons derived from single transgenic animals, indicating cell death. These effects were seen to be diminished in the presence of antioxidants, suggesting elevated reactive oxygen species generation may be the underlying cause[340]. Thus, the 17β-HSD10/Aβ interaction appears to induce mitochondrial dysfunction resulting in elevated levels of reactive oxygen species, which promote cell death.

The aforementioned toxic effects of the 17β-HSD10/Aβ interaction were seen to translate into a cognitive deficit in mAPP/17β-HSD10 dual transgenic animals as indicated by an increase in the number of errors during the radial arm water maze test, characteristic of a defect in spatial learning and memory. Such effects were ameliorated upon treatment with the ABAD-DP, but not with the ABAD-RP (Figure 1.35)[339].

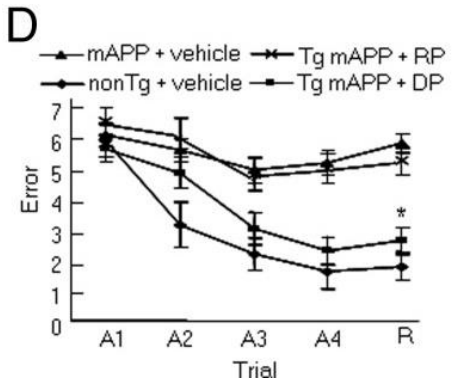

Figure 1.35. Effect of intraperitoneal administration of the ABAD-DP on radial arm test performance. Transgenic mice expressing mAPP were found to have a deficit in spatial learning and memory which was reversed by the intraperitoneal administration of the ABAD-DP, but not the ABAD-RP. Figure reproduced from[339].

The histological examination of cholinergic neuronal density in the subiculum of mAPP expressing mice revealed a significant reduction in mAPP expressing animals, similar to abnormalities associated with AD, a phenotype which was rescued in dual transgenic animals expressing both mAPP and a mitochondrially targeted ABAD-DP peptide[339]. A concomitant decrease in the level of AChE activity was also noted in mAPP transgenic animals, which was not apparent in mAPP/mito-ABAD-DP mice[339]. In terms of behaviour, the transgenic expression of mito-ABAD-DP was seen to induce a similar, but less pronounced effect (Figure 1.36) as compared to the aforementioned intraperitoneal administration of the ABAD-DP (Figure 1.35)[339].

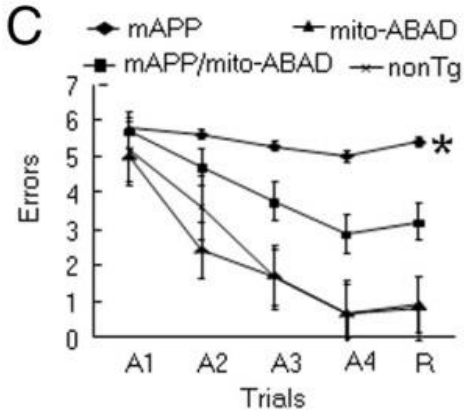

Figure 1.36. Effect of transgenic expression of the ABAD-DP on radial arm test performance. Transgenic mice expressing mAPP were found to have a deficit in spatial learning and memory which was ameliorated, but not reversed, in dual transgenic mice expressing mAPP and a mitochondrial targeted ABAD-DP. Figure reproduced from[339].

In the AD diseased state, the level of expression of the 17β-HSD10 enzyme has been shown to be increased, 28% in the inferior temporal lobe, 40% in the hippocampus[303] and 573% in the CSF[341], with a corresponding enrichment in the 17β-HSD10/Aβ complex in AD patients as compared to non-diseased controls (Figure 1.37)[303].

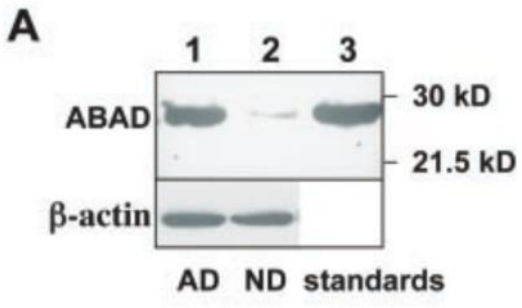

Figure 1.37. 17β-HSD10/Aβ complex in AD brain. Aβ was immunoprecipitated from AD brain lysates, samples separated by SDS-PAGE and immunoblotting performed for 17β-HSD10. In the brains of AD patients a marked enrichment of 17β-HSD10 is observed, indicating elevated levels of the 17β-HSD10/ Aβ complex. Figure reproduced from[303].

The proteomic analysis of the brains of dual transgenic mAPP/17β-HSD10 mice has revealed the up-regulation of peroxiredoxin II, an antioxidant enzyme presumed to represent a compensatory response to the elevated levels of oxidative stress associated with the 17β-HSD10/Aβ interaction (Figure 1.38, left) with a similar up-regulation apparent in the brains of AD patients (Figure 1.38, right)[342].

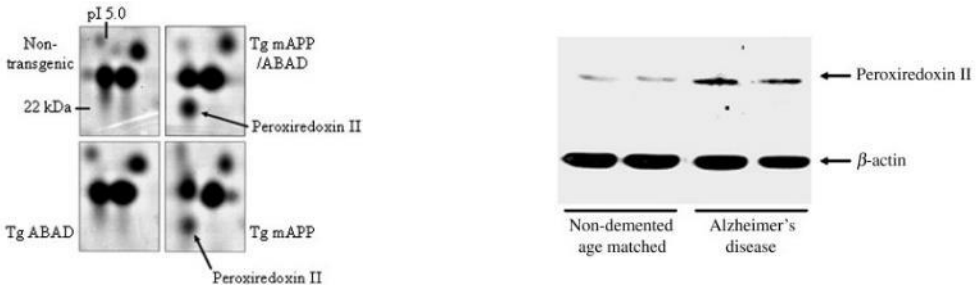

Figure 1.38. Peroxiredoxin II upregulation. The expression of the antioxidant enzyme peroxiredoxin II has been shown to be elevated in the brains of mAPP/17β-HSD10 transgenic mice (left panel) and in the brains of Alzheimer's diseased patients (right panel). Figures reproduced from[342].

Similarly, an upregulation of endophilin I has also been reported in the brains of mAPP/17β-HSD10 transgenic mice and in the brains of AD patients (Figure 1.39), thought to be involved in cell death mediated by an activation of the JNK-1 signalling pathway[343]. pathways.

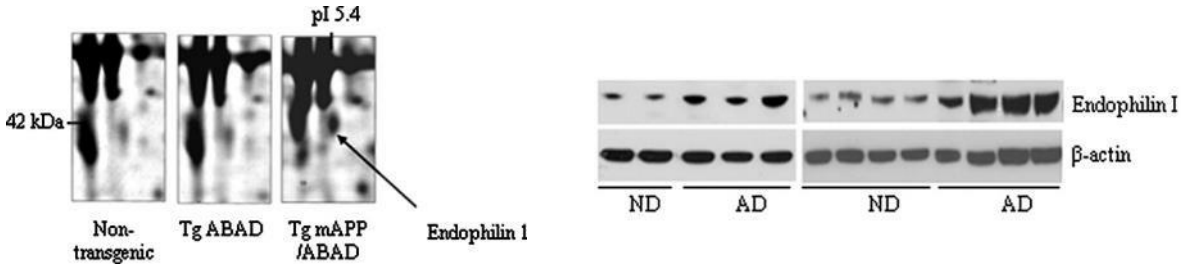

Figure 1.39. Endophilin I upregulation. The expression of endophilin I has been shown to be elevated in the brains of mAPP/17β-HSD10 transgenic mice (left panel) and in the brains of Alzheimer's diseased patients (right panel). Figures reproduced from[343].

The upregulation of peroxiredoxin II and endophilin I in the brains of transgenic mAPP/17β-HSD10 was found to be reversed upon treatment with the ABAD-DP, but not the ABAD-RP, suggesting the enhanced levels of each are a direct response to the toxic effects of the 17β-HSD10/Aβ interaction (Figure 1.40)[342,343]. The fact that such upregulation is also observed in the AD brain suggests the protective effects observed by the disruption of the 17β-HSD10/Aβ interaction in mouse models may translate to a cognitive improvement in patients with AD.

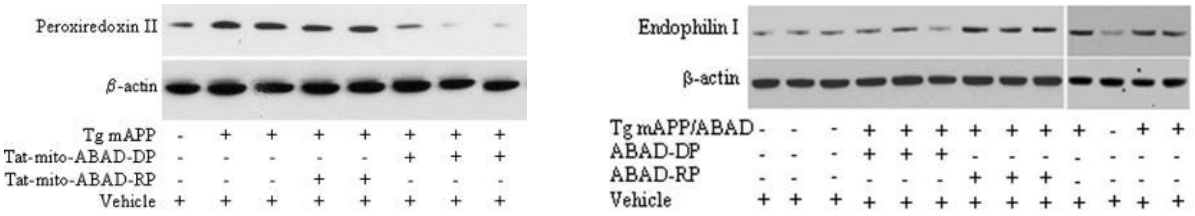

Figure 1.40. 17β-HSD10/Aβ dependency of peroxirdoxin II and enophilin I upregulation. Dual transgenic animals expressing mAPP/17β-HSD10 show upregulation of peroxiredoxin II (left) and endophilin I (right), an effect which is reversed by administration of the ABAD-DP but not the ABAD-RP. Figures reproduced from[342, 343].

In 2006, Xie *et al.* showed that Frentizole, an FDA approved antiviral and immunosuppressant compound, is capable of disrupting the interaction between the 17β-HSD10 enzyme and Aβ[344]. Frentizole, the parent molecule, was found to be relatively poor at doing so with an IC_{50} value of approximately 200 μM. However, further derivatisation of the Frentizole scaffold generated two molecules with markedly improved potency, now with IC_{50} values of approximately 10 μM[344] (Figure 1.42). Frentizole derivatives may therefore hold potential for the generation of novel AD directed therapeutic agents, acting to disrupt the toxic 17β-HSD10/Aβ interaction.

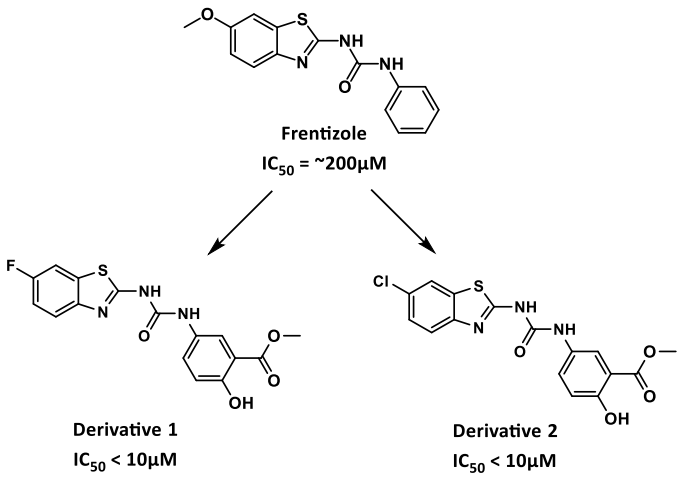

Figure 1.42. Frentizole derived inhibitors of the 17β-HSD10/Aβ interaction. Xie *et al.*[345] identified Frentizole as a compound capable of disrupting the 17β-HSD10/Aβ complex and subsequently developed two derivatives exhibiting enhanced potency. Figure adapted from[344].

Summary:

The amyloid cascade hypothesis was built upon evidence gleaned from the histological analysis of the brains of AD patients, revealing a marked increase in the deposition of insoluble extracellular plaques of Aβ (Section 1.1), and upon genetic based association studies in which mutations in the amyloid-precursor protein, or APP processing enzymes PSEN1 or PSEN2 generate an autosomal dominant form of disease (Section 1.2). In its original guise the amyloid cascade hypothesis posited that insoluble extracellular plaques of Aβ were the main disease driving lesion in the AD brain. However, the observation that plaque load does not correlate with disease severity, and following the failure of several high profile therapies, which were found to dramatically reduce the plaque burden with no marked improvement in cognition or slowing of the disease process (Section 1.32), led to an alteration of the hypothesis, with soluble forms of Aβ now thought to be the main disease driving species (Section 1.41).

Such soluble species of Aβ have been identified within various subcellular compartments where they are hypothesised to interact with cellular proteins, disrupting normal physiological functions and resulting in the synaptic dysfunction and cell death characteristic of AD. Mitochondrial Aβ has been shown to interact with the 17β-HSD10 enzyme with cytotoxic consequences, and interestingly, these cytotoxic effects appear to be dependent on the catalytic activity of the 17β-HSD10 enzyme (Section 1.52). In primary neuronal cultures derived from transgenic mice, the 17β-HSD10/Aβ interaction has been shown to result in overt mitochondrial dysfunction and cell death, effects which was seen to translate into a cognitive deficit in murine models, and were reversed upon disruption of the 17β-HSD10/Aβ interaction. In response to the enhanced levels of stress caused by the 17β-HSD10/Aβ, two proteins were found to be up-regulated; peroxiredoxin II, an antioxidant enzyme and endophilin I, linked to the induction of apoptosis via the JNK pathway. Interestingly, in the brains of AD patients, an enrichment was observed for the 17β-HSD10/Aβ complex, as compared with non-diseased controls, with a concomitant increase in the levels of peroxiredoxin II and endophilin I, possibly suggesting shared mechanistic pathways.

Mutations in the 17β-HSD10 gene have been linked to a neurodegenerative disease termed MHBD deficiency (Section 1.52). Originally, MHBD deficiency was attributed to a defect in the degradation of isoleucine, however the observation that severity of disease did not correlate with the residual level of enzymatic activity suggested otherwise. MHBD deficiency is now thought to result from a defect in a second non-enzymatic function of the 17β-HSD10 protein, which, alongside TRMT10C and PROPR, forms the mtRNase P complex, required for mitochondrial tRNA maturation and protein synthesis. In the context of the mtRNase P complex the enzymatic activity of the 17β-HSD10 enzyme has been shown to be entirely dispensable, with the enzyme instead thought to perform a structural role, stabilising the TRMT10C subunit. Thus, MHBD mutations are thought to perturb the formation of mtRNase P resulting in a generalised mitochondrial dysfunction.

Taken together, these observations suggest that two 17β-HSD10 directed therapeutic approaches may hold merit in treating AD, namely the disruption of the 17β-HSD10/Aβ complex or the direct inhibition of

17β-HSD10 enzymatic activity (Figure 1.40). The latter being viable provided the enzyme remains physically present and capable of performing its function within the mtRNase P complex.

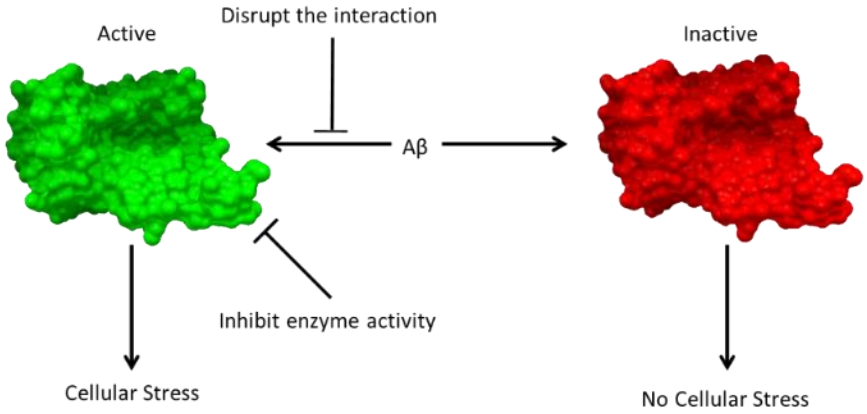

Figure 1.41. 17β-HSD10 directed therapeutic intervention. The formation of the 17β-HSD10/Aβ complex has been shown to result in mitochondrial dysfunction and cell death, with these effects dependent on the catalytic activity of the 17β-HSD10 enzyme. Thus, both the perturbation of the interaction and the direct inhibition of 17β-HSD10 catalytic activity may hold merit in treating AD.

It seems plausible that the ability of the Frentizole scaffold to perturb the interaction between 17β-HSD10 and Aβ may confer the ability to bind directly to the 17β-HSD10 enzyme, and in doing so may inhibit its catalytic activity, potentially allowing both therapeutic avenues to be exploited using a single compound. We sought to investigate this further.

Project Aims:

The primary aim of this project was to identify and characterise novel small molecule inhibitors of the 17β-HSD10 enzyme for the treatment of Alzheimer's disease.

To this end, a series of enzyme and cellular-based assays were developed allowing the identification of small molecules with inhibitory activity against 17β-HSD10. Two initial, enzyme based screening methodologies were employed; a targeted approach using derivatives of the Frentizole scaffold, which we suspected may interact directly with the 17β-HSD10 enzyme, and an explorative approach using a diverse library of small molecules with the aim of identifying a range of novel inhibitor scaffolds. Assays were subsequently developed to assess the drug-like properties of hit compounds; namely potency, specificity and mechanism of action.

Whilst it was unlikely that hit compounds identified herein would in themselves be of use as therapeutic agents, such compounds, once validated, could form the basis of new derivative series with more favourable drug-like properties. The development of robust screening assays would allow the efficient evaluation of compounds of interest and the logical, iterative design of more efficacious compound series.

Chapter 2: Materials and Methods

Section 1: Molecular Cloning

All reagents were purchased from Sigma-Aldrich and all solutions were prepared using MilliQ ultrapure water, unless otherwise stated. DNA sequencing was performed using the services offered by MRC PPU, DNA Sequencing and Services, Dundee.

Reagents:

E. coli BL21(DE3) (NEB: C2527I), *E. coli* DH5-α (NEB: C2988J), calcium chloride (C3306), glycerol (Thermo Fisher: 10021083), agarose (Thermo Fisher: 17850), ethidium bromide (E1510), guanosine (G6752), Antarctic Phosphatase (NEB: M0289), T4 DNA ligase (Promega: M1801), Phusion DNA polymerase (NEB: M0530), GoTaq-polymerase (Promega: M7122), FastDigest Dpn1 (Thermo Fisher: FD1703), SSPI restriction endonuclease (NEB: R0132), T4 DNA polymerase (NEB: M0203S), EDTA (E4884), M-MLV reverse transcriptase (Promega: M1701), oligo-dT primers (Promega: C1101), AMV reverse transcriptase (Promega: M5101).

Equipment:

Agarose gel casting unit (Camlab: H1-set), Qiagen Miniprep Kit (Qiagen: 27104), Qiagen Maxiprep Kit (Qiagen: 12163), Wizard SV Gel and PCR Clean-Up kit (Promega: A9281), RNeasy kit (Qiagen: 74106), QIAShredder column (Qiagen: 79654).

1.01 Competent Cell Generation:

Using aseptic technique, naive *E. coli* strains, BL21 (DE3) and DH5-α, were streaked from a glycerol stock onto agar plates and grown at 37°C overnight. Following incubation, a single colony was picked and transferred to a starter culture of 10 mL Luria Broth and grown overnight at 37°C, with agitation at 225 rpm. 5 mL of overnight culture was added to 500 mL Luria Broth and incubated at 37°C and 225 rpm. Optical density was measured periodically until OD_{600}= 0.4. The culture was split equally into two centrifuge bottles, placed on ice for 20 minutes and centrifuged at 3000g for 15 minutes at 4°C. The cell pellet was resuspended gently (via swirling) in 30 mL ice cold 0.1 M $CaCl_2$ and incubated on ice for 30 minutes. Cells were centrifuged again at 3000g for 15 minutes at 4°C and resuspended gently (via swirling) in 8 mL 0.1 M $CaCl_2$ containing 15% glycerol (v/v). Cells were aliquoted into 1.5 mL microcentrifuge tubes, snap frozen using liquid nitrogen and stored long term at -80°C.

1.02 Heat-Shock Transformation:

Cells were thawed on ice for approximately 30 minutes. An appropriate amount of DNA (typically 50-100 ng of purified plasmid) was added, gently mixed and incubated on ice for 20 minutes. Following incubation, cells were heat-shocked at 42°C for 45 seconds before being transferred back onto ice for 2 minutes. 200 µL of SOC media was added and cells incubated at 37°C and 225 rpm for 1 hour. Cells were spread onto agar plates containing the appropriate antibiotic and grown overnight at 37°C (if using ampicillin, the 1 hour incubation was omitted).

1.03 Glycerol Stock Preparation:

Competent *E. coli* of the appropriate strain (DH5-α for routine cloning) were transformed with the DNA construct of interest via heat-shock, spread onto agar plates containing the appropriate antibiotic and incubated overnight at 37°C. A single colony was picked, added to 10 mL of Luria Broth containing the appropriate antibiotic and grown overnight at 37°C and 225 rpm. 750 µL of saturated culture was mixed with sterile glycerol (20% (v/v) final) in a 1.5 mL microcentrifuge tube. Glycerol stocks were stored long term at -80°C.

1.04 Plasmid DNA Isolation:

Either a single colony or a sample of glycerol stock was picked and grown in an appropriate volume (varied depending upon the desired yield and plasmid copy number) of antibiotic containing Luria Broth. The following morning the culture was harvested via centrifugation at 5000g for 15 minutes at 4°C. DNA extraction was performed using either the Qiagen Miniprep or Maxiprep kit, depending upon the desired yield, as per manufacturer's instructions.

1.05 Restriction Digest:

An appropriate quantity of DNA was employed depending upon the desired application. The appropriate digest buffer was added to a 1 x concentration (typically NEB CutSmart) and a sufficient quantity of restriction endonuclease added (typically a two-fold excess). Total glycerol concentration was maintained below 5% (v/v) to avoid star activity. If high-fidelity restriction endonucleases were employed, digests were performed overnight at 25°C, otherwise a typical reaction time of 1 hour at 37°C was employed. Where possible, dual digests were performed, following appropriate single digest controls, otherwise reactions were performed sequentially.

1.06 Agarose Gel Electrophoresis:

A suitable concentration of agarose was used depending on the size of fragments to be resolved, for routine applications 1% (w/v). Agarose powder was dissolved in 1 x TBE buffer via heating. The gel was cooled, ethidium bromide added (0.5 µg/mL) and the gel cast into a Camlab H1-Set agarose gel electrophoresis unit. Gels were allowed to set for 1 hour at 4°C after which a sufficient volume of 1 x TBE buffer was added to cover both the gel and electrodes. Samples were mixed with 1 x DNA loading dye and dispensed into wells. Samples were separated at 80 V for approximately 1 hour (application depending) and visualised using either a UV-transilluminator or a BioRad ChemiDoc.

1.07 DNA Gel Extraction:

Samples of interest were resolved via agarose gel electrophoresis using 1 x TAE buffer. If using UV illumination, guanosine (1 mM) was added to the agarose gel and 1 x TAE running buffer. The band of interest was excised using a scalpel blade, and DNA extracted using a Promega SV Gel and PCR Clean-Up kit, as per manufacturer's instructions.

1.08 Ligation:

Following gel extraction, cut vector was treated with Antarctic Phosphatase, as per manufacturer's instructions. Vector and insert were mixed at varying molar ratios (typically 50 ng vector, 1:3), higher quantities of insert were employed for difficult ligations. T4 DNA ligase was added and the mixture incubated as per manufacturer's instructions. For difficult ligations, the sample was incubated overnight in a BioRad T100 PCR machine cycling between 10°C and 30°C. Following incubation, a sample of the ligation mixture was transformed into DH5-α *E. coli* via heat-shock, spread onto agar plates harbouring the appropriate antibiotic and incubated overnight at 37°C.

1.09 Diagnostic Digest:

Following ligation, single colonies were picked, cultures grown and DNA extracted via Miniprep. Samples were treated using the appropriate restriction endonucleases, depending upon the cloning strategy employed. Following digestion, products were separated via agarose gel electrophoresis and imaged using a UV-transilluminator, with the presence of a fragment at the expected molecular weight indicating the success of the employed cloning strategy.

1.10 General PCR:

PCR primers were designed as per standard protocol depending on the desired application. PCR reactions for sub-cloning purposes were performed using the high-fidelity Phusion DNA Polymerase, for analytical work, the low fidelity GoTaq-polymerase was employed.

1.11 Site Directed Mutagenesis:

Agilent QuickChange style primers were designed as per manufacturer's specification (25-45 nucleotides in length with 10-15 nucleotides either side of the mismatch, a minimum GC content of 40% and a $T_m \geq$ 78°C) and PCR reactions performed using Phusion polymerase (100 ng template), cycling conditions:

98°C - 5 minutes
98°C- 30 seconds
55-72°C - 30 seconds
72°C - Varied (15-30 seconds/kb)
72°C - 5 minutes
4°C - Hold

PCR product was treated with FastDigest Dpn1 as per manufacturer's instructions and the success of each reaction assessed via agarose gel electrophoresis. Product was transformed into competent DH5-α *E. coli* via heat-shock, cultures grown, DNA was extracted and samples sent for DNA sequencing.

For difficult mutations, a modified primer design described by Liu & Naismith was employed, incorporating comparatively long 3' overhangs on both forward and reverse primers[345].

1.12 Ligation Independent Cloning (LIC):

PCR primers were designed to amplify the sequence of interest out of the current vector and simultaneously add ligation independent cloning tags:

Forward LIC-tag: 5'-TACTTCCAATCCAATGCA-3'
Reverse LIC-tag: 5'-TTATCCACTTCCAATGTTATTA-3'

A standard PCR reaction was performed using Phusion polymerase as per manufacturer's instructions and the product gel purified. The pET-MBP plasmid was a gift from Scott Gradia (Addgene #29656). Vector DNA was treated with SSPI restriction endonuclease, as per manufacturer's instructions, and the linear product gel purified. Gel extracted vector and PCR product were treated with T4 DNA polymerase in the presence of dGTP and dCTP respectively, exploiting the enzyme's intrinsic 3'>5' exonuclease activity to generate complementary overhangs. Vector and insert were mixed at varying molar ratios (50 ng vector, 1:3, 1:5, 1:10) heated to 70°C and allowed to cool to room temperature. EDTA was added to a final concentration of 5 mM and the mixture incubated for 5 minutes at room temperature before being transformed into competent DH5-α *E. coli* via heat-shock. Cultures were grown from single colonies, DNA extracted, and samples sent for DNA sequencing.

1.13 cDNA Cloning:

M-MLV Reverse-Transcriptase:

mRNA was extracted from 5 x 10^6 HEK293 cells using a Qiagen RNeasy kit and a QIAShredder column, as per manufacturer's instructionns. A cDNA library was generated using M-MLV reverse transcriptase and oligo-dT primers as per manufacturer's instructions. The cDNA sequence of interest was subsequently amplified using Phusion polymerase and gene specific primers (designed using NCBI-Primer Blast) harbouring the desired restriction endonuclease sites. The reaction was treated with the corresponding restriction enzymes, products separated using agarose gel electrophoresis and the desired band excised and purified. Empty vector was similarly digested and the fragment of interest purified and dephosphorylated using Antarctic Phosphatase. Fragments were ligated using T4 DNA ligase, transformed into competent DH5-α *E. coli* via heat-shock and spread onto agar plates. Colonies were picked, grown and DNA extracted via Miniprep. A diagnostic digest was performed and analysed via agarose gel electrophoresis, constructs harbouring an insert of the correct size were subsequently sent for sequencing.

AMV Reverse-Transcriptase:

mRNA was extracted from 5 x 10^6 HEK293 cells using a Qiagen RNeasy kit and a QIAShredder column, as per manufacturer's instructions. First strand cDNA synthesis was performed using the reverse gene specific primer and AMV reverse transcriptase over a gradient of temperatures (50-70°C). The cDNA of interest was subsequently amplified using Phusion polymerase and gene specific primers (designed using NCBI-Primer Blast) harbouring the desired restriction endonuclease sites. The reaction was subsequently treated with the appropriate restriction enzymes and products separated using agarose gel

electrophoresis. The desired band was excised and purified via gel extraction. Empty vector was similarly digested and the fragment of interest gel purified and dephosphorylated using Antarctic Phosphatase. Fragments were ligated using T4 DNA ligase, transformed into competent DH5-α *E. coli* via heat-shock and spread onto agar plates harbouring the appropriate antibiotic. Colonies were picked, cultures grown and DNA extracted via Miniprep and sent for sequencing.

Section 2: Protein Purification

All reagents were purchased from Sigma-Aldrich and all solutions were prepared using MilliQ ultrapure water, unless otherwise stated.

Reagents:

HEPES buffer (H3375), sodium chloride (S9888), Tris-HCl (T3253), glycine (Thermo Fisher: 10061073), sodium dodecyl sulfate (L4509), Coomassie Blue R250 (B7920), methanol (Thermo Fisher: 10284580), acetic acid (Thermo Fisher: 10394970), kanamycin (K1377), IPTG (Formedium: IPTG025) DTT (Formedium: DTT010), glycerol (Thermo Fisher: 10021083), ampicillin (A0166), lysozyme (L6876), *E. coli* BL21(DE3) (C2527I), imidazole (I2399), EDTA (E4884), Roche cOmplete EDTA free Protease Inhibitor Tablets (11836170001)

Equipment:

Mini-PROTEAN Tetra Handcast system (BioRad: 1658000FC), Mini PROTEAN TetraCell electrophoresis unit (BioRad: 552BR), 5mL HisTrap HP column (GE Healthcare: 17-5248-01), SnakeSkin Dialysis Membrane 10kDa MWCO (Thermo Fisher: 68100), VivaSpin 20 10kDa MWCO (GE HealthCare: 28932360), HiLoad 16/600 Superdex 75 pg column (GE- Healthcare: 28989333), AKTA-Pure purification rig

2.1 SDS-PAGE:

Polyacrylamide gels were cast using the Mini-PROTEAN Tetra kit at the required percentage. A stacking gel concentration of 4% polyacrylamide (v/v) was routinely employed, resolving gel percentage varied depending upon the resolution required (12% (v/v) for routine work, up to 15% (v/v) for low molecular weight proteins). Gels were loaded into a BioRad Mini-Tetra Cell electrophoresis unit and 1 x Tris-Glycine running buffer added (25 mM Tris, 192 mM glycine, 0.1% SDS, pH 8.5).

An appropriate volume of sample was mixed with 1 x protein loading dye and heated at 95°C for 5-minutes. Samples were briefly centrifuged and loaded onto a gel of the appropriate percentage. Proteins were resolved at 80 V.

2.2 Coomassie Blue Staining:

Polyacrylamide gels were treated with Coomassie Blue R-250 staining solution (0.1% (w/v) Coomassie-R250, 50% (v/v) MeOH, 10% (v/v) glacial acetic acid, 40% (v/v) ddH_2O) for 1 hour. Following staining, gels were destained by boiling in water. The water was replaced periodically until background sufficiently reduced and gels imaged using a BioRad ChemiDoc.

2.3 Small-Scale Expression Optimisation:

An aliquot of competent BL21(DE3) *E. coli* cells were transformed with the appropriate construct (peHISTEV-HSD10, peHISTEV-HSD14 or pET-MBP-HSD8) via heat shock, spread onto Kanamycin containing agar plates (50 µg/mL) and incubated overnight at 37°C. Following incubation, a single colony was picked and transferred to a starter culture of Luria Broth containing the appropriate antibiotic and incubated overnight at 37°C and 225 rpm. The saturated culture was diluted 1:50 into antibiotic containing Luria Broth and grown at 37°C and 225 rpm until OD_{600}= 0.6-0.8. The culture was split into three flasks, placed

at 37°C, 25°C and 15°C, respectively and protein synthesis induced using 1 mM IPTG. 1 mL samples were removed prior to induction and at 1, 2, 4, 6, 12 and 24-hour time points. Cells were pelleted by centrifugation and resuspended in 500 µL lysis buffer (50 mM HEPES, 0.5 M NaCl, 10% glycerol, pH 8.2) and stored at -20°C overnight. The following morning cells were thawed, 25 µL of lysozyme added (0.5 mg/mL final) and samples incubated at room-temperature for 1.5 hours. Following incubation, cells were lysed on ice using sonication (QSonica 500, 2mm probe, 20% amplitude, 10 seconds on, 10 seconds off, 180 seconds total). Cellular debris was pelleted by centrifugation at 16,000g for 5 minutes, the supernatant was transferred to a fresh microcentrifuge tube (soluble fraction). The pelleted debris (insoluble fraction) was resuspended in 525 µL of 1 x SDS-PAGE loading dye and boiled for 5-minutes. 7.5 µL of the soluble fraction was mixed with 7.5 µL 2 x SDS-PAGE loading dye and boiled for 5-minutes. 7.5 µL of the insoluble fraction and the 15 µL of soluble fraction were separated via SDS-PAGE (12% gel). Gels were stained with Coomassie Blue, de-stained and imaged using a BioRad ChemiDoc, allowing the levels of soluble and insoluble protein to be assessed under various induction conditions.

2.4 Tobacco Etch Virus Protease (S219V) Purification:

The pRK793 construct, encoding the catalytic domain of the TEV protease (S219V mutant) fused with a maltose binding domain, was a gift from David Waugh (AddGene Plasmid #8827). An aliquot of competent BL21(DE3) *E. coli* was transformed with the pRK793 construct via heat-shock, spread onto ampicillin containing agar plates (100 µg/mL) and incubated overnight at 37°C. A single colony was picked, transferred to a 100 mL starter culture of Luria Broth (100 µg/mL ampicillin) and grown to saturation overnight at 37°C and 225 rpm. The culture was diluted 1:50 into 3 x 1L flasks of Luria Broth (100 µg/mL ampicillin) and grown at 37°C and 225 rpm until OD_{600}= 0.6-0.8. The temperature was lowered to 25°C and protein expression induced overnight using 1 mM IPTG. Cells were harvested by centrifugation at 5000g for 20 minutes at 4°C and the pellet resuspended in 100 mL of lysis buffer (50 mM HEPES, 200 mM NaCl, 10% glycerol (v/v), pH 8.0, 1 mg/mL lysozyme) and incubated for 1.5 hours at RT with gentle agitation. Cells were lysed using sonication (QSonica 500, 6mm probe, 50% amplitude, 10 seconds on, 20 seconds off, 5 minutes total) on an ice/water/salt slurry and the lysate cleared via centrifugation at 35,000g for 1 hour at 4°C followed by filtration (0.45 µm). Cleared lysate was passed over a 5 mL HisTrap HP column twice at 4°C. The column was loaded onto an AKTA-Pure purification rig and washed with a gradient of imidazole (0-100 mM) until a stable baseline UV absorbance was achieved. Protein was eluted using a linear gradient of imidazole (100-500 mM) and the presence of protein in elution fractions confirmed by SDS-PAGE and Coomassie Blue staining. Protein containing fraction were pooled and loaded into a dialysis membrane (10 kDa MWCO) and incubated in 2 L dialysis buffer (50 mM HEPES, 200 mM NaCl, 2.5 mM DTT, 2 mM EDTA, 10% glycerol (v/v), pH 8.0) at 4°C with stirring for 3 hours. The buffer was exchanged for 2 L of fresh dialysis buffer and incubated overnight. Protein concentration was measured using a NanoDrop 2000 spectrophotometer and adjusted to 1.5 mg/mL. 1 mL aliquots were snap frozen in liquid nitrogen and stored long-term at -80°C

TEV Protease: Abs. 280nm (1% w/v) = 11.26

2.5 17β-HSD8, 17β-HSD10 and 17β-HSD14 Purification:

Competent BL21(DE3) *E. coli* were transformed with the appropriate construct (peHISTEV-HSD10, peHISTEV-HSD14 or pET-MBP-HSD8) via heat-shock. Cells were spread onto agar plates (50 µg/mL kanamycin) and grown overnight at 37°C. A single colony was picked and transferred to a 100 mL Luria Broth starter culture (50 µg/mL kanamycin) and grown overnight at 37°C and 225 rpm. The culture was diluted 1:50 into 3 x 1L flasks of Luria Broth (50 µg/mL kanamycin) and grown at 37°C and 225 rpm, until OD_{600}= 0.6-0.8. The incubation temperature was lowered to 25°C and protein expression induced overnight using 1 mM IPTG. The following morning, cells were harvested by centrifugation at 5000g for 20 minutes at 4°C and resuspended in the appropriate lysis buffer:

17β-HSD8 and 17β-HSD10:
50 mM HEPES, 10% glycerol (v/v), 500 mM NaCl, 10 mM imidazole, 1 x Protease Inhibitor, pH 8.2, 1 mg/mL lysozyme

17β-HSD14:
50 mM HEPES, 10% glycerol (v/v), 100 mM NaCl, 10 mM imidazole, 1 x Protease Inhibitor, pH 8.2, 1 mg/mL lysozyme

Cells were incubated at room temperature for 1.5 hours with gentle agitation before being lysed via sonication (QSonica 500, 6mm probe, 50% amplitude, 10 seconds on, 20 seconds off, 5 minutes total) on an ice/water/salt slurry. Lysate was cleared by centrifugation at 35,000g for 1 hour at 4°C followed by filtration (0.45 µm). Cleared lysate was passed over a 5 mL His-Trap column twice at 4°C.

*Note: The MBP-HSD8 fusion protein was found to have low affinity for the HisTrap HP column, thus the lysate was passed over the column three times to give adequate binding.

The column was loaded onto an AKTA-Pure purification rig and washed with a gradient of imidazole (0-100 mM) until a stable UV absorbance was reached. Protein was eluted using a linear gradient of imidazole (100-500 mM) and the presence of protein in elution fractions confirmed using SDS-PAGE and Coomassie Blue staining. Protein containing fractions were pooled, loaded into a dialysis membrane (10 kDa MWCO) and incubated in 2 L dialysis buffer (50 mM HEPES, 500/150 mM NaCl, 10% glycerol, 20 mM imidazole, 0.5 mM DTT, pH 8.2) at 4°C with stirring for 3 hours. The buffer was exchanged for 2 L of fresh dialysis buffer, TEV protease (S219V) was added at a ratio of 1:25 (w/w) and incubated overnight in a fresh 5 L volume of dialysis buffer.

*Note: The MBP-HSD8 fusion protein is cleaved inefficiently by TEV protease, therefore a ratio of 1:10 (w/w) was used.

Following incubation, TEV cleavage was confirmed by SDS-PAGE and Coomassie Blue staining. Uncleaved protein, free 6 x His-tags, 6 x His-tagged TEV protease and high affinity contaminants were removed by passage through a 5 mL His-Trap column at 4°C. Column flow-through was collected and the presence of

the protein of interest confirmed via SDS-PAGE and Coomassie Blue staining. Fractions were pooled and concentrated using a Vivaspin 20 column (10 kDa MWCO).

*Note: The 17β-HSD8 protein has high intrinsic affinity for the HisTrap HP column and so must be eluted using 50 mM imidazole.

Sample was injected into a pre-equilibriated HiLoad 16/600 Superdex 75 pg column and elution fractions collected periodically. The presence of the protein of interest in peak fractions was confirmed via SDS-PAGE and Coomassie Blue staining. Protein containing fractions were pooled and concentrated (17β-HSD10 and 17β-HSD14: 10 mg/mL, 17β-HSD8: 2 mg/mL) using a VivaSpin 20 spin column (10 kDa MWCO) and NanoDrop 2000 spectrophotometer. Samples were snap frozen in liquid nitrogen and stored long term at -80°C. Protein identity was confirmed using mass spectrometry.

17β-HSD10: Abs. 280nm (1%) = 1.66
17β-HSD14: Abs. 280nm (1%) = 7.04
17β-HSD8: Abs. 280nm (1%) = 3.14

Section 3: Recombinant Enzyme Assays

All reagents were purchased from Sigma-Aldrich and all solutions were prepared using MilliQ ultrapure water, unless otherwise stated.

Reagents:

HEPES buffer (H3375), NADH (N8129), acetoacetyl-CoA (A1625), dimethyl sulfoxide (472301), gelatin (G2500), 17β-estradiol (E8875), NAD^+ (N0632), Tris-HCl (T3253), sodium chloride (S9888) Frentizole (R242640).

Equipment:

SpectraMax M2e spectrophotometer, clear 96 well plates (Thermo Scientific: 167008), black walled 96 well plates (Insight Biotechnology: sc-204468).

3.1 17β-HSD10

Assay Buffer: 10 mM HEPES, 0.5% gelatin (w/v), pH 7.4.

3.11 Michaelis-Menten Kinetics:

Acetoacetyl-CoA:

Solutions containing 500 µM NADH were prepared in assay buffer. Increasing concentrations of acetoacetyl-CoA were added (0-200 µM) and samples dispensed (150 µL/well) into a clear 96 well plate, in triplicate. The plate was loaded into a SpectraMax M2e spectrophotometer, pre-heated to 37°C, and allowed to equilibrate (5 minutes). Following incubation, 17β-HSD10 (0.5 µg/mL, 18.52 nM) was added, the plate shaken and absorbance monitored (340 nm, 600 seconds, 30 second intervals). The rate of reaction was determined during the initial linear period of the progress curve (R^2>0.9). Kinetic parameters were calculated using non-linear regression with GraphPad Prism and the Michaelis-Menten equation.

NADH:

Solutions containing 120 µM acetoacetyl-CoA were prepared in assay buffer. Increasing concentrations of NADH were added (0-600 µM) and samples dispensed (150 µL/well) into a clear 96 well plate, in triplicate. The plate was loaded into a SpectraMax M2e spectrophotometer, pre-heated to 37°C, and allowed to equilibrate (5 minutes). Following incubation, 17β-HSD10 (0.5 µg/mL, 18.52 nM) was added, the plate shaken and absorbance monitored (340 nm, 600 seconds, 30 second intervals). The rate of reaction was determined during the initial linear period of the progress curve (R^2>0.9). Kinetic parameters were calculated using non-linear regression with GraphPad Prism and the Michaelis-Menten equation.

3.12 DMSO Titration:

Solutions containing 120 µM acetoacetyl-CoA and 250 µM NADH were prepared in assay buffer. Increasing concentrations of DMSO were added (0-5% (v/v)) and samples dispensed (150 µL/well) into a clear 96 well plate, in triplicate. The plate was loaded into a SpectraMax M2e spectrophotometer, pre-heated to 37°C, and allowed to equilibrate (5 minutes). Following incubation, 17β-HSD10 (0.5 µg/mL, 18.52 nM) was

added, the plate shaken and absorbance monitored (340 nm, 600 seconds, 30 second intervals). The rate of reaction was taken during the initial linear period of the progress curve (R^2>0.9).

3.13 Small Molecule Screening:

Solutions containing 120 µM acetoacetyl-CoA and 250 µM NADH were prepared in assay buffer. A fixed concentration of each compound of interest, either 100 µM or 25 µM was added. DMSO (1% (v/v)) was used as a vehicle control and samples dispensed (150 µL/well) into a clear 96 well plate, in triplicate. The plate was loaded into a SpectraMax M2e spectrophotometer, pre-heated to 37°C, and allowed to equilibrate (5 minutes). Following incubation, 17β-HSD10 (0.5 µg/mL, 18.52 nM) was added, the plate shaken and absorbance monitored (340 nm, 600 seconds, 30 second intervals). The rate of reaction was determined during the initial linear period of the progress curve (R^2>0.9).

3.14 Dose Response Experiments:

Solutions containing 120 µM acetoacetyl-CoA and 250 µM NADH were prepared in assay buffer. Compounds of interest were added at a range of concentrations (varied depending on potency). DMSO (1% (v/v)) was used as a vehicle control and samples dispensed (150 µL/well) into a clear 96 well plate, in triplicate. The plate was loaded into a SpectraMax M2e spectrophotometer, pre-heated to 37°C, and allowed to equilibrate (5 minutes). Following incubation, 17β-HSD10 (0.5 µg/mL, 18.52 nM) was added, the plate shaken and absorbance monitored (340 nm, 600 seconds, 30 second intervals). The rate of reaction was determined during the initial linear period of the progress curve (R^2>0.9). IC_{50} values were calculated using GraphPad Prism (variable slope - four parameter model).

3.15 Mechanism of Inhibition Experiments:

Acetoacetyl-CoA**:**

Solutions containing 500 µM NADH were prepared in assay buffer. Increasing concentrations of acetoacetyl-CoA (0-120 µM) and a fixed concentration of inhibitor (1.25 µM or 5 µM) were added. DMSO (1% (v/v)) was used as a vehicle control. Samples were dispensed (150 µL/well) into a clear 96 well plate, in triplicate. The plate was loaded into a SpectraMax M2e spectrophotometer, pre-heated to 37°C, and allowed to equilibrate (5 minutes). Following incubation, 17β-HSD10 (0.5 µg/mL, 18.52 nM) was added, the plate shaken and absorbance monitored (340 nm, 600 seconds, 30 second intervals). The rate of reaction was determined during the initial linear period of the progress curve (R^2>0.9). Hanes-Woolf plots were generated for visual representation of the data and absolute kinetic parameters calculated using non-linear regression with GraphPad Prism and the Michaelis-Menten equation.

NADH:

Solutions containing 120 µM acetoaceyl-CoA were prepared in assay buffer. Increasing concentrations of NADH (0-600 µM) and a fixed concentration of inhibitor (1.25 µM or 5 µM) were added. DMSO (1% (v/v)) was used as a vehicle control. Samples were dispensed (150 µL/well) into a clear 96 well plate, in triplicate. The plate was loaded into a SpectraMax M2e spectrophotometer, pre-heated to 37°C, and allowed to equilibrate (5 minutes). Following incubation, 17β-HSD10 (0.5 µg/mL, 18.52 nM) was added, the plate

shaken and absorbance monitored (340 nm, 600 seconds, 30 second intervals). The rate of reaction was determined during the initial linear period of the progress curve (R^2>0.9). Hanes-Woolf plots were generated for visual representation of the data and absolute kinetic parameters calculated using non-linear regression with GraphPad Prism and the Michaelis-Menten equation.

3.16 Small Molecule Aggregation Test:

Solutions containing 120 µM acetoacetyl-CoA and 250 µM NADH were prepared in assay buffer. Compounds of interest were added at a single fixed concentration (2 µM). DMSO (1% (v/v)) was used as a vehicle control. Varying concentrations of Triton X-100 were added (0%, 0.01%, 0.1% (v/v)). Samples were dispensed (150 µL/well) into a clear 96 well plate, in triplicate. The plate was loaded into a SpectraMax M2e spectrophotometer, pre-heated to 37°C, and allowed to equilibrate (5 minutes). Following incubation, 17β-HSD10 (0.5 µg/mL, 18.52 nM) was added, the plate shaken and absorbance monitored (340 nm, 600 seconds, 30 second intervals). The rate of reaction was determined during the initial linear period of the progress curve (R^2>0.9).

3.17 Reversible/Irreversible Inhibition Test:

Solutions containing 120 µM acetoacetyl-CoA and 250 µM NADH were prepared in assay buffer. Compounds of interest were added (K690, K691= 2 µM, AG18051= 200 nM). DMSO (1% (v/v)) was used as a vehicle control. 17β-HSD10 was added and the solution incubated at room temperature for 10 minutes. Following incubation, 17β-HSD10 was diluted to a final concentration of 0.5 µg/mL in 150 µL well solution (assay buffer, 120 µM acetoacetyl-CoA, 250 µM NADH) containing either an equivalent concentration of inhibitor or DMSO. The plate was loaded into a SpectraMax M2e spectrophotometer, pre-heated to 37°C, shaken and absorbance monitored (340 nm, 600 seconds, 30 second intervals). The rate of reaction was determined during the initial linear period of the progress curve (R^2>0.9).

3.18 NCI Diversity IV Screening Assay:

Solutions containing 120 µM acetoacetyl-CoA and 250 µM NADH was prepared in assay buffer. 99 µL of assay buffer were added to wells of a clear 96 well plate containing 1 µL of compound of interest (10 mM) yielding a final concentration of 100 µM. DMSO (1% (v/v)) was used as a vehicle control. The plate was loaded into a SpectraMax M2e spectrophotometer, pre-heated to 37°C, and allowed to equilibrate (5 minutes). Following incubation, 17β-HSD10 (0.25 µg/mL, 9.26 nM) was added, the plate shaken and absorbance monitored (340 nm, 600 seconds, 30 second intervals). The rate of reaction was determined during the initial linear period of the progress curve (R^2>0.9).

3.2 17β-HSD8 and 17β-HSD14

Assay Buffer**:** 50 mM Tris-HCl, 100 mM NaCl, pH 8.2

3.21 17β-HSD8 Activity Test:

Solution containing 50 µM β-estradiol and 500 µM NAD^+ were prepared in assay buffer. 100 µL was added to wells of a black-walled 96 well plate. 17β-HSD8 was added at varying concentrations to buffer containing wells (0, 1, 2.5, 5, 10 µg/mL), in triplicate. The plate was loaded into a SpectraMax M2e

spectrophotometer, pre-heated to 37°C, and fluorescence measured (excitation 340 nm, emission 460 nm, 900 seconds, 30 second intervals). The rate of reaction was determined during the initial linear period of the progress curve (R^2>0.9).

3.22 17β-HSD14 Activity Test:

Solutions containing 50 µM β-estradiol and 500 µM NAD^+ were prepared in assay buffer. 100 µL was added to wells of a black-walled 96 well plate. 17β-HSD14 was added at varying concentrations to buffer containing wells (0, 50, 100, 150, 200, 250 µg/mL), in triplicate. The plate was loaded into a SpectraMax M2e spectrophotometer, pre-heated to 37°C, and fluorescence measured (excitation 340 nm, emission 460 nm, 1 hour, 5 minute intervals). The rate of reaction was determined during the initial linear period of the progress curve (R^2>0.9).

3.23 17β-HSD8 Michaelis-Menten Kinetics:

NAD^+:

Solutions containing 100 µM 17β-estradiol were prepared in assay buffer. Increasing concentrations of NAD^+ (0-1000 µM) were added and samples dispensed (100 µL/well) into a black-walled 96 well plate, in triplicate. The plate was loaded into a SpectraMax M2e spectrophotometer, pre-heated to 37°C, and allowed to equilibrate (5 minutes). Following incubation, 17β-HSD8 was added to each well (5 µg/mL, 185.3 nM), the plate shaken and fluorescence measured (excitation 340 nm, emission 460 nm, 900 seconds, 30 second intervals). The rate of reaction was determined during the initial linear period of the progress curve (R^2>0.9). Kinetic parameters were calculated using non-linear regression with GraphPad Prism and the Michaelis-Menten equation.

17β-estradiol**:**

Solutions containing 1 mM NAD^+ were prepared in assay buffer. Increasing concentrations of 17β-estradiol (0-100 µM) were added and samples dispensed (100 µL/well) into a black-walled 96 well plate, in triplicate. The plate was loaded into a SpectraMax M2e spectrophotometer, pre-heated to 37°C, and allowed to equilibrate (5 minutes). Following incubation, 17β-HSD8 was added to each well (5 µg/mL, 185.3 nM), the plate shaken and fluorescence measured (excitation 340 nm, emission 460 nm, 900 seconds, 30 second intervals). The rate of reaction was determined during the initial linear period of the progress curve (R^2>0.9). Kinetic parameters were calculated using non-linear regression with GraphPad Prism and the Michaelis-Menten equation.

3.24 17β-HSD14 Michaelis-Menten Kinetics:

NAD^+:

Solutions containing 100 µM 17β-estradiol were prepared in assay buffer. Increasing concentrations of NAD^+ (0-500 µM) and samples dispensed (100 µL/well) into a black-walled 96 well plate, in triplicate. The plate was loaded into a SpectraMax M2e spectrophotometer, pre-heated to 37°C, and allowed to equilibrate (5 minutes). Following incubation, 17β-HSD14 was added to each well (150 µg/mL, 5.3 µM), the plate shaken and fluorescence measured (excitation 340 nm, emission 460 nm, 1 hour, 5 minute

intervals). The rate of reaction was determined during the initial linear period of the progress curve (R^2>0.9). Kinetic parameters were calculated using non-linear regression with GraphPad Prism and the Michaelis-Menten equation.

17β-estradiol:

Solutions containing 500 µM NAD^+ were prepared in assay buffer. Increasing concentrations of 17β-estradiol (0-100 µM) were added and samples dispensed (100 µL/well) into a black-walled 96 well plate, in triplicate. The plate was loaded into a SpectraMax M2e spectrophotometer, pre-heated to 37°C, and allowed to equilibrate (5 minutes). Following incubation, 17β-HSD14 was added to each well (150 µg/mL, 5.3 µM), the plate shaken and fluorescence measured (excitation 340 nm, emission 460 nm, 1 hour, 5 minute intervals). The rate of reaction was determined during the initial linear period of the progress curve (R^2>0.9). Kinetic parameters were calculated using non-linear regression with GraphPad Prism and the Michaelis-Menten equation.

3.25 17β-HSD8 Small Molecule Screening:

Solutions containing 50 µM 17β-estradiol and 500 µM NAD^+ were prepared in assay buffer. A saturating dose of inhibitor, as determined against 17β-HSD10 (K690, K691, K1093 = 12.5 µM, AG18051 = 6.25 µM, 88401 = 50 µM) or an equivalent concentration of DMSO (1% (v/v)) was added. Samples were dispensed (100 µL/well) into a black-walled 96 well plate, in triplicate. The plate was loaded into a SpectraMax M2e spectrophotometer, pre-heated to 37°C, and allowed to equilibrate (5 minutes). Following incubation, 17β-HSD8 was added to each well (5 µg/mL, 185.3 nM), the plate shaken and fluorescence measured (excitation 340 nm, emission 460 nm, 900 seconds, 30 second intervals). The rate of reaction was determined during the initial linear period of the progress curve (R^2>0.9).

3.26 17β-HSD14 Small Molecule Screening:

Solutions containing 75 µM 17β-estradiol and 150 µM NAD^+ were prepared in assay buffer. A saturating dose of inhibitor, as determined against 17β-HSD10 (K690, K691, K1093 = 12.5 µM, AG18051 = 6.25 µM, 88401 = 50 µM) or an equivalent concentration of DMSO (1% (v/v)) was added. Samples were dispensed (100 µL/well) into a black-walled 96 well plate, in triplicate. The plate was loaded into a SpectraMax M2e spectrophotometer, pre-heated to 37°C, and allowed to equilibrate (5 minutes). Following incubation, 17β-HSD14 was added to each well (150 µg/mL, 5.3 µM), the plate shaken and fluorescence measured (excitation 340 nm, emission 460 nm, 1 hour, 5 minute intervals). The rate of reaction was determined during the initial linear period of the progress curve (R^2>0.9).

Section 4: Differential Scanning Fluorimetry

All reagents were purchased from Sigma-Aldrich and all solutions were prepared using MilliQ ultrapure water, unless otherwise stated.

Reagents:

HEPES buffer (H3375), sodium chloride (S9888), SYPRO-Orange (S5692), NADH (N8129), NAD^+ (N0632), acetoacetyl-CoA (A1625), $A\beta_{1-42}$ (Abcam: ab120301), Hexafluoroisopropanol (HFIP) (105228), dimethyl sulfoxide (472301).

Equipment:

Viia7 RT-PCR machine (Thermo Fisher: 4453534) MicroAmp 96 well plates (Thermo Fisher: 4346907), MicroAmp Optical Adhesive Film (Thermo Fisher: 4311971), Hamilton Syringe (20703), enhanced chemiluminescence solution (Pierce: 32106).

Assay Buffer: 50 mM Hepes, 0.5 M NaCl, pH 8.2

4.1 Differential Scanning Fluorimetry Assay Optimisation:

Solutions containing varying concentrations of 17β-HSD10 protein (0, 5, 10, 25, 50 μM) and SYPRO-orange (x 0, x 5, x 10, x 20 concentration, absolute values not published) were prepared in assay buffer. Samples were dispensed (25 μL/well) into a 96 well MicroAmp Fast Optical plate, in triplicate. The plate was sealed with optical grade sealing film, centrifuged briefly at 500g and loaded into a ViiA7 RT-PCR machine (ramp speed 0.015°C/second, 25-95°C). Data was exported into GraphPad Prism and T_m values calculated using the Boltzmann sigmoidal curve fit equation.

4.2 NADH Titration:

Solutions containing increasing concentrations of NADH (0, 0.01, 0.02, 0.039, 0.078, 0.156, 0.313, 0.625, 1.25, 2.5, 5 mM) were prepared in assay buffer. 17β-HSD10 (10 μM) and SYPRO-orange (x 20) were added and samples dispensed (25 μL/well) into a 96 well MicroAmp Fast Optical plate, in triplicate. The plate was sealed with optical grade sealing film, centrifuged briefly at 500g and loaded into a ViiA7 RT-PCR machine (ramp speed 0.015°C/second, 25-95°C). Data was exported into GraphPad Prism and T_m values calculated using the Boltzmann sigmoidal curve fit equation.

4.3 NAD^+ Titration:

Solutions containing increasing concentrations of NAD^+ (0, 0.01, 0.02, 0.039, 0.078, 0.156, 0.313, 0.625, 1.25, 2.5, 5, 10 mM) were prepared in assay buffer. 17β-HSD10 (10 μM) and SYPRO-orange (x 20) were added and samples dispensed (25 μL/well) into a 96 well MicroAmp Fast Optical plate, in triplicate. The plate was sealed with optical grade sealing film, centrifuged briefly at 500g and loaded into a ViiA7 RT-PCR machine (ramp speed 0.015°C/second, 25-95°C). Data was exported into GraphPad Prism and T_m values calculated using the Boltzmann sigmoidal curve fit equation.

4.4 Acetoacetyl-CoA Titrations:

Solutions containing increasing concentrations of acetoacetyl-CoA (0, 0.008, 0.016, 0.031, 0.063, 0.125, 0.25, 0.5, 1, 2 mM) were prepared in assay buffer. 17β-HSD10 (10 µM) and SYPRO-orange (x 20) were added and samples dispensed (25 µL/well) into a 96 well MicroAmp Fast Optical plate, in triplicate. The plate was sealed with optical grade sealing film, centrifuged briefly at 500g and loaded into a ViiA7 RT-PCR machine (ramp speed 0.015°C/second, 25-95°C). Data was exported into GraphPad Prism and T_m values calculated using the Boltzmann sigmoidal curve fit equation.

The experiment was subsequently repeated in the presence of 5 mM NAD^+.

4.5 Small Molecule Screening:

Solutions were prepared containing a serial dilution of compounds of interest (K690, K691, K1093= 100-0.098 µM). Samples containing an equivalent concentration of vehicle, DMSO (1% (v/v)) were prepared and analysed concurrently. 17β-HSD10 (10 µM) and SYPRO-orange (x 20) were added and samples dispensed (25 µL/well) into a 96 well MicroAmp Fast Optical plate, in triplicate. The plate was sealed with optical grade sealing film, centrifuged briefly at 500g and loaded into a ViiA7 RT-PCR machine (ramp speed 0.015 °C/sec, 25-95 °C). Data was exported into GraphPad Prism and T_m values calculated using the Boltzmann sigmoidal curve fit equation.

The experiment was subsequently repeated in the presence of 5 mM NAD^+ and 2 mM acetoacetyl-CoA.

4.6 Amyloid-beta Peptide:

1 mg of recombinant $A\beta_{1-42}$ was suspended in 221.7 µL of HFIP using a Hamilton syringe and incubated at room-temperature for 1 hour. The monomerised $A\beta_{1-42}$ was dispensed into 10 µL (0.045 µg) aliquots and microcentrifuge tubes left open inside a fume hood for 48-hours to allow HFIP evaporation. Following incubation, tubes were sealed with parafilm and stored dessicated at -20°C.

Oligomeric amyloid beta-peptide was prepared by dissolving one aliquot (0.045 µg) of monomerised $A\beta_{1-42}$ in 2 µL of DMSO, generating a 5 mM stock. 98 µL of assay buffer was subsequently added generating a 100 µM stock, vortexed for 15-seconds and incubated overnight at 4°C.

Solutions were prepared containing 17β-HSD10 (10 µM) and SYPRO-orange (x 20) in assay buffer. An increasing concentration of oligomeric $A\beta_{1-42}$ (0, 1.562, 3.125, 6.25, 12.5, 25, 50 µM) was added and samples incubated at 4°C for 1 hour. Samples were dispensed (25 µL/well) into a 96 well MicroAmp Fast Optical plate, in triplicate. The plate was sealed with optical grade sealing film, centrifuged briefly at 500g and loaded into a ViiA7 RT-PCR machine (ramp speed 0.015°C/sec, 25-95°C). Data was exported into GraphPad Prism and T_m values calculated using the Boltzmann sigmoidal curve fit equation.

4.7 17β-HSD10/Aβ Interaction Western Blot

Oligomeric $A\beta_{1-42}$ was prepared as described previously (Materials and Methods: Section 4.6). Solutions containing 10 µM 17β-HSD10 and 50 µM oligomeric $A\beta_{1-42}$ were prepared in assay buffer (50 mM Hepes,

0.5 M NaCl, pH 8.2). Compounds of interest were added at varying concentrations (6.25 µM–0.156 µM) and samples incubated at 4°C for 1 hour. DMSO (2% (v/v)) was used as a vehicle control. Following incubation, proteins were separated using SDS-PAGE electrophoresis (15% resolving gel) and transferred to a methanol activated PVDF membrane (25 V, 1-hour). Membranes were blocked for 1-hour at room-temperature (5% BSA), and probed using an anti-amyloid antibody (D54D2) overnight at 4°C. Membranes were washed (3 x 10 minutes TBS-T) incubated with the appropriate secondary antibody, washed (3 x 10 minutes TBS-T) and imaged using an LAS-3000 unit and an enhanced chemiluminescent solution.

Section 5: Cell Culture

All reagents were purchased from Sigma-Aldrich and all solutions were prepared using MilliQ ultrapure water, unless otherwise stated

Reagents:

DMEM-Glutamax (Thermo Fisher: 31966), foetal bovine serum (Gibco: 10270098), Penicillin/Streptomycin (Thermo Fisher: 15140122), TrypLe-Express (Thermo Fisher: 12604013), dimethyl sulfoxide (D2650), Lactate Dehydrogenase Kit (MAK066), polyethylenamine (408727), Opti-MEM (Thermo Fisher: 31985062), magnesium chloride (M8266), potassium chloride (P9541), DTT (Formedium: DTT010), Triton X-100 (T8787), Roche cOmplete EDTA free protease inhibitor tablets **(**11836170001), sodium dodecyl sulfate (L3771), sodium deoxycholate (D6750), methanol (Thermo Fisher: 10284580), Tris-HCl (T3253), glycine (Thermo Fisher: 10061073), bovine serum albumin (A9647), enhanced chemiluminescence solution (Pierce: 32106), $A\beta_{1-42}$ (Abcam: ab120301)

Equipment:

Hemacytometer (Z359629), Mr. Frosty freezing unit (Thermo Fisher: 5100-0001), T75 cell culture flasks (Thermo Fisher: 156499), T25 cell culture flasks (Thermo Fisher: 156340), SH-SY5Y nucleofection kit (Lonza: VACA-1003), 1 mL dounce homogeniser (Thermo Fisher: 357538), BCA Kit (Pierce: 23223), PVDF membrane (MilliPore: IPVH00010), XCell SureLock electrophoresis unit (Thermo Fisher: EI0001)

5.01 Culture Media:

HEK293 cells were maintained in DMEM-Glutamax supplemented with 10% foetal bovine serum, 50 units/mL penicillin and 50 µg/mL streptomycin.

SH-SY5Y cells were maintained in DMEM-F12 supplemented with 10% foetal bovine serum, 50 units/mL penicillin and 50 µg/mL streptomycin.

5.02 Foetal Bovine Serum (FBS) Heat Inactivation:

FBS was heated to 56°C for 30 minutes with periodic agitation. Heat inactivated FBS was dispensed into 50 mL aliquots and stored long term at -20°C.

5.03 Cryogenic Storage of Cell Lines:

The cell line of interest was grown to 70-80% confluency in a T75 cell culture flask. Culture media was removed, cells washed with pre-warmed 1 x PBS, 1 mL of TrypLe added and the flask incubated at 37°C and 5% CO_2 for 15 minutes to allow cell detachment. Cells were taken up in 9 mL of culture media and gently resuspended. Cells were counted using a haemocytometer, pelleted (500g, 5 minutes) and resuspended in a suitable volume of freezing media (90% FBS, 10% DMSO (v/v)) to give the desired concentration (typically 2-4 x 10^6 cells/mL). Cells were dispensed into 1 mL aliquots in cryovials, placed in a Mr. Frosty freezing unit and placed at -80°C overnight. The following morning, vials were moved to liquid nitrogen for long term storage.

5.04 Thawing of Cryogenically Stored Cell Lines:

A cryovial containing the cells of interest was removed from long-term storage in liquid nitrogen. The cryovial was placed in a waterbath pre-warmed to 37°C until thawed and the cells transferred to a T25

cell culture flask containing 8 mL of pre-warmed cell culture media and incubated overnight at 37°C and 5% CO_2. The following morning, the culture media was replaced and cells again incubated at 37°C and 5% CO_2. Culture media was replaced periodically and cells allowed to grow until 70-80% confluent before being transferred to a T75 flask and used experimentally.

5.05 Lactate Dehydrogenase (LDH) Assay:

HEK293 and SH-SHY5Y cells were dispensed into clear 96 well plates at a density of 15,000 cells per well and incubated overnight at 37°C and 5% CO_2. Following incubation, compounds of interest were added at varying concentrations, in triplicate. Control wells containing an equivalent concentration of DMSO (0.5% (v/v)) were prepared and analysed concurrently. Cells were incubated with compounds of interest for 24 at 37°C and 5% CO_2. Following incubation 0.1% Triton X-100 was added to additional control wells, giving a measure of maximum cell death. The LDH assay was then performed as per manufacturer's instructions (MAK066).

To check for compound induced assay interference, the LDH reaction was performed using purified LDH enzyme both in the presence and absence of compounds K690 and K691 (50 µM) as per manufacturer's instructions.

5.06 HEK293 Polyethylenimine (PEI) Transfection:

A stock solution of PEI was prepared at 1 mg/mL in MilliQ water, the pH adjusted to 7.0 and filter sterilised (0.22 µm). Aliquots were stored long term at -80°C.

HEK293 cells were dispensed into a 24 well plate at an appropriate density (60-70% confluency) and incubated overnight at 37°C and 5% CO_2. Transfection mixtures were prepared in serum free Opti-MEM. 25 µL of Opti-MEM was mixed with 750 ng of DNA (ethanol precipitated) and mixed gently via pipetting. 3 µL of PEI (1 mg/mL stock) was added, the microcentrifuge tube vortexed (15 x 1 second pulses) and incubated at room-temperature for 45 minutes. 500 µL of complete media was transferred from the cell containing well, mixed with the transfection solution and transferred back to the well. Cells were incubated for 24 hours at 37°C and 5% CO_2 after which the culture media was replaced. Analysis was performed 24-48 hours post transfection.

The given conditions were optimised using the pmaxGFP plasmid for transfection in a 24 well plate. For alternative cell culture vessels, the PEI:DNA ratio was maintained and the reaction scaled according to total surface area of the culture vessel.

5.07 SH-SY5Y Nucelofection:

Culture media was aspirated from a T75 flask of SH-SY5Y cells (70-80% confluent), cells washed with pre-warmed 1 x PBS, 1 mL of TrypLe added and the flask incubated at 37°C and 5% CO_2 for 15 minutes to allow cell detachment. Cells were taken up in 9 mL of culture media and gently resuspended. Cells were counted using a haemocytometer and 1-2 x 10^6 SH-SY5Y cells pelleted and resuspended in the appropriate

nucleofection solution (Lonza, VACA-1003) containing 2 µg of DNA. Cells were nucleofected using an Amaxa 2b Nucleofector (protocol #A-023). Analysis was performed 24-48 hours post transfection.

5.08 Enzyme Activity in Cell Lysates:

HEK293 cells were seeded at an appropriate density into 60mm dishes and incubated overnight at 37°C and 5% CO_2. Cells were transiently transfected with the desired constructs or empty vector using PEI. Cells were incubated for 24 hours at 37°C and 5% CO_2. Following incubation cells were detached using TrypLe and transferred to 1.5 mL microcentrifuge tubes, pelleted at 2000g and resuspended in 1 mL of hypotonic buffer (10 mM HEPES, 1.5 mM $MgCl_2$, 10 mM KCl, 0.5 mM DTT, pH 7.9) and lysed using a dounce homogeniser (25 strokes). The cell lysate was transferred to fresh microcentrifuge tubes, centrifuged at 16,000g for 3 minutes and the supernatant transferred to new microcentrifuge tubes. Acetoacetyl-CoA and NADH were added to the supernatant (120 µM and 250 µM respectively) the lysate divided 150 µL/well into a clear 96 well plate, in triplicate and absorbance measured at 340 nm (900 seconds, 30 second intervals, 37°C). The rate of reaction was determined during the initial linear period (R^2>0.9) and normalised to total protein content using the BCA assay, as per manufacturer's instructions.

Inhibitors were spiked into lysates from cells transiently transfected with 17β-HSD10 at 50 µM and enzyme activity measured as detailed previously. DMSO (1% (v/v)) was used as a vehicle control.

5.09 Stable Cell Line Generation:

Cells were transiently transfected with the construct of interest using the appropriate methodology (HEK293-PEI, SH-SH5Y-nuclofection) and incubated at 37°C and 5% CO_2. Control cells, harbouring no construct were similarly treated. 48 hours post transfection the culture media was removed and replaced with media containing an appropriate concentration of selection agent (500 µg/mL Geneticin, 250 µg/mL Zeocin). Media was replaced every 2 days and cells maintained in selection until control cells were no-longer viable and foci of resistant cells apparent (typically 1-2 weeks). Selection media was removed and replaced with maintenance media (200 µg/mL Geneticin, 100 µg/mL Zeocin) and cells allowed to grow to confluency before being cryogenically frozen or used experimentally. Protein overexpression was confirmed via western blot.

5.10 Cell Lysate Generation:

Following experimental manipulation, cells were washed with ice-cold PBS and an appropriate volume of ice-cold RIPA lysis buffer added (50 mM Tris, 150 mM NaCl, 1% Triton X-100, 1% sodium deoxycholate, 0.1% SDS, 1 mM EDTA, pH 7.4, 1 x protease inhibitor). Cells were detached via scraping and transferred to pre-cooled microcentrifuge tubes. Tubes were incubated on ice for 30-minutes, centrifuged at 16,000g for 20-minutes at 4°C and the supernatant transferred to fresh microcentrifuge tubes. Protein concentration was determined using the BCA assay as per manufacturer's instructions. Lysates were stored long term at -80 °C.

5.11 Generalised Western Blot:

An appropriate volume of lysate (depending on protein abundance) was resolved via SDS-PAGE (Materials and Methods: Section 2.1). Proteins were transferred to a methanol activated PVDF membrane using a XCell SureLock transfer unit. The transfer of proteins was performed at 25 V for approximately 1.5 hours using 1 x Transfer Buffer (25 mM Tris, 192 mM glycine, 20% (v/v) MeOH) as per manufacturer's instructions. Membranes were blocked using the appropriate blocking agent (typically 5% w/v BSA or NFDM prepared in 1 x TBS-T) for 1 hour at RT and incubated in the appropriate dilution of primary antibody overnight at 4°C. Membranes were washed using TBS-T (3 x 10 minutes) and incubated at room-temperature for 1 hour in the appropriate dilution of secondary antibody (HRP-conjugated). Membranes were washed using TBS-T (3 x 10 minutes) and treated with enhanced chemiluminesence solution before being imaged using an LAS-3000 imaging unit.

If required, membranes were stripped using Abcam mild-stripping buffer, as per manufacturer's instructions, blocked for 1 hour at room-temperature and re-probed using the desired antibody overnight at 4°C. Membranes were washed (3 x 10 minutes TBS-T) incubated with the appropriate secondary antibody, washed (3 x 10minutes TBS-T) and imaged using a LAS-3000 unit and enhanced chemiluminescence solution.

Target	Primary Antibody	Dilution	Secondary Antibody	Dilution
17β-HSD10	ab10260 (5F3)	1:1000 (5% NFDM)	Anti-Mouse- ab6709	1:20,000 (5% NFDM)
β-Actin	A1978	1:10,000 (5% NFDM)	Anti-Mouse- ab6709	1:20,000 (5% NFDM)
Amyloid-Beta	D54D2 (8243)	1:500-1:1000 (5% BSA)	Anti-Rabbit- ab97200	1:75,000 (5% BSA)
Amyloid Precursor Protein	ab32136	1:20,000 (5% NFDM)	Anti-Rabbit- ab97200	1:50,000 (5% NFDM)
4-hydroxynoneal	ab46545	1:500 (5% NFDM)	Anti-Rabbit- ab97200	1:50,000 (5% NFDM)

Chapter 3: 17β-HSD10 Assay Development and Small Molecule Screening

Chapter 3 - Introduction and Aims:

Whilst there are numerous theories related to the underlying cause for the development of Alzheimer's disease (AD), arguably the most widely accepted is the amyloid cascade hypothesis. First described by Hardy and Higgins in 1992[164], the amyloid cascade hypothesis proposes that an abnormal accumulation of amyloid beta-peptide (Aβ) is the main causative factor for the development of AD, disrupting normal cellular processes and giving rise to the characteristic neuronal loss associated with the disease. Although originally attributed to plaque deposition, in recent years there has been a shift in focus from extracellular insoluble plaques of Aβ, to soluble intracellular forms and their binding partners[284,285].

The mitochondrial 17β-HSD10 enzyme is one such binding partner[337,338]. The interaction between the 17β-HSD10 enzyme and Aβ has been shown to be cytotoxic, resulting in oxidative stress and cell death[303,338-340]. Interestingly, hallmarks of this toxicity have been shown to be dependent on the catalytic activity of the 17β-HSD10 enzyme[338] and thus, small molecule inhibitors of the 17β-HSD10 enzyme may be of therapeutic merit in treating AD.

The primary aim of this chapter was to purify the 17β-HSD10 protein to homogeneity and to develop a robust screening assay for measuring catalytic activity. Subsequently, to use this assay to screen several libraries of compounds, with the aim of identifying a range of molecules capable of enzyme inhibition. To confirm such hits through the use of de-selection assays and characterise the most promising molecules in terms of mechanism of action and potency. Once validated, these compounds would form the basis for the development of subsequent series of derivative compounds, with more favourable drug-like properties, which may form the basis for the development of novel therapeutic agents against Alzheimer's disease.

3.01 Protein Purification:

In order to evaluate the potential of compounds of interest to modulate the catalytic activity of the 17β-HSD10 enzyme, first highly pure recombinant protein was required. A previous PhD student within the group, Dr. Kirsty Muirhead, developed and optimised the expression and purification of the 17β-HSD10 enzyme using the peHISTEV vector[346] (Figure 3.01, construct herein referred to as peHISTEV-HSD10) and the BL21(DE3) *E. coli* variant. Expression using this system yields recombinant protein with a TEV cleavable, N-terminal, 6 x His-Tag and was used for large scale protein purification.

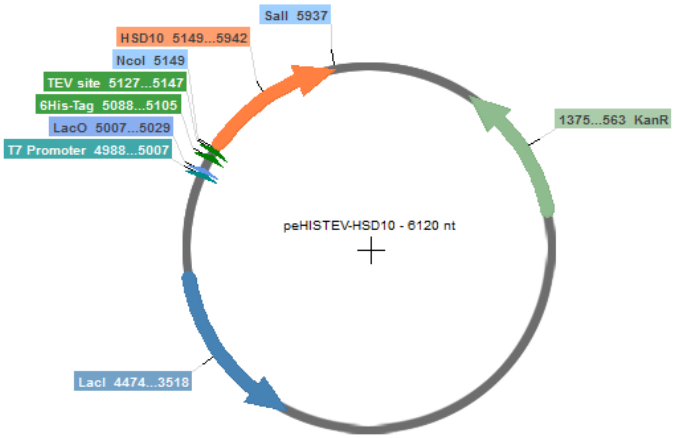

Figure 3.01. peHISTEV-HSD10 expression vector. The 17β-HSD10 cDNA sequence was cloned into the peHISTEV[345] vector by using the NcoI and SalI restriction enzyme sites.

In brief, the peHISTEV-HSD10 construct was transformed into competent *E. coli* BL21(DE3) cells, grown to OD_{600}= 0.6-0.8 and protein expression induced overnight at 25°C. Cells were lysed via sonication and protein purified using a combination of Ni-NTA affinity chromatography and size exclusion chromatography. Samples were analysed throughout the purification procedure to ensure the success of the preceding step, to give a measure of purity and also a rough gauge of yield.

Ni-NTA affinity chromatography exploits the ability of histidine residues to form coordinate bonds to immobilised metal ions, in this case Ni^{2+}. As cell lysate is passed over the purification column, histidine residues within the 6 x HisTag form coordinate bonds to immobilised Ni^{2+} ions held within the Ni-NTA resin and thus remain bound (Figure 3.02). Non-tagged proteins exhibit comparatively low affinity and pass through without binding.

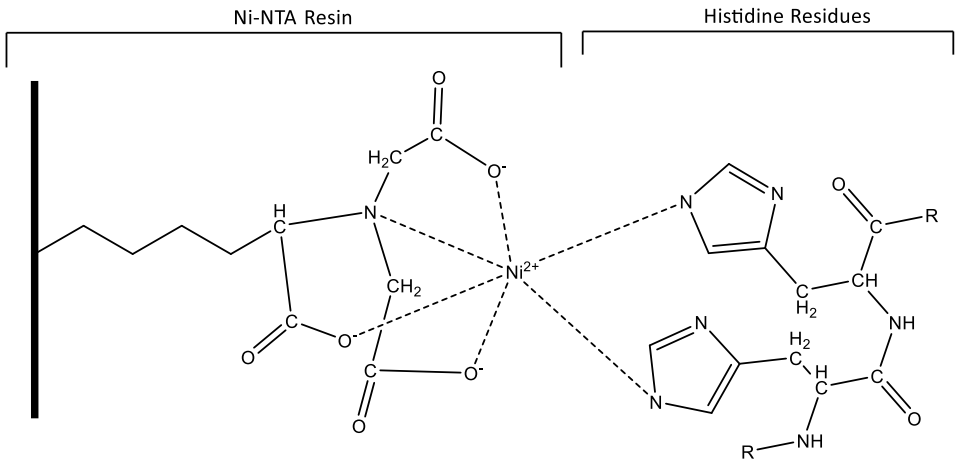

Figure 3.02. Ni-NTA Resin. Histidine residues are able to form coordinate bonds to immobilised Ni^{2+} ions held in the Ni-NTA support, allowing the isolation of tagged proteins of interest.

An initial check for both 17β-HSD10 expression and column binding was made by analysing a sample of cleared lysate and column flow-through via SDS-PAGE and Coomassie Blue staining. A prominent band is apparent in the cleared lysate at approximately 27 kDa, corresponding to the 17β-HSD10 protein. Following passage through a HisTrap HP column, this band is no longer seen, indicating the 17β-HSD10 protein is now bound to the purification column (Figure 3.03).

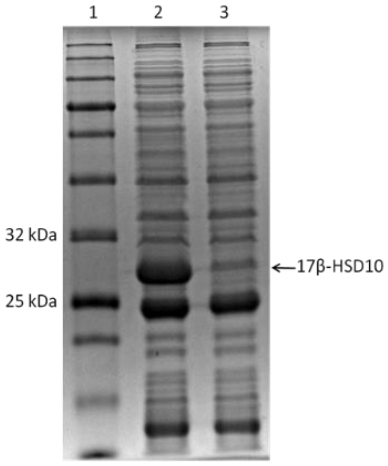

Figure 3.03. Expression and column binding of recombinant 17β-HSD10 protein. A sample of cleared lysate and column flow-through were analysed using SDS-PAGE and Coomassie staining. A prominent band is apparent in the cleared lysate at approximately 27 kDa, but not in the column flow-through, corresponding to the recombinant 17β-HSD10 protein pre and post column binding. Lane 1 = Ladder, Lane 2 = Cleared Lysate, Lane 3 = Column Flow Through.

A number of proteins native to the *E. coli* cell are known to have an intrinsic affinity for the Ni-NTA resin, usually by virtue of a natural abundance of histidine residues, and so bind to the Ni-NTA resin in a non-specific manner[347]. Imidazole will compete with bound proteins for the Ni-NTA resin and at a sufficient concentration cause them to elute from the column. Contaminating proteins typically exhibit low affinity as compared to a 6 x His-tagged protein and therefore by washing the column with a gradient of imidazole low affinity contaminants can be removed leaving the protein of interest bound.

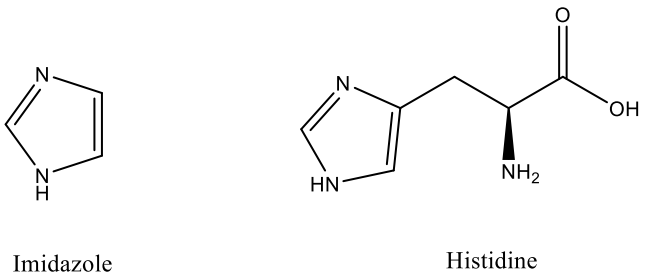

Figure 3.04. Structure of Imidazole and Histidine. Imidazole is able to compete with histidine residues for the Ni-NTA matrix and, at sufficient concentration, causes proteins to elute from the column.

Although a multitude of workflows are possible for column loading, wash and elution steps (syringe based, batch based, gravity flow etc.), the use of an automated purification system makes the procedure significantly less time and labour intensive. Thus, to facilitate wash and elution steps, the HisTrap HP column was loaded onto an AKTA-Pure purification rig and the column washed with a stepwise increase in imidazole concentration (0-100 mM). Once a stable UV baseline was reached, indicating that no further protein was being eluted and low affinity contaminants were removed, the 17β-HSD10 protein was eluted using a linear gradient of imidazole (100-500 mM) and fractions taken periodically. The presence of 17β-HSD10 protein in elution fractions was confirmed using SDS-PAGE and Coomassie Blue staining, with clean 17β-HSD10 protein being observed in fractions 7-10 (Figure 3.05).

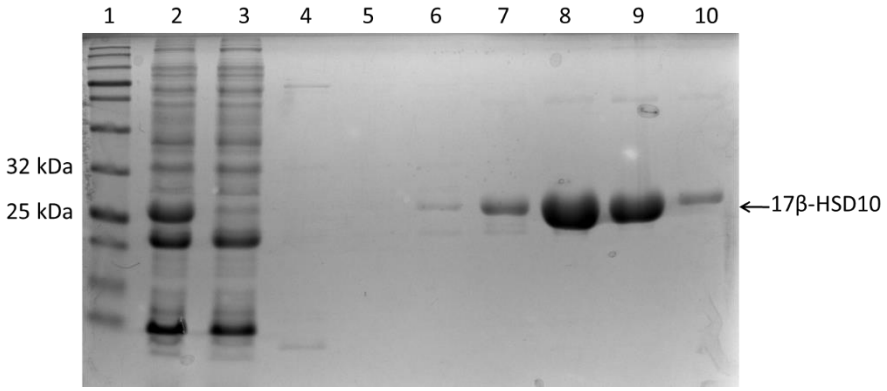

Figure 3.05. 17β-HSD10 wash and elution fractions. The HisTrap HP column, loaded with 17β-HSD10 protein was washed with a stepwise increase in imidazole (0-100 mM) removing low affinity contaminants. 17β-HSD10 protein was subsequently eluted using a linear gradient of imidazole (100-500 mM). Lane 1 = Ladder, Lane 2 = Cleared Lysate, Lane 3 = Column Flow Through, Lanes 4-6 = Wash Fractions, Lanes 7-10 = Elution Fractions

As the 6 x HisTag is relatively small, in many cases it can be left attached to a protein of interest without altering its function. However, previous work has shown that the presence of an N-terminal 6 x HisTag significantly reduces the enzymatic activity of the 17β-HSD10 protein (Dr. Kirsty Muirhead, unpublished observation) and thus it must be removed prior to further analysis, a task accomplished through the use of 6 x His-tagged TEV-protease (S219V variant). TEV protease cuts at the recognition sequence ENLYFQ-G, previously engineered into the peHISTEV vector between the 6 x HisTag and multiple cloning site. As imidazole is known to inhibit TEV protease activity it must be removed prior to cleavage, accomplished here through the use of dialysis. Fractions 7-10 were pooled, loaded into a dialysis membrane and allowed to equilibrate with imidazole free buffer. The dialysis membrane was placed into a second container of fresh buffer, TEV protease added and the mixture incubated at 4°C overnight. TEV cleavage was confirmed via SDS-PAGE and Coomassie Blue staining the following morning.

Following treatment with TEV protease, the band corresponding to the 17β-HSD10 protein was found to be shifted down, corresponding to a loss of mass and charge, indicative of successful cleavage (Figure 3.06, Lane 3). A faint band of un-cleaved protein and TEV protease itself can be seen above.

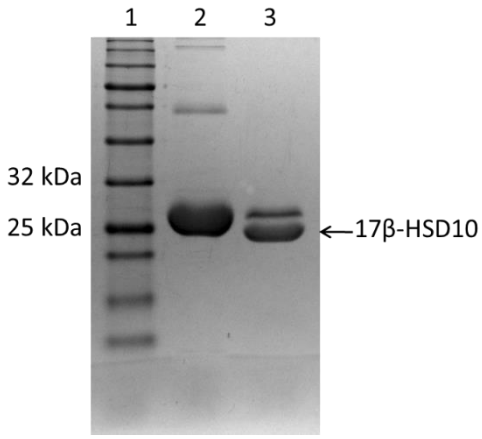

Figure 3.06. 17β-HSD10 TEV cleavage confirmation. TEV protease was employed to remove the 6 x His-tag from the 17β-HSD10 enzyme. A sample of 17β-HSD10 protein was taken pre and post TEV treatment and analysed using SDS-PAGE and Coomassie staining. Following TEV treatment the band corresponding to the 17β-HSD10 protein is shifted down, indicative of successful cleavage. Lane 1 = Ladder, Lane 2 = Pre-TEV, Lane 3 = Post-TEV.

The TEV protease treated sample was again passed over a HisTrap HP column, this time allowing the binding of free 6 x His-tags, 6 x His-tagged-TEV protease, uncleaved 17β-HSD10 protein and any remaining high affinity contaminants. Column flow-through, now containing the protein of interest, was collected and concentrated for gel filtration using a VivaSpin 20 spin-column (10 kDa MWCO). Sample was injected into a pre-equilibrated HiLoad Sephadex 75 prep-grade column and fractions taken periodically. Those corresponding to the start, middle and end of the peak were run on a polyacrylamide gel and stained using Coomassie Blue, confirming the presence of pure 17β-HSD10 protein (Figure 3.07).

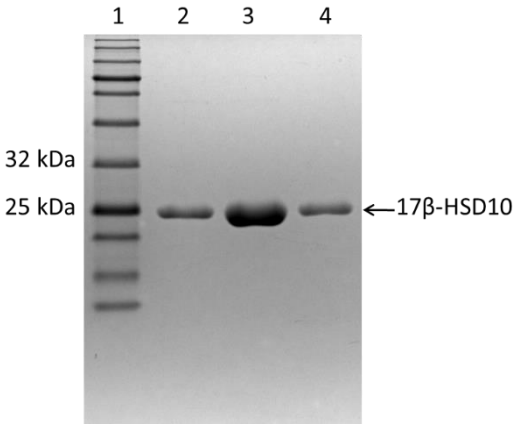

Figure 3.07. 17β-HSD10 post gel filtration. Ni-NTA purified 17β-HSD10 protein was concentrated and loaded onto a pre-equilibrated HiLoad Sephadex 75 prep-grade column. Fractions were taken periodically and those corresponding to the start, middle and end of the peak were analysed using SDS-PAGE and Coomassie staining confirming the presence of pure 17β-HSD10 protein. Lane 1 = Ladder, Lanes 2-4 = Start, middle and end of elution peak.

Gel filtration fractions, harbouring pure 17β-HSD10 protein, were pooled and concentrated to 10 mg/mL before being flash frozen in liquid nitrogen and stored long-term at -80°C. Protein identity was confirmed using mass spectrometry (see Appendix: A).

3.02 Activity Assay Development:

Now that highly pure 17β-HSD10 protein was available, a robust screening assay for measuring enzymatic activity was required. Such an assay has been worked on previously, but with limited success. The conditions utilised were found to have issues associated with reproducibility, throughput, compound solubility and enzyme stability. The screening assay employed measures the 17β-HSD10 catalysed conversion of acetoacetyl-CoA to L-3-hydroxybutyryl-CoA (Scheme 3.01).

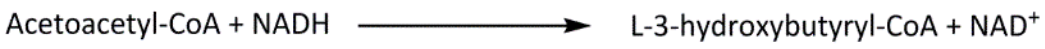

Scheme 3.01. 17β-HSD10 catalysed conversion of acetoacetyl-CoA (forward reaction). The 17β-HSD10 enzyme is known to catalyse the NADH dependent conversion of acetoacetyl-CoA to L-3-hydroxybutyryl-CoA, a reaction which forms the basis for the in-house enzyme activity assay.

In the forward direction, NADH is utilised as a cofactor and becomes oxidised, producing NAD^+. NADH shows marked absorbance at 340 nm, whilst NAD^+ does not, and thus enzymatic activity can be measured by a decrease in absorbance over time as substrate is converted to product and NADH is converted to NAD^+ in a stoichiometric manner. NADH also shows a peak in fluorescence at 460 nm when excited at 340 nm, a property not shared by NAD^+, and thus a fluorescence-based readout could also be employed. Both approaches have merit, with the absorbance assay showing linearity over a wider range of NADH concentrations (Figure 3.08, left) and the fluorescence assay being more sensitive to low concentrations of NADH (Figure 3.08, right).

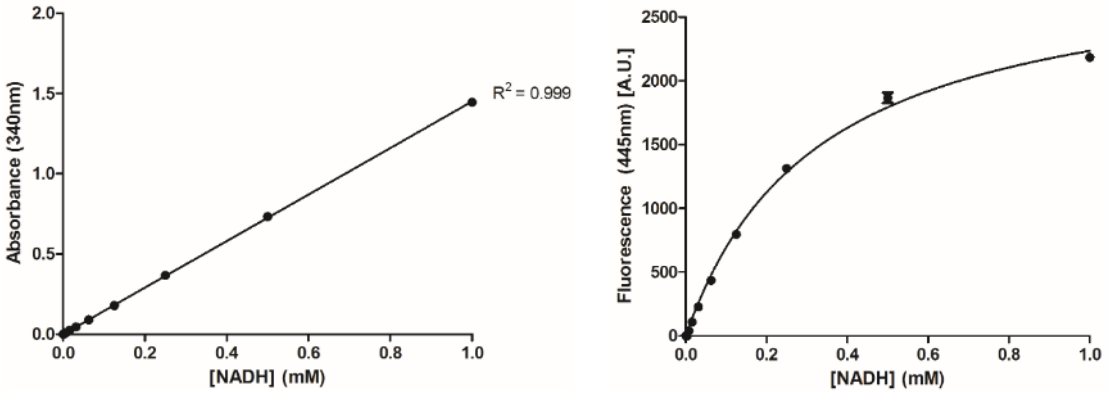

Figure 3.08. Absorbance and fluorescence as a function of NADH concentration. NADH shows marked absorbance (340 nm) and fluorescence (ex. 340 nm, em. 460 nm). An absorbance-based readout shows linearity over a larger range of NADH concentrations (left), whilst the fluorescence-based assay is more sensitive to low concentrations of NADH (right). Values shown are an average from one experiment with three technical repeats ± SEM.

As we are measuring the forward reaction, the initial concentration of NADH will be high causing the associated signal to fall outside of the linear range of the fluorescence-based assay. Therefore, to simplify data analysis, an absorbance based read-out was adopted.

The previous assay buffer consisted of 10 mM HEPES buffer, 100 mM NaCl, 120 µM acetoacetyl-CoA, 250 µM NADH, pH 7.0, 30°C. 17β-HSD10 enzyme was added at a final concentration of 0.5 µg/mL and the rate of reaction determined during the linear period of the progress curve ($R^2 > 0.9$). Under these conditions it was possible to reproducibly measure 17β-HSD10 activity; however, compounds of interest consistently precipitated from the solution giving highly variable results and making useful inference impossible. An illustrative example is provided in Figure 3.09, using a series of Frentizole derivative compounds.

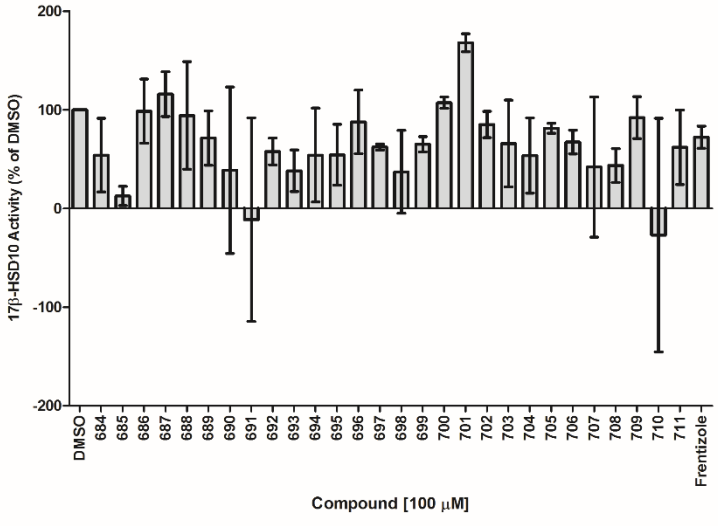

Figure 3.09. Inherited 17β-HSD10 activity assay. Enzyme activity was assessed in the presence of compounds K684-K711 at 100 µM using the inherited assay conditions. The inherited assay was found to produce highly variable results, making meaningful inference impossible. Values shown are an average taken from two independent experiments each with three technical repeats ± SEM.

As such, a number of buffer parameters were altered in an attempt to improve the quality of the assay. Various salt concentrations and temperatures were trialled, with the net effect of NaCl being removed and the temperature of the assay increased to 37°C. The addition of a low concentration of gelatin has previously been shown to improve the solubility of small molecules in aqueous solution[348], and thus 0.5% gelatin was added to the buffer system, simultaneously improving compound solubility and also enzyme stability.

At this point it was deemed necessary to prepare fresh compound solutions from anhydrous stocks. The preparation of fresh 10 mM stocks revealed a marked difference in colouration between the inherited solutions and those freshly prepared, suggesting an error in calculation had been made previously. Examination of the calculations performed confirmed such an error, with the result of the previous compound stocks being 100 mM rather than 10 mM and explaining the associated solubility issues. Once this was known, compound solubility was no longer an issue and the assay became markedly more reproducible.

Initial experiments made use of a BMG FluoStar Optima plate reader. This spectrophotometer was only capable of performing kinetic reads of the required interval on a single well at a time, severely limiting throughput and introducing a large amount of variability into the assay. To rectify this, a different spectrophotometer was used, initially a SpectraMax 250 and later a SpectraMax M2e, both of which are capable of taking readings from an entire 96 well plate at once, ameliorating the aforementioned issues and dramatically improving the reliability of results.

3.03 Michaelis-Menten Kinetics:

When performing screening experiments with the aim of identifying enzyme inhibitors, it is important to select appropriate concentrations of substrate and cofactor for use in the reaction. Michaelis-Menten kinetic parameters, V_{max} and K_m, are typically used to guide this selection. The kinetic parameters of the 17β-HSD10 enzyme were assessed with respect to cofactor, NADH, and substrate, acetoacetyl-CoA, using non-linear regression and the Michaelis-Menten equation. Thus, 17β-HSD10 activity was measured in the presence of a saturating concentration of NADH and increasing concentrations of acetoacetyl-CoA and subsequently, in the presence of a saturating concentration of acetoacetyl-CoA and increasing concentrations of NADH. A V_{max} value of 10.64 ± 0.42 µmol mg^{-1} min^{-1} and K_m of 11.79 ± 1.87 µM were calculated with respect to acetoacetyl-CoA (Figure 3.10, top). A V_{max} value of 15.54 ± 0.96 µmol mg^{-1} min^{-1} and a K_m value of 99.84 ± 21.34 µM were calculated with respect to NADH (Figure 3.10, bottom).

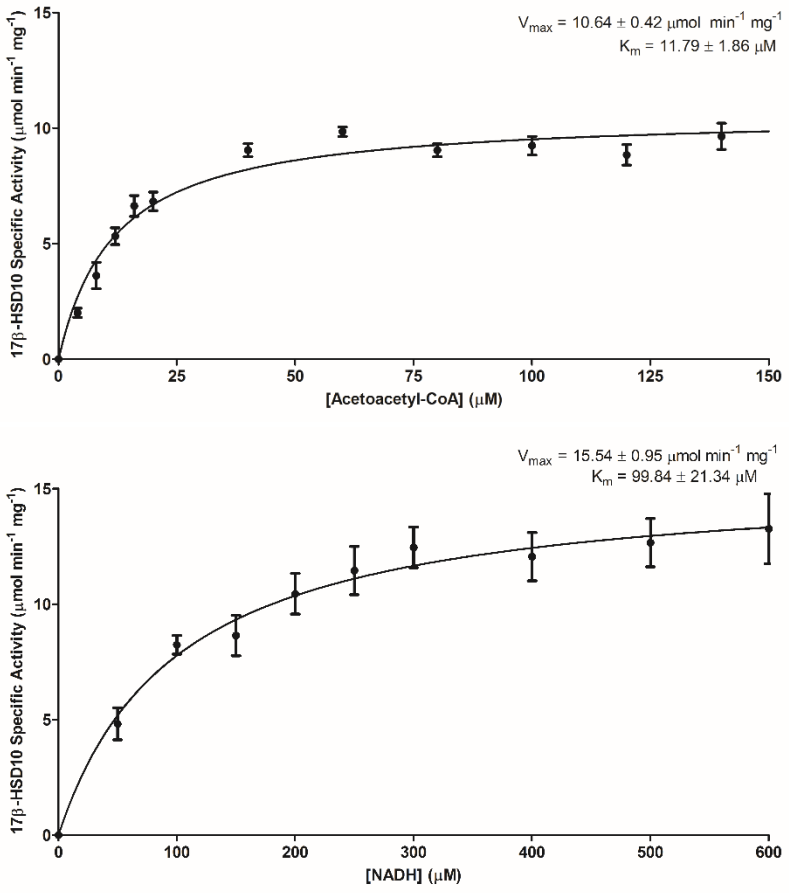

Figure 3.10. 17β-HSD10 enzymatic activity as a function of acetoacetyl-CoA concentration (Top) and NADH concentration (Bottom). The rate of reaction was measured in the presence of increasing concentrations of acetoaceyl-CoA or NADH, allowing the calculation of kinetic parameters V_{max} and K_m. A V_{max} value of 10.64 ± 0.42 µmol mg^{-1} min^{-1} and a K_m value of 11.79 ± 1.87 µM were calculated with respect to acetoacetyl-CoA. A V_{max} value of 15.54 ± 0.96 µmol mg^{-1} min^{-1} and a K_m value of 99.84 ± 21.34 µM were calculated with respect to NADH. Values shown are an average taken from two independent experiments each with three technical repeats ± SEM.

Typically, screening assays with the aim of identifying enzyme inhibitors will utilise substrate and co-factor concentrations at or around the value of K_m, ensuring that the assay is capable of identifying inhibitors acting via a competitive mechanism, as they will not be out-competed by either substrate or co-factor. The concentrations of acetoacetyl-CoA and NADH utilised in the inherited assay were both markedly above the K_m value at 120 µM and 250 µM respectively, effectively masking the influence of inhibitors acting via a competitive mechanism; however, compounds acting via a non-competitive mechanism would still be apparent. The active site of the 17β-HSD10 enzyme is known to undergo a marked conformational change once bound to Aβ[303,349] and as such, competitive inhibitors are unlikely to remain active against the disease relevant 17β-HSD10/Aβ complex. Therefore, a decision was made to continue with the previous concentrations of 120 µM acetoacetyl-CoA and 250 µM NADH and to focus on the identification of non-competitive inhibitors of the 17β-HSD10 enzyme.

3.04 DMSO Titration:

To facilitate ease of screening, all in-house compounds were prepared using dimethyl sulfoxide (DMSO), a polar, aprotic solvent capable of dissolving both polar and non-polar compounds. Prior to the commencement of small molecule screening, an initial experiment was performed to assess the effect of increasing concentrations of solvent on 17β-HSD10 enzymatic activity. Any changes in enzyme activity observed in the presence of compounds of interest could then reliably be attributed to the said compound and not simply solvent effects. As such, the activity of the 17β-HSD10 enzyme was assessed in the presence of increasing concentrations of DMSO (0-5% (v/v)). A measurable decrease in activity was seen even at the lowest concentration tested (0.5% (v/v)), suggesting the 17β-HSD10 enzyme is reasonably sensitive to this solvent. A concentration of 1% DMSO (v/v) was deemed to induce an acceptable decrease in activity (4.8%) whilst allowing a reasonable range of compound concentrations to be tested and thus was employed for subsequent compound screening experiments.

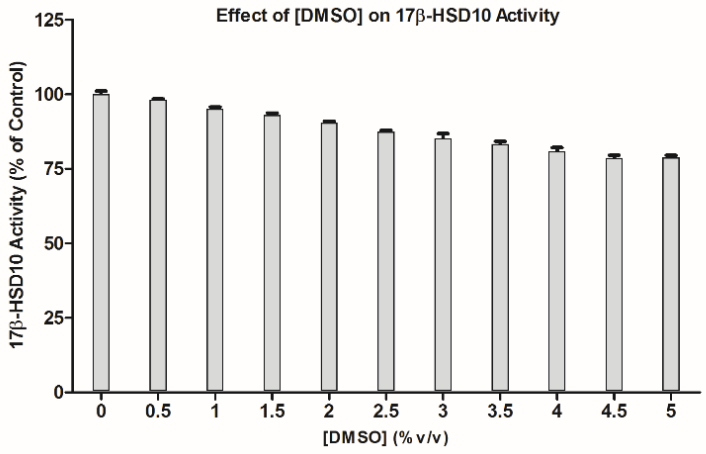

Figure 3.11. Effect of increasing DMSO concentration on 17β-HSD10 enzymatic activity. The catalytic activity of the 17β-HSD10 enzyme was measured in the presence of increasing concentrations of DMSO (0-5 % (v/v)) . A concentration of 1% (v/v) was selected for subsequent compound screening experiments. Values shown are an average taken from one experiment with three technical repeats ± SEM.

3.05 Assay Validation: AG18051 Dose-Response and Z-Factor calculation

As validation of the aforementioned 17β-HSD10 activity assay, an IC_{50} value was calculated using compound AG18051. Identified in 2004 by Kissinger *et al.,* AG18051 is a known potent inhibitor of the 17β-HSD10 enzyme with a reported IC_{50} value of 92 nM[350] (Figure 3.12).

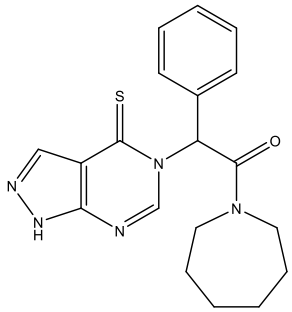

Figure 3.12. Structure AG18051. Compound AG18051 was identified as a potent inhibitor of the 17β-HSD10 enzyme by Kissinger *et al.* in 2004[350].

Using the previously defined in-house enzyme based assay, an IC_{50} value of 68.61 nM (95% CI = 64.5-72.99) was calculated for compound AG18051 (Figure 3.13).

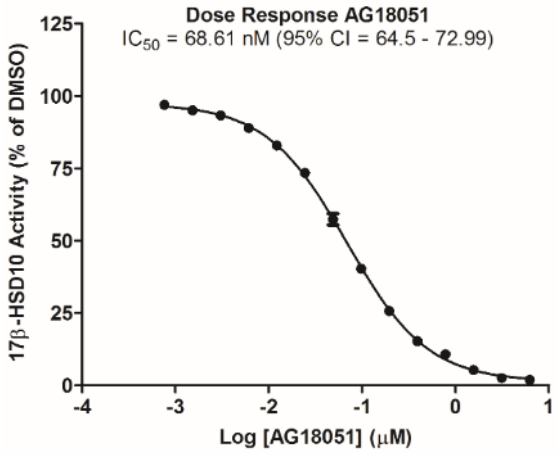

Figure 3.13. Compound AG18051 dose response. 17β-HSD10 enzyme activity was measured in the presence of increasing concentrations of compound AG18051, a known potent inhibitor of the 17β-HSD10 enzyme. An IC_{50} value of 68.61 nM (95% CI = 64.5-72.99) was calculated using GraphPad Prism. Values shown are an average taken from two independent experiments each with three technical repeats ± SEM.

The IC_{50} values reported herein and previously by Kissinger *et al*. were found to correlate well, showing the in-house enzyme assay is functioning as expected and is suitable for further explorative screening experiments.

Repeat experiments using a saturating concentration of compound AG18051 were performed on three sequential days, indicating an extremely high degree of reproducibility (data not shown). As the experiments are performed using purified 17β-HSD10 enzyme there should, with the exception of human and equipment error, be no biological variation between repeat experiments, as was indicated by the observed high degree of reproducibility. Thus, for small molecule characterisation based assays, two

independent experiments would be performed on sequential days, each harbouring three technical repeats and an average taken. The inclusion of technical repeats would allow equipment error to be controlled for, whilst performing two entirely independent experiments would account for any biological variation between enzyme aliquots, and allow any gross human error to be readily identified, whilst also acting to conserve limited compound and protein stocks.

To test the robustness of such an experimental design, a Z-factor value was calculated for the assay. The Z-Factor, described by Zhang *et al.,* is commonly used to assess the robustness of a screening assay, providing a measure of both dynamic range and reproducibility[351]. A Z-Factor value was calculated for the 17β-HSD10 activity assay using data taken from two independent experiments, each with three technical repeats (comparable to conditions used for subsequent screening experiments), using the formula:

$$Z = 1 - \frac{(3SD\ of\ Sample + 3SD\ of\ Control)}{(Mean\ of\ sample - Mean\ of\ Control)}$$

Z = 1, An ideal assay

1>Z> 0.5, An excellent assay

0.5>Z>0, A marginal assay

Z= 0, An assay unsuitable for screening purposes

DMSO (1% (v/v)) was employed as a vehicle control and a saturating concentration of compound AG18051 used as a positive control for inhibition. A Z-Factor value of 0.895 was obtained, falling well within the "excellent assay" bracket and indicating that the described screening assay is robust in nature and suitable for further explorative screening experiments.

Whilst potent, the mechanism of action utilised by compound AG18051 involves the formation of a covalent bond to cofactor, NAD^+, altering the conformation of the Rossmann fold motif and thereby inhibiting enzyme activity[350]. As both NAD^+ and the Rossmann fold are features common to many families of enzyme[352], it was hypothesised that compound AG18051 would be promiscuous in nature and hence a poor drug candidate, prompting the search for alternatives.

3.06 Frentizole Derivatives - Initial Screens:

In 2006, Xie *et al.* showed that Frentizole, an FDA approved antiviral and immunosuppressant compound, is capable of perturbing the interaction between the 17β-HSD10 enzyme and Aβ, albeit poorly with an IC_{50} value of approximately 200 μM[344]. Two derivatives of the parent Frentizole scaffold were generated with markedly improved potency against the 17β-HSD10/Aβ interaction, with IC_{50} values <10 μM (Figure 3.14)[344].

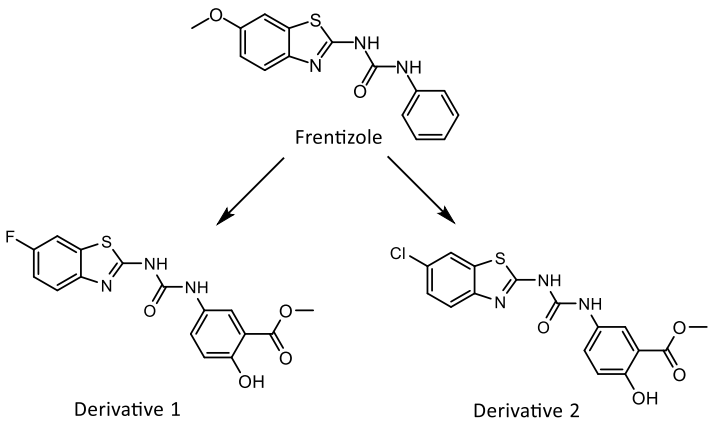

Figure 3.14. 17β-HSD10/Aβ interaction perturbing compounds. Frentizole, the parent compound was found to be capable of disrupting the interaction between the 17β-HSD10 enzyme and Aβ (IC_{50}>200 μM) derivatives 1 and 2 were found to be markedly more potent (IC_{50}<10 μM). Redrawn from[344].

We hypothesised that the ability of the compounds described by Xie *et al.* to perturb the interaction between the 17β-HSD10 enzyme and Aβ, may confer the ability to bind directly to 17β-HSD10 and in doing so may inhibit the catalytic activity of the enzyme. Thus, Frentizole derivatives may hold the potential for the generation of dual purpose therapeutics, simultaneously disrupting the 17β-HSD10/Aβ interaction, whilst also inhibiting the catalytic activity of the enzyme.

To investigate this further, our collaborators in the Czech Republic synthesised derivative compounds 1 and 2 (Figure 3.14, Table 3.01: K710-K711) and an additional 25 compounds harbouring various substitutions on the phenylurea moiety, with the aim of generating novel inhibitors of the 17β-HSD10 enzyme (Table 3.01: K684-K709). Frentizole, the parent molecule, was available commercially and thus was purchased, allowing comparative biological evaluation (see Appendix: C for compound NMR).

Table 3.01. Series 1: Frentizole derivative compounds (K684-K711). A series of 25 Frentizole derivatives were synthesised with the aim of generating novel inhibitors of the 17β-HSD10 enzyme (K684-K709). Two known 17β-HSD10/Aβ interaction disrupting compounds were also synthesised (K710-K711)[344].

K-Code	Structure	K-Code	Structure
K684	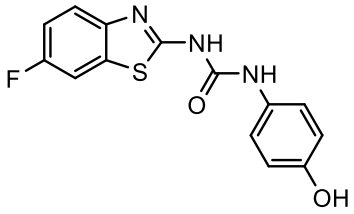	K690	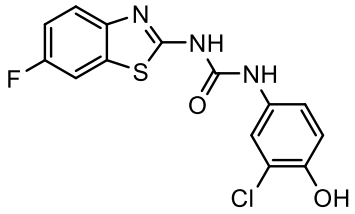
K685	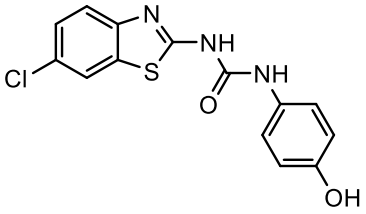	K691	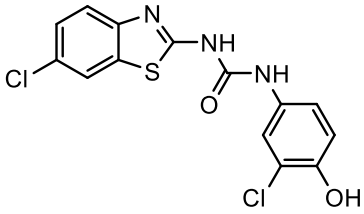
K686	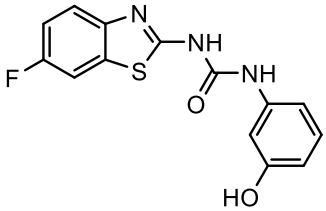	K692	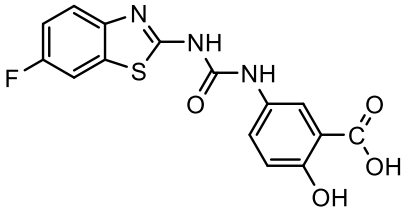
K687	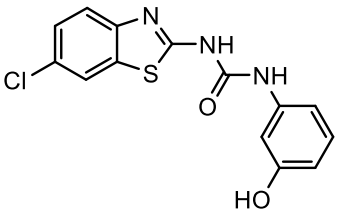	K693	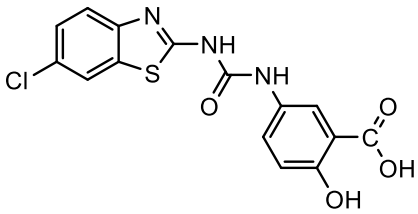
K688	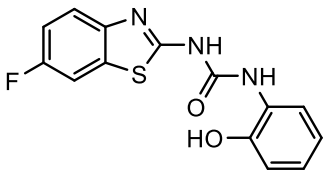	K694	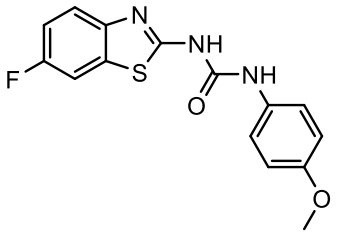
K689	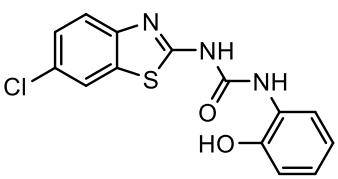	K695	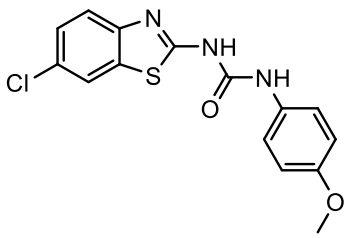

K-Code	Structure	K-Code	Structure
K696	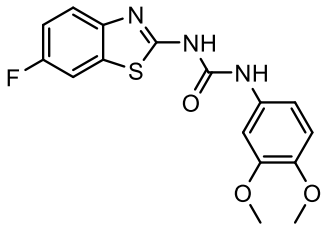	K701	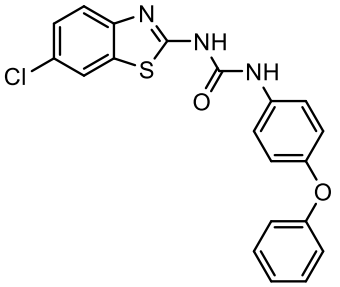
K697	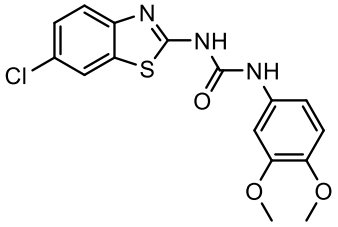	K702	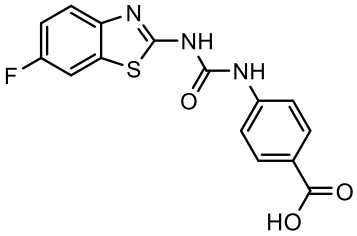
K698	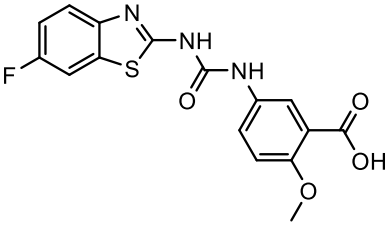	K703	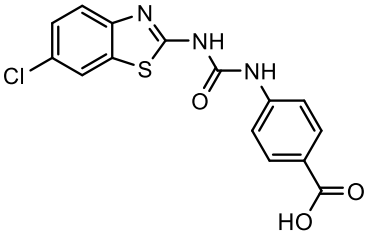
K699	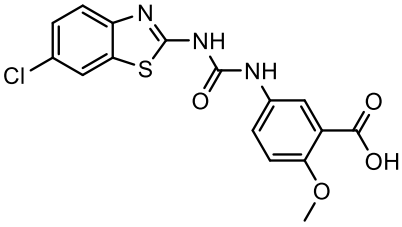	K704	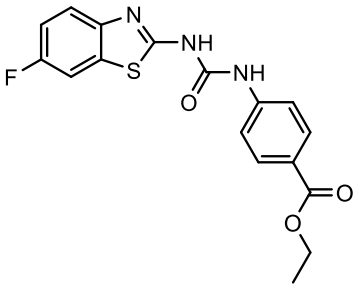
K700	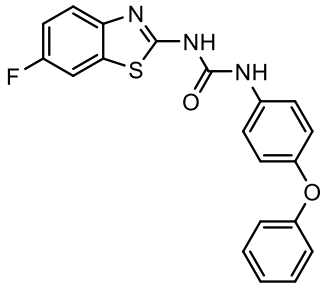	K705	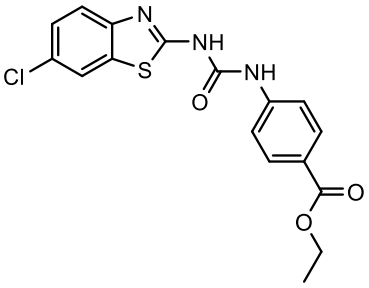

K-Code	Structure	K-Code	Structure
K706	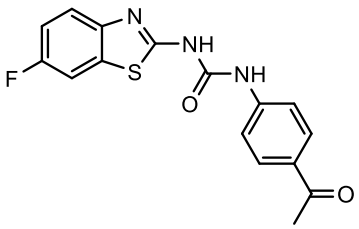	K709	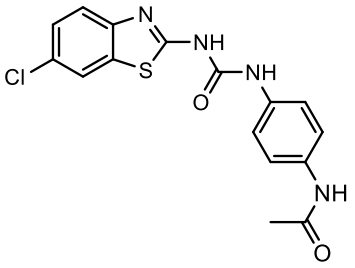
K707	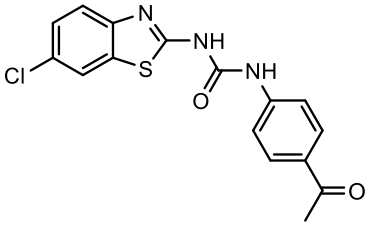	K710	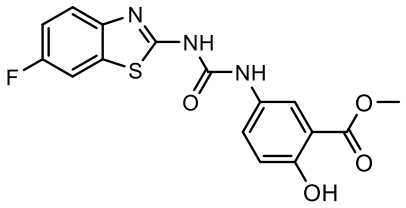
K708	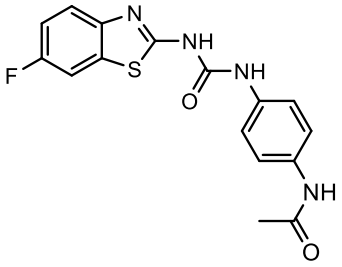	K711	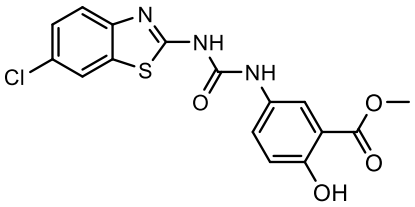

Using the aforementioned 17β-HSD10 activity assay (Chapter 3: Section 3.02), an initial screen of the synthesised Frentizole derivatives was performed at 100 µM. At this concentration five compounds capable of inhibiting the 17β-HSD10 enzyme were identified; compounds K688, K689, K690, K691 and K693 (Figure 3.15). Interestingly, compounds known to perturb the 17β-HSD10/Aβ interaction (Frentizole, K710-K711) were found to be incapable of directly inhibiting the catalytic activity of the enzyme.

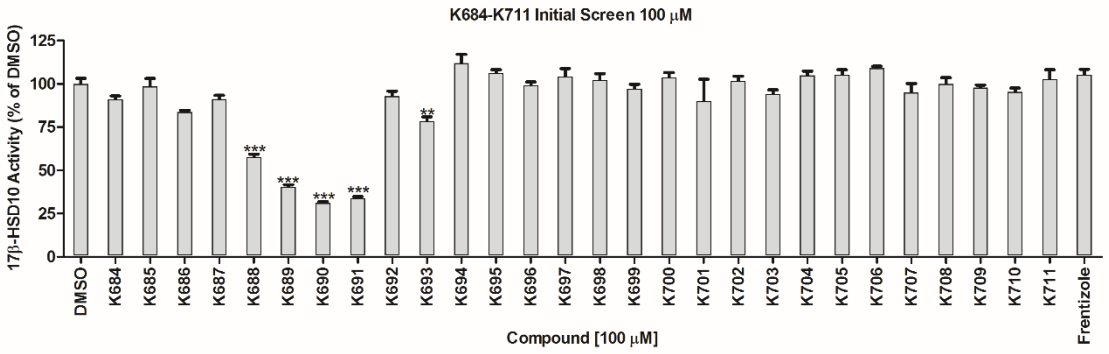

Figure 3.15. 17β-HSD10 activity in the presence of compounds K684-K711 at 100 μM. An initial screen of the synthesised frentizole derivatives was performed at 100 μM. At this concentration 5 compounds, K688, K689, K690, K691 and K693, were found to be capable of significantly inhibiting the catalytic activity of the 17β-HSD10 enzyme. Values shown are an average taken from two independent experiments each with three technical repeats ± SEM. Statistical analysis was performed using GraphPad Prism and a one-way ANOVA with Bonferonni multiple comparisons. * = P ≤ 0.05, ** = P ≤ 0.01, *** = P ≤ 0.001, **** = P ≤ 0.0001.

In an attempt to identify the most potent inhibitors, a second compound screen was subsequently performed at 25 μM. At this concentration compounds K690 and K691 were found to retain a similar level of inhibition to that seen at 100 μM whilst compounds K688, K689 and K693 showed less marked inhibition, suggesting compounds K690 and K691, harbouring a hydroxyl group in the *para* position and chloro group in the *meta* position of the phenylurea moiety, are the most potent inhibitors within this series (Figure 3.16).

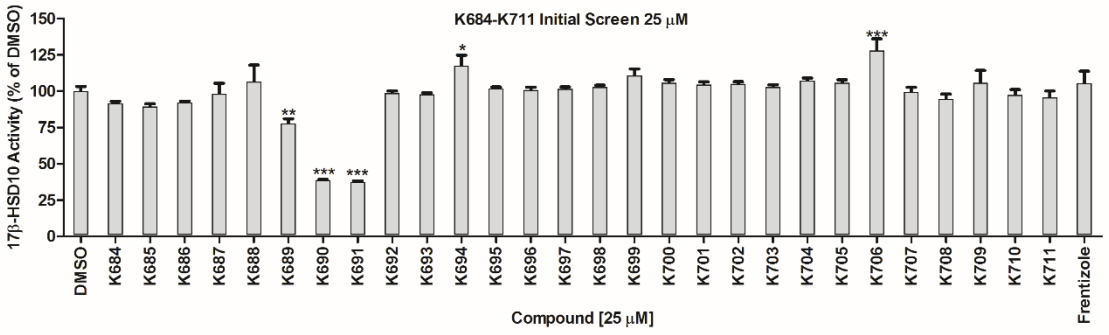

Figure 3.16. 17β-HSD10 activity in the presence of compounds K684-K711 at 25 μM. A second screen of the synthesised frentizole derivatives was performed at 25 μM. At this concentration 3 compounds, K689, K690 and K691 were found to be capable of significantly inhibiting the 17β-HSD10 enzyme. Values shown are an average from two independent experiments each with three technical repeats ± SEM. Statistical analysis was performed using GraphPad Prism and a one-way ANOVA with Bonferonni multiple comparisons. * = P ≤ 0.05, ** = P ≤ 0.01, *** = P ≤ 0.001, **** = P ≤ 0.0001.

A second compound series was designed on the basis of information obtained from the first (Table 3.02: K795-K805). Substitution of the benzothiazole moiety with a chloro group at position 5 was retained and the phenylurea moiety substituted with chloro and hydroxyl groups, in various combinations and positions, in the hope of generating structure activity relationships, and more potent inhibitors of the 17β-HSD10 enzyme (see Appendix: C for compound NMR).

Table 3.02. Series 2: Frentizole derivative compounds (K795-K805). A second series of 11 Frentizole derivatives were synthesised with the aim of further characterising the structural motifs required for inhibition of the 17β-HSD10 enzyme.

K-Code	Structure	K-Code	Structure
K795	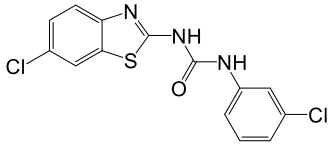	**K801**	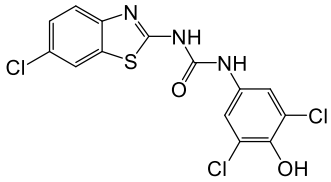
K796	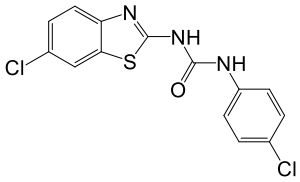	**K802**	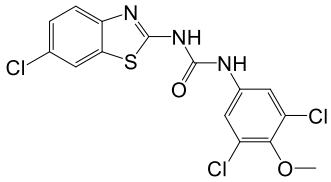
K797	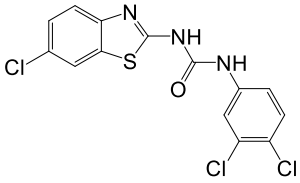	**K803**	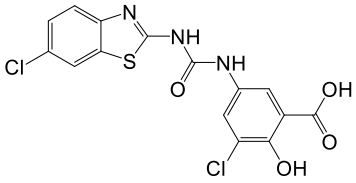
K798	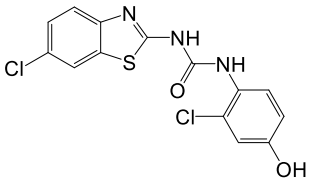	**K804**	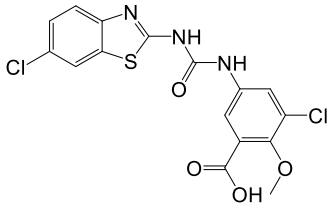
K799	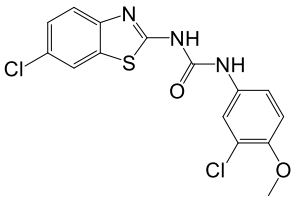	**K805**	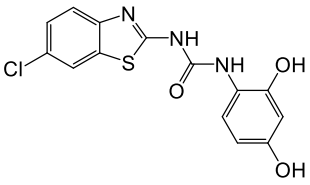
K800	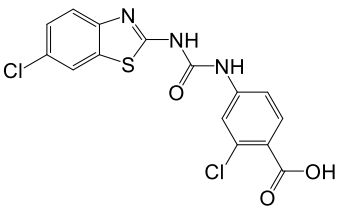		

As before, compounds K795-K805 were first screened at 100 µM and subsequently at 25 µM. At the 100 µM concentration compounds K798, K801, K803 and K805 were found to be capable of significantly reducing enzyme activity (Figure 3.17).

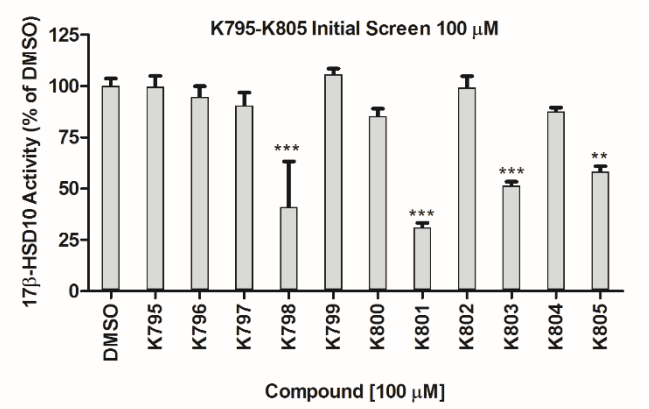

Figure 3.17. 17β-HSD10 activity in the presence of compounds K795-K805 at 100 µM. An initial screen of the synthesised frentizole derivatives was performed at 100 µM. At this concentration 4 compounds, K798, K801, K803 and K805, were found to be capable of significantly inhibiting the catalytic activity of the 17β-HSD10 enzyme. Values shown are an average taken from two independent experiments each with three technical repeats ± SEM. Statistical analysis was performed using GraphPad Prism and a one-way ANOVA with Bonferonni multiple comparisons. * = P ≤ 0.05, ** = P ≤ 0.01, *** = P ≤ 0.001, **** = P ≤ 0.0001.

A second screen, performed at a lower 25 µM concentration, identified compound K801 as the most potent inhibitor within this series (Figure 3.18).

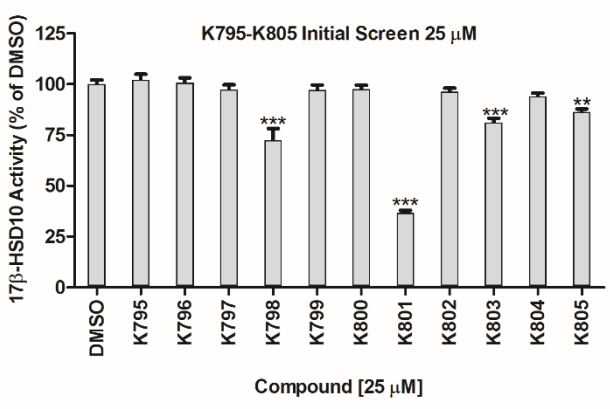

Figure 3.18. 17β-HSD10 activity in the presence of compounds K795-K805 at 25 µM. A subsequent screen of the synthesised frentizole derivatives was performed at 25 µM. At this concentration 4 compounds, K798, K801, K803 and K805, were found to be capable of significantly inhibiting the catalytic activity of the 17β-HSD10 enzyme. Values shown are an average taken from two independent experiments each with three technical repeats ± SEM. Statistical analysis was performed using GraphPad Prism and a one-way ANOVA with Bonferonni multiple comparisons. * = P ≤ 0.05, ** = P ≤ 0.01, *** = P ≤ 0.001, **** = P ≤ 0.0001.

As was seen previously with compounds K690 and K691 (Figures 3.15 and 3.16), substitution of the phenylurea moiety with a hydoxyl group in the *para* position and chloro group in the *meta* position was found to give rise to the highest level of enzyme inhibition, seen here with compound K801.

3.07 K690, K691 and K801 Dose-Response Curves:

Whilst an initial compound screen using a single fixed concentration is useful for identifying compounds capable of inhibition, it does little to describe their relative potencies, making meaningful comparisons between inhibitors difficult. The generation of dose response curves and the calculation of IC_{50} values provides a much more descriptive assessment of potency and allows robust comparisons between compounds of interest, critical for the assessment of subsequent generations of, hopefully, more potent series of compounds.

Dose response curves were generated for compounds K690, K691 and K801 (Figure 3.19, A, B and C). As would be expected given their close structural similarity all three compounds were found to be similarly potent, with IC_{50} values of 1.89 µM (95% CI = 1.52-2.35), 1.67 µM (95% CI = 1.30-2.13) and 1.94 µM (95% CI = 1.75-2.10) calculated for compounds K690, K691 and K801, respectively. At saturation, all three inhibitors were found to result in incomplete inhibition of the 17β-HSD10 enzyme with approximately 30-40% residual activity observed.

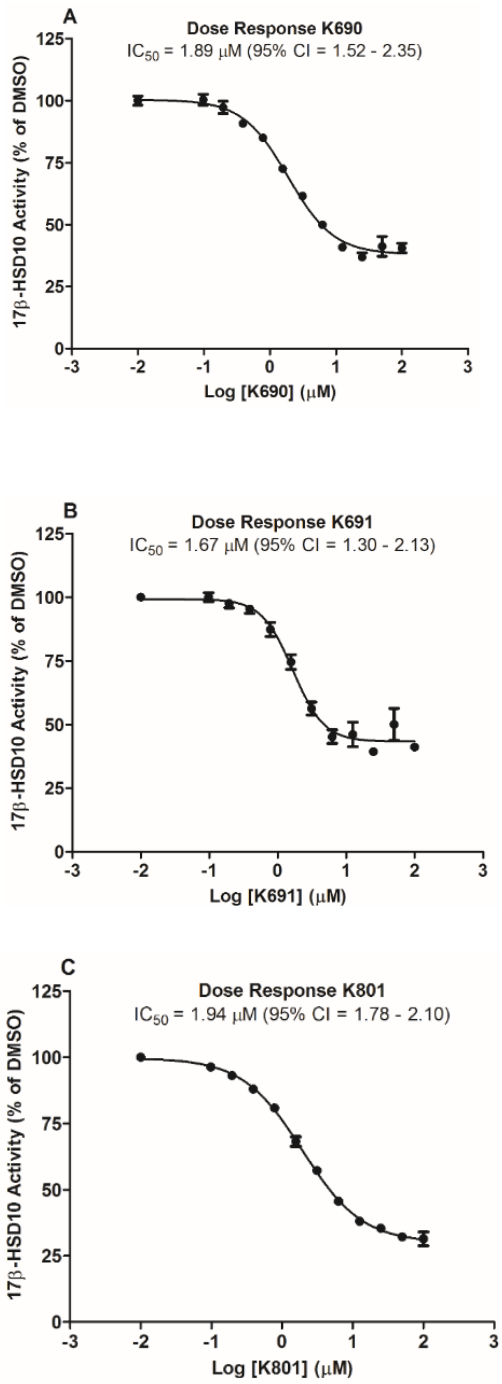

Figure 3.19. Dose response K690, K691, K801. 17β-HSD10 activity was measured in the presence of increasing concentrations of compound K690, K691 and K801. IC_{50} values of 1.89 µM (95% CI= 1.52-2.35), 1.67 µM (95% CI= 1.30-2.13) and 1.94 µM (95% CI= 1.78-2.10) were calculated for compounds K690, K691 and K801 respectively. Values shown are an average of two independent experiments each with three technical repeats ± SEM

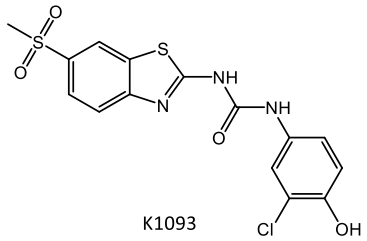

K1093

Figure 3.20. Structure K1093. Additional series of compounds were designed on the basis of inhibitors K690 and K691. Various substitutions of the benzothiazole moiety were trialled with the aim of improving potency and solubility. Compound K1093 was found to be both more potent and more soluble than K690 and K691.

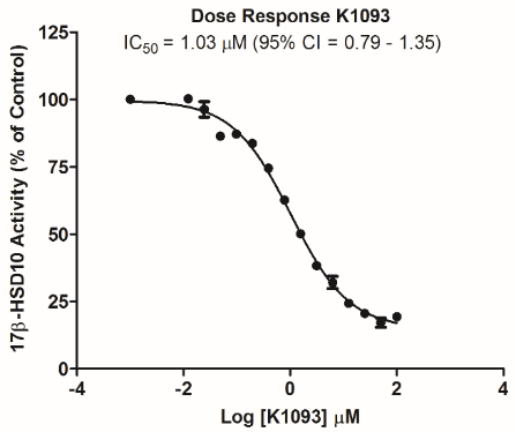

Figure 3.21. Dose Response K1093. 17β-HSD10 activity was measured in the presence of increasing concentrations of compound K1093. An IC_{50} value of 1.03 μM (95% CI = 0.79-1.35) was calculated for compound K1093. Values shown are an average of two independent experiments each with three technical repeats ± SEM

Compound K801 is substituted with an additional chloro group on the phenylurea moiety, as compared to compounds K690 and K691, resulting in a compound with less favourable physiochemical properties and no corresponding increase in potency. As such, it was deemed a less promising candidate and was not further pursued.

Subsequent generations of compounds with alternative substitutions of the benzothiazole moiety were designed on the basis of inhibitors K690, K691 and K801. The screening of these compounds, performed by Becka Hughes, a Masters student in the lab, identified compound K1093 (Figure 3.20) as being both more potent and more soluble than the parent molecules, as indicated by the lower IC_{50} value and the lower residual activity observed at saturation (Figure 3.21). Compound K1093 was thus passed forward into further testing.

3.08 K690 and K691 Mechanism of Inhibition:

Arguably, the gold standard for understanding the mechanism by which an enzyme inhibitor exerts its effect is through the generation of a crystal structure of the enzyme-inhibitor complex, allowing a detailed understanding of the interactions formed and the subsequent rational design of molecules with enhanced potency and specificity. Whilst a number of crystal structures of the 17β-HSD10 enzyme have been published previously (PDB identifiers: 2O23, 1U7T, 1SO8), our group has been unable to replicate these results. As such, in an attempt to characterise the mechanism of inhibition utilised by compounds K690 and K691, a kinetics based appraisal was instead undertaken.

By assessing their effect on the Michaelis-Menten parameters, V_{max} and K_m, enzyme inhibitors can be placed into three main classes; competitive, non-competitive and uncompetitive. Competitive inhibitors are typically structural analogues of either substrate or cofactor and occupy the substrate or cofactor binding site. In doing so, competitive inhibitors prevent reactant binding via steric-occlusion and thereby halt catalysis. In the presence of increasing concentrations of substrate/cofactor the inhibitor molecule will eventually be outcompeted, giving a restoration in enzymatic activity. Thus, in the presence of a competitive inhibitor, V_{max} will remain constant but a higher concentration of substrate will be required to reach it, indicated by an elevation in the value of K_m. Non-competitive inhibitors bind outside of the active site and therefore increasing concentrations of substrate/cofactor will be unable to relieve inhibition. As such, V_{max} will be reduced but as the binding of the inhibitor does not alter the binding of cofactor or substrate, K_m will remain constant. Uncompetitive inhibitors bind solely to the enzyme-substrate complex resulting in a decrease in V_{max} and a corresponding decrease in K_m.

Traditionally, Lineweaver-Burk plots have been used to determine the values of V_{max} and K_m from Michaelis-Menten curves, providing a linear transformation of such data. However, the transformation used (1/V vs 1/[S]) results in unequal error distribution across the dataset potentially influencing results[353]. The Hanes-Woolf transformation ([S]/V vs [S]) gives a more uniform distribution of error and likely more accurate estimations of kinetic parameters[353]. With the invention of computers and the comparative ease with which non-linear regression analysis can now be performed, both have been superseded but remain useful for providing a visual representation of the data. As such, Hanes-Woolf plots were used to visually display the produced kinetic data, whilst absolute values for V_{max} and K_m were determined via non-linear regression using GraphPad Prism and the Michaelis-Menten equation.

With respect to NADH, both K690 and K691 were found to act via a non-competitive mechanism of inhibition. Both inhibitors were found to induce a reduction in V_{max}, indicated by an increase in the slope of the line, with no apparent change in K_m, as shown by the convergence on the x-axis (Figure 3.22). These results indicate that the binding of NADH and the binding of inhibitor are not mutually exclusive and that increasing concentrations of NADH are not able to prevent inhibition. As such, it can be reasoned that compounds K690 and K691 are not binding to the cofactor binding site.

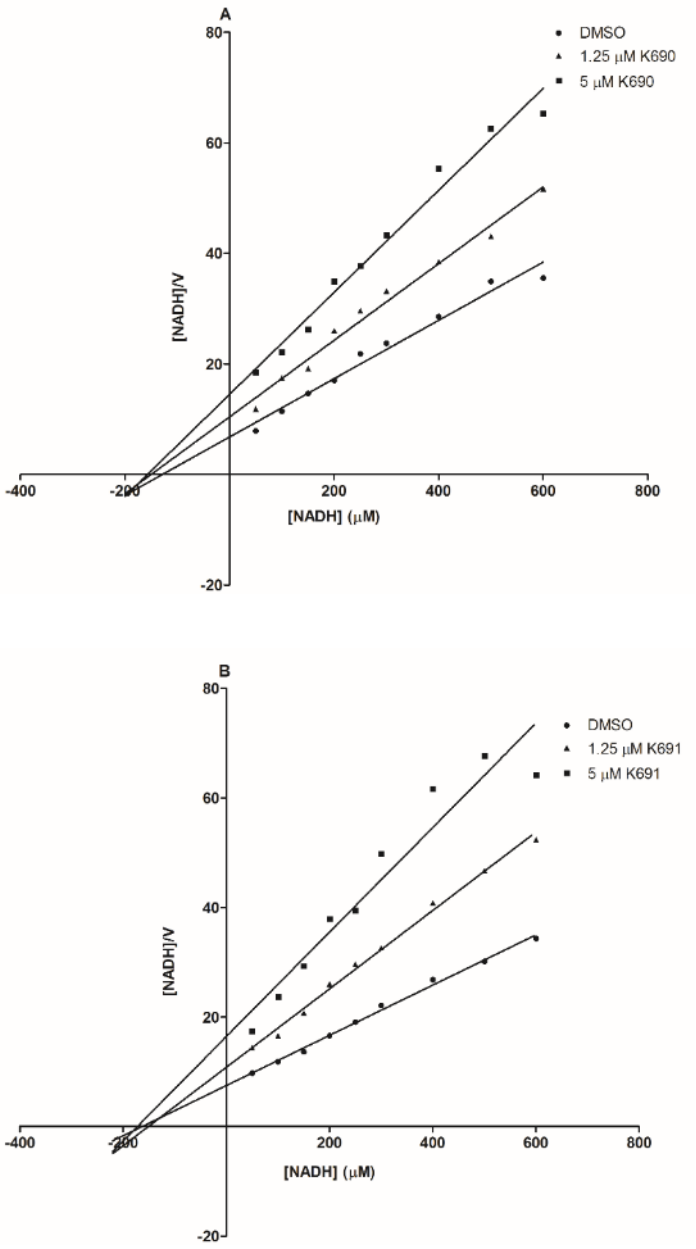

Figure 3.22. Hanes-Woolf plot: K690 and K691 vs NADH. Initial velocities of the 17β-HSD10 enzyme were measured with the indicated concentrations of NADH, both in the absence and presence of compounds K690 (A) and K691 (B) (1.25 μM and 5 μM). Values shown are an average of two independent experiments, each with two technical repeats.

Such conclusions are supported by the values of V_{max} and K_m as determined by non-linear regression using the Michaelis-Menten equation. In the presence of either inhibitor, V_{max} was found to be significantly decreased whilst K_m was unchanged (Table 3.03).

Table 3.03. Effect of compounds K690 and K691 on V_{max} and K_m, with respect to NADH. Compounds K690 and K691 were found to induce a significant decrease in V_{max} with no significant alteration in K_m. Values shown are an average of two independent experiments each with two technical repeats. Statistical analysis was performed with GraphPad Prism using a sum of squares F-test. NS = P > 0.05, * = P ≤ 0.05, ** = P ≤ 0.01, *** = P ≤ 0.001, **** = P ≤ 0.0001.

	V_{max} (µmol min^{-1} mg^{-1})	Significance	K_m	Significance
DMSO	18.28 ± 0.99		115.2 ± 20.27	
1.25 µM K690	14.21 ± 0.75	*	145.3 ± 22.09	NS
5 µM K690	10.56 ± 0.57	***	146.2 ± 22.74	NS
DMSO	21.51 ± 0.58		157.3 ± 11.92	
1.25 µM K691	15.04 ± 1.02	***	176.2 ± 31.78	NS
5 µM K691	10.24 ± 1.05	****	162.6 ± 45.70	NS

With respect to substrate, acetoaceyl-CoA, both K690 and K691 were found to act via a mixed non-competitive mechanism of inhibition, as shown by both the slope of the line and the x-intercept being altered in the presence of either compound, indicative of a reduction in both V_{max} and K_m and suggesting compounds K690 and K691 are able to bind to both the free enzyme and to the enzyme-substrate complex with differing affinities for each (Figure 3.23).

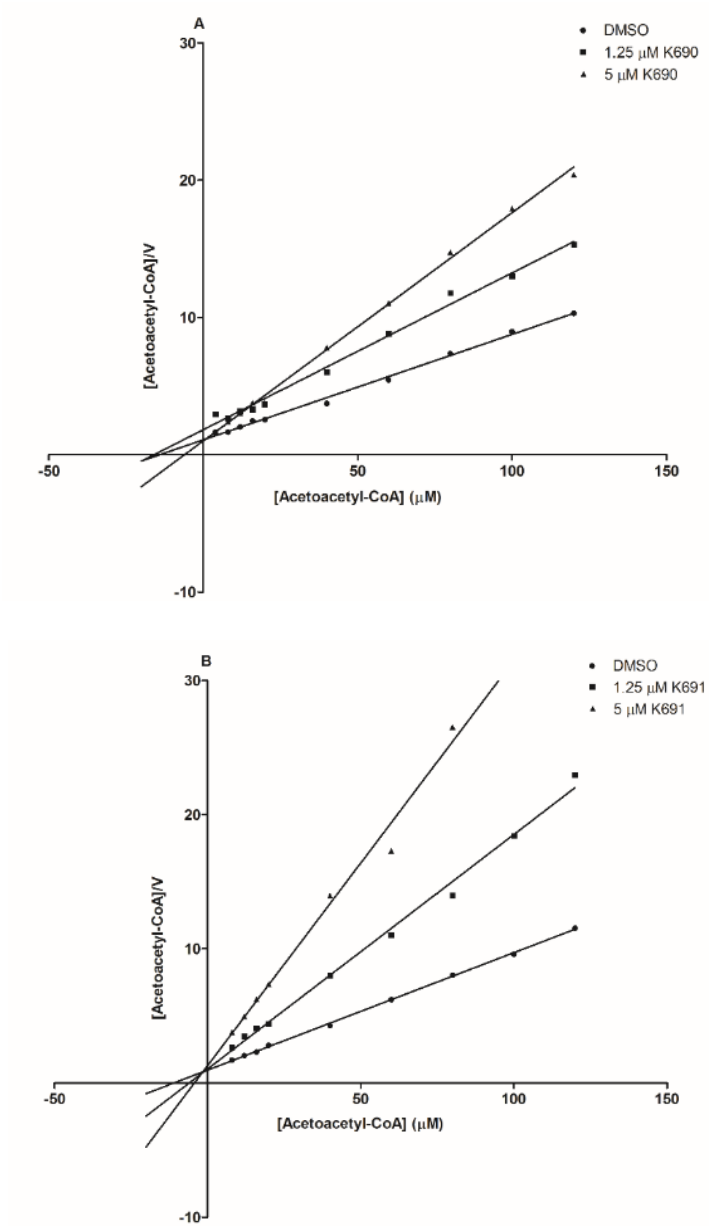

Figure 3.23. Hanes-Woolf plot: K690 and K691 vs acetoacetyl-CoA. Initial velocities of the 17β-HSD10 enzyme were measured with the indicated concentrations of acetoacetyl-CoA, both in the absence and presence of compounds K690 (A) and K691 (B) (1.25 μM and 5 μM). Values shown are an average of two independent experiments, each with two technical repeats.

Such conclusions are supported by the results of non-linear regression analysis using GraphPad Prism and the Michaelis-Menten equation. With respect to acetoacetyl-CoA, compounds K690 and K691 were found to induce a significant decrease in both V_{max} and K_m (Table 3.04).

Table 3.04. Effect of compounds K690 and K691 on V_{max} and K_m with respect to acetoacetyl-CoA. Compounds K690 and K691 were found to induce a significant decrease in both V_{max} and K_m. Values shown are an average of two independent experiments each with two technical repeats. Statistical analysis was performed with GraphPad Prism using a sum of squares F-test. NS = P > 0.05, * = P ≤ 0.05, ** = P ≤ 0.01, *** = P ≤ 0.001, **** = P ≤ 0.0001.

	V_{max} (µmol min^{-1} mg^{-1})	Significance	K_m	Significance
DMSO	13.23 ± 0.39		14.52 ± 1.51	
1.25 µM K690	8.63 ± 0.28	****	14.32 ± 1.64	NS
5 µM K690	6.01 ± 0.29	****	4.73 ± 1.25	***
DMSO	11.53 ± 0.14		11.49 ± 0.54	
1.25 µM K691	6.01 ± 0.15	****	8.36 ± 0.91	**
5 µM K691	3.42 ± 0.17	****	5.12 ± 1.34	**

3.09 K690 and K691 Small Molecule Aggregation Test:

A frequent problem encountered during small molecule screening is the identification of false positives. Often, small molecules form aggregates which sequester and inactive enzyme molecules in a non-specific fashion, yielding what appear promising hits[354]. To test this, enzyme activity can be measured with a suspected inhibitor both in the presence and absence of a detergent, such as Triton X-100[354]. The addition of detergent will disrupt aggregate formation and thus if enzyme activity were to be restored in the presence of Triton X-100, it would imply that the inhibitor is indeed acting via a non-specific aggregation based mechanism. The effect of compounds K690 and K691 on enzyme activity was assessed in the presence and absence of two concentrations of Triton X-100. In both cases no reversal of inhibition was observed suggesting a non-specific aggregation based mechanism is not at work (Figure 3.24).

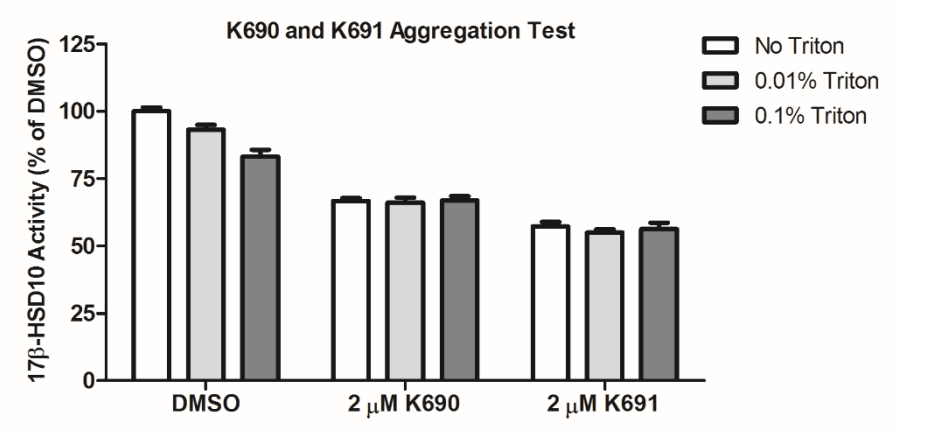

Figure 3.24. Small molecule aggregation test. 17β-HSD10 activity was assessed with 2μM K690, K691 or DMSO both in the presence and absence of Triton X-100 (0.1%, 0.01%). In both cases, no reversal of inhibition was observed in the presence of Triton X-100. Values shown are an average of one experiment with three technical repeats ± SEM.

In addition, a check was made for known troublesome chemical motifs using the Pan Assay Interference Compounds (PAINS) database, a web-based tool aimed at the identification of compounds likely to exert a biological effect in a non-specific manner[355]. A database search was performed using the structures of compounds K690 and K691, with no reported issues.

3.10 K690, K691 and AG18051 - Reversible/Irreversible Inhibition

Depending upon the nature of the interaction formed between protein and ligand, enzyme inhibition can be either reversible or irreversible in nature. To test whether the mechanism of action used by compounds K690, K691 and AG18051 was reversible or irreversible, the 17β-HSD10 enzyme was treated with a saturating dose of inhibitor molecule (12.5 µM for K690/K691 and 0.39 µM for AG18051) and subsequently diluted into well solution containing an equivalent concentration of inhibitor molecule, yielding no net dilution, or no inhibitor molecule, yielding a dilution to a non-saturating dose. If reversible, activity should be restored upon dilution. In all cases, enzyme activity was found to be restored upon dilution, indicating all three inhibitors act via a reversible mechanism (Figure 3.25).

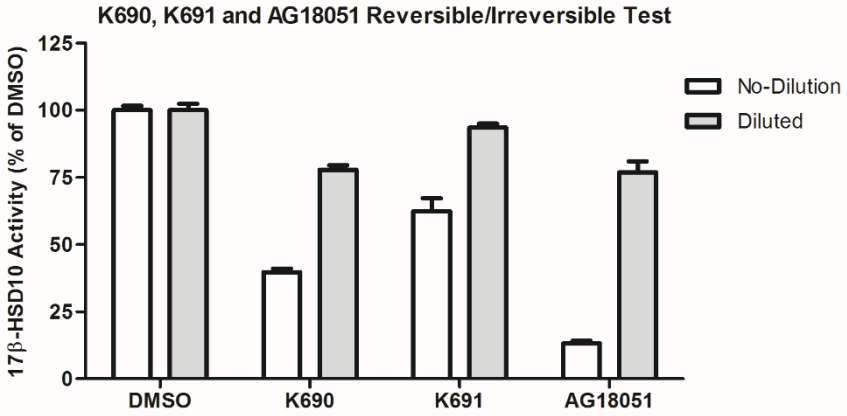

Figure 3.25. K690, K691, AG18051 reversible/irreversible inhibition. 17β-HSD10 was treated with a saturating dose of compounds K690, K691 or AG18051 and subsequently diluted into well solution containing an equal concentration of inhibitor (no dilution) or no-inhibitor (diluted). Following dilution, 17β-HSD10 activity was seen to be restored, indicating all three inhibitors act via a reversible mechanism of inhibition. Values shown are an average of one experiment with three technical repeats ± SEM.

3.11 Frentizole Derivatives - Differential Scanning Fluorimetry

Through the use of an enzyme activity assay, we have identified three novel, reasonably potent inhibitors of the 17β-HSD10 enzyme, termed K690, K691 and K1093. To confirm suspected hit compounds a second independent technique is often employed, reducing the chance of such hits being an artefact of the primary screening methodology. As confirmation of a direct interaction between the 17β-HSD10 enzyme and compounds K690, K691 and K1093, differential scanning fluorimetry (DSF/thermal shift/thermofluor) was utilised.

When correctly folded, hydrophobic residues in the primary structure of a protein are held within the core of the tertiary structure, sequestered away from water in the external environment. Depending upon the nature of the protein, this tertiary structure has an intrinsic stability, which can be measured using DSF as the temperature at which the protein becomes denatured. SYPRO orange, a fluorophore which shows low fluorescence in an aqueous environment, but marked fluorescence in a hydrophobic environment, is employed for this purpose. As the temperature of the reaction is increased, the protein of interest will at a certain point become denatured, exposing the hydrophobic core and allowing SYPRO orange to bind and resulting in a peak in fluorescence. Therefore, the melting temperature (T_m) of a protein can be determined as a function of SYPRO orange fluorescence. The binding of ligand to protein will often result in a stabilisation or destabilisation of the tertiary structure, measured here as an increase or decrease in T_m, providing direct biophysical evidence of an interaction being formed[356].

An initial range-finding experiment was performed to identify optimal concentrations of SYPRO orange and 17β-HSD10 protein, giving a high signal to noise ratio and a sharp transition from the native to denatured state. A combination of x 20 SYPRO Orange (absolute concentration not published) and 10 µM 17β-HSD10 was found to give the highest signal to noise ratio (approximately 5-fold) and a sharp transition, whilst also using a reasonable amount of protein. Using an initial buffer system of 50 mM HEPES (pH 8.2) and 0.5 M NaCl, a T_m of 55.32 ± 0.01°C was calculated for 17β-HSD10.

To validate that the DSF experiment was functioning correctly and was capable of detecting a known protein-ligand interaction, GraphPad Prism and the Boltzmann sigmoidal curve fit equation were used to calculate T_m values for both the free enzyme, and the enzyme in the presence of increasing concentrations of NADH, a known binding partner of 17β-HSD10. The addition of NADH to the buffer system induced a dose dependent increase in T_m from 56.28 ± 0.10°C for the free enzyme to 63.16 ± 0.02°C with 5 mM NADH (Figure 3.26, Table 3.05), validating that the DSF experiment was functioning correctly.

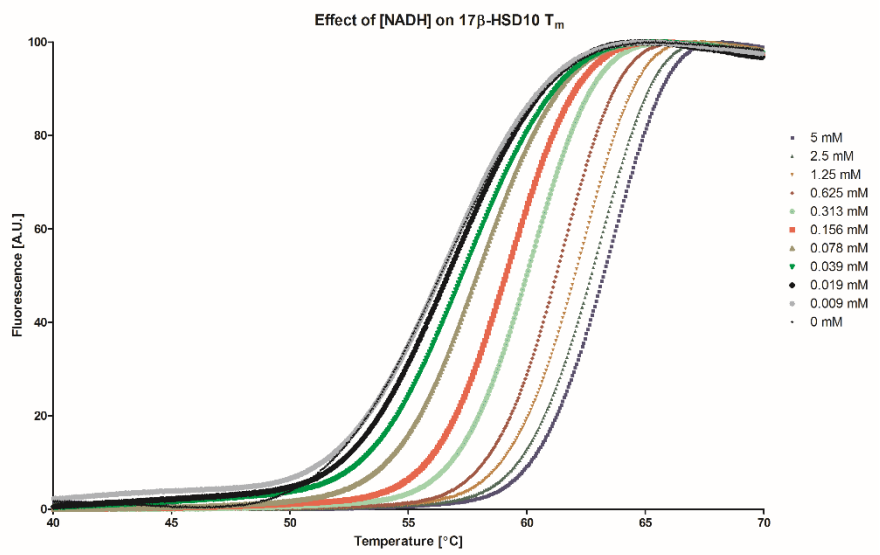

Figure 3.26. Melt-profile of 17β-HSD10 in the presence of increasing concentrations of NADH. The melting temperature of the 17β-HSD10 enzyme was measured in the presence of increasing concentrations of NADH. Binding of NADH was found to result in a dose dependent increase in T_m. Values shown are an average of raw fluoresence taken from two experiments each with three technical repeats. For clarity, error bars have been omitted.

Table 3.05. Effect of increasing NADH concentration on 17β-HSD10 T_m. Binding of NADH was found to result in a dose dependent increase in the T_m value of the 17β-HSD10 enzyme. Values shown are an average of best-fit T_m values taken from two independent experiments each with three technical repeats, relative to the free enzyme.

[NADH] mM	ΔT_m (°C)	SEM
0.00	0.00	0.12
0.02	0.25	0.14
0.04	0.88	0.02
0.08	1.62	0.11
0.16	2.74	0.02
0.31	3.58	0.09
0.63	4.85	0.06
1.25	5.62	0.08
2.50	6.32	0.03
5.00	6.88	0.07

With the assay validated, compounds K690 and K691 were screened against the free 17β-HSD10 enzyme at 25 µM. However, no change in T_m was observed in the presence of either compound.

Based upon previous kinetic based experiments (Section 3.08), inhibitors K690 and K691 act via a non-competitive mechanism of inhibition with respect to cofactor, NADH, and thus the binding of NADH does not impact upon the binding of either inhibitor molecule. However, a mixed mechanism of inhibition was observed with respect to substrate, acetoacetyl-CoA suggesting K690 and K691 are capable of binding to both the free enzyme and the enzyme substrate complex, with differing affinities for each. As such, compounds K690 and K691 may preferentially bind to the enzyme-substrate complex, explaining the lack of a shift in T_m with the free enzyme. A dose-response experiment was performed using acetoacetyl-CoA in an attempt to identify a saturating concentration against which compounds K690 and K691 could be screened.

At the lower concentrations of acetoacetyl-CoA tested, no alternation in T_m was apparent. A modest decrease in T_m was observed at higher concentrations (Figure 3.27, Table 3.06).

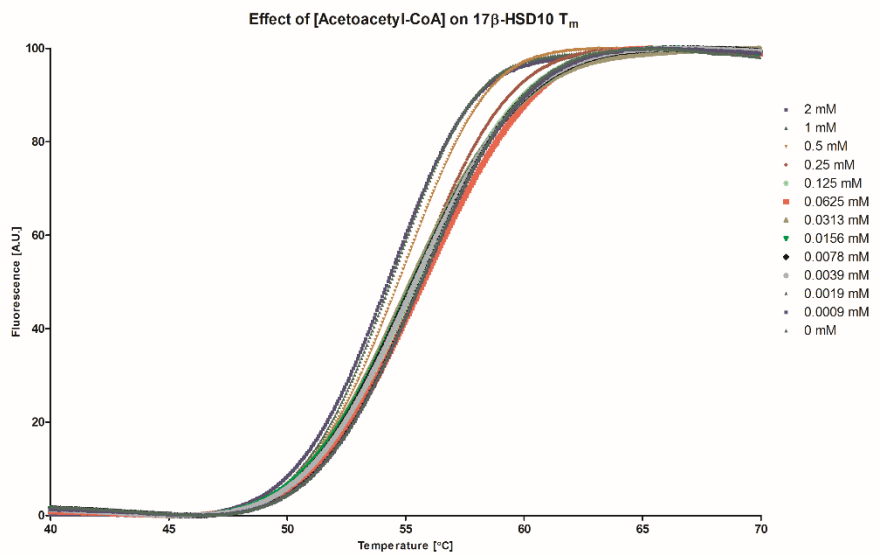

Figure 3.27. Melt-profile of 17β-HSD10 in the presence of increasing concentrations of acetoacetyl-CoA. The melting temperature of the 17β-HSD10 enzyme was measured in the presence of increasing concentrations of acetoacetyl-CoA. At the higher concentrations tested, a dose dependent decrease in T_m was seen. Values shown are an average of raw fluoresence taken from two experiments each with three technical repeats. For clarity, error bars have been omitted

Table 3.06. Effect of increasing acetoacetyl-CoA concentration on 17β-HSD10 T_m. Binding of acetoacetyl-CoA was found to result in a dose dependent decrease in the T_m value of the 17β-HSD10 enzyme. Values shown are an average of best-fit T_m values taken from two independent experiments each with three technical repeats, relative to the free enzyme.

[Acetoacetyl-CoA] mM	ΔT_m (°C)	SEM
0.00	0.00	0.20
0.13	-0.28	0.07
0.25	-0.43	0.08
0.50	-1.17	0.16
1.00	-1.32	0.12
2.00	-1.59	0.07

Based on previously derived K_m values, acetoacetyl-CoA should have a higher affinity for the 17β-HSD10 enzyme as compared to NADH (Chapter 3: Section 3.03). Using DSF, a measurable shift in T_m was observed at NADH concentrations as low as 0.04 mM and as such, a shift in T_m due to the binding of acetoacetyl-CoA would be expected at or below 0.04 mM, however, this was not observed (Figure 3.27, Table 3.06). Two possibilities may underlie the lack of a shift in T_m observed with acetoacetyl-CoA, either the binding of this molecule gives rise to no marked alteration in the stability of the 17β-HSD10 enzyme, or, the reaction may progress via an order sequential mechanism with the binding of acetoacetyl-CoA being dependent on the 17β-HSD10 enzyme having already bound cofactor. The addition of NADH to the reaction system would provide all necessary components for catalysis, and thus there would be continually changing levels of reactants in the reaction mixture until an equilibrium was reached, potentially influencing results.

NAD^+ is identical to NADH, with the exception of a single hydrogen atom and so any conformational changes in the 17β-HSD10 enzyme observed with NADH are likely to also be seen with NAD^+, however catalysis of acetoacetyl-CoA would not occur. Thus, a dose response experiment was performed using NAD^+ in place of NADH. As before, with increasing cofactor concentration, a dose dependent increase in T_m was observed (Figure 3.28, Table 3.07). However, the maximum increase in T_m was found to be lower with NAD^+ as compared to NADH, 3.38°C and 6.88°C respectfully, suggesting the conformational changes associated with the binding of each molecule may not be identical.

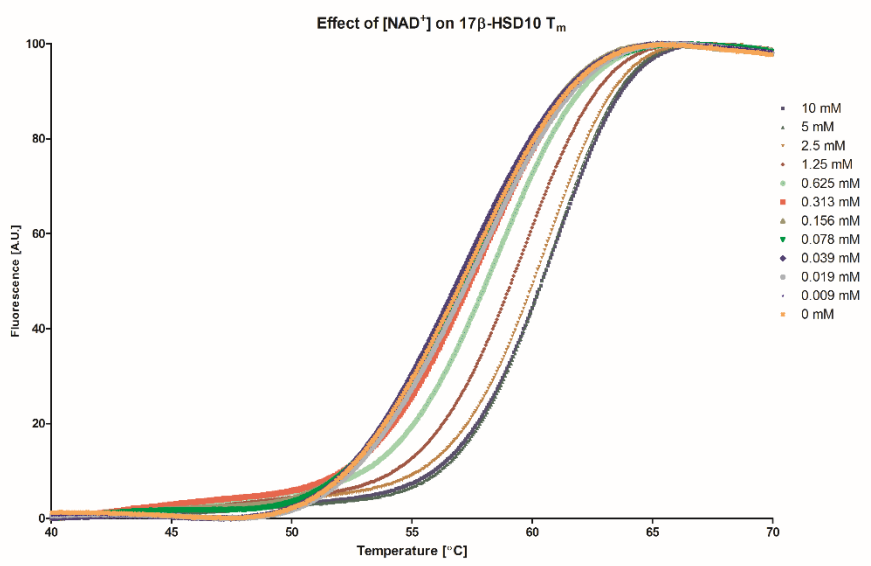

Figure 3.28. Melt-profile of 17β-HSD10 in the presence of increasing concentrations of NAD⁺. The melting temperature of the 17β-HSD10 enzyme was measured in the presence of increasing concentrations of NAD⁺. Binding of NAD⁺ was found to induce a dose dependent increase in T_m. Values shown are an average of raw fluoresence taken from two experiments each with three technical repeats. For clarity, error bars have been omitted.

Table 3.07. Effect of increasing NAD⁺ concentration on 17β-HSD10 T_m. Binding of NAD⁺ was found to result in a dose dependent increase in the T_m value of the 17β-HSD10 enzyme. Values shown are an average of best-fit T_m values taken from two independent experiments each with three technical repeats, relative to the free enzyme.

[NAD⁺] mM	ΔT_m (°C)	SEM
0.00	0.00	0.09
0.31	0.29	0.08
0.63	1.13	0.09
1.25	2.03	0.12
2.50	2.97	0.09
5.00	3.34	0.03
10.00	3.40	0.13

Irrespective, a saturating concentration of 5 mM NAD⁺ was passed forward and a titration of acetoacetyl-CoA concentrations again tested. In contrast to the free enzyme, in the presence of 5 mM NAD⁺ a dose dependent elevation in T_m was observed with increasing acetoacetyl-CoA concentration, indicating that high affinity binding of acetoacetyl-CoA is dependent on the enzyme having previously bound cofactor, and thus suggesting that the reaction does indeed proceed via an order sequential mechanism (Figure 3.29, Table 3.08). As was seen previously in the absence of cofactor, at the highest concentrations of acetoacetyl-CoA tested this elevation in melting temperature was reversed, with a decrease in T_m observed.

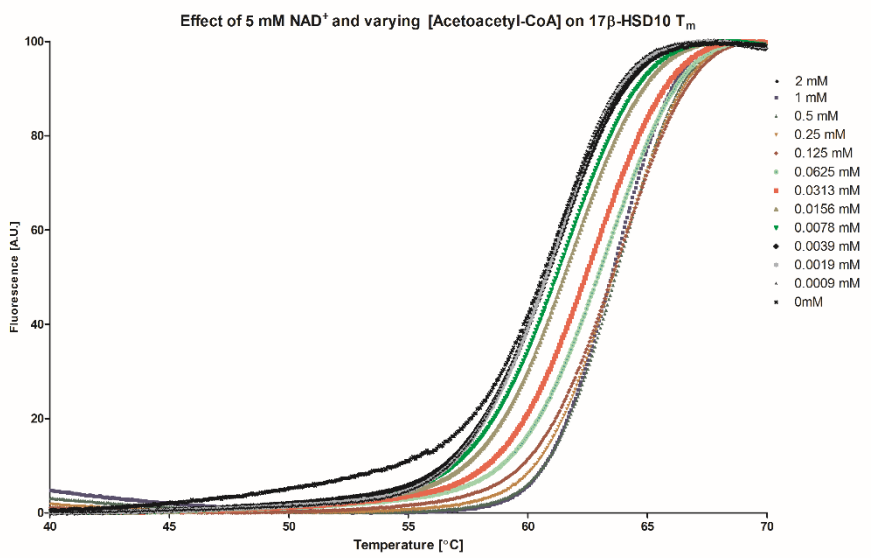

Figure 3.29. Effect of increasing acetoacetyl-CoA concentration on the melting temperature of the 17β-HSD10 enzyme in the presence of 5 mM NAD⁺. In the presence of a saturating concentration of NAD^+, a dose dependent increase in T_m was observed with increasing acetoacetyl-CoA concentration. At the highest concentrations of acetoacetyl-CoA tested this stabilisation was seen to be reversed, indicated via a decrease in T_m. Values shown are an average of raw fluoresence taken from two experiments each with three technical repeats. For clarity, error bars have been omitted

Table 3.08. Effect of increasing acetoacetyl-CoA concentration on the melting temperature of the 17β-HSD10 enzyme in the presence of 5 mM NAD⁺. In the presence of a saturating concentration of NAD^+, a dose dependent increase in T_m was observed with increasing acetoacetyl-CoA concentration. At the highest concentrations of acetoacetyl-CoA tested this stabilisation was seen to be reversed. Values shown are an average of best-fit T_m values taken from two independent experiments each with three technical repeats, relative to the free enzyme.

5 mM NAD^+ + [Acetoacetyl-CoA] mM	ΔT_m (°C)	SEM
0.000	0.00	0.08
0.002	0.07	0.03
0.004	0.20	0.08
0.008	0.56	0.04
0.016	1.09	0.10
0.031	1.74	0.03
0.063	2.20	0.05
0.125	2.66	0.13
0.250	2.81	0.10
0.500	3.06	0.04
1.000	2.65	0.16
2.000	2.54	0.04

A saturating concentration of both NAD^+ (5 mM) and acetoacetyl-CoA (0.5 mM) were utilised for the screening of compounds K690 and K691, but again no consistent alteration in T_m was observed.

Compound K1093, a derivative of K690 and K691, shows both improved aqueous solubility and enhanced potency against the free 17β-HSD10 enzyme (Section 3.07). As such, this compound was similarly screened using DSF. In this instance, a dose dependent increase in T_m was observed, indicative of a direct interaction between inhibitor and the 17β-HSD10 enzyme (Figure 3.30, Table 3.09). This increase was only apparent at 25 µM and above, beyond the limit of solubility profile of compounds K690 and K691.

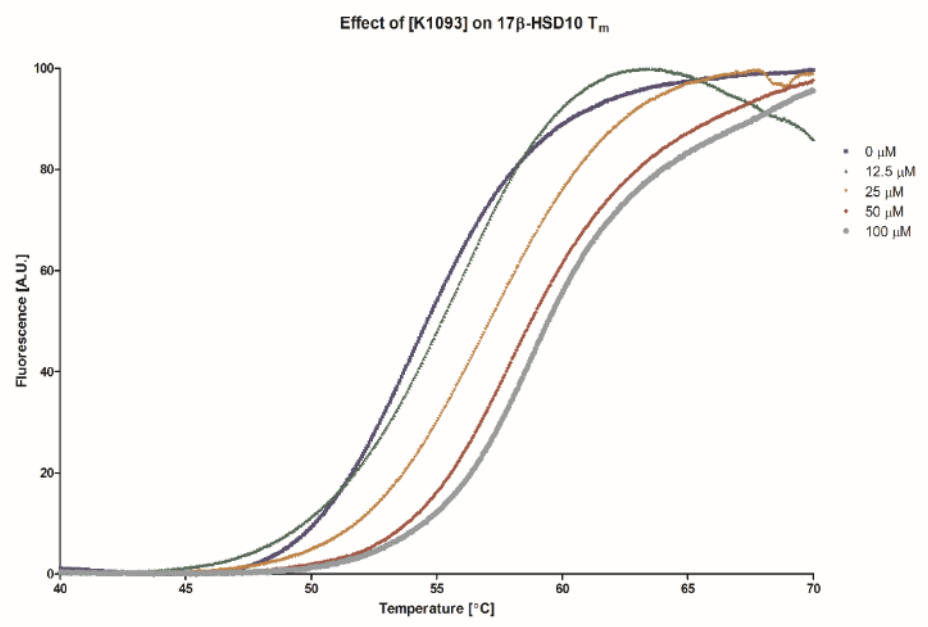

Figure 3.30. Effect of increasing concentrations of K1093 on the melting temperature of the 17β-HSD10 enzyme. A dose dependent increase in T_m was observed in the presence of increasing concentrations of compound K1093 Values shown are an average of raw fluoresence taken from two experiments each with three technical repeats. For clarity, error bars have been omitted.

Table 3.09. Effect of increasing concentrations of K1093 on the melting temperature of the 17β-HSD10 enzyme. A dose dependent increase in T_m was observed in the presence of increasing concentrations of compound K1093. Values shown are an average of best-fit T_m values taken from two independent experiments each with three technical repeats, relative to the free enzyme.

[K1093] µM	ΔT_m (°C)	SEM
0	0.00	0.07
12.5	0.20	0.09
25	2.49	0.14
50	4.32	0.09
100	5.04	0.06

3.12 Quantifying The 17β-HSD10-Aβ Interaction

In 2006, Xie *et al.* identified Frentizole as a compound capable of disrupting the interaction between the 17β-HSD10 enzyme and Aβ, albeit relatively poorly with an IC_{50} value of approximately 200 μM[344]. Subsequent derivatization of the parent scaffold generated two analogues (here referred to as K710 and K711, Table 3.01) with markedly improved potency against this interaction[344]. Through the use of a 17β-HSD10 based enzyme assay, we have shown that both Frentizole and its derivatives K710 and K711 are unable to directly inhibit the catalytic activity of the 17β-HSD10 (Chapter 3: Section 3.06). However, further modification of the Frentizole scaffold was found to generate three reasonably potent 17β-HSD10 inhibitors, termed K690, K691 and K1093 (Section 3.07). As both the direct inhibition of 17β-HSD10 activity[338], and the disruption of the 17β-HSD10/Aβ interaction[303] have been shown to be of therapeutic merit in treating Alzheimer's disease, we were curious as to whether compounds K690 and K691 would retain the ability to perturb the 17β-HSD10-Aβ complex, potentially allowing both therapeutic avenues to be pursued with a single compound.

Previously, an ELISA based technique was used to investigate the interaction between the 17β-HSD10 enzyme and Aβ[344]. Here, a combination of differential scanning fluorimetry and western blotting was instead used.

Initial experiments employed differential scanning fluorimetry with the aim of identifying a concentration of oligomeric $Aβ_{1-42}$ capable of saturating a given concentration of 17β-HSD10 (10 μM). With increasing $Aβ_{1-42}$ concentration, a dose dependent decrease in T_m was observed, suggesting that the binding of $Aβ_{1-42}$ to 17β-HSD10 results in destabilisation of the tertiary structure of the enzyme. At the higher concentrations of $Aβ_{1-42}$ tested, this reduction in T_m was seen to plateau, indicating saturation of the 17β-HSD10 enzyme (Figure 3.31). In the absence of the 17β-HSD10 enzyme, no marked melt transition was observed, suggesting that either the $Aβ_{1-42}$ protein harbours no hydrophobic core or that the tertiary structure of the protein is too stable to unfold in the temperature range tested. An increase in background fluorescence was however observed, suggesting the surface of the $Aβ_{1-42}$ protein may harbour hydrophobic residues capable of binding to SYPRO-orange. A saturating concentration of 50 μM $Aβ_{1-42}$ was passed forward into western blotting based experiments.

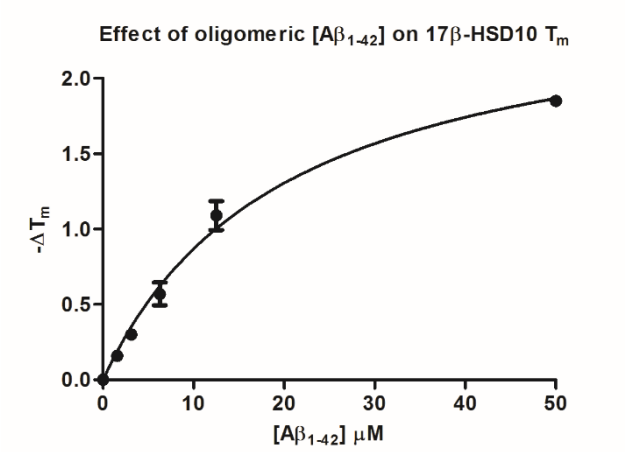

Figure 3.31. Best fit T_m values for the 17β-HSD10 enzyme in the presence of the indicated concentrations of $Aβ_{1-42}$. Oligomeric $Aβ_{1-42}$ was found to induce a dose-dependent decrease in the melting temperature of the 17β-HSD10 enzyme. Values shown are an average taken from two independent experiments, each with three technical repeats ± SEM.

As an initial trial experiment, solutions containing 10 μM 17β-HSD10, 50μM $Aβ_{1-42}$, or the two combined were prepared in assay buffer. Additional samples containing both 17β-HSD10 and $Aβ_{1-42}$ were prepared in the presence of increasing concentrations of compound K711, known to disrupt the interaction between 17β-HSD10 and $Aβ_{1-42}$[344]. Samples were incubated for 1 hr at 4°C after which proteins were resolved using SDS-PAGE and the localisation of the $Aβ_{1-42}$ protein assessed via western blot. A faint band was observed with the 17β-HSD10 enzyme in isolation, subsequently found to be due to non-specific binding of the secondary antibody (Figure 3.32, Lane 1). $Aβ_{1-42}$ was found to give rise to a number of bands, indicating a mixture of oligomeric forms, but none at 27 kDa, the molecular weight of the 17β-HSD10 enzyme (Figure 3.32, Lane 2). Following incubation together, a prominent band was observed at 27 kDa, indicative of an interaction between 17β-HSD10 and $Aβ_{1-42}$ (Figure 3.32, Lane 3). In the presence of increasing concentrations of compound K711, this interaction was found to be disrupted in a dose dependent manner, confirming the work of Xie *et al.,* and validating the assay is capable of identifying compounds which disrupt this interaction (Figures 3.32, Lanes 3-6).

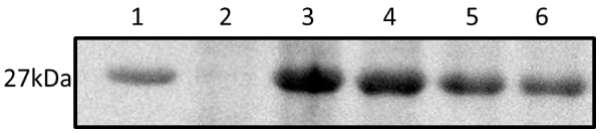

Figure 3.32. Western blot for the 17β-HSD10/$Aβ_{1-42}$ interaction. Samples were prepared containing 17β-HSD10 and Aβ both in isolation and together. Additional samples were prepared containing both 17β-HSD10 and Aβ with varying concentrations of compound K711, known to prevent the 17β-HSD10/Aβ interaction. Samples were subjected to western blot analysis using an anti-amyloid antibody, indicating the presence of an interaction between 17β-HSD10 and Aβ, and the disruption of this interaction by compound K711. Lane 1 = 17β-HSD10, Lane 2 = Aβ, Lane 3 = 17β-HSD10 + Aβ + DMSO, Lane 4 = 17β-HSD10 + Aβ +1.56 μM K711, Lane 5 = 17β-HSD10 + Aβ + 3.125 μM K711, Lane 6 = 17β-HSD10 + Aβ + 6.25 μM K711.

Densitometry based analysis was found to confirm the visual assessment, again showing compound K711 induces a dose dependent decrease in $A\beta_{1-42}$ binding to the 17β-HSD10 enzyme (Figure 3.33).

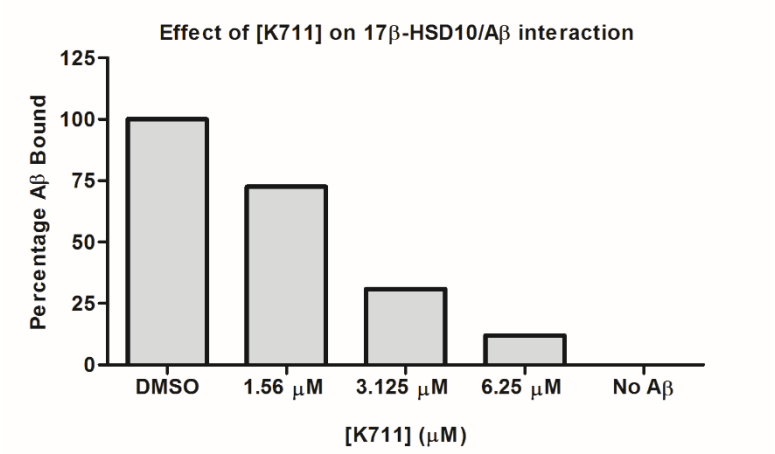

Figure 3.33. Densitometry 17β-HSD10/$A\beta_{1-42}$ interaction. Denistometry based analysis of Figure 3.32 was performed using ImageJ. A dose-dependent decrease in bound $A\beta_{1-42}$ was observed in the presence of increasing concentrations of compound K711.

The experiment was repeated to confirm the observed results but was not found to be consistently reproducable, possibly due to the procedure used to generate monomeric $A\beta_{1-42}$. Due to time constraints, this experiment was not further persued.

3.13 NCI Diversity IV Initial Screen:

Whilst a number of Frentizole derived 17β-HSD10 inhibitors have thus far been identified (Section 3.07) it is unlikely that any one hit scaffold will fulfil all requirements (ie. specific, non-toxic, membrane permeable, potent etc). As such, a decision was made to try and identify additional compound scaffolds capable of 17β-HSD10 inhibition, thereby diversifying the portfolio of compounds available and increasing the chance of success. The National Cancer Institute (NCI) houses an extensive compound library, comprising around 150,000 drug-like molecules, samples of which are available to academic researchers for the cost of shipping and handling. In addition, a diversity set of 1596 pre-plated compounds is also available. This comparatively small library holds compounds representative of the majority of the core scaffolds found within the complete library, allowing smaller screening institutions to sample a much larger chemical space than would otherwise be possible. Each compound within the diversity library typically has a number of structural analogues, which are similarly available and thus the procurement of follow-up samples and the generation of structure-activity relationships are both possible.

In an attempt to identify additional core scaffolds, which could form the basis for subsequent series of 17β-HSD10 inhibitors, an application was made to the NCI for the plated NCI Diversity Library (at the time of application, the fourth iteration) which was subsequently granted. Compounds were supplied as 10 mM stocks in DMSO and were screened using a modification of the aforementioned recombinant 17β-HSD10 screening assay (Materials and Methods: 3.18). Due to the high cost in terms of both labour and consumables, an initial screen of the entire library was run once with promising hit compounds further characterised thereafter.

An initial 100 µM screen of the entire compound library identified a number of potential enzyme inhibitors. Suspected hit compounds were ranked on the basis of residual 17β-HSD10 activity (Table 3.10, see Appendix: D for a more comprehensive list of hit compounds). An effort was made to focus on compounds for which a relatively large number of analogues were available in the hope of generating structure-activity relationships. Compound 17796 was deemed to be of interest due to its small size and relatively high potency, whilst compound 88402 was found to have a large range of analogues available and so was also selected for further evaluation.

Table 3.10. NCI Diversity IV derived 17β-HSD10 inhibitors. An initial screen of the NCI Diversity IV compound library was performed at 100 µM. Compounds were ranked on the basis of residual enzyme activity relative to control (1% DMSO (v/v)).

NSC #	Structure	% Activity
120622	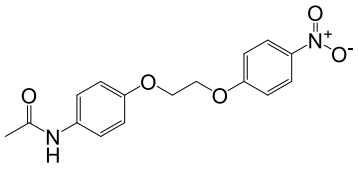	0.70
63001	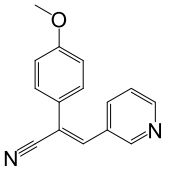	2.99
339161	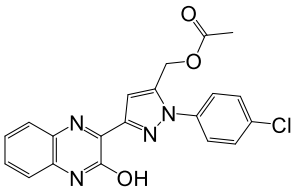	3.77
33005	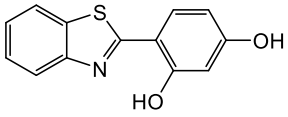	4.27
328111	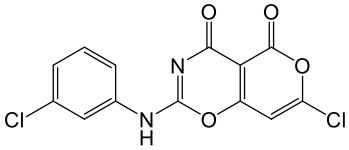	5.54
17796	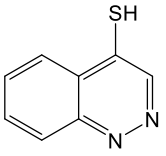	6.28
106231	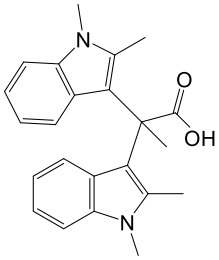	6.67
55453	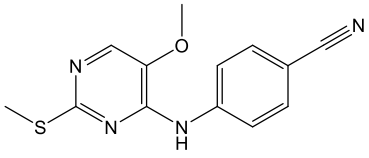	9.00

NSC #	Structure	% Activity
73735	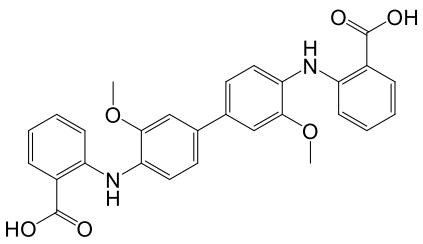	9.37
19063	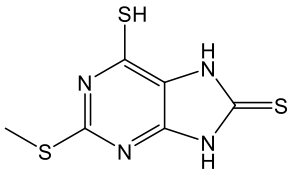	10.33
378719	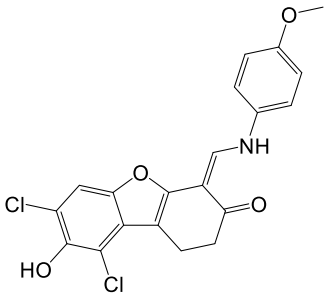	10.54
246415	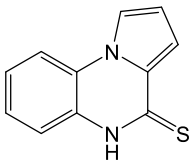	11.01
622608	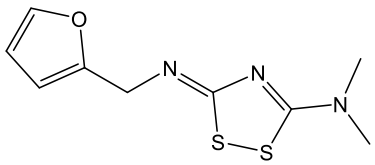	11.80
67307	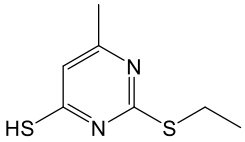	12.04
43013	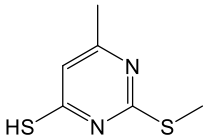	13.22
88402	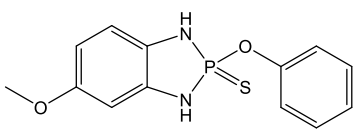	13.34

17796 Analogues

To confirm 17796 as a true hit and in an attempt to generate structure activity relationships, a request was sent for a follow up sample of compound 17796 and also 31 analogues of this molecule. Upon receipt, an initial screen was performed at 100 μM confirming compound 17796 as an active 17β-HSD10 inhibitor and also identifying four related compounds capable of high level enzyme inhibition, NSC numbers: 114063, 350076, 66128 and 77847 (Figure 3.34, Table 3.11).

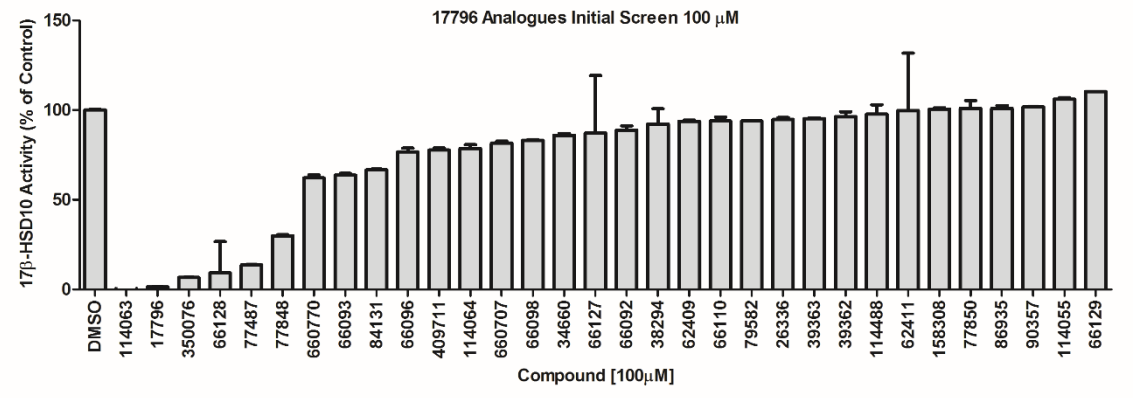

Figure 3.34. Compound 17796 analogues. 31 analogues of compound 17796 were screened at 100 μM, confirming 17796 as a 17β-HSD10 inhibitor and identifying additional inhibitors; compounds 114063, 350076, 66128 and 77847. Values are an average of one experiment with three technical repeats ± SEM

Table 3.11. Molecular structures of 17796 derived 17β-HSD10 inhibitors . The screening of 31 analogues of inhibitor 17796 identified three additional compounds of interest; 114063, 350076 and 77847.

NSC #	Structure
114063	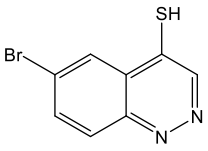
350076	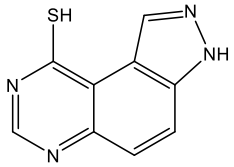
17796	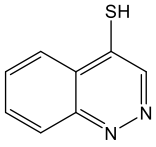
77847	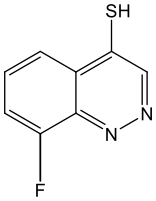

Compounds 114063, 17796, 350076 and 77847 were re-screened at 100 µM and 25 µM, highlighting compounds 114063 and 350076 as the most potent inhibitors identified within this series thus far (Figure 3.35). Compound 66128 was found to interfere with the assay and so was not further pursued.

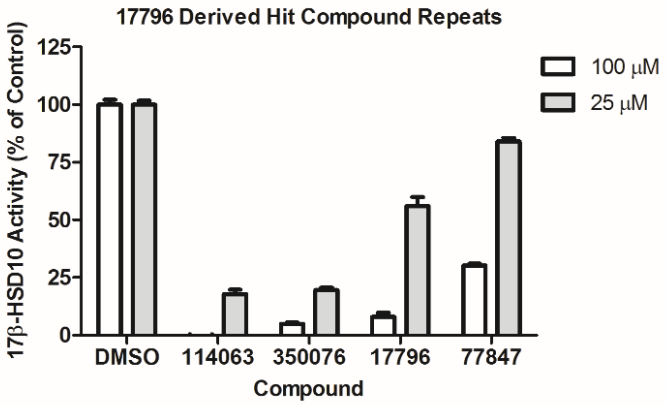

Figure 3.35. 17796 derived 17β-HSD10 inhibitors. Inhibiting compounds derived from compound 17796 were re-screened at 100 µM and 25 µM, identifying compounds 114063 and 350076 as the most potent inhibitors within this series. Values shown are an average taken from two independent experiments, each with three technical repeats ± SEM.

To give a more robust measure of potency, IC_{50} curves were generated for compounds 114063, 350076 and 17796. IC_{50} values of 10.44 µM (95% CI = 9.62-11.33), 7.87 µM (95% CI = 7.36-8.40) and 20.33 µM (95% CI= 16.45-25.12) were calculated for compounds 114063, 350076 and 17796 respectively, again highlighting compounds 114063 and 350076 as the most potent inhibitors identified within this series.

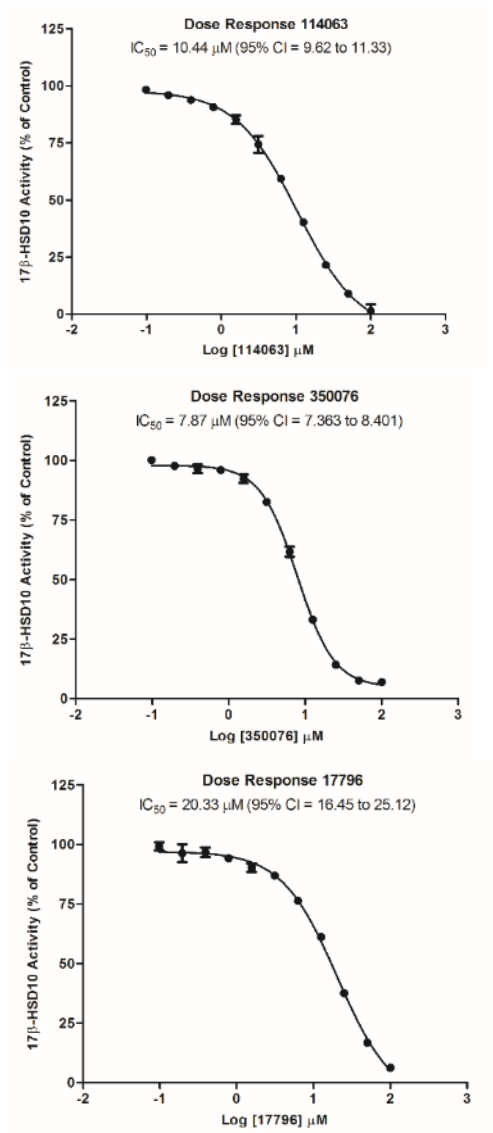

Figure 3.36. Dose-response curves for compound 114063 (Top), 350076 (Middle) and 17796 (Bottom). 17β-HSD10 activity was measured in the presence of increasing concentrations of compounds 114063, 350076 and 17796 with IC_{50} values of 10.44 µM (95% CI = 9.62-11.33), 7.87 µM (95% CI = 7.36-8.40) and 20.033 µM (95% CI = 16.45-25.12) calculated for each compound respectfully. Values shown are an average of two independent experiments each with three technical repeats ± SEM

At this point it was noted that all inhibiting compounds of this series harbour a thiol group, whilst non-inhibiting compounds do not, suggesting that this group may be key for inhibition. To test this hypothesis further, our collaborators in the Czech Republic synthesised a custom series of compounds (Table 3.12: K945-K950). Should the thiol group seen in compounds 11796, 114063 and 350076 be acting as a hydrogen bond donor, compound K947 harbouring a primary amine group should be similarly active. Should the thiol group be acting as a hydrogen bond acceptor compounds K945 and K947, harbouring a keto and primary amine group respectively, should also be active. However, if compounds 11796, 114063 and 350076 are utilising the thiol as a potential nucleophile for disulphide bond formation, only compounds K946, K948 and K950 should be active, each harbouring a thione group, predicted to be in resonance with a thiol.

Table 3.12 Compounds K945-K950. A series of compounds were synthesised with the indicated substiutions with the aim of investigating the mechanism of action utilised by compound 17796 and its analogues 114063 and 350076.

K-Code	Structure
K945	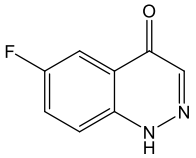
K946	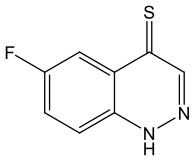
K947	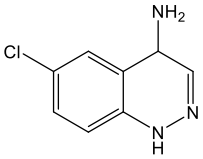
K948	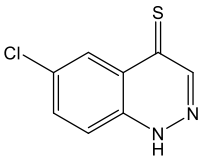
K949	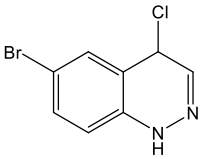
K950	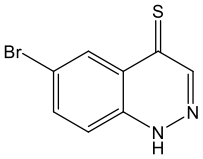

When screened at 100 µM using the in-house 17β-HSD10 assay, only compounds K946, K948 and K950, harbouring a thione group, showed marked inhibitory activity, suggesting that the thiol group is indeed required for inhibition and possibly that a disulphide bridge may be being formed to an active site cysteine residue, although the mechanism by which this may occur is not clear. This inhibition was seen to be reversible upon the addition of DTT, again providing further evidence for such an effect (Figure 3.37).

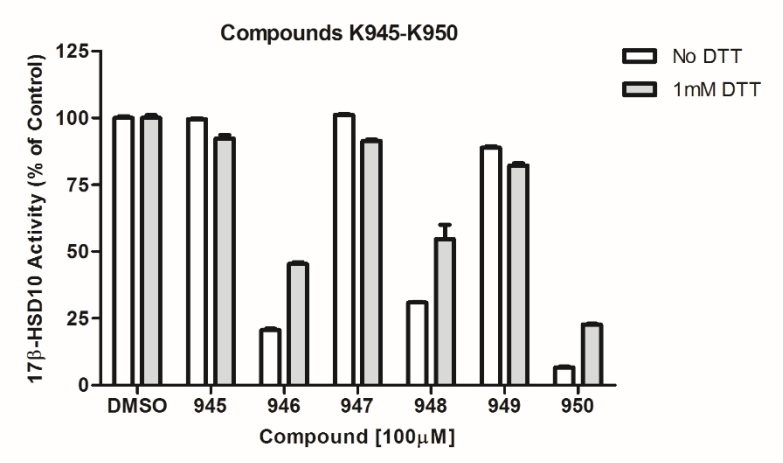

Figure 3.37. 17β-HSD10 inhibition induced by compounds K945-K950. Compounds K945-K950 were assessed for the ability to inhibit the 17β-HSD10 enzyme at 100 μM. Only compounds harbouring a thione group, K946, K948 and K950 were found to induce marked inhibition and this was shown to be reversed by the addition of DTT, suggesting the formation of a disulphide bridge is responsible for the observed inhibition. Values shown are an average of two experiments each with three technical repeats ± SEM.

Upon examination of the crystal structure of the 17β-HSD10 enzyme, an active site cysteine is indeed present, located in the cofactor binding site (Figure 3.38). Whilst this cysteine residue is not predicted to form part of catalytic triad, or shown to form bonds to cofactor, the binding of compound 17796 or its derivatives may prevent cofactor binding through steric-occlusion thereby halting catalysis.

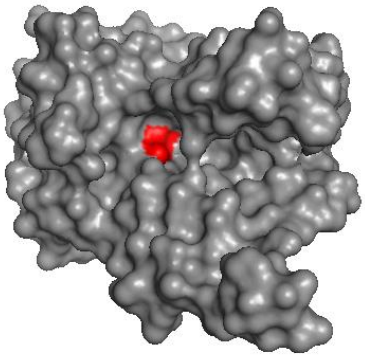

Figure 3.37. Crystal structure of 17β-HSD10 (PDB:1U7T). The 17β-HSD10 enzyme was found to harbour an active site cysteine residue (Residue C91: Red), potentially explaining the mechanism of action utilised by thiol containing inhibitors 17796, 350076 and 114063.

88402 Analogues

Subsequently, to confirm compound 88402 as a true hit and in an attempt to generate structure activity relationship which could inform the design of subsequent compound series, an additional sample of compound 88402 was requested, as well as samples of eighteen structural analogues. When screened at 100 μM compound 88402 was confirmed as a true inhibitor, and a range of additional molecules of interest were identified (Figure 3.39).

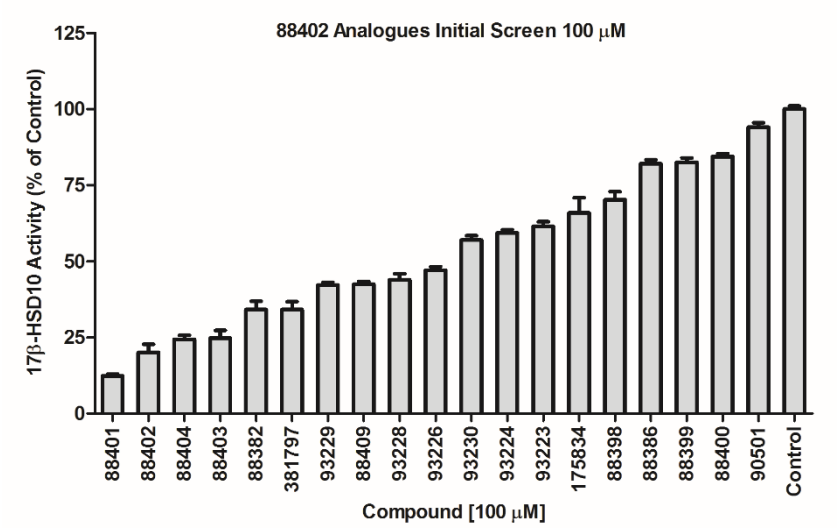

Figure 3.39. 88402 Analogues. 18 analogues of compound 88402 were procured from the NCI and screened against the 17β-HSD10 enzyme at 100 μM. Values shown are an average of two independent experiments each will three technical repeats ± SEM.

A dose response experiment was performed for the most potent inhibitor identified in this series, compound 88401, and an IC_{50} value of 10.30 μM (95% CI = 9.51-11.16) calculated (Figure 3.40).

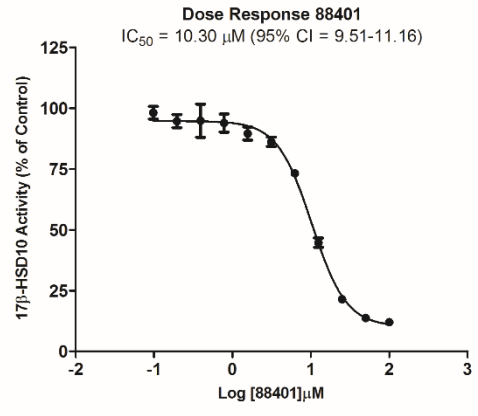

Figure 3.40. Dose response curve compound 88401. 17β-HSD10 enzyme activity was measured in the presence of increasing concentrations of compounds 88401. An IC_{50} value of 10.30 μM (95% CI = 9.51-11.16) was calculated using GraphPad Prism. Values shown are an average of two independent experiments each with three technical repeats ± SEM.

Chapter 3 - Discussion

Previous work has shown that the 17β-HSD10 enzyme forms a toxic complex with Aβ, resulting in oxidative stress and cell death[303,337,338]. Interestingly, hallmarks of this toxicity appear to be dependent on the catalytic activity of the 17β-HSD10 enzyme and as such two 17β-HSD10 directed therapeutic approaches may hold merit in treating Alzheimer's disease, namely the disruption of the 17β-HSD10/Aβ interaction or the direct inhibition of 17β-HSD10 catalytic activity.

Here, I have developed a highly robust screening assay for measuring the activity of the 17β-HSD10 enzyme and have subsequently shown for the first time that derivatives of Frentizole, a compound known to be capable of perturbing the interaction between 17β-HSD10 and Aβ, can be turned into reasonably potent inhibitors of 17β-HSD10 enzymatic activity, potentially allowing both therapeutic approaches to be pursued with a single compound. From two initial series of Frentizole derivatives, three novel inhibitors of the 17β-HSD10 enzyme were identified, termed K690, K691 and K801 (Figure 3.41).

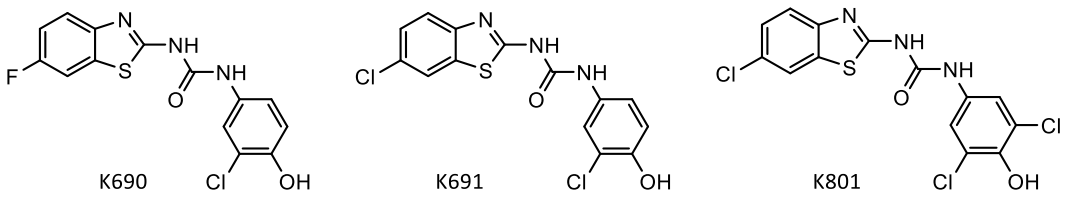

Figure 3.41. Frentizole derived 17β-HSD10 inhibitors. From two initial series of Frentizole derivatives, three 17β-HSD10 inhibiting compounds were identified, termed compounds K690, K691 and K801.

One additional inhibitor, K1093, with improved potency and solubility was identified thereafter as a result of a subsequent series of derivative compounds (Figure 3.42).

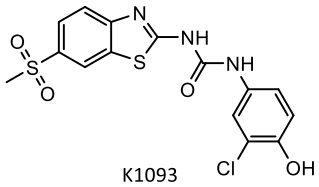

Figure 3.42 Frentizole derived 17β-HSD10 inhibitors (2). Screening of a number of follow-up series of Frentizole derivatives, identified inhibitor K1093 with improved potency and solubility.

Based upon the results of the initial screens of compounds K684-K711, it would appear that for the direct inhibition of 17β-HSD10 activity substitution of the benzothiazole moiety with a chlorine atom is preferable to fluorine, as evidenced by the enhanced levels of inhibition seen with chloro-substituted compounds K689 and K693 versus fluoro-substituted compounds K688 and K692 (Figure 3.15) and between compounds K689 and K688 (Figure 3.16). The presence of a hydroxyl group on the phenylurea moiety appears to be required for inhibition, likely involved in the formation of a hydrogen bond to the

17β-HSD10 enzyme. The position of this substitution on the phenylurea moiety also appears vital. A single hydroxyl group in the *ortho* position (Figures 3.15 and 3.16, K688 and K689) was found to be sufficient for inhibition, whilst substitution in the *para* position gave rise to no marked decrease in enzymatic activity (Figures 3.15 and 3.16, K684 and K685).

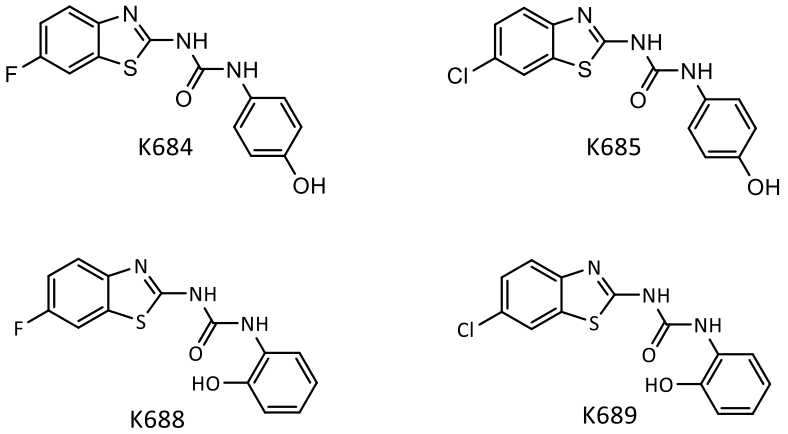

Figure 3.43. Frentizole derived enzyme inhibitors. Compounds K684 and K685 harbouring a hydroxyl group in the *para* position of the phenylurea moiety were found to be incapable of direct inhibition of the 17β-HSD10. Whilst compounds K688 and K689, with substitution in the *ortho* position gave rise to significant levels of inhibition.

Interestingly, substitution with a hydroxyl group in the *para* position in combination with a chloro group in the *meta* position gave rise to the most potent inhibitors (Figure 3.16 and Figure 3.18, K690, K691, K801) with movement of either group or alternative substitution found to result in a decreased level of inhibition (Tables 3.01 and 3.02, Figures 3.16 and 3.18). As substitution with a hydroxyl group in the *ortho* position was found to be sufficient in itself for inhibition (Figure 3.15 and 3.16, K688 and K689), it may be advantageous to add this substitution to the scaffold of compound K691, potentially improving potency (Figure 3.44). Similarly, on the basis of the enhanced solubility and potency of inhibitor K1093, (Figure 3.42) further substitution of the benzothiazole moiety at position 5 should be investigated. Such compound series are currently in the process of being designed, synthesised and evaluated by Dr. Laura Aitken, in collaboration with Professor Kamil Musilek, Ondrej Benek and Lukas Hroch.

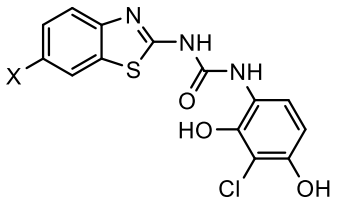

Figure 3.44. Proposed Frentizole derived inhibitor. On the basis of previously identified inhibitors, the addition of a hydroxyl group in the *ortho* position of the phenylurea moiety of inhibitor K691 may generate a more potent inhibitor. Additional substation at position X should also be investigated.

At saturation, all compounds were found to result in incomplete inhibition of the 17β-HSD10 (Figures 3.19 and 3.21). Originally, this was attributed to a partial mechanism of inhibition, in which the enzyme-

substrate-inhibitor complex would continue to generate product at a diminished rate. However, it now seems such a phenomenon is instead due to the limited solubility profiles of these initial hit compounds, forming a point of focus for subsequent series.

In the absence of an X-ray crystallography derived model, the exact stereochemistry of binding is difficult to ascertain. As such, in an attempt to gain more insight into the mechanism of action utilised by compounds K690 and K691, a kinetics based appraisal was undertaken. Both compounds were found to act via a non-competitive mechanism with respect to cofactor, NADH, and a mixed non-competitive mechanism with respect to substrate, acetoacetyl-CoA (Section 3.08), somewhat unsurprising given that the assay conditions were designed to predispose to the identification of inhibitors of this type (Section 3.03). In terms of drug like properties, non-competitive inhibitors are generally viewed favourably. In the presence of a competitive inhibitor, enzyme activity will be reduced resulting in a build-up of substrate and cofactor until a level is reached at which the inhibitor is outcompeted and activity restored. Inhibitors acting via a non-competitive mechanism do not suffer from this limitation, and thus typically require lower doses to maintain the desired effect, decreasing off-target effects and toxicity[357]. The generated data suggests that the binding of substrate, cofactor and inhibitor are not mutually exclusive events and thus both NADH and acetoacetyl-CoA may be of use as stabilising agents to facilitate the generation 17β-HSD10-inhibitor crystals, an approach not previously attempted within the group. The generation of such a crystal would be highly advantageous allowing a detailed understanding of the interactions formed between inhibitor and protein and thus, the rational design of improved derivatives.

As a confirmation assay, differential scanning fluorimetry was employed, providing direct biophysical evidence of an interaction between inhibitor, K1093, and the 17β-HSD10 enzyme and reducing the chance of such hits simply being the result of screening artefacts. Compounds K690 and K691 were not found to elicit a marked shift in the melting temperature of either the free 17β-HSD10 enzyme, or the enzyme in complex with cofactor and substrate. The lack of an observed shift in T_m may be due to the fact that the binding of compounds K690 and K691 induces no significant alteration in the stability of the 17β-HSD10 enzyme, or more likely, due to an inherent limitation of the assay. DSF based experiments require ligand to remain bound at significantly elevated temperatures, 40-70°C, as compared to the initial enzymatic screening assay, performed at 37°C (Section 3.07), possibly effecting binding affinity. Given the reversible nature of inhibition exerted by compounds K690 and K691 (Figure 3.25) and the limited aqueous solubility of both molecules, the concentration of inhibitor required for significant binding to occur under the conditions necessary for DSF may simply be unattainable. Compound K1093, with enhanced potency and solubility, was found to induce a dose dependent stabilisation of the enzyme structure but only at concentrations above 25 μM, beyond the limited solubility profile of compounds K690 and K691, providing further evidence that the lack of an observed shift with these molecules was due to inherent limitations of the DSF experiment and confirming Frentizole derived inhibitors as true hits.

One of the main advantages of compounds derived from the Frentizole scaffold is the potential for such compounds to simultaneously inhibit the catalytic activity of the 17β-HSD10 enzyme whilst also preventing binding to Aβ. The parent Frentizole scaffold has previously been shown to be capable of disrupting the 17β-HSD10/Aβ complex[344] and thus we sought to ascertain whether inhibitors K690, K691 and K1093 would retain this ability. Through the use of differential scanning fluorimetry and western blotting an attempt was made to generate a means of quantifying the amount of Aβ bound to the 17β-HSD10 enzyme (Section 3.12). Although a lack of reproducibility meant that these experiments were deemed unsuitable for compound screening, it seems likely that with further optimisation a western blot based approach may be viable as a means of quantifying the ability of compounds of interest to perturb the 17β-HSD10/Aβ interaction. Whilst the exact cause for the observed lack of reproducbility is difficult to decipher, the most likely reason seems to be inconsistencies in the preparation of oligomeric Aβ. Commercially available recombinant Aβ must first be treated with a monomerising agent prior to an aging step to generate the desired oligomeric state. Traditionally, hexafluoroisopropanol (HFIP) has been used for this purpose, however the efficiency of such treatment has since been called into question. HFIP-treated Aβ has been shown to harbour a mixture of species, indicated by the presence of a range of elution products following size exclusion chromatography (Figure 3.45)[358] with the presence of such oligomeric species subsequently shown to speed the rate of fibril formation using a thioflavin-T assay, presumably through a seeding based mechanism (Figure 3.45)[358].

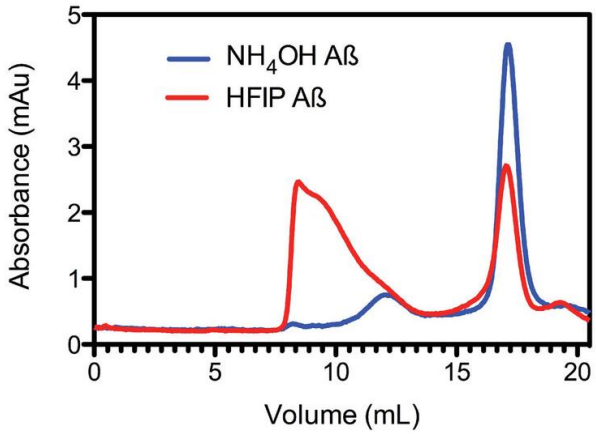

Figure 3.45. HFIP treatment results in a range of oligomeric species of Aβ. HFIP was found to result in incomplete monomerisation of Aβ, indicated here using size exclusion chromatography. NH_4OH was shown to result in a more homogeneous monomeric preparation. Figure from[358].

The 17β-HSD10 enzyme has been proposed to interact with oligomeric forms of Aβ[349]. Thus, if the starting material were to contain a mixture of monomeric and oligomeric species, as a result of incomplete monomerisation via HFIP, varying levels of oligomers and fibrils would be present following an amyoid aging step, resulting in varying levels of 17β-HSD10 bound Aβ and explaining the observed experimental variance. The use of NaOH has been proposed as an alternative method of amyloid monomerisation and has been shown to produce a more homogenious monomeric starting solution (Figure 3.45)[358]. Therefore,

the use of NaOH in place of HFIP may serve to ameloriate the observed variance between replicate experiments and make the assay viable for small molecule screening.

Whilst Frentizole derived inhibitors offer a promising starting point for the generation of disease modifying compounds, it is unlikely that any one series of compounds will fulfil all requirements and as such, a search for addition inhibitor scaffolds was made allowing a diversification of the portfolio of compounds available for evaluation and thereby increasing the chance of success. Additionally, in the absence of a crystal structure, pharmacophore mapping may be used to compare validated inhibitors and identify common structural features, providing insight into the key moieties necessary for inhibition, on the proviso that such inhibitors are confirmed to be operating at the same site. A large explorative screening experiment, using the NCI diversity IV compound library, identified a range of 17β-HSD10 inhibitors, which, following further evaluation, may prove useful for such purposes (Section 3.13).

Two inhibitors identified as a result of the NCI Diversity IV screen, compounds 17796 and 88402, were further investigated (Section 3.13). Compound 17796 and its associated derivatives with inhibitory activity were found to all harbour a thiol group, suggesting inhibition may be due to the formation of a disulphide bridge to an active site cysteine residue. Inhibition was found to be reversible in the presence of DTT, a reducing agent, providing further support for this hypothesis. As further validation of such a mechanism, 17β-HSD10 activity could be assessed in the presence of increasing concentrations of N-ethylmaleimide, a compound which will irreversibly react with exposed thiol groups on cysteine residues.

The screening of derivatives of compound 88402, identified compound 88401, harbouring substitution of the heterocyclic ring with two chloro groups at positions 5 and 6, which was more potent than the original hit compound, 88402, substituted at the 5 position with a methoxy group (Figure 3.39). A lack of substitution at this position, compounds 175834, 88398, 88400, 90501, was seen to result in comparatively poor inhibition, as did substitution with a methyl group, compound 88399. Thus suggesting the addition of small electronegative groups, particularly at position 5 of the heterocyclic moiety enhances inhibition (Table 3.13).

Table 3.13. 17β-HSD10 inhibition by analogues of compound 88402 analogues (subset 1). 17β-HSD10 enzyme activity was assessed in the presence of the indicated compound at 100 µM. Compound are ranked on the basis of residual enzyme activity. Values shown are an average of two independent experiments each with three technical repeats ± SEM.

NSC #	Structure	Residual Activity (%)
88401	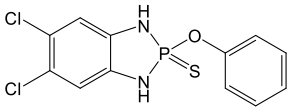	12.39 ± 0.61
88402	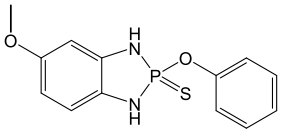	20.07 ± 2.73
175834	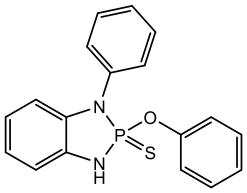	65.87 ± 4.98
88398	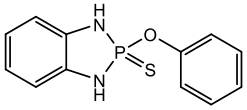	70.21 ± 2.67
88399	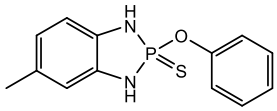	82.56 ± 1.43
88400	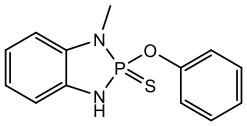	84.40 ± 0.95
90501	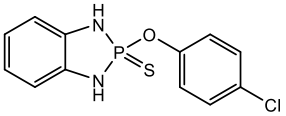	94.07 ± 1.38

The presence of a methoxybenzene extension was also found to be important for inhibition, with substitution with a methylbenzene group resulting in less marked inhibition, as seen with compounds 88402 and 88382 (Table 3.14).

The presence of a secondary amine on the heterocyclic ring was also found to be crucial for inhibition. Replacement with a tertiary amine, as with compound 88386, resulted in dramatically reduced inhibition as compared with compound 88382, suggesting the secondary amine is acting as a hydrogen bond donor and that the formation of this bond is critical for the inhibition of the 17β-HSD10 enzyme. The position of this secondary amine appears to become more important when substitution at position 5 of the heterocyclic ring is also present. The replacement of one of the two secondary amine groups with a tertiary amine, in the absence of an electron withdrawing group at position 5 of the heterocyclic moiety, had comparatively little effect on inhibition, as seen with compounds 88398 and 88400 (Table 3.13). In the absence of substitution on the heterocyclic ring, the inhibitor molecule may be more flexible, which may allow the second secondary amine to form this key hydrogen bond. Once an electron withdrawing group is added, the bound inhibitor molecule may become sterically restricted, preventing this hydrogen bond from being formed and explaining the comparatively large reduction in inhibition seen between compounds 88382 and 88386 (Table 3.14).

Table 3.14. 17β-HSD10 inhibition by analogues of compound 88402 analogues (subset 2). 17β-HSD10 activity was assessed in the presence of the indicated compound at 100 µM. Compound are ranked on the basis of residual enzyme activity. Values shown are an average of two independent experiments each with three technical repeats ± SEM.

NSC #	Structure	Residual Activity (%)
88402	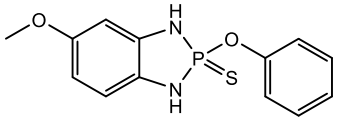	20.07 ± 2.73
88382	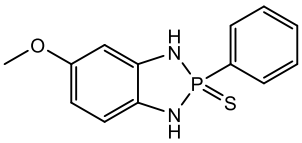	34.17 ± 2.73
88386	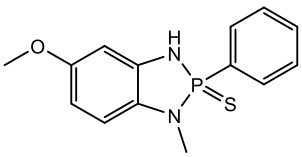	82.09± 1.21

In summary, we now have a highly robust method for measuring the catalytic activity of the 17β-HSD10 enzyme, forming the basis of our primary small molecule screening assay. Alongside this, we have a second robust de-selection assay in the form of differential scanning fluorimetry, allowing the validation of suspected small molecule inhibitors. Through the use of these experiments we have identified 3 derivatives of the Frentizole scaffold which are capable of enzyme inhibition, termed K690, K691 and K1093. As a result of a comparatively large NCI Diversity IV screen, a range of additional inhibitor scaffolds were identified., with two, compounds 17796 and 88402, being further investigated and possibly forming the basis for new inhibitor series. Subsequent experiments were conducted to assess inhibitor specificity

(Chapter 4) and to generate a cellular disease model against which compounds of interest could be tested (Chapter 5).

Chapter 4: Inhibitor Specificity - Molecular Cloning and Purification of 17β-HSD8 and 17β-HSD14

Chapter 4 - Introduction and Aims:

A frequent issue associated with the development of small molecule enzyme inhibitors is specificity of action. Enzymes are clustered into families, based on substrate utilisation and primary sequence similarities and into super-families on the basis of shared mechanistic and structural features. Whilst a decrease in the level of activity of one enzyme within a family may be therapeutically beneficial, the simultaneous inhibition of closely related homologues can often give rise to toxicity. Thus, an understanding of the specificity of a compound of interest for a given target is highly valuable during the drug development process. The 17β-HSD10 enzyme represents but one of fourteen enzymes within the 17β-hydroxysteroid dehydrogenase family and therefore the possibility of off target affects appears high and worthy of investigation.

In terms of primary sequence similarity, members of the 17β-HSD family are diverse in nature, typically sharing less than 30% identity, and thus enzymes of this class are primarily grouped on the basis of shared mechanistic and structural features[359]. A structural similarity search was performed using the previously published 17β-HSD10 crystal structure (PDB ID: 2O23) and the RCSB Protein Data Bank web-interface, identifying two closely related enzymes within the same family, 17β-HSD8 (PDB: 2PD6) and 17β-HSD14 (PDB: 1YDE). As expected, an alignment of the primary sequences of 17β-HSD8 and 17β-HSD14 to that of 17β-HSD10 revealed a low degree of identity between the proteins, 32% and 31% respectively. However, a structural alignment, performed using Pymol, revealed a high degree of structural homology (Figure 4.01), with RMSD scores of 0.919 and 0.997 calculated for 17β-HSD8 and 17β-HSD10, and 17β-HSD14 and 17β-HSD10, respectively. The aim of this chapter was to clone the cDNA sequences encoding the 17β-HSD8 and 17β-HSD14 enzymes, purify both proteins to homogeneity and develop enzyme activity assays for each, allowing a measure of the specificity of known 17β-HSD10 enzyme inhibitors to be made.

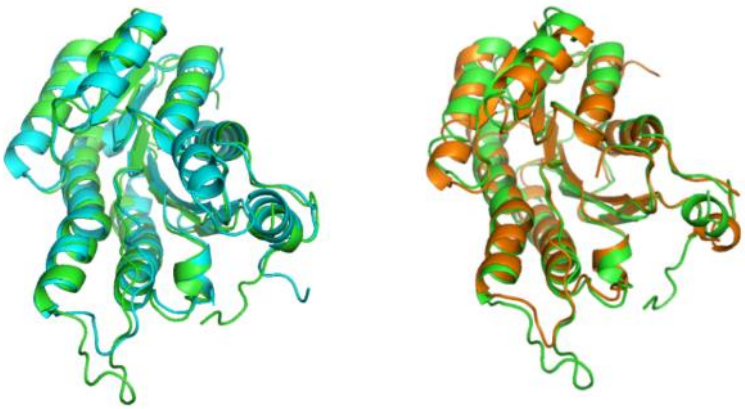

Figure 4.01. Structural alignment of 17β-HSD8 and 17β-HSD14 to 17β-HSD10. Using PyMOL, a structural alignment was made between the 17β-HSD8, 17β-HSD14 and 17β-HSD10 enzymes. In both instances, a high degree of structural similarity was seen, as indicated by RMSD values of 0.919 and 0.997. Left Image= Alignment 17β-HSD8 and 17β-HSD10. Right Image= Alignment 17β-HSD14 and 17β-HSD10. Green cartoon = 17β-HSD10.

4.1: 17β-HSD8 and 17β-HSD14 cDNA Cloning

4.11 peHISTEV-HSD8

In recent years, the ability to artificially synthesise entire genes has become both feasible and economically viable. In brief, short oligonucleotide fragments encompassing the sequence of interest are synthesised *de novo* and subsequently ligated using a DNA polymerase reaction, producing the full length coding sequence. The product is sequence verified and typically provided to the end user in a maintenance vector. The GeneArt service offered by ThermoFisher was used for this project.

As the sole purpose of this project was the production of recombinant protein, the human 17β-HSD8 coding sequence, as provided by Ensembl website[360], was codon optimised for expression using *E. coli.* NcoI and SalI sites were added 5' and 3' respectively, allowing downstream cloning into the desired expression vector. The generated construct was delivered in a pMAT vector backbone harbouring an ampicillin resistance marker (Figure 4.02).

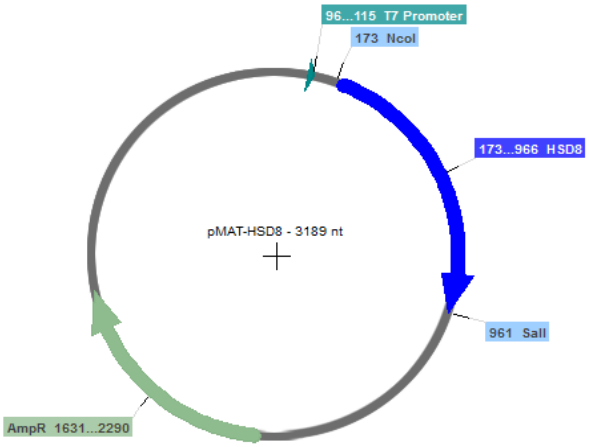

Figure 4.02. pMAT-HSD8 Vector Map. The 17β-HSD8 cDNA sequence was synthesised using the GeneArt service offered by ThermoFisher and was delivered in a pMAT maintenance vector.

Our in-house expression system for 17β-HSD10 utilises the peHISTEV expression vector which produces a TEV-cleavable, N-terminal 6 x His-tagged protein for subsequent purification using Ni-NTA affinity chromatography (Chapter 3 - Section 3.01). The 17β-HSD10 cDNA sequence had previously been ligated into the multiple cloning site of the peHISTEV-vector using the NcoI and SalI restriction enzymes (Figure 4.03).

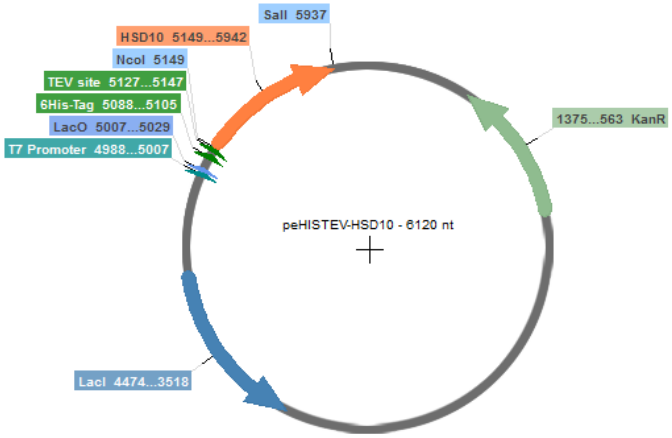

Figure 4.03. peHISTEV-HSD10 Vector Map. The cDNA sequence encoding the 17β-HSD10 enzyme had previously been cloned into the peHISTEV expression vector using the NcoI and SalI restriction enzyme sites. The peHISTEV vector produces a TEV cleavable, 6 x His-tagged protein for subsequent purification using Ni-NTA affinity chromatography.

Thus, the initial cloning strategy entailed the digestion of the peHISTEV-HSD10 expression vector using the NcoI and SalI restriction endonucleases, liberating the 17β-HSD10 cDNA sequence. Following digestion, the 17β-HSD8 cDNA sequence would subsequently be ligated within the vector, producing a peHISTEV-HSD8 expression construct (Figure 4.04).

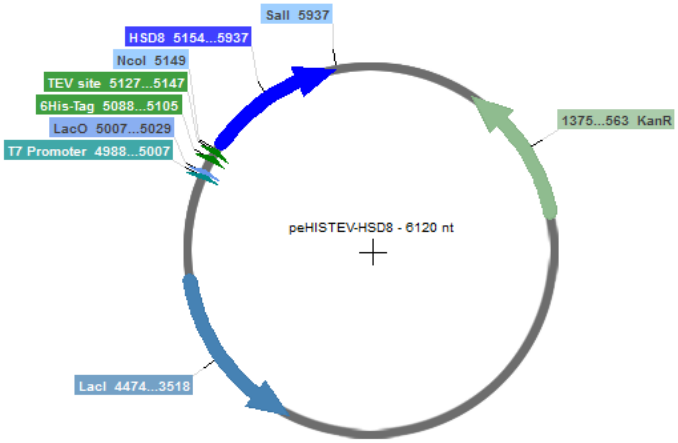

Figure 4.04 peHISTEV-HSD8 initial cloning strategy. The peHISTEV-HSD10 construct was to be cut using the NcoI and SalI restriction endonucleases, liberating the 17β-HSD10 cDNA sequence and allowing the 17β-HSD8 cDNA sequence to be ligated in its place, producing a peHISTEV-HSD8 expression vector.

However, a cursory check that the NcoI and SalI restriction enzymes were behaving as expected identified an issue. Diagnostic digests were performed with the pMAT-HSD8 and peHISTEV-HSD10 constructs using the NcoI and SalI enzymes, both individually and in a dual digest. Each enzyme in isolation would be expected to cut the supercoiled pMAT-HSD8 construct once, producing a single linear fragment of approximately 3.2 kb. Dual digestion with both enzymes would liberate the 17β-HSD8 coding sequence, producing two linear fragments, one corresponding to the empty pMAT vector, approximately 2.4 kb in

size, the second corresponding to the 17β-HSD8 coding sequence, approximately 0.8 kb in size. Similarly, with the peHISTEV-HSD10 construct, cleavage with each enzyme individually should yield a single linear fragment, approximately 6.1 kb in length. Digestion with both the NcoI and SalI enzymes should yield two linear fragments, of approximately 5.3 kb and 0.8 kb, corresponding to the empty peHISTEV vector and the 17β-HSD10 insert respectively.

Cleavage with NcoI was found to produce a single linear fragment, as expected. However, with both constructs, cleavage with SalI was found to produce a mixture of linear fragments as opposed to the expected one (Figures 4.05 and 4.06, Lane 4). In the case of the pMAT-HSD8 construct, three distinct species are apparent, the largest being equal in size to the NcoI digested DNA (Figure 4.05, Lane 3) and thus likely representing the expected linear digestion product (Figure 4.05, Lane 4). Two additional smaller species are however also apparent (Figure 4.05, Lane 4).

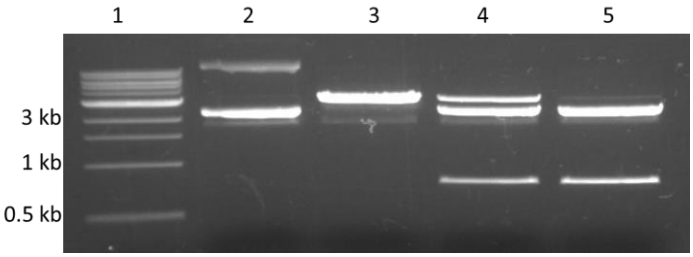

Figure 4.05. pMAT-HSD8 digestion with NcoI and SalI. Cleavage of the pMAT-HSD8 construct with NcoI was found to generate a single linear fragment, as expected. However, cleavage using SalI was found to produce three linear fragments. Lane 1 = Ladder, Lane 2 = Uncut pMAT-HSD8, Lane 3 = NcoI, Lane 4 = SalI, Lane 5 = NcoI + SalI.

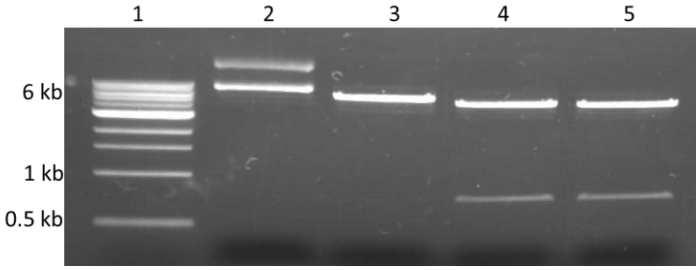

Figure 4.06. peHISTEV-HSD10 digestion with NcoI and SalI. Cleavage of the peHISTEV-HSD10 construct with NcoI was found to generate a single linear fragment, as expected. However, cleavage using SalI was found to produce two linear fragments. Lane 1 = Ladder, Lane 2 = Uncut peHISTEV-HSD10, Lane 3 = NcoI, Lane 4 = SalI, Lane 5 = NcoI + SalI.

The most likely explanations for the observed dual cleavage by SalI were checked, namely cross contamination of enzyme stocks and the inadvertent introduction of a second SalI site during cloning, neither of which offered an explanation for the observed digestion pattern. The SalI enzyme used was a high-fidelity variant and thus star activity was unlikely. The exact cause for this dual cleavage remains unknown.

To circumvent this issue, the peHISTEV-HSD10 construct was replaced with a naive peHISTEV vector, precluding the possibility of issues introduced during the previous cloning strategy. In addition, the next 3' restriction enzyme site within the MCS, HindIII, was used in place of SalI. A diagnostic digest was

performed using the NcoI and HindIII restriction endonucleases and the empty peHISTEV construct, yielding the expected digestion products.

With the NcoI and HindIII restriction enzymes validated as cutting correctly, a pair of PCR primers were designed to amplify the 17β-HSD8 coding sequence out of the pMAT backbone and simultaneously change the 3'-SalI restriction enzyme site to a HindIII recognition sequence:

Forward: 5'-atctg**CCATGG**CGAGCCAGCTGC-3'

Reverse: 5'-tcga**AAGCTT**ACATAAACAGACCACCGGTCACTTCAACG-3'

(Lowercase = Spacer Sequence, Bold = Restriction enzyme site)

To optimise primer annealing temperatures, three small scale PCR reactions were performed with primer annealing at 72°C, 65°C and 55°C. A prominent band was seen in each reaction at the correct size, 0.8 kb, and thus an annealing temperature of 72°C was selected for further use (Figure 4.07).

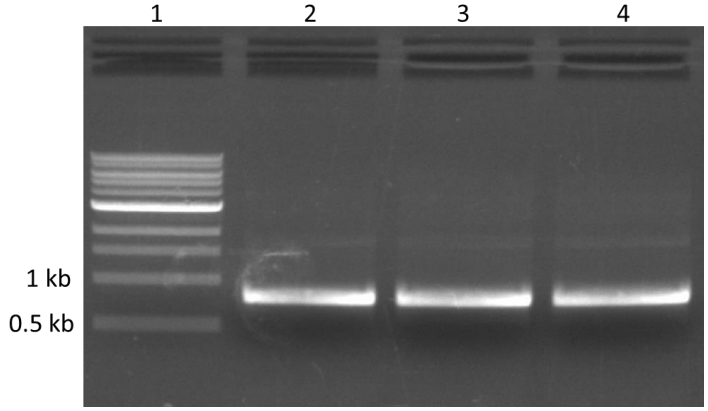

Figure 4.07. 17β-HSD8 PCR primer check. PCR primers were designed to amplify the 17β-HSD8 cDNA sequence out of the pMAT backbone and simultaneously exchange the 3'SalI restriction site to a HindIII recognition sequence. To optimise primer annealing, three temperatures were trialled. Lane 1= Ladder, Lane 2= 72°C annealing, Lane 3= 65°C annealing, Lane 4= 55°C annealing.

The amplified 17β-HSD8 insert and the empty peHISTEV backbone were cleaved using the NcoI and HindIII restriction endonucleases, the products separated using agarose gel electrophoresis and the fragments of interest gel extracted. The purified vector and insert were ligated using T4 DNA ligase, yielding the desired construct (Figure 4.08), herein referred to as peHISTEV-HSD8.

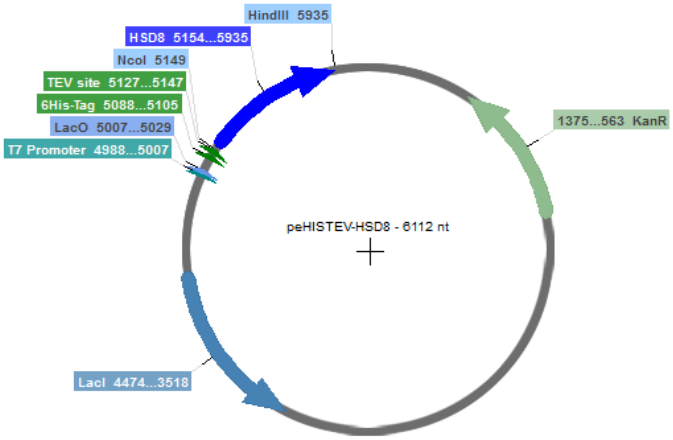

Figure 4.08. peHISTEV-HSD8 expression vector. The 17β-HSD8 cDNA sequence was ligated into the empty peHISTEV vector using the NcoI and HindIII restriction endonucelease sites producing a peHISTEV-HSD8 expression vector.

4.12 peHISTEV-HSD14

An alternative cloning strategy was employed for 17β-HSD14. Rather than having the gene synthesised, reverse-transcription of an mRNA template was instead used. At the mRNA level, the 17β-HSD14 gene is known to be highly expressed in kidney tissue, as shown by the Protein Atlas[361] and so mRNA was extracted from a human embryonic kidney cell line (HEK293) for use as a template. Initially, a cDNA library corresponding to the poly-A tailed mRNA transcripts was generated using M-MLV reverse transcriptase and oligo(dT) primers. Gene specific primers were subsequently used to amplify the cDNA of interest, here the 17β-HSD14 coding sequence, from the cDNA library and simultaneously add appropriate restriction enzyme sites, 5'-NcoI and 3'-XhoI, for downstream cloning:

Forward: 5'-gatcga**CCATGG**CTACGGGAACGCGCTATGC-3'

Reverse: 5'-catgta**CTCGAG**TCAGGAAGGGATATCGGGGGCGTCC-3'

(Lowercase = Spacer sequence, Bold = Restriction enzyme site)

To verify that first strand cDNA synthesis had been successful, and in an attempt to generate the cleanest PCR product possible, three small scale PCR reactions were performed with varying primer annealing temperatures (72°C, 65°C and 55°C). Amplification of the 17β-HSD14 cDNA sequence was observed at each temperature tested, as indicated by the presence of a band at approximately 0.8 kb, suggesting first strand cDNA synthesis had been successful (Figure 4.09). A primer annealing temperature of 72°C was selected for further use, giving the most stringent binding and likely most specific product.

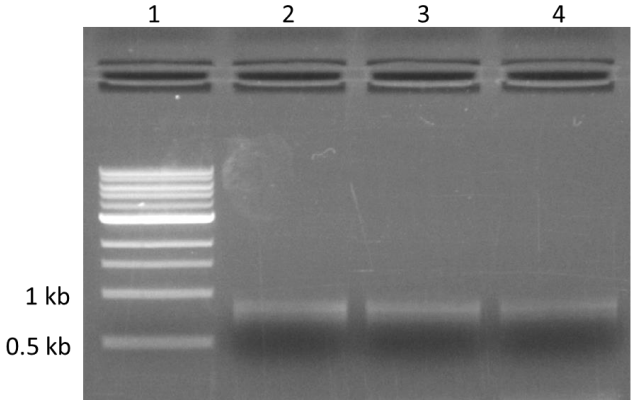

Figure 4.09. 17β-HSD14 cDNA amplification. The 17β-HSD14 cDNA sequence was PCR amplified using gene specific primers and a cDNA template generated using M-MLV reverse transcriptase and oligo(dT) primers. Three annealing temperatures were trialled, with 72°C being selected for further use. Lane 1= Ladder, Lane 2= 72°C annealing, Lane 3 = 65°C annealing, Lane 4= 55°C annealing.

As issues had been related to non-specific cleavage had been encountered previously during restriction digests (Section 4.11), a check was made to ensure the naive peHISTEV vector was cleaved correctly using the NcoI and XhoI restriction endonucleases. In both cases, the expected digestion pattern was observed and thus the amplified 17β-HSD14 cDNA sequence and the empty peHISTEV vector were cleaved using

the NcoI and XhoI restriction endonucleases, the products separated via agarose gel electrophoresis, the fragments of interested gel extracted and ligated using T4 DNA ligase. Product was transformed into competent DH5-α *E. coli*, cells plated, cultures grown and DNA extracted.

Sequencing of the resultant peHISTEV-HSD14 constructs showed perfect alignment with the expected coding sequence at both the 5' and 3' ends of the cDNA sequence. However, short regions within the coding sequence were consistently absent (Figure 4.10). Initially, it was presumed that these missing sections may be a consequence of alternate splicing and thus represent different isoforms of the protein, of which there are four. However, using the Ensembl website[360], the produced sequencing results were not found to correspond to any known splice variant of the 17β-HSD14 enzyme and were therefore assumed to be a consequence of mRNA secondary structure during first strand cDNA synthesis.

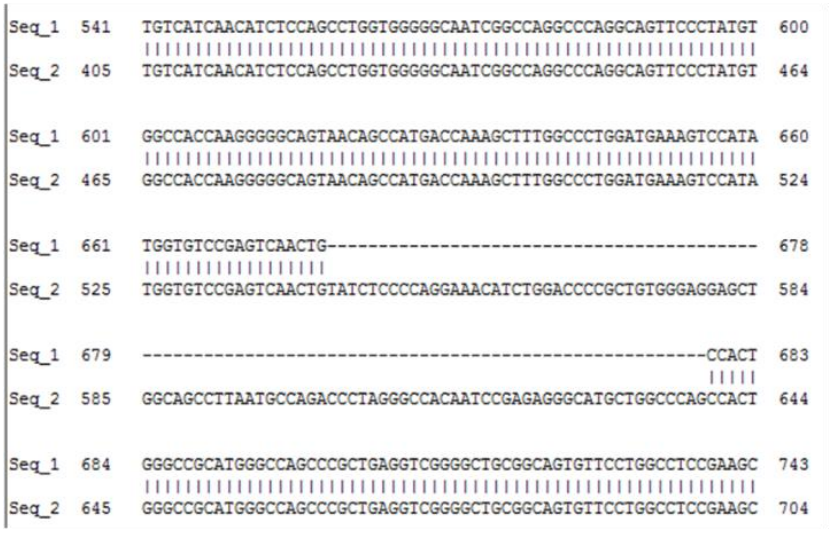

Figure 4.10. peHISTEV-HSD14 example sequencing result. Sequencing of the resultant peHISTEV-HSD14 constructs revealed perfect alignment with the expected coding sequence at the 5' and 3' ends of the cDNA sequence. However, short stretches within the sequence were found to be absent, assumed to be a consequence of secondary structure within the mRNA template.

To rectify this, AMV reverse transcriptase, which has been shown to be able to tolerate higher reaction temperatures[362], was used in place of M-MLV for first strand cDNA synthesis and the cDNA synthesis step performed over a gradient of temperatures (50-72°C). Oligo(dT) primers will not anneal efficiently at these elevated temperatures and so were replaced with the reverse gene specific primer for 17β-HSD14. Thus, rather than a library of cDNA molecules, only one corresponding to the 17β-HSD14 mRNA transcript would be produced. This would have the added benefit of likely decreasing non-specific priming during the second round of cDNA amplification via PCR, giving a cleaner product.

To check for successful cDNA generation, a test PCR reaction was performed using a sample of cDNA from each reaction temperature and the products visualised by agarose gel electrophoresis. In all reactions, a fragment was observed at the expected size, approximately 0.8 kb, suggesting cDNA synthesis was successful at all temperatures trialled. An additional smaller fragment was also observed at every temperature, which may still be a consequence of off target amplification (Figure 4.11).

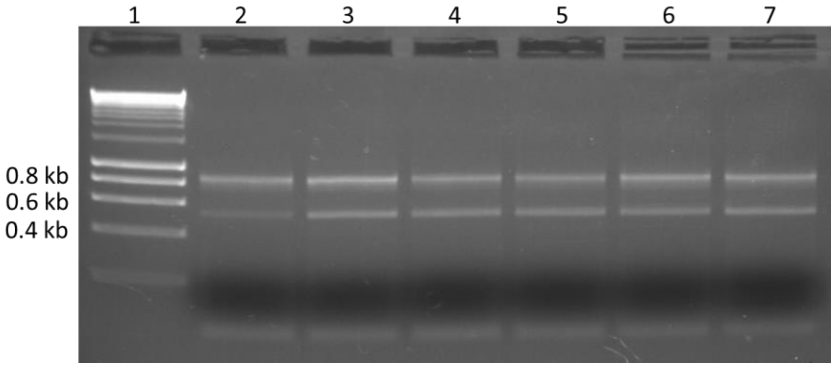

Figure 4.11. 17β-HSD14 AMV cDNA synthesis. In an attempt to overcome issues related to secondary structure in the mRNA template, 17β-HSD14 cDNA was synthesised over a range of reaction temperatures. A trial PCR reaction was performed a sample of cDNA generated at each reaction temperature. A band of the correct size was observed in each case (0.8 kb), verifying the success of cDNA synthesis. Lane 1 = Ladder, Lanes 2-7 = 72°C-50°C reaction temperature.

Concerns that the AMV-RT enzyme may exhibit reduced fidelity at elevated incubation temperatures led to the cDNA generated at 55°C being selected for use as a template for the PCR amplification of the 17β-HSD14 cDNA sequence. The resultant PCR product and the empty peHISTEV vector were cut using the NcoI and XhoI restriction enzymes and the products separated using agarose gel electrophoresis. The fragments of interest were gel extracted and ligated using T4 DNA ligase. Sequencing was found to confirm that the elevated cDNA synthesis temperature had indeed resulted in the production of a full length transcript, but also that concerns regarding enzyme fidelity were correct. Two missense mutations were found to be present within the coding sequence of the 17β-HSD14 gene (A91>G and G303>A).

Thus, to restore the native coding sequence, two rounds of site directed mutagenesis were performed sequentially as per the Liu & Naismith protocol[345] with prominent product observed at each reaction temperature trialled (Figures 4.12 and 4.13).

A91>G Forward: 5'-CCTTCGTG**a**ACAGCGGGGCCCGAGTGGTTATCTGC-3'

A91>G Reverse: 5'- GCTGT**t**CACGAAGGCGCGCACGATCCC-3'

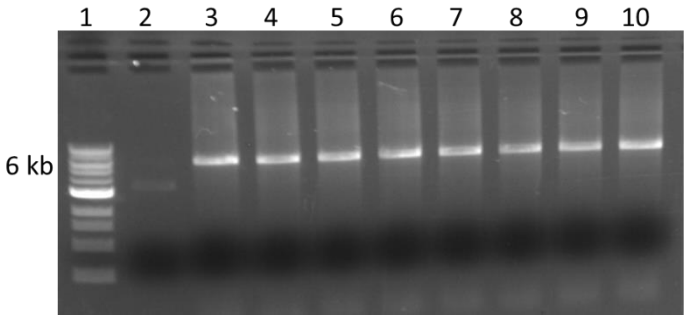

Figure 4.12. 17β-HSD14 SDM #1. Using Liu & Naismith style SDM primers the A>91G missense mutation was corrected. Lane 1 = Ladder, Lane 2 = Dpn1 Control, Lanes 3-10 = Annealing Thermal Gradient 72°C-50°C.

G303>A Forward: 5'-CCTGAGGA**g**ACCTCTGCCCAGGGATTCC-3'

G303>A Reverse: 5'- CAGAGGT**c**TCCTCAGGCCTCTGTGG-3'

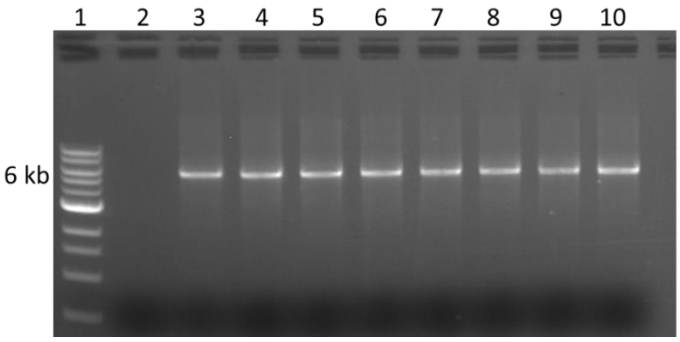

Figure 4.13. 17β-HSD14 SDM #2. Using Liu & Naismith style SDM primers the A440G missense mutation was corrected. Lane 1 = Ladder, Lane 2 = Dpn1 Control, Lanes 3-8 = Annealing Thermal Gradient 72°C-50°C.

Sequencing of the resultant constructs confirmed the restoration of the native coding sequence (see Appendix: B for sequencing results), construct herein referred to as peHISTEV-HSD14 (Figure 4.17)

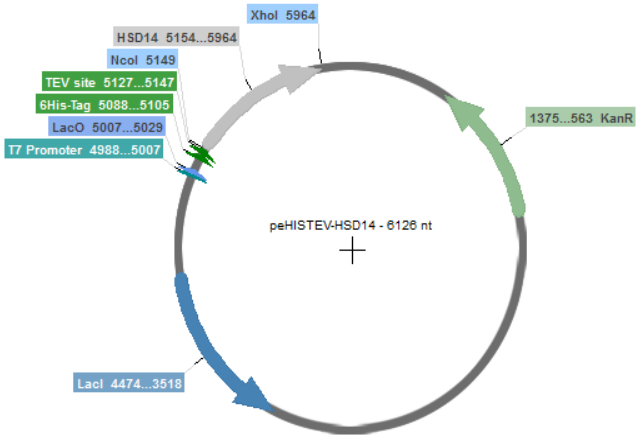

Figure 4.14. peHISTEV-HSD14 Vector Map. The 17β-HSD14 cDNA sequence was cloned into the empty peHISTEV vector using the NcoI and XhoI restriction endonuclease sites producing a peHISTEV-HSD14 protein expression construct.

4.2: 17β-HSD8 and 17β-HSD14 Protein Expression

4.21 Whole Cell Lysates:

The expression of eukaryotic protein in a prokaryotic system allows for the quick and cheap purification of large quantities of a protein of interest. However, in some instances such expression can prove toxic to the host cell, resulting in little to no protein production. Thus, an initial check for expression was made by examining whole cell lysates.

The expression constructs generated for 17β-HSD8 and 17β-HSD14 (Section 4.11 and 4.12) were transformed into BL21(DE3) *E. coli.* A single colony was picked, grown and protein expression induced overnight. Whilst the optimal temperature for *E. coli* growth is 37°C, the induction of protein synthesis at a lower temperature often improves both protein solubility and yield, presumably by slowing the rate of synthesis and thereby giving the cell more time to fold the protein into the correct conformation[363]. As such, protein expression was induced overnight at three temperatures, 15°C, 25°C and 37°C. The following morning whole cell lysates were taken from both induced and non-induced cultures, proteins separated by SDS-PAGE and gels stained using Coomassie Blue. In both instances a prominent band was observed post induction at approximately the expected molecular weight (Figures 4.18 and 4.19). The bands of interest were excised and sent for mass-spectrometry, confirming the identity of both proteins.

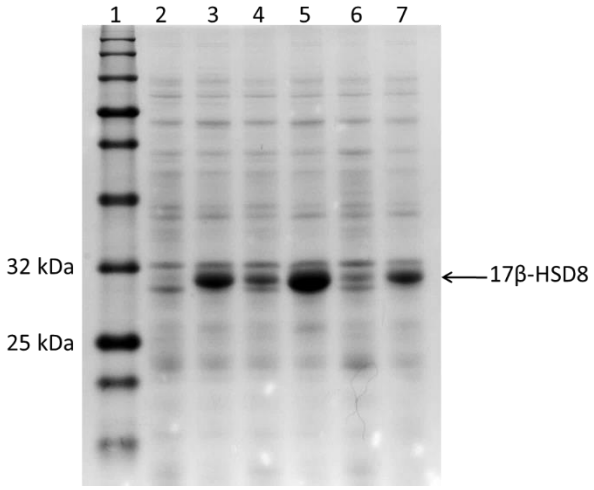

Figure 4.18. peHISTEV-HSD8 expression trial. Protein expression was induced overnight at 15°C, 25°C and 37°. The following morning samples were taken and whole cell lysates generated. Protein expression was assessed via SDS-PAGE and Coomassie Blue staining. Lane 1 = Ladder, Lanes 2/3 = 15°C Non-Induced/Induced, Lanes 4/5 = 25°C Non-Induced/Induced, Lanes 6/7 = 37°C Non-Induced/Induced.

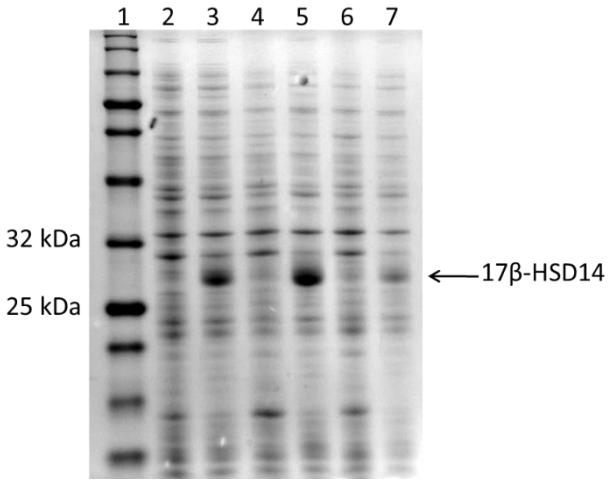

Figure 4.19. peHISTEV-HSD14 expression trial. Protein expression was induced overnight at 15°C, 25°C and 37°. The following morning samples were taken and whole cell lysates taken and assessed via SDS-PAGE and Coomassie Blue staining. Lane 1 = Ladder, Lanes 2/3 = 15°C Non-Induced/Induced, Lanes 4/5 = 25°C Non-Induced/Induced, Lanes 6/7 = 37°C Non-Induced/Induced.

4.22 Optimisation of *E. coli* Cell Lysis:

Whilst the assessment of protein levels using whole-cell lysates is useful for confirming protein expression, it gives no information regarding whether the protein of interest is soluble or insoluble under the induction conditions used. Although it is possible to purify proteins from the insoluble fraction, this typically involves the denaturation and subsequent refolding of the protein of interest, introducing the possibility that the protein may refold into a non-native conformation with downstream implications. Thus, it is generally preferable to induce expression in such a way that the produced protein is synthesised in a soluble form. Before the partitioning of the 17β-HSD8 and 17β-HSD14 proteins between the insoluble and soluble fractions could be assessed, thorough cell lysis conditions were first required.

To this end, *E. coli* BL21 (DE3) cells were transformed with the peHISTEV-HSD10 construct, an expression construct known to produce reasonable levels of soluble protein. The following morning a single colony was picked, grown and protein expression induced overnight at 25°C. Samples were taken, treated with lysozyme and subsequently lysed via sonication for varying lengths of time (0-600 seconds). Cellular debris was pelleted via centrifugation and the total protein content in the soluble fraction assessed using the Bradford assay. Sonication for 180 seconds was found to be sufficient for thorough cell lysis following pre-treatment with lysozyme, as indicated by the plateau in soluble protein levels after this time-point (Figure 4.20). Thus, lysozyme pre-treatment followed by 180 seconds of sonication was used for the subsequent optimisation of induction parameters for the 17β-HSD8 and 17β-HSD14 proteins.

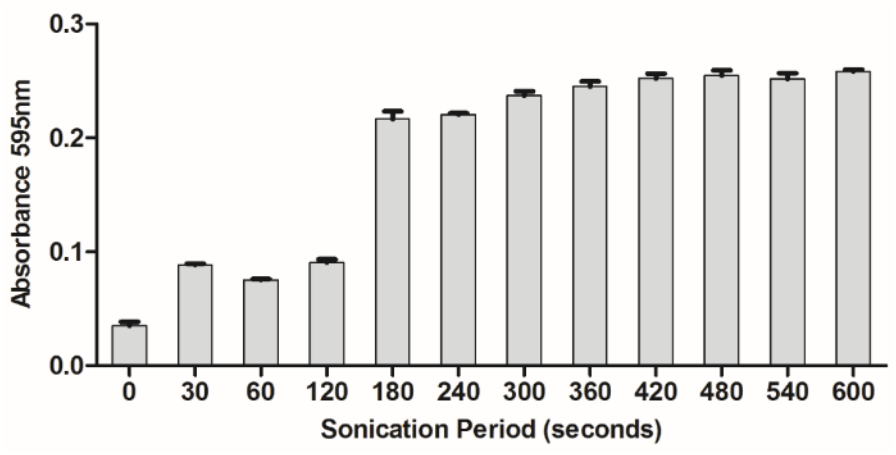

Figure 4.20. *E. coli* sonication optimisation. BL21(DE3) *E. coli* harbouring the peHISTEV-HSD10 construct were grown and protein synthesis induced overnight at 25°C. Following lysozyme treatment, cells were lysed using sonication and total protein level in the soluble fraction assessed using the Bradford assay. Lysozyme treatment followed by 180 seconds of sonication was used for subsequent experiments. Values shown are an average taken from one experiment with three technical repeats ± SEM.

4.23 Recombinant 17β-HSD8 and 17β-HSD14 Solubility Assessment

Samples of peHISTEV-HSD8 and peHISTEV-HSD14 expressing BL21(DE3) *E. coli* were taken following overnight induction at 15°C, 25°C and 37°C and lysed using the aforementioned conditions (Section 4.22), allowing the partitioning of each protein into the soluble and insoluble fractions to be assessed. Following SDS-PAGE analysis and Coomassie Blue staining, no soluble 17β-HSD8 protein was observed at any induction temperature (Figure 4.21).

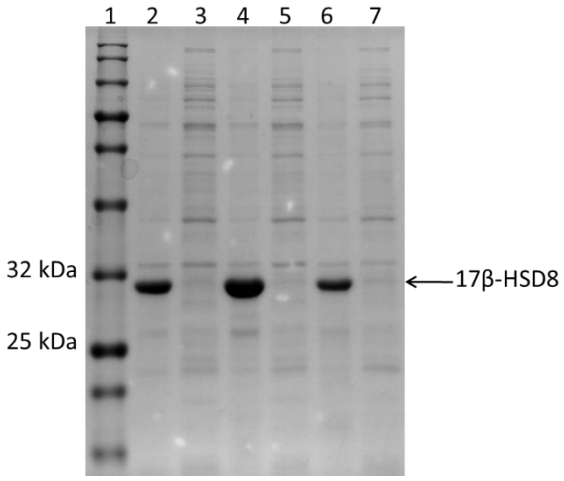

Figure 4.21. peHISTEV-HSD8 insoluble/soluble partitioning. Protein expression was induced overnight at 15°C, 25°C and 37°. The following morning samples were taken and lysed via lysozyme treatment and sonication. Levels of soluble and insoluble protein were assessed via SDS-PAGE and Coomassie Blue staining. Lane 1 = Ladder, Lanes 2/3 = 15°C Insoluble/Soluble, Lanes 4/5 = 25°C Insoluble/Soluble, Lanes 6/7 = 37°C Insoluble/Soluble.

In contrast, the peHISTEV-HSD14 construct was found to yield soluble protein at all temperatures tested (Figure 4.22). The highest level of soluble 17β-HSD14 protein was observed with induction at 25°C and therefore, overnight induction at 25°C was used for the subsequent large-scale purification of the 17β-HSD14 protein.

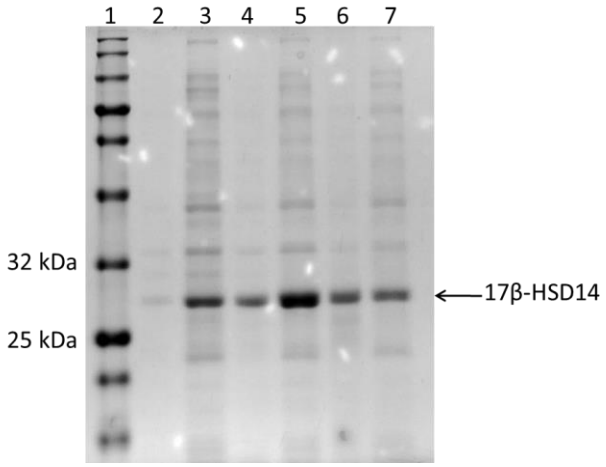

Figure 4.22. peHISTEV-HSD14 insoluble/soluble partitioning. Protein expression was induced overnight at 15°C, 25°C and 37°. The following morning samples were taken and lysed via lysozyme treatment and sonication. Levels of soluble and insoluble protein were assessed via SDS-PAGE and Coomassie Blue staining. Lane 1 = Ladder, Lanes 2/3 = 15°C Insoluble/Soluble, Lanes 4/5 = 25°C Insoluble/Soluble, Lanes 6/7 = 37°C Insoluble/Soluble.

A more thorough time-course of induction was undertaken using the peHISTEV-HSD8 construct and BL21(DE3) *E. coli* to ascertain if the solubility of the 17β-HSD8 protein shows a time dependency. Three cultures were prepared and protein expression induced at 15°C, 25°C and 37°C. Samples were taken pre-induction and at 1, 2, 4, 6, 12 and 24-hours post-induction. The relative levels of soluble and insoluble 17β-HSD8 protein was assessed using the aforementioned methodology (Section 4.22). In all instances, a time-dependent increase in 17β-HSD8 expression was observed, with the rate of expression slower at lower temperatures, as would be expected. However, the 17β-HSD8 protein was found to be insoluble irrespective of the temperature or time of induction (Figure 4.23).

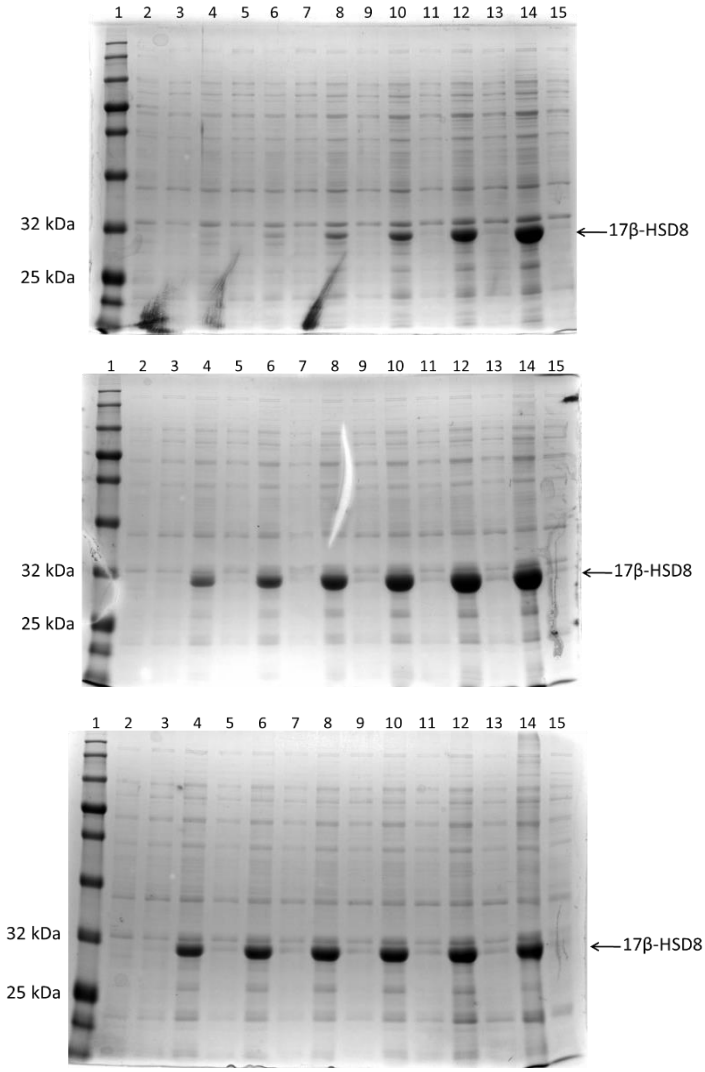

Figure 4.23. peHISTEV-HSD8 temperature and time-course of induction. Protein expression was induced at 15°C (top), 25°C (middle) and 37°C (bottom),. Samples were taken pre-induction and at 1, 2, 4, 6, 12 and 24hr timepoints. Levels of soluble and insoluble protein were assessed via SDS-PAGE and Coomassie Blue staining. Lane 1 = Ladder, Lanes 2/3 = Pre-induction insoluble/soluble, Lanes 4/5 = 1hr insoluble/soluble, Lanes 6/7= 2hr insoluble/soluble, Lanes 8/9= 4hr insoluble/soluble, Lanes 10/11= 6hr insoluble/soluble, Lanes 12/13= 12hr insoluble/soluble, Lanes 14/15= 24hr insoluble/soluble.

4.24 17β-HSD8-Maltose Binding Protein Fusion

A common approach used to improve the solubility of a protein of interest is to generate a fusion protein with a solubility enhancing tag, such as the Maltose-Binding-Protein (MBP). A pET derived expression construct was obtained from AddGene (#29656), herein referred to as pET-MBP, allowing the generation of an N-terminal, 6 x His-tagged, TEV cleavable MBP fusion protein through the use of ligation independent cloning (LIC) (Figure 4.24).

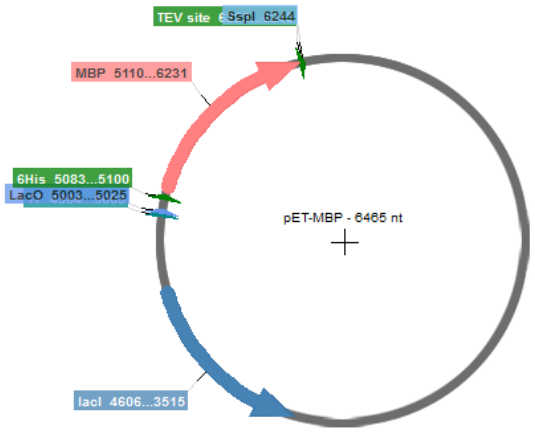

Figure 4.24. pET-MBP Vector Map. The pET-MBP plasmid (AddGene #29656) allows the generation of an N-terminal, 6 x His-tagged, TEV cleavable MBP fusion protein.

LIC exploits the 3' to 5' exonuclease activity of T4 DNA polymerase. Under normal reaction conditions, in which saturating concentrations of dNTPs are present, the 5' to 3' DNA synthesis activity of T4 DNA polymerase counter-acts its 3' to 5' exonuclease activity, meaning as soon as a base is removed from the 3' end of a DNA strand, a new base is added. However, the reaction conditions for LIC are designed such that only a single dNTP is present in the reaction mixture and therefore bases will be removed from the 3' end of a DNA strand until this base is encountered, at which point the polymerase activity will cause the exonuclease activity to stall. Through the design of appropriate primers, this property can be used to rapidly generate long complementary overhangs on both vector and insert. Such overhangs are stable enough to survive transformation without being covalent linked via ligation and thus this time consuming and inefficient step is omitted.

Primers were designed to amplify the 17β-HSD8 cDNA sequence out of the peHISTEV backbone and add 5' and 3' ligation independent cloning tags.

Forward: 5'-**TACTTCCAATCCAATGCA**ATGGCGAGCCAGCTGC-3'

Reverse: 5'-**TTATCCACTTCCAATGTTATTA**TTACATAAACAGACCACCGGTCACTTCA-3'

(Bold = LIC tag)

In order to identify an optimal primer annealing temperature, three trial PCR reactions were performed with annealing at 72°C, 65°C and 55°C. In all reactions, product was observed at the expected size, approximately 0.8 kb, and thus a 72°C annealing temperature was selected (Figure 4.25).

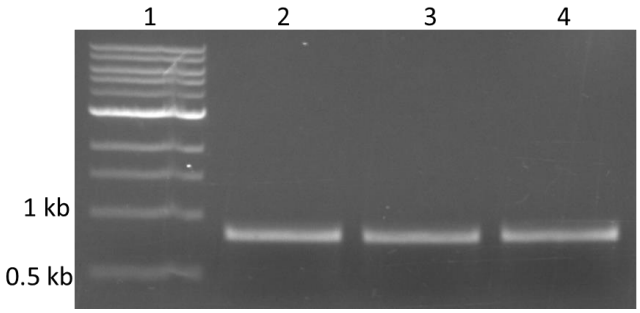

Figure 4.25. 17β-HSD8 PCR primer check. PCR primers were designed to amplify the 17β-HSD8 coding sequence out of the pMAT backbone and simultaneously add LIC cloning tags. To allow for the selection of an optimal annealing temperature, a trial PCR reaction was performed at three temperatures. Lane 1=72°C annealing, Lane 2= 65°C annealing, Lane 3 = 55°C annealing.

The PCR product was purified by agarose gel electrophoresis followed by gel extraction (required to ensure the removal of dNTP molecules present in the PCR reaction prior to T4 DNA polymerase treatment). The insert was subsequently treated with T4 DNA polymerase in the presence of dCTP, exploiting the enzymes intrinsic 3' to 5' exonuclease activity to generate long 15 bp overhangs.

pET-MBP vector DNA was treated with SSPI restriction endonuclease to generate a linear fragment which was subsequently gel extracted and treated with T4 DNA polymerase in the presence of dGTP generating 15 bp overhangs, complementary to the insert. Vector and insert were mixed at varying molar ratios and transformed into competent DH5-α *E. coli*. The following morning colonies were picked, grown, DNA purified and analysed by agarose gel electrophoresis. All colonies were found to harbour an insert of the correct size, and the generation of the desired expression construct confirmed via DNA sequencing (see Appendix: B for sequencing results). Construct herein referred to as pET-MBP-HSD8 (Figure 4.26).

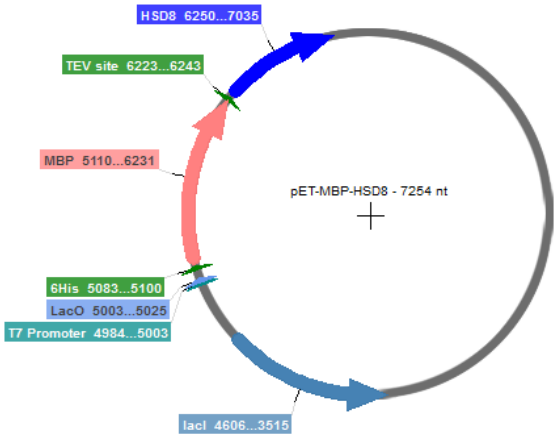

Figure 4.26. pET-MBP-HSD8 Vector Map. The 17β-HSD8 cDNA sequence was cloned into the pET-MBP vector using ligation independent cloning, generating a pET-MBP-HSD8 protein expression vector.

The pET-MBP-HSD8 construct was transformed into BL21(DE3) *E. coli* and protein expression induced at 15°C, 25°C and 37°C overnight. The following morning, expression of the MBP-HSD8 fusion protein was assessed using whole cell lysates. Following induction, a band was observed at approximately 67 kDa, the expected size of the MBP-HSD8 fusion protein (Figure 4.27).

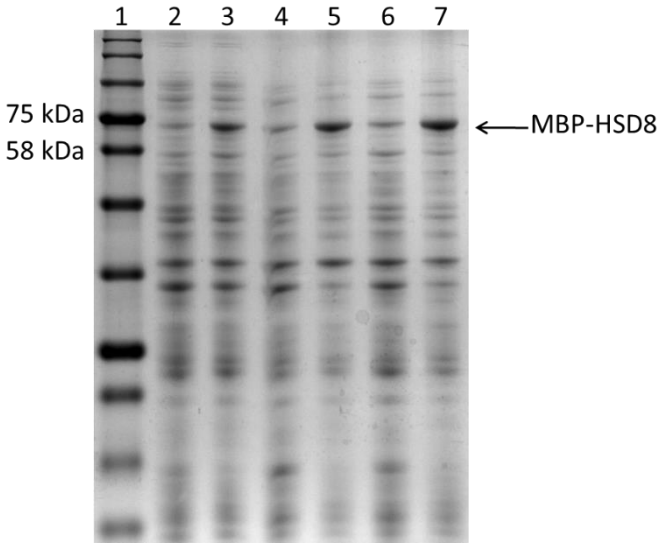

Figure 4.27. MBP-HSD8 expression trial. Protein expression was induced overnight at 15°C, 25°C and 37°. The following morning samples were taken and whole cell lysates generated. Protein expression was assessed via SDS-PAGE and Coomassie Blue staining. Lane 1 = Ladder, Lanes 2/3 = 15°C Non-Induced/Induced, Lanes 4/5 = 25°C Non-Induced/Induced, Lanes 6/7 = 37°C Non-Induced/Induced.

An assessment of the solubility of the MBP-HSD8 fusion protein was made using the previously described methodology (Section 4.22). Soluble protein was observed with induction at 15°C and 25°C, whilst induction at 37°C gave rise to high levels of insoluble protein (Figure 4.28). Overnight induction at 25°C was found to give rise to the highest level of soluble protein and therefore was used for the large scale

purification of the MBP-HSD8 fusion protein. The band corresponding to the MBP-HSD8 protein was excised and sent for mass-spectrometry, confirming protein identity.

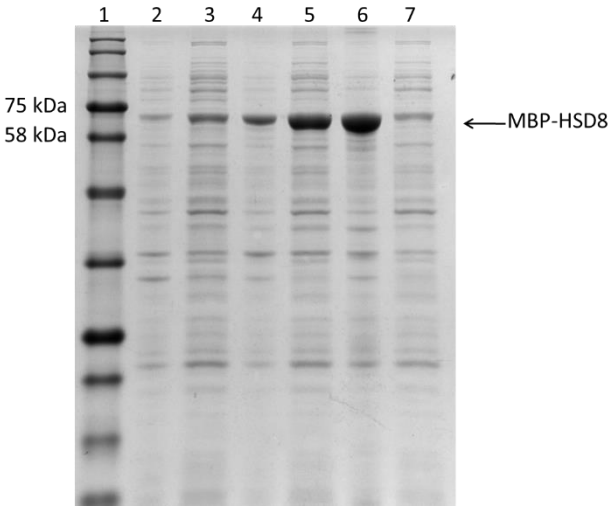

Figure 4.28. MBP-HSD8 insoluble/soluble partitioning. Protein expression was induced overnight at 15°C, 25°C and 37°. The following morning samples were taken and lysed via lysozyme treatment and sonication. Levels of soluble and insoluble protein were assessed via SDS-PAGE and Coomassie Blue staining. Lane 1 = Ladder, Lanes 2/3 = 15°C Insoluble/Soluble, Lanes 4/5 = 25°C Insoluble/Soluble, Lanes 6/7 = 37°C Insoluble/Soluble.

4.25 17β-HSD14: Large-Scale Purification

Initial attempts at the large scale purification of the 17β-HSD14 protein employed the lysis buffer used previously for 17β-HSD10, resulting in significant protein precipitation during loading of the HisTrap Ni-NTA column, clogging the column and resulting in extremely low yields. Optimisation of pH, temperature and NaCl concentration resulted in a reduction of the NaCl concentration used in the cell lysis buffer, from 500 mM to 100 mM, maintaining protein solubility and dramatically improving yield.

Using the newly optimised lysis buffer, a large scale purification of the 17β-HSD14 enzyme was undertaken. In brief, BL21(DE3) *E. coli* cells harbouring the peHISTEV-HSD14 construct were grown to OD_{600}= 0.6-0.8 and protein expression induced overnight at 25°C. Cells were harvested, lysed and the crude lysate applied to a 5 mL HisTrap column. An initial check for protein expression and column loading was made by analysing a sample of cleared lysate and column flow through using SDS-PAGE and Coomassie Blue staining. A prominent band can be seen in the cleared lysate, at approximately 28 kDa, which is no-longer apparent in the column flow-through indicating both 17β-HSD14 expression and column binding (Figure 4.29).

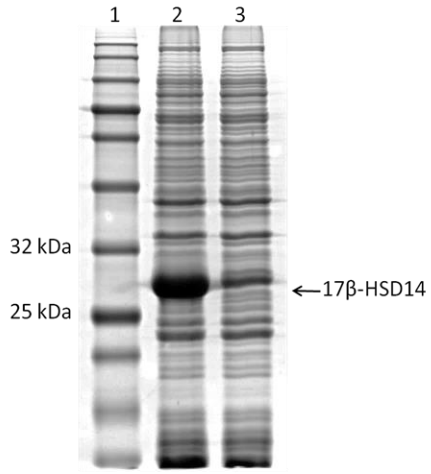

Figure 4.29. 17β-HSD14 expression and column binding. A sample of cleared lysate and column flow-through were analysed using SDS-PAGE and Coomassie Blue staining. A prominent band is apparent in the cleared lysate at approximately 28 kDa, but not in the column flow-through, corresponding to the recombinant 17β-HSD10 protein pre and post column binding Lane 1 = Ladder, Lane 2 = Cleared Lysate, Lane 3 = Column Flow Through.

The column was loaded onto an AKTA-Pure purification rig and washed with a stepwise increase in imidazole concentration until a stable UV baseline was reached. Protein was eluted using a linear gradient of imidazole (100-500 mM) and elution fractions collected periodically. The presence of the 17β-HSD14 enzyme in elution fractions was confirmed by SDS-PAGE and Coomassie Blue staining. A band was observed in all elution fractions, at approximately 28 kDa, corresponding to the 17β-HSD14 enzyme (Figure 4.30). In all cases, a second band was also observed at a lower molecular weight. Using mass-spectrometry, this band was also identified as being 17β-HSD14 and thus may represent a truncated

isoform of the protein. As elution fraction 5 (Figure 4.30, lane 8) was found to harbour comparatively little of this contaminant, it was carried forward for further processing.

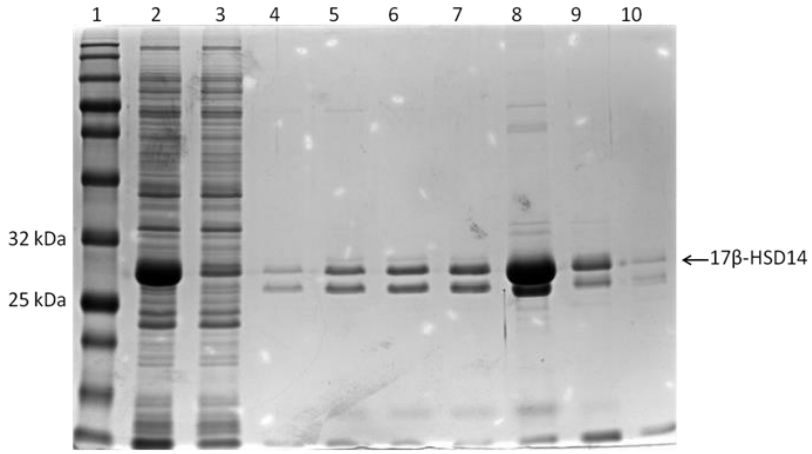

Figure 4.30. 17β-HSD14 Elution Fractions. The HisTrap HP column, loaded with 17β-HSD10 protein was washed with a stepwise increase in imidazole (0-100 mM) removing low affinity contaminants. 17β-HSD10 protein was subsequently eluted using a linear gradient of imidazole (100-500 mM). Lane 1 = Ladder, Lane 2 = Cleared Lysate, Lane 3 = Column Flow Through, Lanes 4-10 = Elution Fractions.

The protein containing sample was dialysed to remove imidazole, TEV-protease added and the solution incubated overnight at 4°C. The following morning TEV cleavage was confirmed via SDS-PAGE and Coomassie Blue staining. Following TEV treatment the band of interest was found to be shifted down, indicative of successful cleavage (Figure 4.31, lane 3).

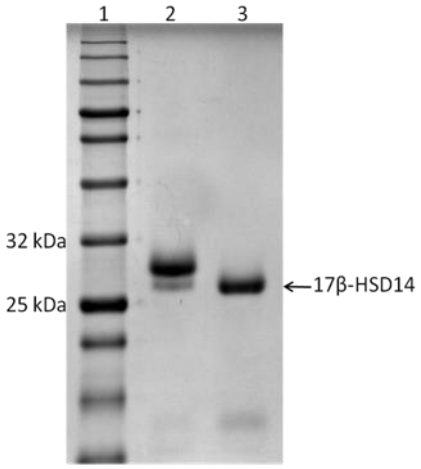

Figure 4.31. 17β-HSD14 TEV cleavage confirmation. TEV protease was employed to remove the 6 x His-tag from the 17β-HSD14 enzyme. A sample was taken pre and post-TEV treatment and analysed using SDS-PAGE and Coomassie Blue staining. Following TEV treatment the band corresponding to the 17β-HSD14 protein is shifted down, indicative of successful cleavage. Lane 1 = Ladder, Lane 2 = Pre-TEV, Lane 3 = Post-TEV.

The TEV cleaved protein was again passed over a HisTrap column, this time allowing the binding of uncleaved protein, 6 x His-tagged TEV protease, free 6 x His-tags and any residual high affinity contaminants. Column flow-through, now containing the protein of interest, was collected.

As a final step, gel filtration was employed. The sample was concentrated using a VivaSpin column (10 kDa MWCO), loaded onto a pre-equilibrated HiLoad Sephadex 75 prep-grade column and elution fractions collected periodically. Samples corresponding to the start, middle and end of the peak were analysed using SDS-PAGE and Coomassie Blue staining, showing high levels of pure 17β-HSD14. The enzyme is known to form a dimer, observed as a faint band present at approximately 56 kDa (Figure 4.32).

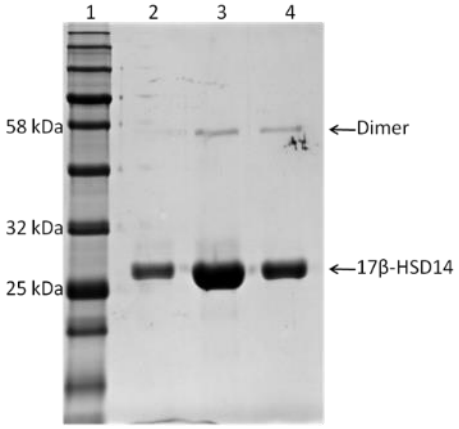

Figure 4.32. 17β-HSD14 Gel Filtration. 17β-HSD14 protein was further purified using gel filtration. Fractions were taken periodically and those corresponding to the start, middle and end of the peak were analysed using SDS-PAGE and Coomassie Blue staining confirming the presence of pure 17β-HSD14 protein. Lane 1 = Ladder, Lanes 2-4 = Start, middle and end of elution peak.

Peak fractions were pooled and concentrated to 10 mg/ml before being snap frozen in liquid nitrogen and stored long term at -80°C. Protein identity confirmed via mass spectrometry.

4.26 17β-HSD8: Large-Scale Purification:

The pET-MBP-HSD8 construct was transformed into BL21(DE3) *E. coli.,* grown to OD_{600}= 0.6-0.8 and protein expression induced overnight at 25°C. The following morning cells were harvested, lysed and the lysate passed over a 5 mL HisTrap Ni-NTA column. To confirm protein expression and column loading, a sample of cleared lysate and column flow through were analysed using SDS-PAGE and Coomassie Blue staining. A prominent band is apparent in the cleared lysate at approximately 67 kDa, corresponding to the MBP-HSD8 fusion protein. This band decreases in intensity in the flow-through but, unlike 17β-HSD10 and 17β-HSD14, does not disappear entirely, indicating that the MBP-HSD8 protein exhibits a lower affinity for the Ni-NTA resin, or that the 5 mL HisTrap column has become saturated with the comparatively large fusion protein (Figure 4.33).

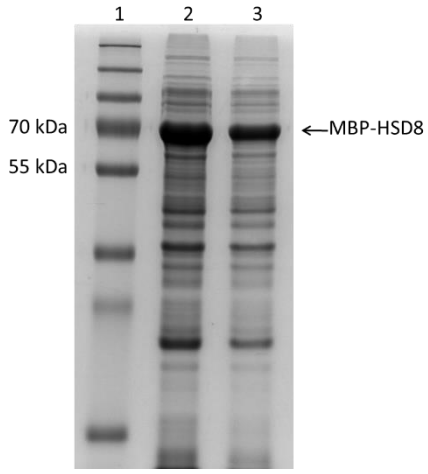

Figure 4.33. MBP-HSD8 expression and column binding. A sample of cleared lysate and column flow-through were analysed using SDS-PAGE and Coomassie Blue staining. A prominent band is apparent in the cleared lysate at approximately 67 kDa, and decrease in intensity in the column flow-through, corresponding to the MBP-HSD8 fusion protein pre and post column binding. Lane 1 = Ladder, Lane 2 = Cleared Lysate, Lane 3 = Column Flow Through.

The column was loaded onto an AKTA-Pure purification rig and washed with a stepwise increase in imidazole concentration (0-100 mM) until a stable UV baseline was reached, indicating low affinity contaminants had been removed. The MBP-HSD8 protein was eluted using a linear gradient of imidazole (100-500 mM) and fractions taken periodically. The presence of MBP-HSD8 protein in elution fractions was confirmed by SDS-PAGE and Coomassie Blue staining (Figure 4.34), with clean protein observed in elution fractions 2 and 3 (lanes 8 and 9).

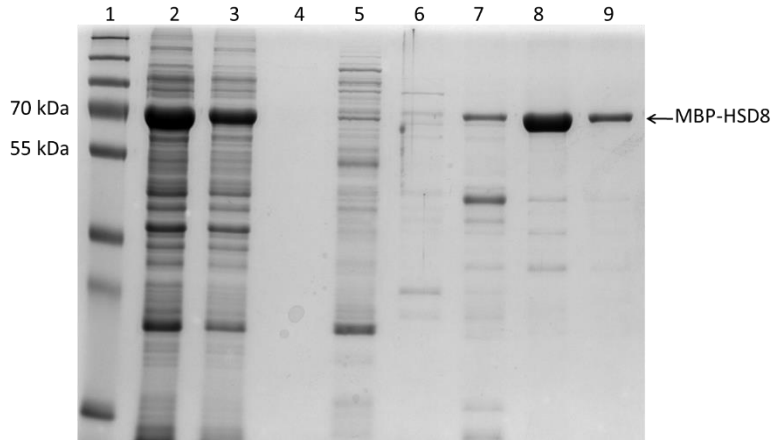

Figure 4.34. MBP-HSD8 wash and elution fractions. The HisTrap HP column, loaded with MBP-HSD8 fusion protein was washed with a stepwise increase in imidazole (0-100 mM) removing low affinity contaminants. MBP-HSD8 protein was subsequently eluted using a linear gradient of imidazole (100-500 mM). Lane 1 = Ladder, Lane 2 = Cleared Lysate, Lane 3 = Column Flow Through, Lanes 4-6 = Wash Fractions, Lanes 7-10 = Elution Fractions.

Elution fractions 2 and 3 were pooled, loaded into a dialysis membrane (10 kDa MWCO) and incubated in fresh buffer, removing imidazole. TEV protease was added and the sample incubated overnight at 4°C. The following morning cleavage was assessed using SDS-PAGE and Coomassie Blue staining. Following TEV treatment, the bands corresponding to the free MBP-tag and free 17β-HSD8 proteins are markedly more prominent, indicating TEV cleavage was successful (Figure 4.25, lane 3). TEV protease itself can be seen below 17β-HSD8 and a faint band of uncleaved fusion protein remains.

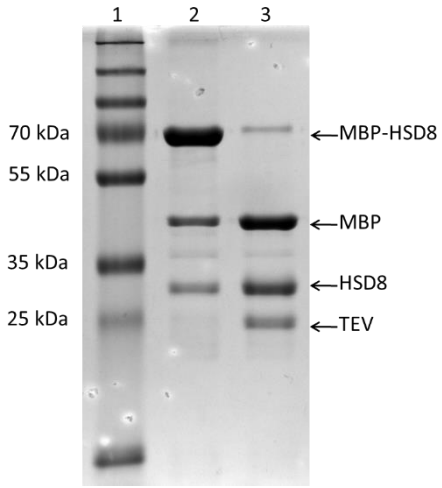

Figure 4.35. MBP-HSD8 TEV cleavage confirmation. TEV protease was employed to remove the MBP-tag from the 17β-HSD8 enzyme. A sample of MBP-HSD8 fusion protein was taken pre and post TEV treatment and analysed using SDS-PAGE and Coomassie Blue staining. Following TEV treatment two bands were apparent, corresponding to the free MBP protein and the 17β-HSD8 enzyme, indicative of successful cleavage. Lane 1 = Ladder, Lane 2 = Pre-TEV, Lane 3 = Post-TEV.

The TEV treated sample was again passed over a HisTrap column, this time allowing the binding of uncleaved protein, 6 x His-tagged TEV protease, 6 x His-tagged MBP protein and any residual high affinity contaminants. A sample pre and post-column loading was assessed via SDS-PAGE and Coomassie Blue staining, showing removal of uncleaved fusion protein, the 6 x His-tagged-MBP protein and 6 x His-tagged-TEV protease (Figure 4.36).

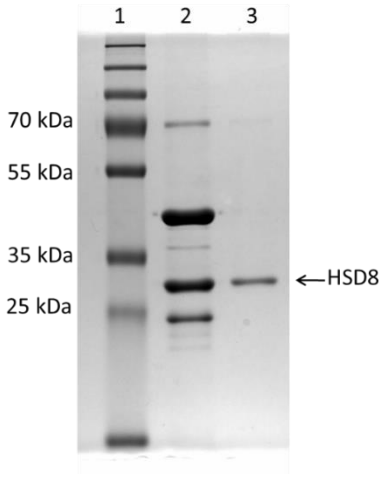

Figure 4.36. 17β-HSD8 Second Affinity. Following TEV cleavage, the sample was again passed over a Histrap HP column, allowing the binding of uncleaved MBP-HSD8, His-Tagged-MBP, His-tagged TEV and any remaining high affinity contaminants, leaving clean 17β-HSD8 protein. Lane 1 = Ladder, Lane 2 = Pre-second affinity, Lane 3 = Post second affinity.

The quantity of 17β-HSD8 in the column flow-through was found to be comparatively low, suggesting the protein has an intrinsic affinity for the Ni-NTA resin. Thus, a stepwise increase in imidazole was used to elute protein bound to the column, dramatically improving yield. Two clean fractions of 17β-HSD8 protein were obtained (Figure 4.37, lanes 2 and 3), with the 6 x His-tagged-MBP protein and 6 x His-tagged-TEV protease eluting in later fractions (Figure 4.37, lanes 4-6).

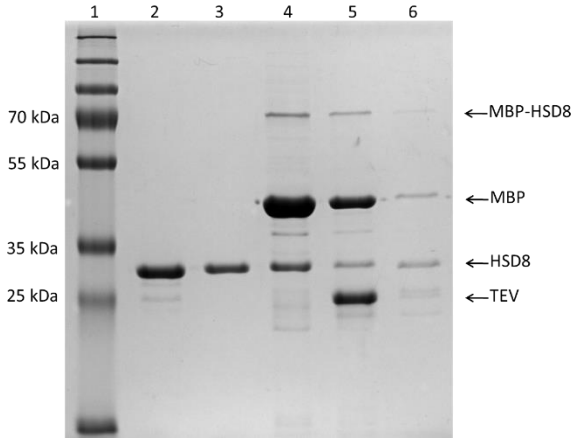

Figure 4.37. 17β-HSD8 Second Affinity Elution. To elute bound 17β-HSD8 protein following a second affinity step, a stepwise increase in imidazole concentration was used, with two clean fractions of 17β-HSD8 protein obtained. Lane 1 = Ladder, Lanes 2-6 = Elution fractions.

Protein containing fractions were pooled, concentrated and loaded onto a pre-equilibrated HiLoad Sephadex 75 prep-grade column. Elution fractions were collected periodically with two peaks observed. Fractions corresponding to the start, middle and end of each peak were analysed via SDS-PAGE and Coomassie Blue staining. A faint high molecular weight band was observed in fractions taken from the first peak (Figure 4.37, Lanes 2-4), possibly a multimer of the 17β-HSD8 enzyme. Clean monomeric 17β-HSD8 protein was observed in fractions corresponding to the second peak (Figure 4.38, Lanes 6-8).

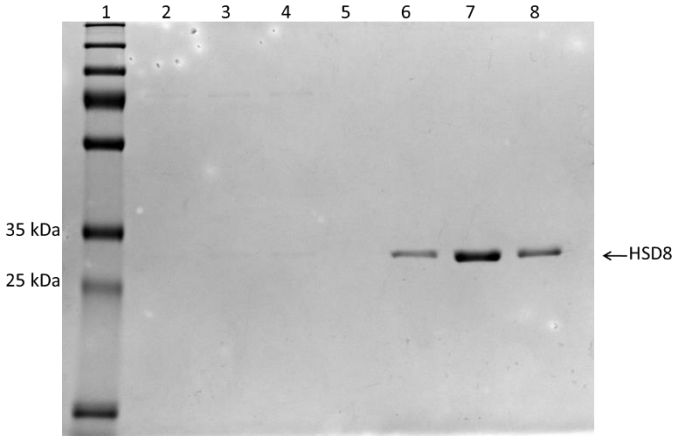

Figure 4.38. 17β-HSD8 Gel Filtration. 17β-HSD8 protein was further purified by gel filtration. Fractions were taken periodically and those corresponding to the start, middle and end of the two observed peaks were analysed using SDS-PAGE and Coomassie Blue staining confirming the presence of pure 17β-HSD8 protein. Lane 1 = Ladder, Lanes 2-4 = Start, middle and end of elution peak 1, Lanes 6-8= Start, middle and end of elution peak 2.

Fractions 6-8 were pooled, concentrated to 2 mg/mL, flash frozen in liquid nitrogen and stored long term at -80°C. Protein identity confirmed via mass-spectrometry.

4.27 Purified Protein Concentration Check:

The extinction coefficients calculated for the 17β-HSD8, 17β-HSD10 and 17β-HSD14 and subsequently used to monitor protein concentration throughout the purification procedure are known to be reasonably inaccurate. Using a training set of 116 proteins, the predicted extinction coefficients have been shown to vary from the experimental calculated value by an average of 3.17%, however in the absence of tryptophan residues, this error can increase to greater than 10%[364]. As the 17β-HSD8, 17β-HSD10 and 17β-HSD14 proteins harbour relatively low numbers of tryptophan residues (1, 0 and 2 respectively), there is the possibility that the calculated extinction coefficient, and thus the estimated protein concentration, may be inaccurate. For compound screening experiments, where enzyme activity is reported as a percentage of control, the absolute enzyme concentration is arguably less important than for the calculation kinetic constants, where activity is reported per unit enzyme (mg^{-1}). Prior to undertaking a kinetics based appraisal of the 17β-HSD8 and 17β-HSD14 enzymes, a check was made to ensure the protein concentrations determined via absorbance at 280 nm were reasonably accurate. Samples of 17β-HSD8, 17β-HSD10 and 17β-HSD14 were diluted to an expected concentration of 0.5 mg/mL and the actual protein concentration determined using the BCA assay. In all cases, the protein concentration as determined by BCA assay was extremely close to that estimated using absorbance at 280 nm (Figure 4.39).

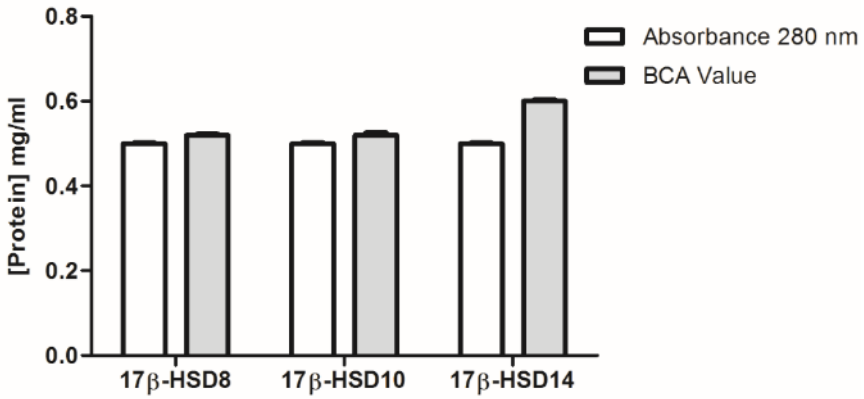

Figure 4.39. Expected vs actual protein concentration. Samples of purified 17β-HSD8, 17β-HSD10 and 17β-HSD14 were diluted to an expected 0.5mg/mL concentration, as determined by absorbance at 280 nm. The actual protein concentration was determined using the BCA assay. In all cases the protein concentration as determined via absorbance at 280 nm was found to be accurate. Values shown are an average taken from one experiment with three technical repeats ± SEM.

4.3 17β-HSD8 and 17β-HSD14 Recombinant Enzyme Assays:

4.31 Initial Activity Tests

An initial test for activity was made using high, saturating concentrations of substrate, β-estradiol, and cofactor, NAD^+, and varying concentrations of 17β-HSD8 and 17β-HSD14 enzyme. The reported specific activity values for the conversion of estradiol to estrone by both 17β-HSD8[365] and 17β-HSD14[366,367] are significantly lower than that observed previously for 17β-HSD10 and acetoacetyl-CoA (section 1.03), being in the realms of nmol/min^{-1}/mg^{-1} as opposed to µmol/min^{-1}/mg^{-1} and as such, the absorbance assay used previously was exchanged for a fluorescence based read-out, giving increased sensitivity. As would be expected, with increasing enzyme concentration, a dose dependent increase in the rate of reaction was observed (Figures 4.40 and 4.41).

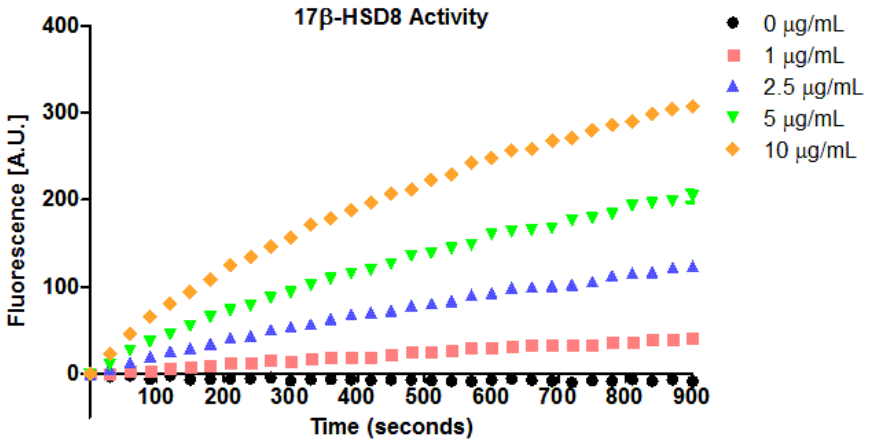

Figure 4.40. 17β-HSD8 enzymatic activity. The rate estadiol conversion to estrone was monitored over time as a function of NADH fluorescence in the presence of increasing concentrations of 17β-HSD8 enzyme. Values shown are an average of one experiment with three technical ± SEM.

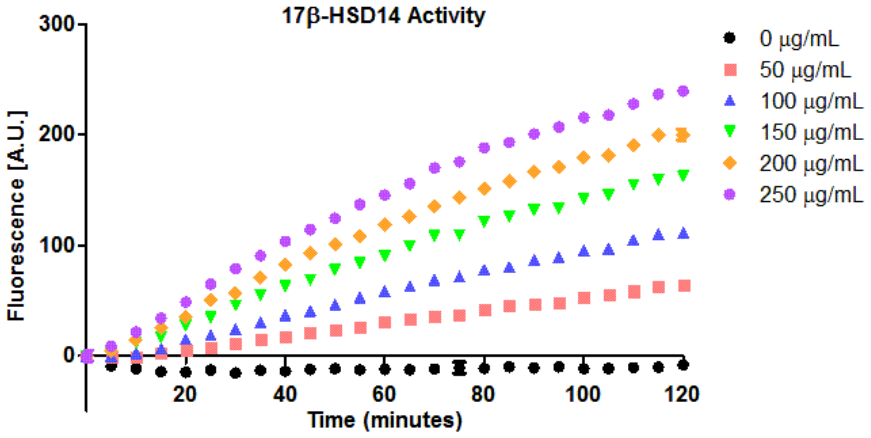

Figure 4.41. 17β-HSD14 enzymatic activity. The rate estadiol conversion to estrone was monitored over time as a function of NADH fluorescence in the presence of increasing concentrations of 17β-HSD14 enzyme. Values shown are an average of one experiment with three technical repeats ± SEM.

The rate of reaction was determined during the linear period of the progress curve for both the 17β-HSD8 and 17β-HSD14 enzymes, again confirming a dose dependent increase in activity with increasing enzyme concentration (Figures 4.42 and 4.43). Concentrations of 5 µg/mL 17β-HSD8 and 150 µg/mL 17β-HSD14 were selected for subsequent experiments, ensuring linearity over a suitable time-interval, giving a high signal to noise ratio and also conserving protein.

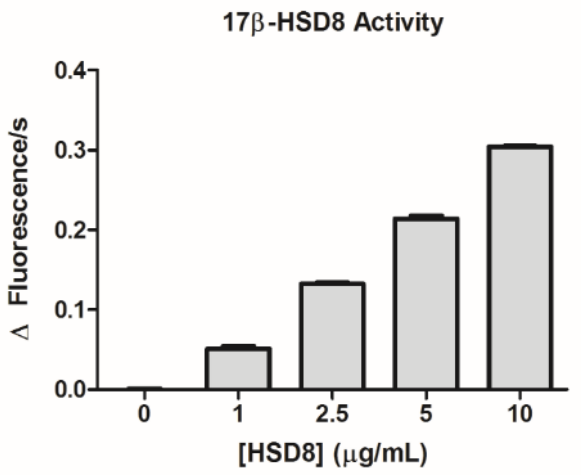

Figure 4.42. 17β-HSD8 rate of reaction. The rate of the 17β-HSD8 catalysed conversion of estradiol to estrone was measured as a function of NADH fluorescence over time. With increasing enzyme concentration, a dose dependent increase in the rate of reaction was observed, suggesting the purified 17β-HSD8 enzyme is catalytically active. Values are an average taken from one experiment with three technical repeats ± SEM.

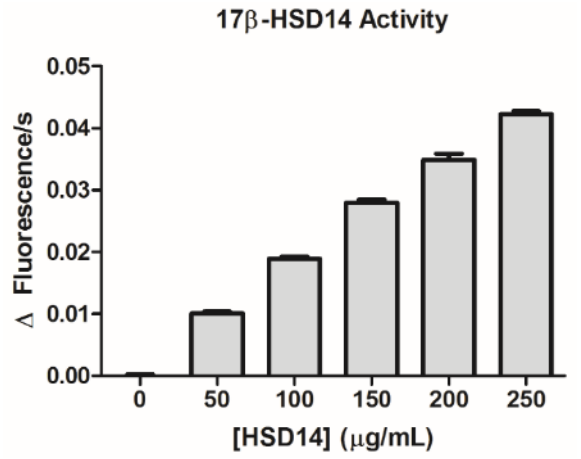

Figure 4.43. 17β-HSD14 rate of reaction. The rate of the 17β-HSD14 catalysed conversion of estradiol to estrone was measured as a function of NADH fluorescence over time. With increasing enzyme concentration, a dose dependent increase in the rate of reaction was observed, suggesting the purified 17β-HSD14 enzyme is catalytically active. Values are an average taken from one experiment each with three technical repeats ± SEM.

4.32 Michaelis-Menten Kinetics

Michaelis-menten kinetics were derived for 17β-HSD8 with respect to substrate, estradiol and cofactor, NAD^+. A V_{max} value of 657.6 ± 28.6 nmol min^{-1} mg^{-1} and a K_m value of 30.7 ± 3.3 µM were calculated for 17β-HSD8 with respect to estradiol. With respect to cofactor, NAD^+, a V_{max} value of 573.5 ± 17.0 nmol min^{-1} mg^{-1} and a K_m value of 367.1 ± 27.8 µM were calculated (Figure 4.44). Substrate and cofactor concentrations of 50 µM estradiol and 500 µM NAD^+ were passed forward into compound screening experiments using 17β-HSD8.

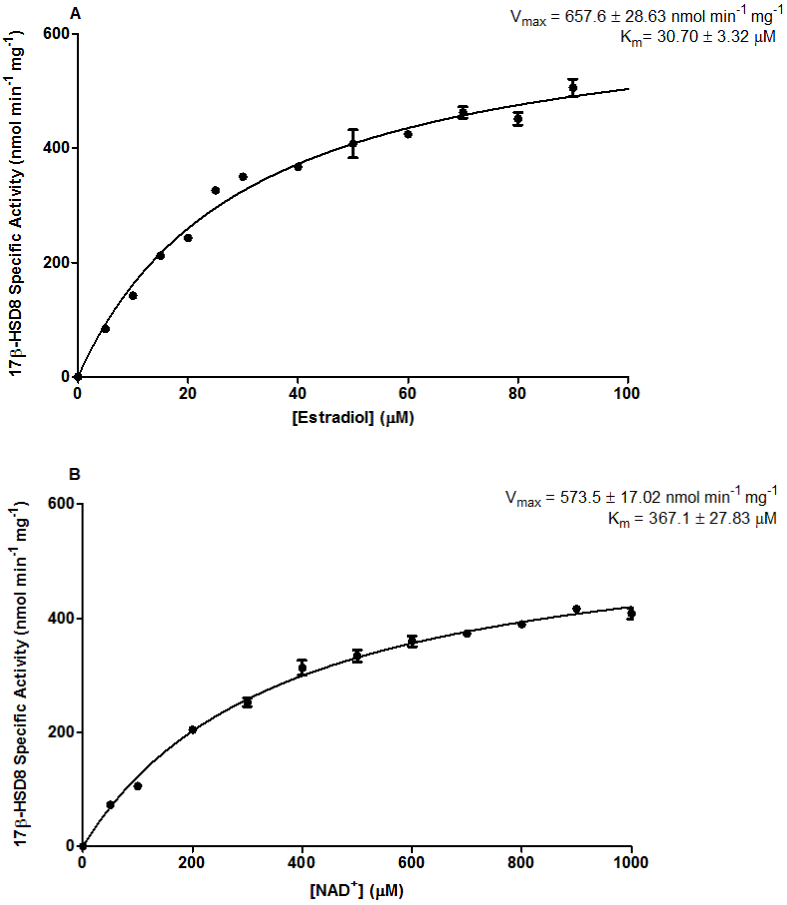

Figure 4.44. 17β-HSD8 Michaelis-Menten kinetics. V_{max} and K_m were calculated with respect to estradiol (top) and NAD^+ (bottom) for the 17β-HSD8 enzyme. A V_{max} value of 657.6 ± 28.6 nmol min^{-1} mg^{-1} and a K_m value of 30.7 ± 3.3 µM were calculated with respect to estradiol. A V_{max} value of 573.5 ± 17.0 nmol min^{-1} mg^{-1} and a K_m value of 367.1 ± 27.8 µM were calculated with respect to NAD^+. Values shown are an average of two independent experiments each with three technical repeats ± SEM.

Michaelis-Menten kinetics were similarly derived for 17β-HSD14 with respect to substrate, estradiol and cofactor, NAD^+. A V_{max} value of 3.5 ± 0.1 nmol min^{-1} mg^{-1} and a K_m value of 33.4 ± 2.7 µM were calculated for the 17β-HSD14 enzyme with respect to estradiol. With respect to cofactor, NAD^+, a V_{max} value of 2.4 ± 0.1 nmol min^{-1} mg^{-1} and a K_m value of 73.0 ± 7.2 µM were calculated (Figure 4.45). Substrate and cofactor

concentrations of 50µM estradiol and 150 µM NAD^+ were passed forward into compound screening experiments using 17β-HSD14.

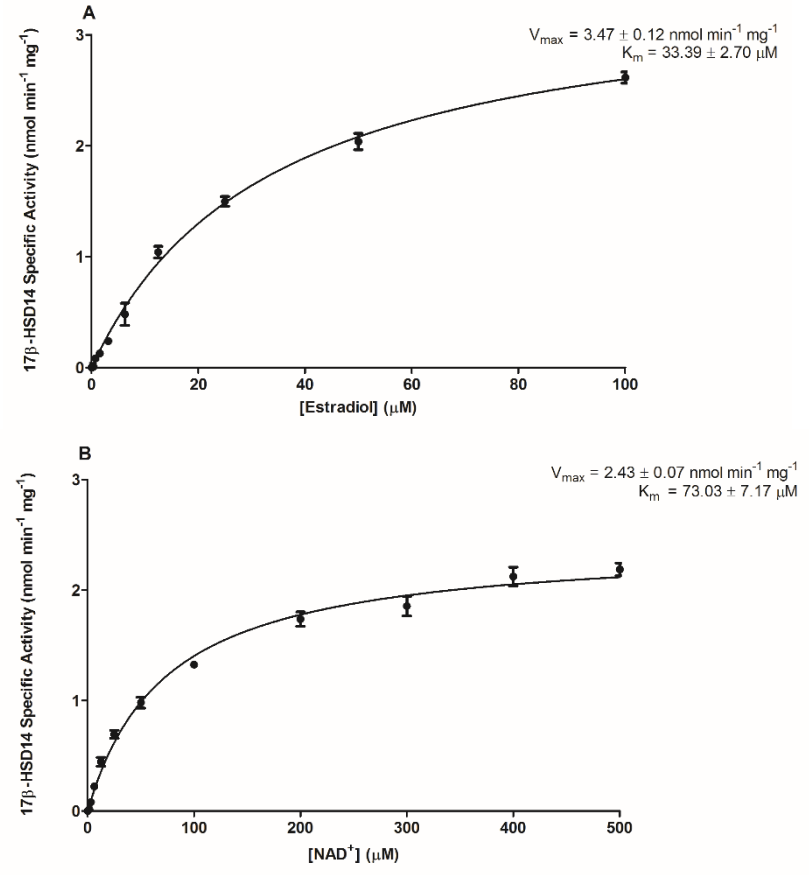

Figure 4.45. 17β-HSD14 Michaelis-Menten Kinetics. V_{max} and K_m were calculated with respect to estradiol (top) and NAD^+ (bottom) for the 17β-HSD8 enzyme. A V_{max} value of 657.6 ± 28.6 nmol min^{-1} mg^{-1} and a K_m value of 30.7 ± 3.3 µM were calculated with respect to estradiol. A V_{max} value of 573.5 ± 17.0 nmol min^{-1} mg^{-1} and a K_m value of 367.1 ± 27.8 µM were calculated with respect to NAD^+. Values shown are an average of two independent experiments each with three technical repeats ± SEM.

4.33 Inhibitor Screening 17β-HSD10, 17β-HSD8 and 17β-HSD14

To give a measure of compound specificity, known inhibitors of the 17β-HSD10 enzyme were screened against 17β-HSD8 and 17β-HSD14 at a saturating concentration, as determined previously against 17β-HSD10 (K690/K691/K1093 = 12.5 µM, 88401= 50 µM, AG18051= 6.25 µM, Chapter 3: Sections 3.05, 3.07, 3.13). Compound AG18051 was found to be extremely specific resulting in 96.80 ± 0.49% inhibition of 17β-HSD10, 7.10 ± 3.14% inhibition of 17β-HSD8 and 4.87 ± 5.39% inhibition of 17β-HSD14. Compound 88401 resulted in a significant and approximately equal decrease in activity of both 17β-HSD10 and 17β-HSD8, 67.36 ± 1.22% and 63.99 ± 3.26%, respectively. A non-significant decrease in activity of the 17β-HSD14 enzyme, 11.13 ± 4.52%, was also observed in the presence of this compound. Frentizole derived compounds; K690, K691 and K1093 induced a significant decrease in activity of all three enzymes with 17β-HSD10 showing 57.89 ± 1.71% inhibition, 63.24 ± 5.26% inhibition and 82.09 ± 0.85% inhibition in the presence of compounds K690, K691 and K1093, respectively. In the presence of compounds K690, K691 and K1093, 17β-HSD8 exhibited 66.16 ± 1.49% inhibition, 78.62 ± 2.70% inhibition and 59.00 ± 1.37% inhibition respectively whilst 17β-HSD14 showed 25.18 ± 3.28% inhibition, 21.18 ± 2.04% inhibition and 19.71 ± 2.56% inhibition (Figure 4.46).

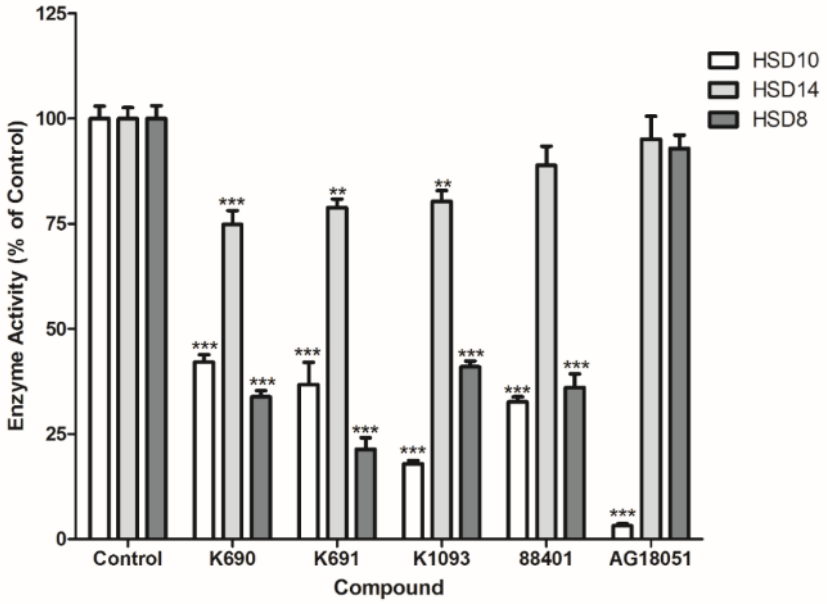

Figure 4.46. Inhibitor specificity 17β-HSD10, 17β-HSD8 and 17β-HSD14. Validated 17β-HSD10 inhibitors were subsequently screened against 17β-HSD8 and 17β-HSD14 at a saturating concentration (as determined against 17β-HSD10). Values shown are an average of two independent experiment, each with three technical repeats ± SEM. Statistical analysis was performed using a one-way ANOVA with Bonferonni multiple comparisons. * = P ≤ 0.05, ** = P ≤ 0.01, *** = P ≤ 0.001, **** = P ≤ 0.0001.

Chapter 4 - Discussion:

A key property of any drug molecule is specificity of action, allowing the therapeutic modulation of a protein of interest, whilst sparing closely related homologues and thereby avoiding off-target affects and toxicity. The 17β-hydroxysteroid dehydrogenase family, to which 17β-HSD10, our target enzyme belongs, contains a further 13 closely related enzymes and thus the likelihood of off-target effects appears high and worthy of investigation. On the basis of a structural similarity search, performed using the RCSB Protein Data Bank website, two closely related enzymes, 17β-HSD8 and 17β-HSD14, were identified. The coding sequence for each enzyme was cloned, proteins purified and activity assays developed allowing a measure of inhibitor specificity to be generated.

The 17β-HSD8 cDNA sequence was custom synthesised using the GeneArt service offered by Thermo Fisher and was cloned into our standard peHISTEV expression vector. Protein expressed using the resultant peHISTEV-HSD8 construct and BL21(DE3) *E. coli* was found to be insoluble under all conditions tested (Figure 4.23) and thus the 17β-HSD8 cDNA sequence was subcloned into a second pET derived expression vector, generating a fusion protein with the solubility enhancing maltose binding protein (MBP-HSD8). The MBP-HSD8 fusion protein was soluble and subsequently purified successfully (Section 4.26).

The 17β-HSD14 cDNA sequence was reverse transcribed from an mRNA template and cloned into our standard peHISTEV expression vector, yielding soluble protein when expressed in Bl21(DE3) *E. coli*. During protein elution from the Ni-NTA affinity column, two bands were observed with both subsequently being identified as 17β-HSD14 via mass spectrometry (Figure 4.30). Whilst under ideal conditions, a recombinant protein would be expressed in a single homogenous form, this is not always the case. The lower molecular weight of the second minor band of 17β-HSD14 protein suggests it may represent a truncated isoform of the protein. Due to differing tRNA abundance and the concomitant differential codon usage between prokaryotic and eukaryotic organisms, some mammalian proteins can be difficult to express using a bacterial system[368]. The presence of such rare codons can result in premature termination of translation, particularly when such residues are present sequentially within the coding sequence, potentially explaining the observed secondary minor band of 17β-HSD14.

A check was made for rare codons within the 17β-HSD14 coding sequence using the Rare Codon Calculator[369], identifying a number of potentially problematic residues, although not sequentially within the coding sequence (see Appendix: E). To circumvent this issue, the cDNA sequence could be codon-optimised for expression using *E. coli,* requiring the gene to be custom synthesised, or extensive rounds of site directed mutagenesis. A different strain of *E. coli* could also be utilised in-place of BL21(DE3). Two such variants, BL21-Codon Plus and BL21-Rosetta, are engineered to express higher than normal levels of these rare tRNA molecules, preventing stalling of the translation machinery and thus resulting in higher yields of full length protein. Alternatively, the 6 x His-tag used for Ni-NTA mediated protein purification could also be moved from the N-terminus of the protein, to the C-terminus thereby only isolating full

length 17β-HSD14. A second explanation for this minor band of 17β-HSD14 protein, relates to the fact that the 17β-HSD14 protein is predicted to harbour an internal disulphide bridge (DIANNA webserver[370]) and thus the second band may represent an incompletely reduced isoform of the protein, possibly due to the use of old loading dye, resulting in a protein with altered secondary structure and a modified migration through the gel.

To characterise the catalytic properties of the 17β-HSD8 and 17β-HSD14 enzymes, and to guide subsequence compound screening experiments, a kinetics based appraisal was undertaken for both enzymes. Michaelis-Menten parameters, V_{max} and $K_{m,}$ were calculated for both enzymes with respect to substrate, estradiol, and cofactor, NAD^+.

The V_{max} and K_m values calculated here for the 17β-HSD14 enzyme with respect to estradiol, V_{max} = 3.47 ± 0.12 nmol min^{-1} mg^{-1}, K_m = 33.39 ± 2.70 µM, are in line with those previously reported in the literature, V_{max} = 2.5 ± 1.0 nmol min^{-1} mg^{-1} and K_m = 5.6 ± 1.2 µM[367]. However, the values calculated for 17β-HSD8, V_{max} = 657.6 ± 28.63 nmol min^{-1} mg^{-1}, K_m = 30.70 ± 3.32 µM, are dramatically higher than those reported previously, V_{max} =0.405 ± 0.046 nmol min^{-1} mg^{-1} and K_m = 0.110 ± 0.02 µM[365]. This discrepancy may be attributed to a number of experimental differences, or, more likely, a combination of these factors.

First, the previously reported rate constants were derived from protein generated using the murine coding sequence for the 17β-HSD8 enzyme[365], as opposed to the human sequence employed here, possibly contributing to the observed differences in catalytic activity. However, an alignment of the primary sequences for both human and mouse variants of the 17β-HSD8 enzyme reveals a high degree of sequence identity (87.1%, Figure 4.47). In addition, the differential amino acids map to non-conserved regions outside of the active site and thus it seems unlikely that primary sequence differences are in of themselves able to account for the dramatically differing levels of reported enzymatic activity.

```
87.1% identity in 256 residues overlap; Score: 1138.0; Gap frequency: 0.0%

Human           6 QNRLRSALALVTGAGSGIGRAVSVRLAGEGATVAACDLDRAAAQETVRLLGGPGSKEGPP
Mouse           4 QLRLRSALALVTGAGSGIGRAISVRLAAEGAAVAACDLDGAAAQDTVRLLGSPGSEDGAP
                  * ******************** ***** *** ******* **** ****** ***  * *

Human          66 RGNHAAFQADVSEARAARCLLEQVQACFSRPPSVVVSCAGITQDEFLLHMSEDDWDKVIA
Mouse          64 RGKHAAFQADVSQGPAARRLLEEVQACFSRPPSVVVSCAGITRDEFLLHMSEEDWDRVIA
                  ** *********   *** *** ******************** ********* *** ***

Human         126 VNLKGTFLVTQAAAQALVSNGCRGSIINISSIVGKVGNVGQTNYAASKAGVIGLTQTAAR
Mouse         124 VNLKGTFLVTQAAAQALVSSGGRGSIINISSIIGKVGNIGQTNYASSKAGVIGLTQTAAR
                  ****************** * ********** ***** ****** **************

Human         186 ELGRHGIRCNSVLPGFIATPMTQKVPQKVVDKITEMIPMGHLGDPEDVADVVAFLASEDS
Mouse         184 ELGRHGIRCNSVLPGFIATPMTQKMPEKVKDKVTAMIPLGHMGDPEDVADVVAFLASEDS
                  ************************ * ** ** * *** ** ******************

Human         246 GYITGTSVEVTGGLFM
Mouse         244 GYITGASVEVSGGLFM
                  ***** **** *****
```

Figure 4.47. Amino acid sequence alignment of human and mouse 17β-HSD8 protein. The primary amino acid sequence for human and murine 17β-HSD8 protein were aligned using the ExPASY SIM alignment tool, identifying a number of differences.

A more likely explanation relates to the protein purification methodologies utilised here and previously by Fomitcheva *et al.*[365], which would likely result in preparations of differing purity. Here, a combination of Ni-NTA chromatography and size exclusion chromatography were employed and, although somewhat unnecessary given the small size of the 6 x His-tag (0.84 kDa), an additional pass over the Ni-NTA column was included to remove free 6 x His-tags following TEV cleavage, resulting in a reasonably pure protein preparation as indicated by SDS-PAGE and Coomassie Blue staining (Figure 4.38). For the purification of the murine homologue of the 17β-HSD8 enzyme, a single chromatography step was employed using a GST-tag and a glutathione sepharose column. A single chromatography step is also unlikely to result in a pure protein product, as is indicated by the additional bands present in the final preparation (Figure 4.48)[365], likely contributing to the described discrepancies in catalytic efficiency. In addition, following thrombin cleavage, no additional step was employed to remove the now free and contaminating GST-tags[365]. As the GST-tag and 17β-HSD8 enzyme are comparable in size, 26 kDa and 27 kDa respectively, and will be present at a one to one molar ratio, the accurate determination of the concentration of 17β-HSD8 protein in the final protein preparation will be difficult, if not impossible.

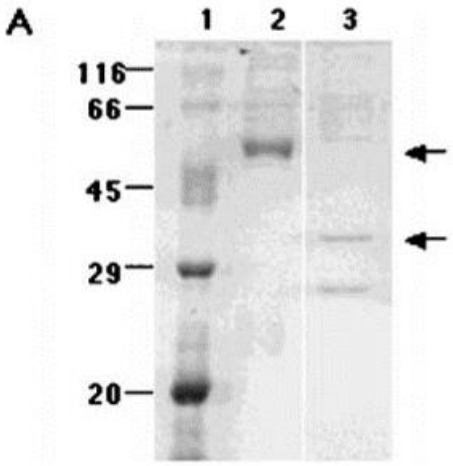

Figure 4.48. Fomitcheva *et al.* 17β-HSD8 purification. 17β-HSD8 was purified from crude cell lysate using a single GST based chromatography step resulting in an impure final preparation. Lane 1= Ladder, Lane 2= 17β-HSD8-GST protein, Lane 3= Thrombin cleaved 17β-HSD8 protein (Top arrow= 17β-HSD8-GST Fusion in Lane 2, Bottom Arrow= Thrombin cleaved 17β-HSD8 in Lane 3, Bottom Band in Lane 3= Free GST-tag, Top smear in Lane 3= Unknown). Figure reproduced from[365].

Finally, the 17β-HSD8 enzyme appears to have an intrinsic tendency to fold incorrectly, indicated by the formation of inclusion bodies when overexpressed in *E. coli*, classically considered a marker of protein misfolding[371] (Figure 4.23). The MBP-tag has been shown to be comparably more effective than the GST-tag in promoting protein solubility, and presumably correct folding, resulting in preparations of higher enzymatic activity[372-375]. Thus, a higher proportion of the 17β-HSD8 purified here using an MBP-tag may be correctly folded and thus relatively more active, per unit mass, than that produced previously using the GST-tag.

In contrast to our expectation, in terms of inhibitor potency and specificity, compound AG18051 (Figure 4.49) was found to be by far and away the best, resulting in almost complete inhibition of 17β-HSD10, the target enzyme, and no significant decrease in the activity of 17β-HSD8 and 17β-HSD14 (Figure 4.46).

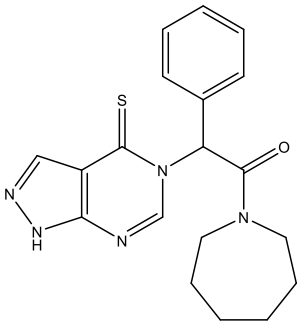

Figure 4.49. Structure AG18051. Compound AG18051 was identified as a potent inhibitor of the 17β-HSD10 by Kissinger *et al.* in 2004[350].

The small molecule inhibitors identified as a result of this investigation; compounds K690, K691, 88401 and K1093 (Figure 4.50), appear to show specificity for 17β-HSD10 over 17β-HSD14, with compound 88401 resulting in no significant decrease in activity of 17β-HSD14, whilst compounds K690, K691 and K1093 resulted in a significant but comparably small decrease in activity, as compared to that seen with 17β-HSD10 (Figure 4.46). However, all four compounds were found to induce a large and significant decrease in activity of the 17β-HSD8 enzyme (Figure 4.46).

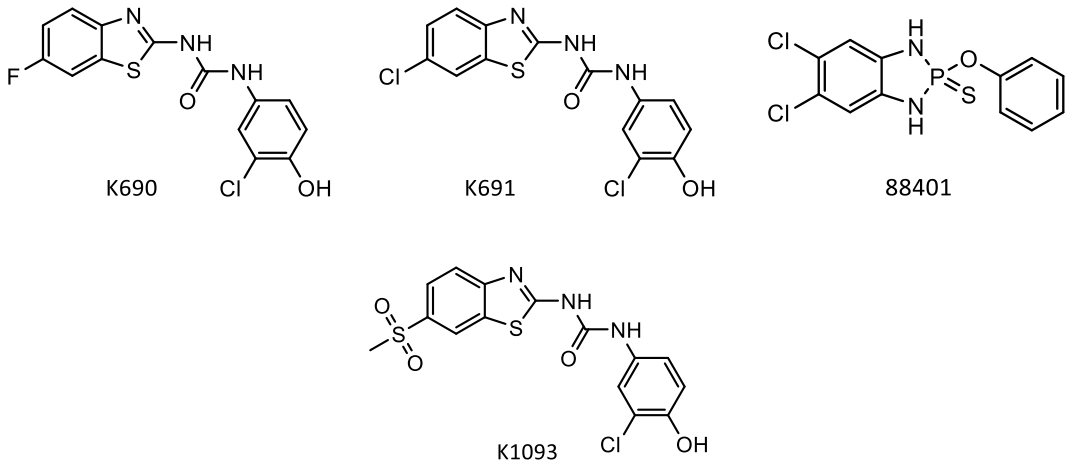

Figure 4.50. Identified 17β-HSD10 enzyme inhibitors. As a result of this investigation, a number of inhibitors of the 17β-HSD10 enzyme were identified. K690, K691 and K1093, derived from the Frentizole parent scaffold and 88401 identified as a result of a large screen of the NCI diversity IV compound library (Sections 3.06 and 3.13)

Whilst the compounds identified herein compare poorly with AG18051, all, with the exception of compound K1093, represent initial screening hits and thus are likely to be suboptimal in terms of potency and specificity. Compound K1093, with alternate substitution at position 5 of the benzothiazole moiety,

exhibits increased potency against 17β-HSD10 and decreased potency against 17β-HSD8 as compared to compounds K690 and K691, suggesting further substitution of the benzothizaole moiety at position 5 may be advantageous for subsequent generations of more specific inhibitors.

The results obtained here again re-emphasise the need for a crystal structure of the 17β-HSD10 enzyme and now also the 17β-HSD8 enzyme in complex with inhibitor, allowing the rational design of subsequent compound series with improved potency against 17β-HSD10, and specificity as measured against 17β-HSD8. Whilst previous attempts have been made within the group to generate a crystal structure of the 17β-HSD10 enzyme, all have failed. All previously published crystal structures of 17β-HSD10 (PDB ID: 2023, 1SO8, 1U7T) harbour at least one ligand, presumably stabilising the structure of the enzyme and, now that the mechanism of inhibition utilised by our Frentizole derived inhibitors is understood (Section 3.08), such an approach appears viable for the generation of enzyme-inhibitor-cofactor complexes. In addition, now validated, differential scanning fluorimetry may prove of use allowing the rational optimisation of buffer composition and the identification of stabilising additives which may further improve the chances of crystal formation. To illustrate the point, previous crystal trials were performed at pH values as low as 4.0, however, using DSF and a three buffer system (citric acid, HEPES, CHES), allowing the effects of buffer composition and pH to be delineated, it becomes apparent that below pH 5.5-5.0 the 17β-HSD10 enzyme is denatured, indicated by an altered melt profile and increased initial fluorescence (Figure 4.51). As such, DSF may be used to narrow the range of conditions trailed in a logical manner, concentrating time and resources into the most promising avenues of investigation and thereby increasing the chances of success.

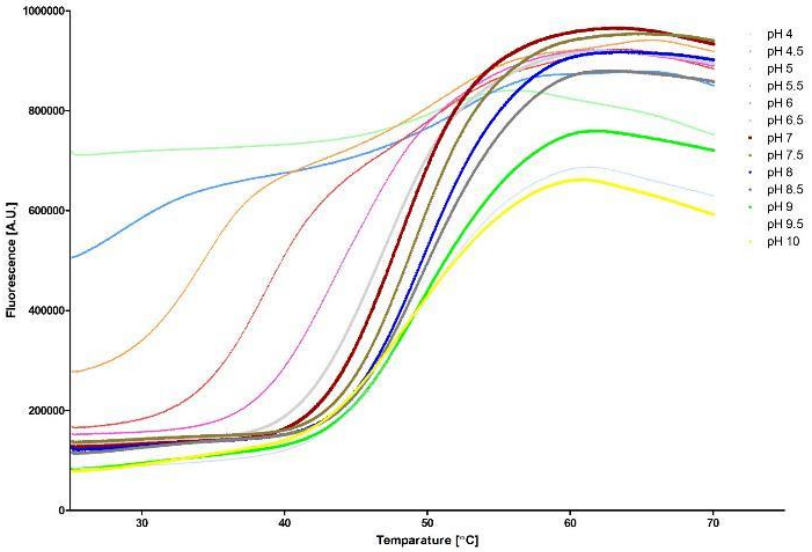

Figure. 4.51. Differential scanning fluorimetry mediated buffer optimisation. DSF can be used to rationally alter buffer composition, improving protein stability and thereby improving the chances of crystal formation, indicated here using a gradient from pH 4-10. Values shown are an average of two independent experiments, each with three technical repeats. For clarity, error bars have been omitted.

Chapter 5: Development of a 17β-HSD10 Driven Cellular AD Model

Chapter 5 - Introduction and Aims:

So far I have developed a highly robust screening assay for our target enzyme 17β-HSD10, leading to the identification of a number of novel enzyme inhibitors (Chapter 3). In addition, I have cloned, purified and developed screening assays for two close structural homologues of the 17β-HSD10 enzyme, 17β-HSD8 and 17β-HSD14, allowing a measure of inhibitor specificity to be generated (Chapter 4). Whilst such assays are useful as initial explorative screening tools, given their high-throughput and low cost, they do little to recapitulate the complex environment found within the cell. Thus, it would be advantageous to develop a robust cellular based disease model against which compounds of interest can be tested. Previous work performed by Shi du Yan *et al.* has shown that the co-expression of catalytically active 17β-HSD10 enzyme with Aβ results in a marked increase in oxidative stress, whilst the overexpression of a catalytically inactive mutant of the 17β-HSD10 enzyme with Aβ does not[338], a property which could potentially be exploited to generate a cellular screening tool.

Using site directed mutagenesis, a catalytically inactive mutant of the 17β-HSD10 enzyme would first be generated. The wild-type 17β-HSD10 and the catalytically inactive mutant would subsequently be introduced into a mammalian cell line alongside Aβ, after which relative levels of oxidative stress would be assessed using a commercially available probe. If previous work is correct, treatment with Aβ should induce a marked increase in oxidative stress when catalytically active 17β-HSD10 enzyme is present. Validated 17β-HSD10 inhibitors would be titrated onto a wild-type 17β-HSD10/Aβ background, hopefully showing for the first time a reversal of a disease relevant phenotype and confirming that the direct inhibition of 17β-HSD10 activity is of therapeutic merit in treating AD. Cells harbouring a catalytically inactive mutant of the 17β-HSD10 enzyme would act as a no-stress control, accounting for intrinsic levels of reactive oxygen species and in doing so, defining the window for intervention (illustrated in Figure 5.01). The aim of this chapter was to develop such an assay.

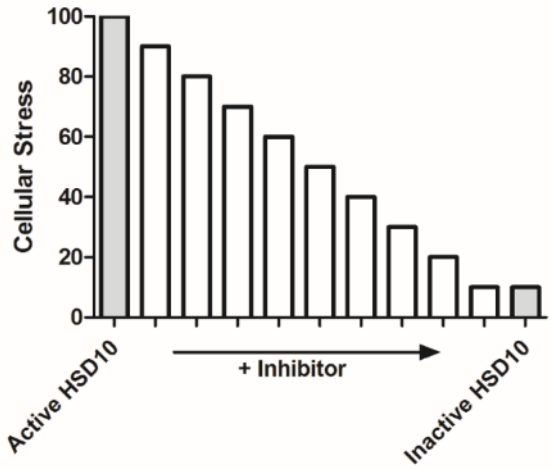

Figure 5.01. Hypothetical 17β-HSD10 based cellular disease model. The combined expression of active 17β-HSD10 with Aβ has been shown to induce a marked increase in oxidative stress, whilst inactive 17β-HSD10 does not. Thus, through the use of a reactive oxygen species marker a high throughput screening tool could be generated allowing compounds of interest to be tested in a cellular environment.

5.1 Mammalian 17β-HSD10 Inhibition

When producing recombinant protein, a number of expression systems can be utilised; broadly divided into prokaryotic, eukaryotic or cell free. Here, a prokaryotic *E. coli* based system was used, primarily due to the facilities available, in-house expertise and ultimately, cost. However, such heterologous expression can generate undesirable affects, such as a lack of post-translational modification or incorrect folding of a protein of interest, potentially influencing downstream applications. Thus, a check was made to ensure that the Frentizole derived 17β-HSD10 enzyme inhibitors, K690 and K691, identified using recombinant protein produced in *E. coli,* remain active against mammalian expressed 17β-HSD10 protein.

To this end, HEK293 cells were transiently transfected with the pcDNA3-HSD10 construct. 24 hours post transfection, cells were treated with a hypotonic buffer, rendering them fragile, and lysates generated using a dounce homogeniser. Inhibitors K690, K691 or vehicle (DMSO) were added after which substrate (acetoacetyl-CoA) and cofactor (NADH) were spiked in, and the change in absorbance monitored over time at 340 nm. A significant decrease in activity was observed in the presence of compounds K690 and K691, as compared to vehicle treated 17β-HSD10 (Figure 5.02). Approximately 30-40% residual activity was observed in the presence of saturating concentrations of K690 and K691, comparable to previous results (Figures 3.15 and 3.16), suggesting there is no difference between prokaryotic and eukaryotic expressed enzyme and the results obtained previously are valid. As such, provided they are capable of membrane penetration, compounds K690 and K691 should be active in a cellular environment.

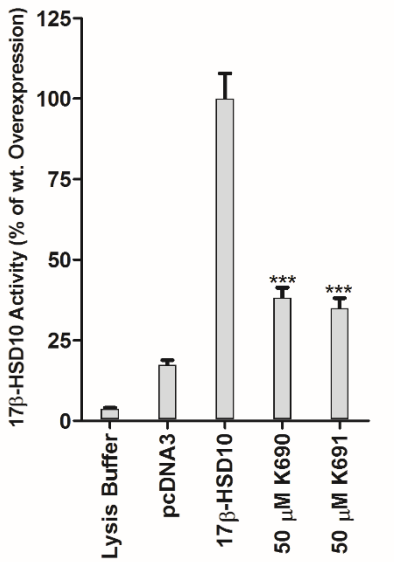

Figure 5.02. Inhibition of mammalian expressed 17β-HSD10. 17β-HSD10 expressed in HEK293 cells, after which cells were lysed, inhibitors K690 and K691 added, follwed by acetoacetyl-CoA and NADH and activity monitored at 340 nm. A comparable level of inhibition was with compounds K690 and K691 using both bacterial and mammalian expressed 17β-HSD10. Values shown are an average of three independent experiments each with three technical repeats ± SEM. Statistical anaylsis was performed using a one-way ANOVA with Bonferroni mutiple comparisons. * = P ≤ 0.05, ** = P ≤ 0.01, *** = P ≤ 0.001, **** = P ≤ 0.0001.

5.2 Inhibitor Toxicity

Compounds which are acutely toxic are unlikely to be developed into a successful therapeutic agent. As such, a measure of the toxicity of compounds K690 and K691 was made using a lactate dehydrogenase assay (LDH) assay. The LDH assay provides a measure of cell death on the basis of enhanced membrane permeability and thus serves as a useful indicator for both necrotic and apoptotic cell death[376]. The assay is based around a coupled reaction, in which the lactate dehydrogenase enzyme converts lactate to pyruvate using NAD^+ as a cofactor, producing NADH. NADH is subsequently used by diaphorase to convert iodonitrotetrazolium (INT) to formazan, giving a coloured product which can be measured using spectrophotometry via absorbance at 490 nm (Scheme 5.01).

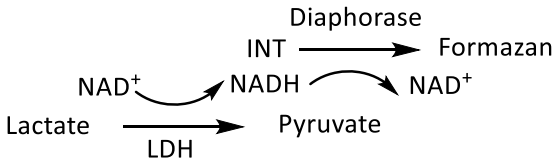

Scheme 5.01. Lactate dehydrogenase assay. The lactate dehydrogenase enzyme converts lactate to pyruvate, generating NADH. NADH is subsequent utilised by diaphorase to convert a tetrazolium salt (INT) to formazan, a coloured product which can be measured via absorbance at 490 nm.

During the LDH assay procedure, compounds of interest are added to the culture media, which is then used directly in the assay. As such, there is the potential for compound induced inhibition of either the lactate dehydrogenase enzyme or the coupled diaphorase enzyme, possibly leading to false negative results.

Therefore, to ensure that compounds K690 and K691 do not interfere with the LDH assay, an initial trial experiment was performed using purified LDH and diaphorase enzymes. The LDH assay was performed in the presence of 50 µM K690, K691 or vehicle (DMSO). No significant alteration in signal was observed in the presence of either compound, as compared to vehicle (DMSO), indicating compounds K690 and K691 do not inhibit the LDH or diaphorase enzymes and thus the assay is suitable for assessing compound induced cytotoxicity (Figure 5.03).

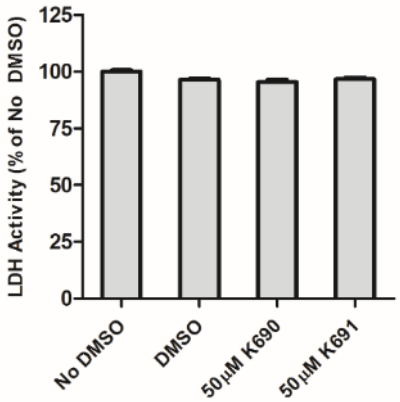

Figure 5.03. K690 and K691 induced LDH interference. A check was made to ensure that compounds K690 and K691 do not interfere with the LDH assay. No signfiicant decrease in signal was apparent in the presence of compound K690 or K691. Values shown are an average of three biological repeats each with three technical repeats ± SEM. Statistical anaylsis was performed using a one-way ANOVA with Bonferroni mutiple comparisons.

With the assay validated, HEK293 and SH-SY5Y cells were treated with varying concentrations of compounds K690 and K691 for 24 hours, after which cell death was assessed using the LDH assay. In all cases, no increase in cell death was observed (Figure 5.04). A high background signal is apparent due to the presence of foetal bovine serum in the culture media, which is known to contain LDH[376].

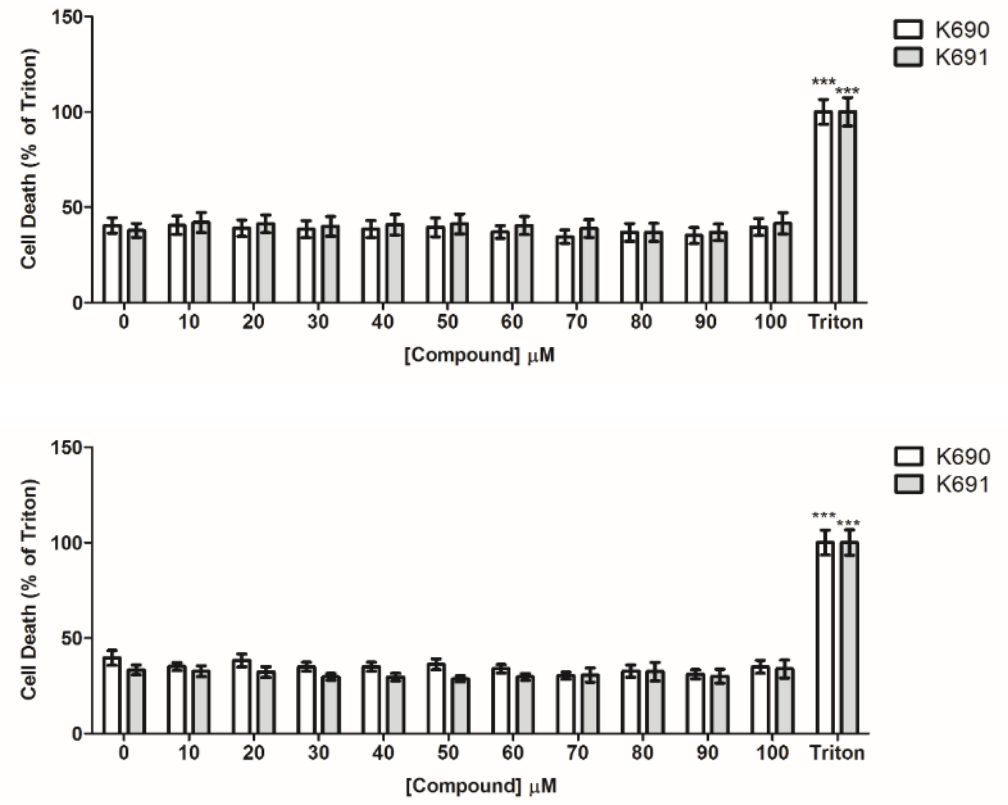

Figure 5.04. K690 and K691 induced cytotoxicity. HEK293 and SH-SY5Y cells were treated with the indicated concentrations of compounds K690 and K691 and incubated for 24 hours. Following incubation, a measure of cell death was made using the LDH assay. In all cases, no significant increase in cell death was observed following incubation with compounds K690 and K691 for 24 hours. Top= HEK293, Bottom= SH-SY5Y. Values shown are an average of three independent experiments, each with three technical repeats ± SEM. . Statistical anaylsis was performed using a one-way ANOVA with Bonferroni mutiple comparisons. * = $P \leq 0.05$, ** = $P \leq 0.01$, *** = $P \leq 0.001$, **** = $P \leq 0.0001$.

5.3 17β-HSD10 Site-Directed Mutagenesis:

In order to develop a 17β-HSD10 centred cellular disease model, a catalytically inactive mutant of the 17β-HSD10 enzyme was first required. Two such mutations have previously been reported in the literature, Q165H[320] and Y168G[338]. The first, Q165H, has been proposed to prevent cofactor binding, thereby rendering the enzyme inactive, whilst the Y168G mutation alters a conserved residue within the enzyme catalytic triad, again rendering the enzyme catalytically dead.

Site directed mutagenesis (SDM) was used to introduce both mutations into the coding sequence of the 17β-HSD10 enzyme, previously cloned into the pcDNA3 vector for mammalian expression (Figure 5.05). Previous work conducted by Dr. Margaret Taylor, a past PhD student within the group, has shown that the subcellular localisation of the 17β-HSD10 enzyme changes when overexpressed, becoming dispersed throughout the cell as opposed to solely mitochondrial, presumably due to the overloading of the cellular translocation machinery (unpublished observation). Therefore, the expression construct was previously modified to add an N-terminal mitochondrial targeting sequence, taken from the COX8 gene, ensuring correct subcellular localisation (Figure 5.05). The COX8 mitochondrial targeting sequence is subsequently cleaved from the protein within the mitochondrial matrix, giving wild-type 17β-HSD10 in its native cellular location.

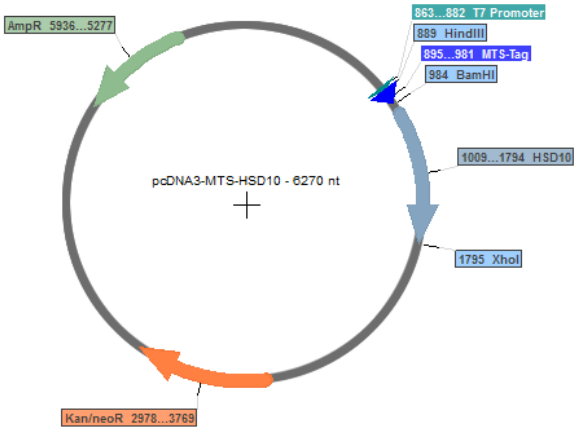

Figure 5.05. pcDNA3-HSD10 vector map. The 17β-HSD10 coding sequence was cloned into the pcDNA3 mammalian expression vector. An N-terminal mitochodrial targeting sequence (MTS) was previously added ensuring the correct sub cellular localisation of the expressed 17β-HSD10 enzyme .

Q165H Mutant

Using standard QuickChange style SDM primers the Q165H mutation was successfully introduced into the 17β-HSD10 coding sequence (Figure 5.06, see Appendix: B for sequencing results).

Forward Primer: 5'-GGGTCAGGTTGGACA**c**GCTGCATACTCTGCTTCC-3

Reverse Primer: 5'-GGAAGCAGAGTATGCAGC**g**TGTCCAACCTGACCC-3

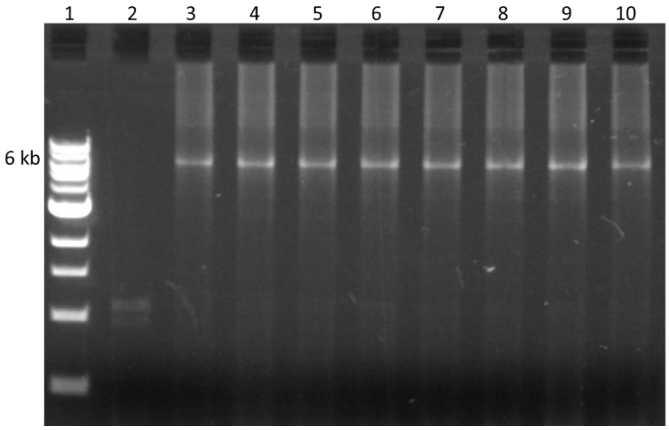

F**igure 5.06. Q165H site directed mutagenesis.** The Q165H mutation was introduced into the coding sequence of the 17β-HSD10 enzyme, held within the pcDNA3 expression construct, using QuickChange style SDM primers. Lane 1= Ladder, Lane 2= Dpn1 Control, Lanes 3-10= Thermal gradient 72 -50°C.

Y168G Mutant

Initial attempts to generate the Y168G mutant using standard QuickChange style primers were unsuccessful.

Forward Primer: 5'-GGACAAGCTGCA**gg**CTCTGCTTCCAAGG-3'

Reverse Primer: 5'-CCTTGGAAGCAGAG**cc**TGCAGCTTGTCC-3'

Whilst additional optimisation would likely have given rise to the desired mutation, an altered, more efficient SDM methodology, has been described by Liu & Naismith[345]. In this case, primers are designed with a short extension 5' to the desired mutation and a comparatively long 3' extension thereafter, with the result that the produced primers have a higher affinity for the template as compared to one another and giving an exponential amplification of product, as opposed to the linear amplification seen with QuickChange style primers. Using this style of primer, the Y168G mutation was successfully introduced into the 17β-HSD10 cDNA sequence (Figure 5.07, see Appendix: B for sequencing results).

Liu & Naismith Forward Primer: 5'-GCTGCA**gg**CTCTGCTTCCAAGGGGGGAATAGTGGGC-3'

Liu & Naismith Reverse Primer: 5'-GCAGA**cc**TGCAGCTTGTCCAACCTGACCCTCG-3'

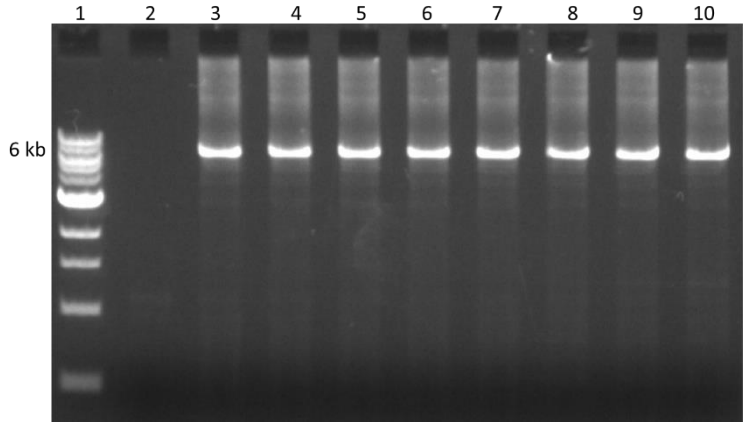

Figure 5.07. Y168G site directed mutagenesis. The Y168G mutation was introduced into the coding sequence of the 17β-HSD10 enzyme, held within the pcDNA3 expression construct, using Liu& Naismith style SDM primers[345]. Lane 1= Ladder, Lane 2= Dpn1 Control, Lanes 3-10= Thermal gradient 72 -50°C.

5.4: 17β-HSD10 Mutant Characterisation

5.41 Mutant 17β-HSD10 Expression

With the putative inactivating mutations successfully introduced into the 17β-HSD10 coding sequence, and sequence verified, a check was made to ensure each is expressed equally well to the wild-type enzyme. With the introduction of amino acid substitutions into a protein sequence there is the potential that the efficiency of translation may be altered, resulting in lower than usual protein levels. Here, such an effect would present as an apparent loss of enzymatic activity, when in-fact the effect would be due to a decrease in enzyme expression, influencing the validity of subsequent conclusions.

As such, a check was made to ensure both the Y168G and Q165H mutants are expressed equally well to the wild-type enzyme. HEK293 cells were transiently transfected with each construct and 17β-HSD10 expression assessed via western blot following 24-hours incubation. Following transfection with the empty pcDNA3 vector, a faint single band is observed, corresponding to endogenous 17β-HSD10 enzyme (Figure 5.08, Lanes 1-3). After transfection with the pcDNA3 vector harbouring either the wild-type enzyme, the Q165H mutant or the Y168G mutant, two prominent bands are seen, corresponding to the free enzyme (lower band) and MTS-tagged enzyme (upper band) (Figure 5.08, Lanes 4-12). The intensity of the observed bands was found to be comparable with each construct, as determined via densitometry based analysis, suggesting the Q165H and Y168G mutants of the 17β-HSD10 enzyme are expressed equally well to the wild-type enzyme and thus any changes in activity observed between them can be attributed to differences in catalytic efficiency and not simply a lack of enzyme being present.

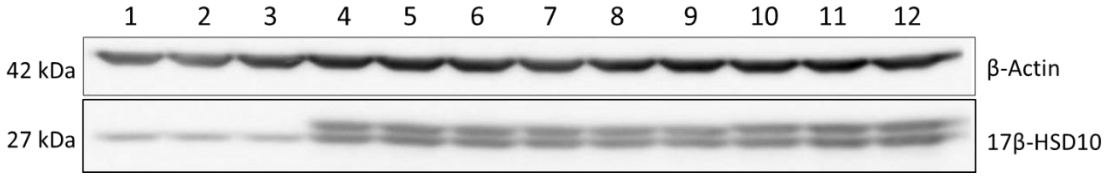

Figure 5.08. Expression of wild-type 17β-HSD10, the Q165H mutant and the Y168G mutant. HEK293 cells were transiently transfected with the indicated 17β-HSD10 constructs. 24 hours post transfection, the expression of the 17β-HSD10 enzyme assessed via western blot. Each mutant of the 17β-HSD10 enzyme was found to be expressed to a comparable level as the wild-type. Lanes 1-3= pcDNA3 empty vector, Lanes 4-6= Wild-type 17β-HSD10, Lanes 7-9= Q165H, Lanes 10-12= Y168G.

5.42 Mutant 17β-HSD10 Enzymatic Activity

With the Y168G and Q165H mutants of the 17β-HSD10 enzyme confirmed as being expressed equally well to the wild-type enzyme, a valid comparison of their relative catalytic efficiencies could now be made. In order to confirm that the Q165H and Y168G mutants of the 17β-HSD10 enzyme are indeed catalytically inactive, HEK293 cells were again transiently transfected with each construct. 24 hours post transfection, cells were treated with a hypotonic buffer rendering them fragile and subsequently lysed using a dounce homogeniser. Cellular debris was pelleted via centrifugation and substrate (acetoacetyl-CoA) and cofactor, (NADH) spiked into the supernatant. 17β-HSD10 catalytic activity was measured as a function of NADH conversion to NAD^+, via absorbance at 340 nm. pcDNA3 empty vector transfected cells were used as a control, allowing the activity of endogenous levels of 17β-HSD10 and any additional enzymes which are capable of catalysing the same reaction to be controlled for. Any increase in activity following transfection with each construct could then reliably be attributed to the introduced enzyme. Activity was normalised to total protein content using the BCA assay, accounting for any variation in plating density or lysis efficiency.

In contrast to previous reports[320], the Q165H mutation was found to reduce the catalytic activity of the 17β-HSD10 enzyme, but not completely inactivate it (Figure 5.09).

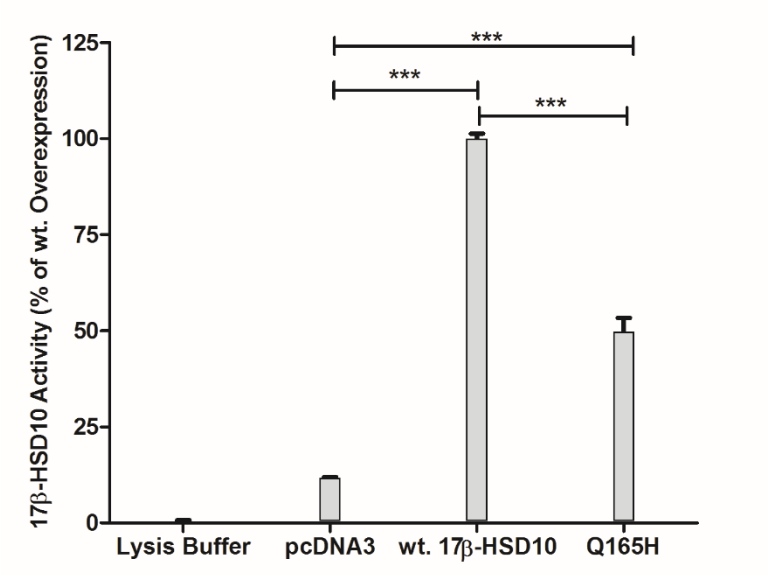

Figure 5.09. Catalytic activity of the 17β-HSD10-Q165H mutant. HEK293 cells were transiently transfected with the empty pcDNA3 vector, wild-type 17β-HSD10 or the Q165H mutant. 24 hours post transfection, cells were lysed and enzyme activity measured as a function of NADH conversion to NAD^+. The Q165H mutant of the 17β-HSD10 enzyme was found to be less active than the wild-type enzyme but not catalytically dead. Values shown are an average of three independent experiments each with three technical repeats ± SEM. Statistical anaylsis was performed using a one-way ANOVA with Bonferroni mutiple comparisons. * = P ≤ 0.05, ** = P ≤ 0.01, *** = P ≤ 0.001, **** = P ≤ 0.0001.

As previously reported[338], the Y168G mutation was found to completely inactivate the 17β-HSD10 enzyme, with only background levels of activity observed.

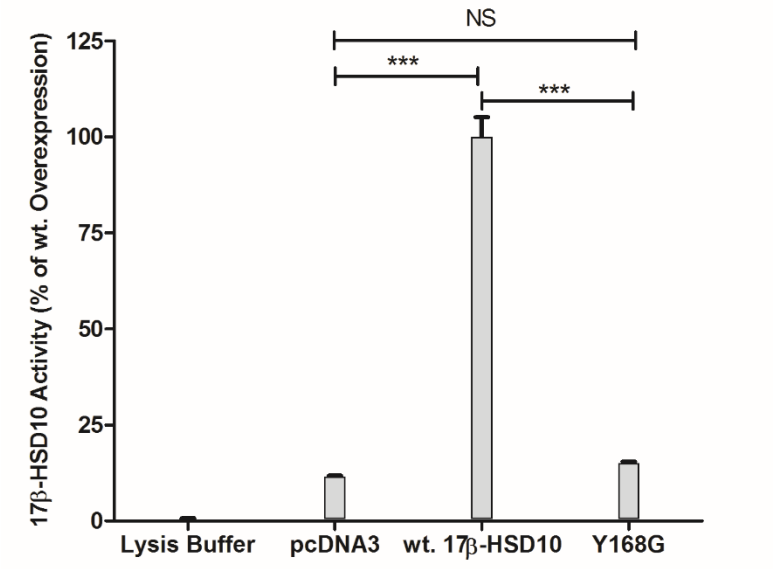

Figure 5.10. Catalytic activity of the 17β-HSD10-Y168G mutant. HEK293 cells were transiently transfected with the empty pcDNA3 vector, wild-type 17β-HSD10 or the Y168G mutant. 24 hours post transfection, cells were lysed and enzymatic activity measured as a function of NADH conversion to NAD^+. The Y168G mutant of the 17β-HSD10 enzyme was found to be catalytically dead, as reported previously. Values shown are an average of three independent experiments each with three technical repeats ± SEM. Statistical anaylsis was performed using a one-way ANOVA with Bonferroni mutiple comparisons. NS = Non-significant, * = P ≤ 0.05, ** = P ≤ 0.01, *** = P ≤ 0.001, **** = P ≤ 0.0001.

5.5 APP Transfection Optimisation

In cell culture based experiments, the application of amyloid beta-peptide is typically performed using one of two methodologies; cells are either dosed with purified recombinant amyloid beta-peptide of the desired oligmeric state or transfected with a mutant of the amyloid precursor protein (APP), leading to elevated levels of Aβ being generated endogenously.

Commercially available recombinant amyloid beta-peptide must first be treated with a monomerising agent and subsequently incubated under the appropriate conditions to generate the desired oligomerised state. The methodologies employed for such steps are divergent in nature with varying efficiencies and levels of characterisation[358]. Previously, in the original paper reporting the 17β-HSD10/Aβ interaction as toxic, COS-7 cells were transiently transfected with both APP (V171G), generating increased levels of $A\beta_{1-42}$, and 17β-HSD10 resulting in elevated levels of oxidative damage and cell death[337,338]. As such, cells were here transiently transfected with APP harbouring the Swedish mutation (APPswe), generating enhanced levels of $A\beta_{1-40}$ and $A\beta_{1-42}$ endogenously, the species with which the 17β-HSD10 enzyme interacts[338].

The APPswe gene had previously been cloned into the pcDNA3 mammalian expression vector using the HindIII and XbaI restriction sites (Figure 5.11).

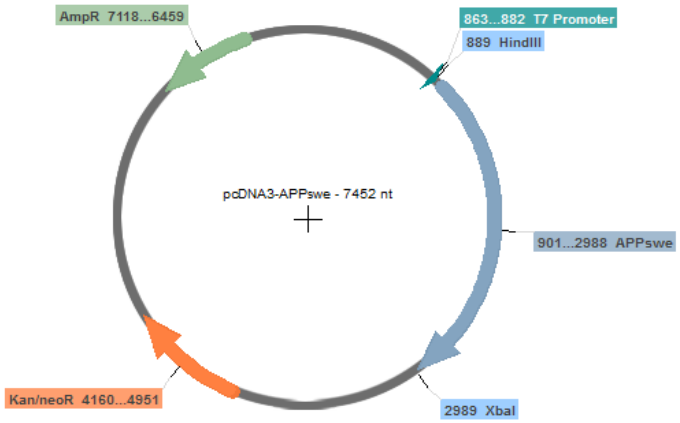

Figure 5.11. pcDNA3-APPswe Vector Map. The amyloid precursor protein coding sequence, harbouring the Swedish mutation, was cloned into the pcDNA3 vector using the HindIII and XbaI restriction enzyme sites.

In order to optimise the transfection and expression of the APPswe construct, HEK293 cells were transiently transfected with the empty pcDNA3 vector or the pcDNA3-APPswe construct. Cell lysates were generated 24 and 48 hours post transfection, and the levels of amyloid precursor protein and Aβ assessed via western blot. Following transfection with the pcDNA3-APPswe construct, prominent bands corresponding to the amyloid-precursor protein and Aβ are apparent at both 24 and 48 hours post transfection (Figure 5.12). A 48-hour incubation period post transfection was passed forward into future experiments.

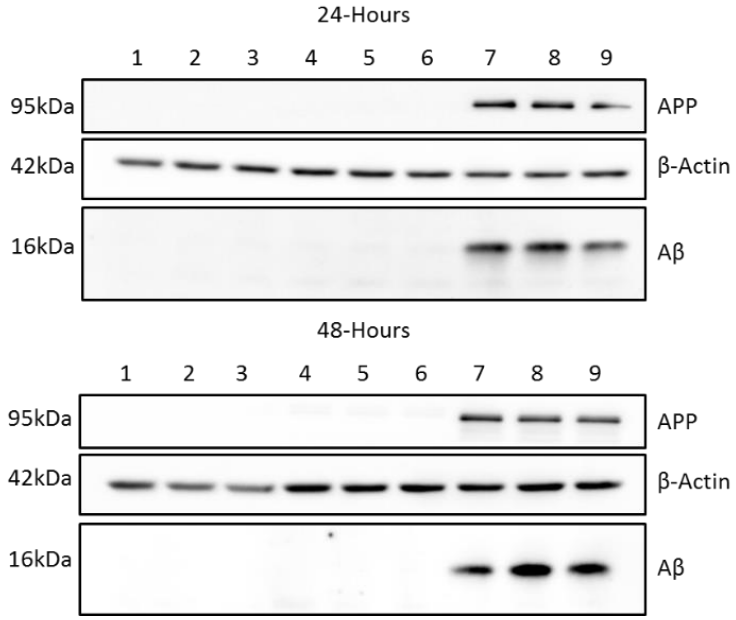

Figure 5.12. APP and Aβ expression at 24-hour and 48-hours post transfection. HEK293 cells were transfected with the empty pcDNA3 vector or the pcDNA3-APPswe construct. 24 and 48 hours post transfection, the expression of the amyloid precursor protein and Aβ was assessed via western blot. Following transfection with the pcDNA3-APPswe construct a marked increase in both amyloid precursor protein and Aβ expression can be seen. Lanes 1-3= Wild-type cells, Lanes 4-6= pcDNA3 empty vector, Lanes 7-9= pcDNA3-APPswe.

5.6 HEK293

5.61 HEK293 17β-HSD10 Stable Cell Line Generation

Whilst it would be possible to transiently transfect cells with both the 17β-HSD10 and APPswe constructs simultaneously, the efficiency of such a dual transfection would likely be low, introducing a large degree of variation between repeat experiments. Thus, a decision was made to generate stable cell lines expressing pcDNA3 empty vector, the wild-type 17β-HSD10 enzyme, the Q165H mutant or the Y168G mutant. The produced cell lines would subsequently be transiently transfected with the pcDNA3 empty vector or the pcDNA3-APPswe construct, after which the levels of 4-HNE, a marker of oxidative stress employed previously as a measure of 17β-HSD10/Aβ induced oxidative damage [338], would be assessed.

Wild-type HEK293 cells were transiently transfected with the empty pcDNA3 vector, the wild-type 17β-HSD10 enzyme, the Q165H mutant or the Y168G mutant. 48 hours post transfection, cells were placed into selection media, containing Geneticin, and selection maintained for a sufficient period to kill both non-transfected and transiently transfected cells. Stably transfected cells were allowed to propagate in maintenance media and the expression of the 17β-HSD10 enzyme confirmed via western blot (Figure 5.13). Densitometry based analysis revealed an approximate 8-fold upregulation of 17β-HSD10 with each expression construct.

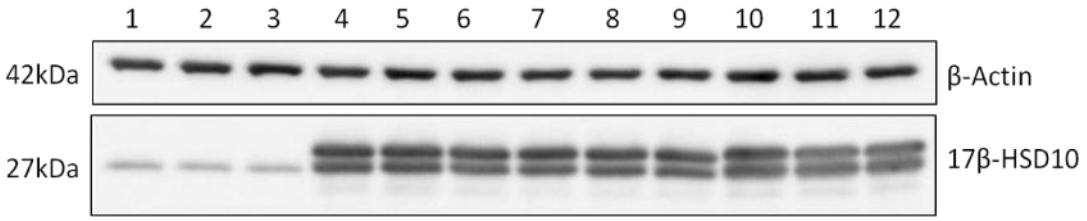

Figure 5.13. 17β-HSD10 expressing HEK293 stable cell lines. HEK293 cells were stably transfected with the pcDNA3 empty vector, the 17β-HSD10 enzyme, the Q165H mutant or the Y168G mutant and expression confirmed via western blot. Lanes 1-3= pcDNA3 stable expression, Lanes 4-6= Wild-type 17β-HSD10, Lanes 7-9= Q165H mutant, Lanes 10-12= Y168G mutant.

5.62 HEK293 17β-HSD10 Stable Cell Lines + APP - 4-HNE Western Blot:

Previously, immunocytochemistry was used to measure intracellular levels of 4-hydroxynoneal (4-HNE), a marker of oxidative stress, in cells expressing catalytically active and inactive 17β-HSD10 enzyme alongside Aβ, with enhanced levels of 4-HNE observed in the presence of the active enzyme[338]. Here, western blotting was instead employed. To confirm that the antibody against 4-HNE was indeed capable of detecting such an antigen, HEK293 cells were treated with either purified 4-HNE or vehicle (ethanol) and cell lysates taken thereafter. The relative levels of 4-HNE modified proteins were subsequently assessed via western blot. A marked increase in 4-HNE modified proteins was observed in samples treated with purified 4-HNE, as would be expected, confirming that the antibody is capable of detecting this antigen (Figure 5.14).

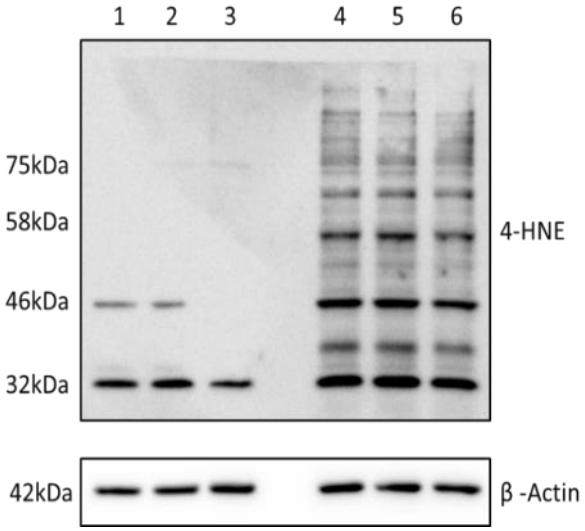

Figure 5.14. 4-HNE antibody validation. HEK293 cells were treated with purified 4-HNE, or vehicle and cell lysates taken. Levels of 4-HNE modified proteins were assessed via western blot, showing a marked increase in 4-HNE treated samples. Lanes 1-3=Vehicle treated, Lanes 4-6= 4-HNE treated.

HEK293 cells stably expressing the pcDNA3 empty vector, the wild-type 17β-HSD10 enzyme or the Y168G mutant were transiently transfected with the APPswe construct. 48 hours post-transfection, the relative levels of 4-HNE modified proteins were assessed via western blot, with the expectation that cells expressing the 17β-HSD10 enzyme would show a marked increase in 4-HNE levels. However, no marked difference in 4-HNE levels was observed between cells expressing pcDNA3 empty vector, the wild-type 17β-HSD10 enzyme or the Y168G mutant (Figure 5.15).

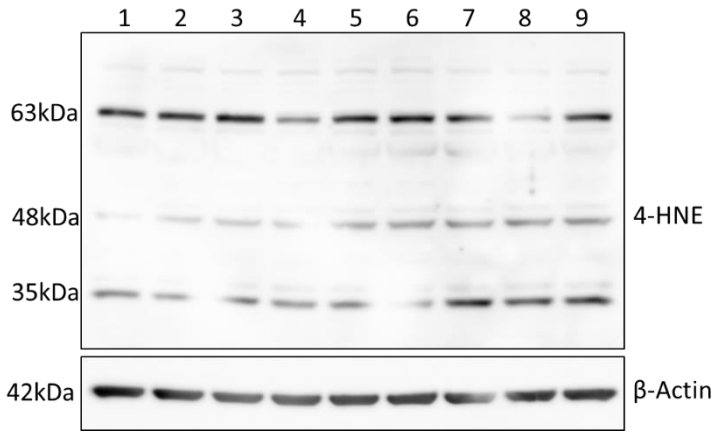

Figure 5.15. 4-HNE western blot. HEK293 cells stably expressing the pcDNA3 empty vector, the wild-type 17β-HSD10 enzyme or the Y168G mutant were transiently transfected with the APPswe construct. 48 hours post transfection the relative levels of 4-HNE were assessed via western blot. No marked difference was observed. Lanes 1-3 = pcDNA3 empty vector + APPswe, Lanes 4-6= 17β-HSD10 stable + APPswe, Lanes 7-9= Y168G stable + APPswe.

5.7 SH-SY5Y Dual Stable Cell Line Generation

One potential explanation for the discrepancy between the results described herein and those reported previously, is the length of incubation post-transfection with the amyloid precursor protein. No time interval was reported previously[338] raising the possibility that a 48-hour incubation may be too long, in which case the cell may compensate, or too short in which case no signal will be apparent.

In an attempt to produce a more robust phenotype, an alternative strategy was employed. Firstly, a more disease relevant cell line, in the form of the neuroblastoma derived SH-SY5Y cell line, was used and, in an attempt to maximise phenotypic differences between control and amyloid expressing cells, a decision was made to move from the transient transfection of the APPswe gene used previously, to stable expression.

Chemical transfection reagents are known to show relatively poor efficiency with neuronal derived cell lines and so nucleofection was instead used. SH-SY5Y cells were nucleofected with the pcDNA3 empty vector, the wild-type 17β-HSD10 enzyme or the catalytically inactive Y168G mutant. 48-hours post nucleofection cells were placed into selection media, containing Geneticin, and selection maintained for a sufficient length of time to kill both non-transfected and transiently transfected cells. Stably transfected cells were allowed to propagate in maintenance media and the expression of the 17β-HSD10 protein confirmed via western blot. As expected, a marked increase in 17β-HSD10 expression was observed in

both the wild-type 17β-HSD10 and Y168G mutant expressing cells as compared to the pcDNA3 empty vector (Figure 5.16, lanes 4-9).

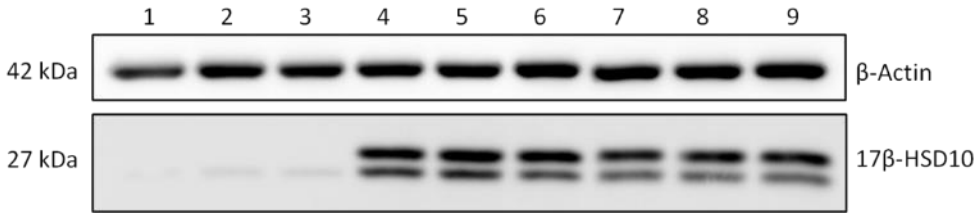

Figure 5.16. 17β-HSD10 Expressing SH-SY5Y stable cell lines. SH-SY5Y cells were nucleofected with the empty pcDNA3 vector, the wild-type 17β-HSD10 enzyme or the Y168G mutant. Stably expressing cells were selected using Geneticin and 17β-HSD10 expression confirmed via western blot. Lanes 1-3= pcDNA3, Lanes 4-6= Wild-type 17β-HSD10, Lanes 7-9 = Y168G mutant.

The 17β-HSD10 and APPswe constructs had both previously been generated using the pcDNA3 vector and thus both harbour a Geneticin resistance marker, precluding the sequential selection of dual stable transfectants. As such, the APPswe gene was PCR amplified out of the pcDNA3 backbone and 5'HindIII and 3'NotI restriction enzyme sites simultaneously added for downstream cloning.

APPswe Forward: 5'- taagca**AAGCTT**ATGCTGCCCGGTTTGGCA-3'

APPswe Rev:erse 5'-tgctta**GCGGCCGC**TTACTAGTTCTGCATCTGCTCAAAGAACTTGTAGG-3'

(Lower case= Spacer sequence, Bold = Restriction Site

To optimise primer annealing temperatures, three small scale PCR reactions were performed with primer annealing at 72°C, 65°C and 55°C. Clean product was observed at the expected size, 2.1 kb, at each temperature tested (Figure 5.17) and thus a 72°C annealing temperature was used subsequently.

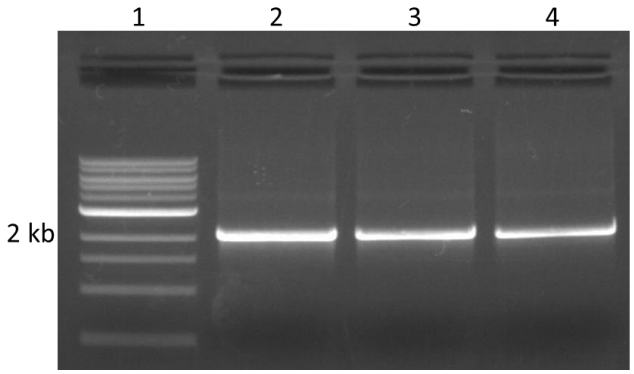

Figure 5.17. APPswe PCR primer check. PCR primers were designed to amplify the APPswe cDNA sequence out of the pcDNA3 backbone and simultaneously add 5'HindIII and 3'NotI restriction enzyme sites. To optimise primer annealing, three temperatures were trialled. Lane 1= Ladder, Lane 2= 72°C annealing, Lane 3= 65°C annealing, Lane 4= 55°C annealing. Clean product was observed at each temperature trialled and thus 72°C was used subsequently.

The PCR amplified APPswe gene was ligated into the pcDNA4/TO vector, harbouring a Zeocin selection marker, generating a pcDNA4-APPswe construct (Figure 5.18, see Appendix: B for sequencing results).

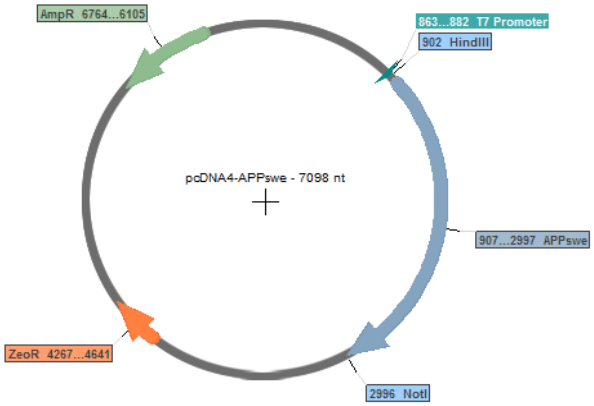

Figure 5.18 pcDNA4-APPswe Vector Map. The amyloid precursor protein coding sequence, harbouring the Swedish mutation, was cloned into the pcDNA4 vector using the HindIII and NotI restriction enzyme sites.

The pcDNA4/TO vector comes in multiple variations. The one to hand was designed to add C-terminal myc and 6 x His tags, allowing the identification of protein expression using an anti-myc antibody, and subsequent protein purification via Ni-NTA affinity chromatography. In this instance neither feature was desired and so two stop codons were added to the C-terminal end of the APPswe gene, preventing their expression. The pcDNA4/TO vector has an additional advantage, in that it can be used in conjunction with the pcDNA6/TR vector to generate a tetracycline inducible expression system. Due to time constraints, a decision was made that in the first instance, tetracycline control of APPswe expression would not be employed and thus both the 17β-HSD10 enzyme and the APPswe gene would be constitutively expressed. However, should this combination prove to be toxic it would be a relatively simple matter to introduce tetracycline mediated control of APPswe expression, requiring an additional round of stable selection, this time using the pcDNA6/TR vector and Blasticidin.

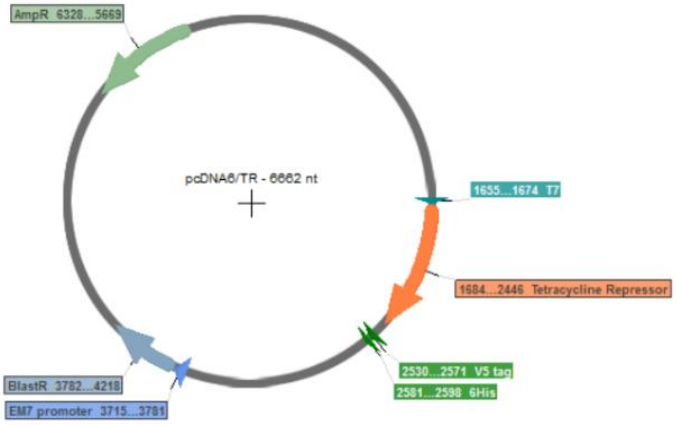

Figure 5.19. pcDNA6/TR Vector Map. The pcDNA6/TR vector can be used in conjunction with the pcDNA4/TO vector to generate a tetracycline inducible expression system.

Stably transfected SH-SH5Y cells, harbouring the empty pcDNA3 vector, the wild-type 17β-HSD10 enzyme or the Y168G mutant were subsequently nucleofected with the empty pcDNA4 vector or the pcDNA4-APPswe construct. 48-hours post nucleofection cells were placed into Zeocin containing media and selection maintained for a sufficient period to kill non-transfected and transiently transfected cells. Following selection, cells were placed into maintenance media and allowed to propagate.

The expression of both APPswe and 17β-HSD10 were subsequently confirmed via western blot (Figure 5.20). Densitometry based analysis revealed approximately equal levels of overexpression for the wild-type 17β-HSD10 enzyme and Y168G mutant, as compared to empty vector controls (5 to 7-fold overexpression). The endogenous levels of APP in pcDNA4-empty vector transfected cell lines were found to be almost undetectable, preventing a comparison being made via densitometry, however visual inspection of the blots indicates a marked increase in APP expression following transfection with the pcDNA4-APPswe construct.

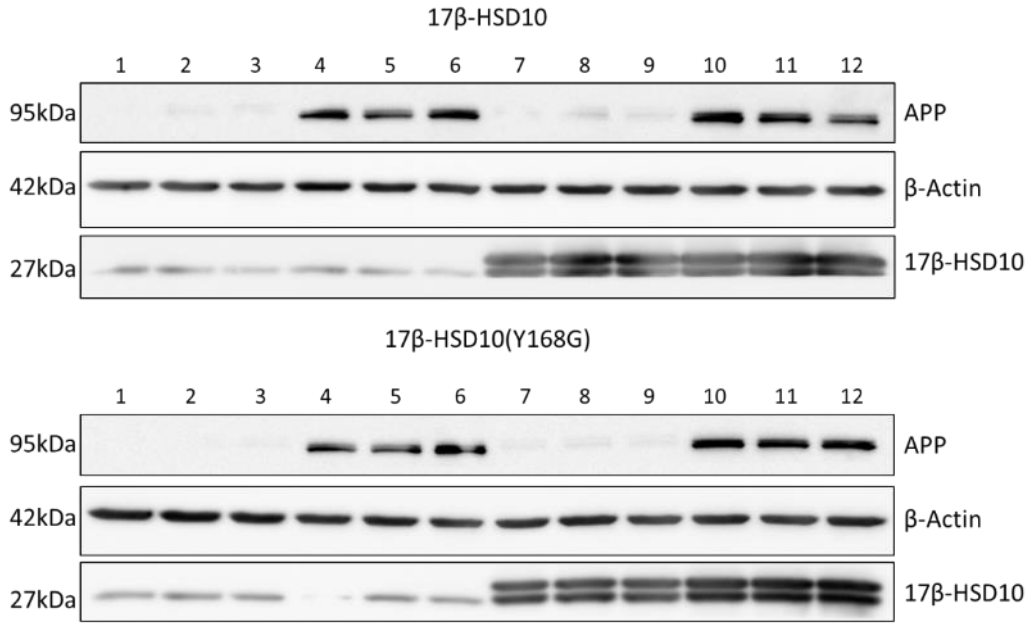

Figure 5.20. 17β-HSD10/17β-HSD10(Y168G) and APPswe dual stable SH-SY5Y cell lines. SH-SY5Y cells were nucleofected with the pcDNA3 empty vector, the pcDNA3-HSD10 or pcDNA3-HSD10(Y168G) constructs and stable transfectants selected. Subsequently, cells were nucleofected with the pcDNA4 empty vector or pcDNA4-APPswe construct and dual stable transfectants selected. Lanes 1-3 = pcDNA3/pcDNA4 empty vector, Lanes 4-6= pcDNA3/pcDNA4-APPswe, Lanes 7-8= pcDNA3-HSD10/pcDNA4 empty vector, Lanes 10-12= pcDNA3-HSD10/pcDNA4-APPswe.

The relative levels of 4-HNE modified proteins in the SH-SY5Y pcDNA3 empty-vector/pcDNA4-APPswe, pcDNA3-17β-HSD10/pcDNA4-APPswe and pcDNA3-Y168G/pcDNA4-APPswe dual stable cell lines were assessed via western blot. No marked difference in 4-HNE levels were observed between the three cell lines (Figure 5.21). Identical results were obtained using the generalised reactive oxygen species marker, H2DCFDA, and mitochondrial superoxide marker MitoSox (data not shown).

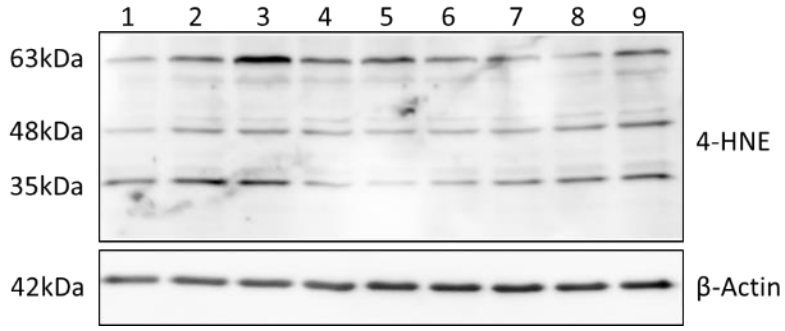

Figure 5.21. Relative levels of 4-HNE modified proteins in SH-SY5Y dual stable cell lines. Lanes 1-3= pcDNA3 empty vector/pcDNA4-APPswe, Lanes 4-6= pcDNA3-17β-HSD10/pcDNA4-APPswe, Lanes 7-9= pcDNA3-17β-HSD10(Y168G)/pcDNA4-APPswe. No marked difference in the level of 4-HNE modified proteins was observed between the indicated cell lines.

Chapter 5 - Discussion:

Two publications from the group of Shi du Yan, have shown that the overexpression of the 17β-HSD10 enzyme alongside Aβ results in a marked increase in oxidative stress and cell death, and through the use of an inactive mutant (mutERAB), that this stress is dependent on the catalytic activity of the 17β-HSD10 enzyme[337,338] (Figure 5.22).

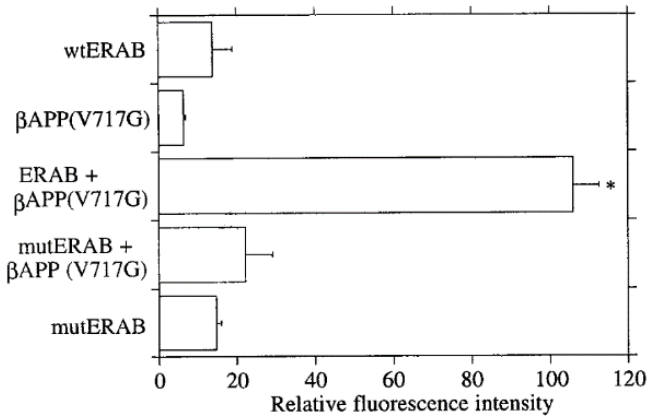

Figure 5.22. Effect of 17β-HSD10 catalytic activity on 17β-HSD10/Aβ cytotoxicity. Co-transfection of COS-7 cells with wild-type 17β-HSD10 (ERAB) and Aβ resulted in a marked increase in 4-hydoxynoneal levels, whilst a catalytically inactive mutant of the 17β-HSD10 enzyme (Y168G/K172G, mutERAB) with Aβ did not. Figure reproduced from[338].

Further work has shown that this oxidative stress and cell death is due to a perturbation of mitochondrial function[340] and translates into a cognitive deficit in mouse models, expressing neuronally targeted mutant amyloid precursor protein and 17β-HSD10 enzyme[303,339]. The administration of a selective agent shown to disrupt the 17β-HSD10/Aβ interaction (ABAD-DP) was shown to reverse these effects, suggesting causation[303,339]. Here, I have failed to replicate the aforementioned studies in both the HEK293 and SH-SY5Y cells, human embryonic kidney and human neuroblastoma cell lines, respectively.

Two missense mutations, Q165H[320] and Y168G[338], have been reported in the literature as rendering the 17β-HSD10 enzyme catalytically inactive. Through the use of site directed mutagenesis, I have generated both mutants, and confirmed comparable expression of each in a mammalian cell line (Figure 5.08). However, in contrast to previous reports, further characterisation revealed that whilst the Q165H mutation reduces the catalytic activity of the 17β-HSD10 enzyme, it does not completely abolish it (Figure 5.09). This discrepancy between experiments is difficult to reconcile. The Q165H mutation was reported to prevent the binding of cofactor NADH/NAD^+, as measured using differential scanning fluorimetry, thereby preventing activity against all known substrates[320]. The activity observed herein however suggests otherwise. An examination of the crystal structure of the 17β-HSD10 enzyme (PDB: 1U7T) reveals that the Q165H amino acid substitution sits far from the cofactor binding site, instead residing in the putative substrate binding cleft (Figure 5.23), potentially influencing substrate binding affinity. The enzyme activity assay performed previously utilised 2-methyl-3-hydoxybutyryl-CoA as substrate and thus the Q165H

mutation may alter 2-methyl-3-hydoxybutyrl-CoA binding affinity, an effect which may be less apparent with acetoacetyl-CoA, explaining the activity observed here and lack thereof. Alternatively, as no substrate concentration is reported for the aforementioned activity assay, the Q165H mutation may lower affinity such that no significant substrate binding occurred under the conditions utilised previously, whilst the 120 µM acetoacetyl-CoA utilised here may be sufficient for binding and catalysis.

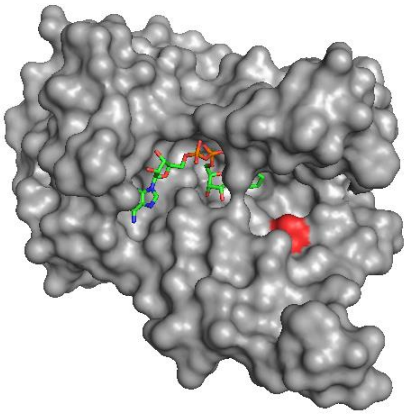

Figure 5.23. 17β-HSD10 Q165H Mutation. The 17β-HSD10 enzyme was co-crystalised with bound cofactor, NAD^+ (stick diagram). The Q165H mutation was found to reside outside of the cofactor binding site.

In concordance with previous reports[338], the Y168G mutation was however found to completely inactivate the 17β-HSD10 enzyme (Figure 5.10). However, when HEK293 cells stably expressing either the wild-type 17β-HSD10 enzyme or the Y168G mutant (Figure 5.13) were transfected with the APPswe construct, giving elevated levels of $A\beta_{1-40}$ and $A\beta_{1-42}$, the species with which 17β-HSD10 interacts[338], no marked increase in 4-HNE levels were observed, as measured by western blot (Figure 5.15). The previously reported increase in 4-HNE levels following transient transfection with the 17β-HSD10 enzyme and Aβ was detected using immunocytochemistry and is large, almost 5 fold (Figure 5.22)[338], suggesting a signal should have been seen even when assessed via a comparatively indirect western blot. The expression constructs generated here have been sequence verified, the subsequently produced stable cell lines verified via western blot and the antibody against 4-HNE has been shown to be capable of detecting this antigen, as such the cause of this discrepancy is not immediately obvious.

In an attempt to generate a more robust phenotype, dual stable SH-SY5Y cells were generated, expressing either the wild-type 17β-HSD10 or the Y168G mutant alongside APPswe (Figure 5.20). However, similar results were obtained with no marked increase in 4-HNE levels being observed (Figure 5.21). In addition, the generalised ROS probe, H2DCFDA, and the superoxide probe, MitoSox, also showed no increase in oxidative stress, although due to time constraints these experiments were not repeated adequately and thus provide only anecdotal evidence.

A number of experimental differences may explain these alternate results. Firstly, the original reports regarding the toxic interaction between the 17β-HSD10 enzyme and Aβ reported subcellular localisation

of 17β-HSD10 to the endoplasmic reticulum and, upon topical treatment with Aβ, a mobilisation to the plasma membrane[337]. The former result has now categorically been disproven, with the 17β-HSD10 localised solely to the mitochondria[313], whilst the latter has yet to be repeated. However, both of these observations correlate with those made by Dr. Margaret Taylor, who noted that upon overexpression the localisation of the 17β-HSD10 changes, becoming dispersed throughout the cell and localised to the plasma membrane (unpublished observations). Such observations prompted the addition of a N-terminal mitochondrial targeting sequence to our 17β-HSD10 overexpression construct, ensuring correct subcellular localisation, a plasmid which has become the archetypal mammalian expression construct used within the group. Therefore, the observed cytotoxicity may in fact represent an artefact caused by the overexpression methodology utilised. Subsequent work using transgenic mice employed the PDGF-β promoter to drive the production of APP and 17β-HSD10, ensuring neuronal expression, but again no mitochondrial targeting sequence was used raising the possibility that the same artefact may have been propagated[303,339,340]. Such a theory would be reasonably easy to test, requiring a round of site directed mutagenesis to remove the mitochondrial targeting sequence from our expression construct, the subsequent overexpression of non-tagged 17β-HSD10 and APPswe, and a second appraisal of toxicity. Should toxicity now be apparent, it would suggest such an effect was indeed responsible.

In which case, a thorough appraisal of the subcellular localisation of the 17β-HSD10 enzyme in the AD brain should be undertaken. The expression of the 17β-HSD10 enzyme has been shown to be increased in the Alzheimer's diseased state, 28% in the temporal grey matter and 40% in the hippocampus[303], and 573% in the CSF[341]. Should the subcellular localisation of the 17β-HSD10 enzyme change in the AD brain in a similar manner to that seen in cell culture based experiments, the conclusions derived from the work conducted of Shi du Yan *et al.* would remain valid, and he therapeutic targeting of 17β-HSD10 would remain viable.

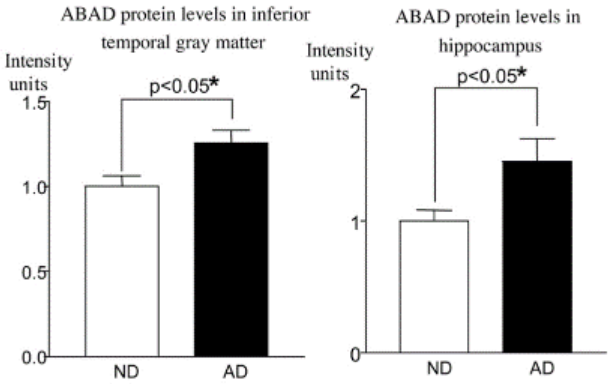

Figure 5.24. 17β-HSD10 upregulation in the AD brain. The expression of the 17β-HSD10 enzyme has been shown to increase approximately 28% in the temporal grey matter, and 40% in the hippocampus of patients with AD. Figure reproduced from[303].

An alternative explanation may relate to compensatory mechanisms described previously in both transgenic mAPP/17β-HSD10 mice and in the brains of AD patients. In both transgenic mice and brain samples derived from Alzheimer's diseased patients an increase in the level of expression of endophilin I and peroxiredoxin II have been reported, linked to cell death and antioxidant activities, respectively[342,343].

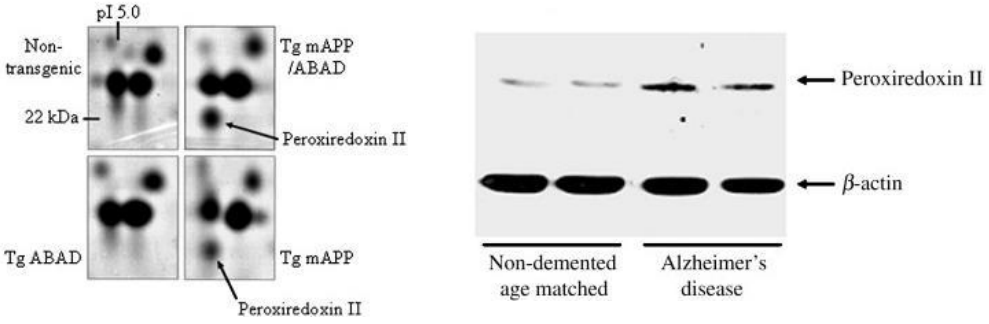

Figure 5.25. Peroxiredoxin II upregulation. The expression of the antioxidant enzyme peroxiredoxin II has been shown to be elevated in the brains of mAPP/17β-HSD10 transgenic mice (left panel) and in the brains of Alzheimer's diseased patients (right panel). Figures reproduced from[342].

Following transfection, a marked increase in cell death was apparent in cells harbouring the pcDNA4-APPswe construct as compared to the pcDNA4 empty vector and as such, the surviving cells may represent a subpopulation better able to cope with the elevated levels of stress associated with the 17β-HSD10/Aβ interaction. Dead or dying cells would have been lost during the wash steps required for lysate generation, biasing results and possibly explaining the lack of 4-HNE signal observed here. Such a theory could be tested in two ways, firstly a western blot for peroxiredoxin II could be performed using the lysates derived previously, should a significant upregulation be observed in samples transfected with both 17β-HSD10 and Aβ it would suggest such a compensatory mechanism is at work. Alternatively, the transfections could be repeated and an LDH assay performed using culture media derived from each condition, such an assay would retain the signal derived from dead and dying cells, giving a more representative appraisal of cellular stress. If such an effect were to be observed, it may prove advantageous to generate clonal cell lines expressing equal levels of active and inactive 17β-HSD10 enzyme and introduce a tetracycline mediated control of APPswe expression, allowing cells to be propagated to a sufficient level prior to induction and preventing the selection pressure induced by the constitutive stable expression employed here.

Chapter 6 - Final Discussion and Future Perspectives

As a result of this project we now have expression constructs and optimised purification protocols for our target enzyme, 17β-HSD10 (Chapter 3), and two related enzymes showing close structural homology, 17β-HSD8 and 17β-HSD14 (Chapter 4). In addition, we have robust enzyme activity assays developed for each, allowing the effect of small molecules of interest on catalytic activity to be assessed in a reasonably high-throughput manner, currently 96-well format.

Following small molecule screening experiments conducted herein, we have identified a subset of Frentizole derived compounds which appear capable of inhibiting the catalytic activity of the 17β-HSD10 enzyme (Chapter 3: Section 3.06) and on the basis of a comparatively large screen of the NCI Diversity IV library we have a range of inhibitor molecules which are currently in the process of being further evaluated (Chapter 3: Section 3.13). In addition, early in 2015, we entered into a collaboration with a large European screening initiative, representing a collaboration between academic and industrial partners and resulting in the screening of hundreds of thousands of small molecules against our target. A qualified hit-list of validated inhibitors is expected in the near future. As a small academic institution, our ability to characterise such a large number of potential hit compounds is limited, and as such the assays developed here will prove vital, allowing the efficient triage on compounds on the basis of potency, specificity, and hopefully, with some optimisation, efficacy in a cellular environment, allowing resources to be channelled into only the most promising hit molecules.

One consistent frustration within the group has been the inability to generate crystal structures of the 17β-HSD10 enzyme in complex with inhibitor, meaning that the design of subsequent compound series has up to this point been based on trial and error, and although progress is being made, as evidenced by the enhanced potency and solubility seen with compound K1093 (Chapter 3: Figure 3.21) as compared to initial hits K690 and K691 (Chapter 3: Figure 3.19), it has been slow. However, we are now working in collaboration with the Structural Genomics Consortium in Oxford, renowned for their structural biology expertise and who have previously successfully crystallised the 17β-HSD10 enzyme (PDB: 2O23), to generate a crystal structure of the 17β-HSD10 in complex with inhibitor. The analysis of such a model will hopefully lead to a more detailed understanding of the interactions formed between protein and ligand, allowing subsequent series to be designed in a more logical fashion and thereby expediting the development process. The results of the kinetic based investigations conducted here (Chapter 3: Section 3.08) suggested that Frentizole derived inhibitors, K690 and K691, act via a non-competitive mechanism and therefore both cofactor and substrate may be of use in stabilising the enzyme-inhibitor complex, likely improving the chances of crystal formation, as evidenced by all known crystal structures requiring the presence of a co-crystallising ligand. Now optimised, such experiments could be swiftly performed to characterise the mechanism of inhibition utilised by other inhibiting molecules identified as a result of the NCI Diversity IV screen or as part of the large-scale screen currently being undertaken, guiding subsequent crystallography experiments.

The lack of correlation between experiments performed here (Chapter 5), demonstrating no enhanced toxicity with overexpression of 17β-HSD10 and Aβ, and those conducted previously, where overt toxicity was reported[337,338], is disconcerting. In my opinion, a detailed appraisal of the cytotoxic effects of the 17β-HSD10/Aβ complex should be performed as a matter of urgency, simultaneously validating the inhibition of the 17β-HSD10 enzyme as a therapeutic strategy in treating Alzheimer's disease and potentially generating an extremely useful screening tool. Several reasons could underlie the aforementioned discrepancy, most notably; the altered subcellular localisation of the 17β-HSD10 enzyme upon overexpression and the lack of a mitochondrial targeting sequence being used in experiments reporting toxicity[337,338], the differing methods of assessing toxicity (previously immunocytochemistry and here western blotting) and possible compensatory mechanisms as a result of stably overexpressing these toxic components (detailed in Chapter 5 – Discussion).

Should the toxic effects of the 17β-HSD10/Aβ complex be confirmed, the 17β-HSD10 enzyme offers an attractive drug target for the treatment of AD. It has been suggested that the failure of plaque clearing therapeutics, AN1792, Solaneuzumab and Bapenuzumab, to improve cognitive performance may relate to the fact that intervention was made too late in the disease process. Such a theory is supported by mouse models expressing ADAD associated mutants of the APP protein, where cognitive defects become apparent prior to plaque deposition[270-272], and in AD patients where plaque burden does not correlate with disease severity and patients with plaque deposition sufficient for a diagnosis of AD, remain cognitively normal[273,276]. Interestingly, soluble oligomeric forms of Aβ, the forms which are known to interact with the 17β-HSD10 enzyme[338,349], have been suggested as the true disease driving form of Aβ in the AD brain, correlating with synapse loss[285,292,293], which is in of itself is the strongest correlate for cognitive performance[274]. The formation of oligomeric forms of Aβ has been shown to precede plaque deposition and thus the formation of the cytotoxic 17β-HSD10/Aβ may represent an early event in the AD brain, driving mitochondrial dysfunction and the synapatic loss characteristic of the disease, making it an attractive target for intervention.

Aside from its potential role in AD, 17β-HSD10 has also been implicated in a range of additional disorders. MHBD deficiency is caused by mutations in the gene encoding 17β-HSD10 and, although originally attributed to a defect in isoleucine degradation[316], it now Instead appears to be related to perturbations of a structural role performed by the 17β-HSD10 enzyme in the formation of the mtRNase P complex[320], with disease causing mutations appearing to affect its ability to interact with and thereby stabilise the TRMT10C subunit[330,377]. One common disease causing mutation, R130C, has been suggested to destabilise the 17β-HSD10 enzyme, as evidenced by a time-dependent decrease in activity and a decrease in the level of detectable protein in patient fibroblasts[320]. As a result of work conducted by Xie *et al.* we know that Frentizole, and two derivatives thereof (Figure 6.01) are capable of perturbing the 17β-HSD10/Aβ interaction[344], and as a result of work conducted here, we know that these molecules are not capable of directly inhibiting the catalytic activity of the enzyme, but several derivatives are, suggesting that the perturbation of the 17β-HSD10/Aβ interaction is likely due to an interaction with the 17β-HSD10 enzyme

as opposed to Aβ (Figures 3.15 and 3.16). In concordance with this one inhibiting derivative, K1093 was found to induce a marked stabilisation of the enzyme, as measured using DSF, indicative of a direct protein-ligand interaction (Figure 3.30).

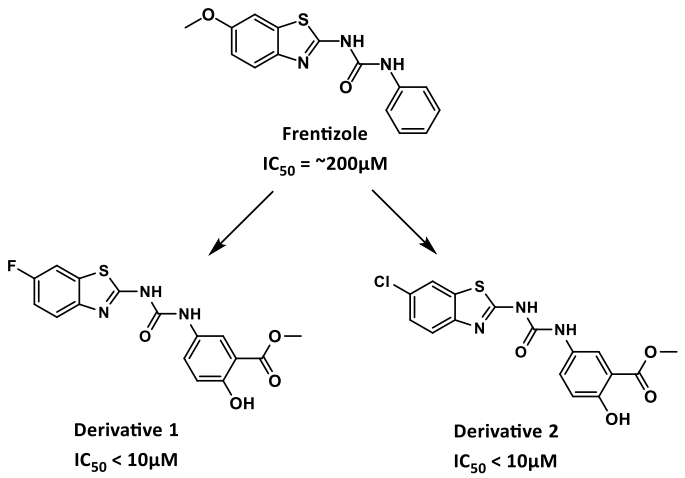

Figure 6.01. 17β-HSD10/Aβ interaction perturbing compounds. Frentizole, the parent compound was found to be capable of disrupting the interaction between the 17β-HSD10 enzyme and Aβ (IC_{50}>200 µM) derivatives 1 and 2 were found to be markedly more potent (IC_{50}<10 µM). Redrawn from[344].

As such, it may be interesting to clone and purify the R130C mutant of the 17β-HSD10 enzyme and perform differential scanning fluorimetry in the presence of Frentizole derivatives, particularly K1093 (Figures 3.15 and 3.16) to assess whether any are capable of stabilising the R130C mutant enzyme potentially allowing the formation of a functional mtRNase P complex and thereby generating a novel therapeutic agent against the currently untreatable MHBD deficiency. Such an effect could be assessed in cell culture by introducing the R130C mutation using CRISPR or by culturing patient fibroblasts and assessing the ability of such a compound to reverse mutation induced mitochondrial abnormalities using electron microscopy, as was done previously[320].

In addition to being implicated in both Alzheimer's disease and MHDB deficiency, the 17β-HSD10 enzyme has also been suggested to play a role in certain forms of cancer. Firstly, an approximately 3-fold upregulation of 17β-HSD10 has been reported in epithelial cells derived from malignant prostate tumours, resulting in elevated synthesis of DHT, a potent androgen, which may promote tumour growth[378]. 17β-HSD10 overexpression has also been shown to promote cell proliferation both in *in vitro* and, using a xenograft based mouse model, *in vivo,* as well as increasing cellular resistance to oxidative stress[379]. Upregulation of 17β-HSD10 has also been shown in patients with certain forms of osteosarcomas who fail to respond to chemotherapy, and was proposed as a potential target for inervention[380] and also in prostate cancer metastases[381].

On the basis of these observations, it appears that, although a focus has been placed here on Alzheimer's disease, the assays developed and the compounds identified as a result of this project may have far

reaching applications in both the treatment of MHBD deficiency and in the development of novel therapeutic agents for the treatment of certain forms of cancer.

References

1 Alzheimer's Society. *Dementia 2014 infographic* <https://www.alzheimers.org.uk/infographic> (2014).

2 Qiu, C., Kivipelto, M. & von Strauss, E. Epidemiology of Alzheimer's disease: occurrence, determinants, and strategies toward intervention. *Dialogues Clin Neurosci* **11**, 111-128 (2009).

3 Alzheimers Disease International. *World Alzheimer Report 2015: The Global Impact of Dementia*, <https://www.alz.co.uk/research/world-report-2015> (2015).

4 Alzheimer, A., Stelzmann, R. A., Schnitzlein, H. N. & Murtagh, F. R. An English translation of Alzheimer's 1907 paper, "Uber eine eigenartige Erkankung der Hirnrinde". *Clin Anat* **8**, 429-431, doi:10.1002/ca.980080612 (1995).

5 Serrano-Pozo, A., Frosch, M. P., Masliah, E. & Hyman, B. T. Neuropathological alterations in Alzheimer disease. *Cold Spring Harb Perspect Med* **1**, a006189, doi:10.1101/cshperspect.a006189 (2011).

6 Musicco, M. *et al.* Predictors of progression of cognitive decline in Alzheimer's disease: the role of vascular and sociodemographic factors. *J Neurol* **256**, 1288-1295, doi:10.1007/s00415-009-5116-4 (2009).

7 Blessed, G., Tomlinson, B. E. & Roth, M. The association between quantitative measures of dementia and of senile change in the cerebral grey matter of elderly subjects. *Br J Psychiatry* **114**, 797-811 (1968).

8 Jucker, M. & Walker, L. C. Self-propagation of pathogenic protein aggregates in neurodegenerative diseases. *Nature* **501**, 45-51, doi:10.1038/nature12481 (2013).

9 Masliah, E., Terry, R. D., Mallory, M., Alford, M. & Hansen, L. A. Diffuse Plaques Do Not Accentuate Synapse Loss in Alzheimers-Disease. *American Journal of Pathology* **137**, 1293-1297 (1990).

10 Itagaki, S., McGeer, P. L., Akiyama, H., Zhu, S. & Selkoe, D. Relationship of microglia and astrocytes to amyloid deposits of Alzheimer disease. *J Neuroimmunol* **24**, 173-182 (1989).

11 Pike, C. J., Cummings, B. J. & Cotman, C. W. Early association of reactive astrocytes with senile plaques in Alzheimer's disease. *Exp Neurol* **132**, 172-179 (1995).

12 Urbanc, B. *et al.* Neurotoxic effects of thioflavin S-positive amyloid deposits in transgenic mice and Alzheimer's disease. *Proc Natl Acad Sci U S A* **99**, 13990-13995, doi:10.1073/pnas.222433299 (2002).

13 Vehmas, A. K., Kawas, C. H., Stewart, W. F. & Troncoso, J. C. Immune reactive cells in senile plaques and cognitive decline in Alzheimer's disease. *Neurobiol Aging* **24**, 321-331 (2003).

14 Thal, D. R., Rub, U., Orantes, M. & Braak, H. Phases of A beta-deposition in the human brain and its relevance for the development of AD. *Neurology* **58**, 1791-1800 (2002).

15 Thal, D. R., Walter, J., Saido, T. C. & Fandrich, M. Neuropathology and biochemistry of Abeta and its aggregates in Alzheimer's disease. *Acta Neuropathol* **129**, 167-182, doi:10.1007/s00401-014-1375-y (2015).

16 Braak, H. & Braak, E. Neuropathological stageing of Alzheimer-related changes. *Acta Neuropathol* **82**, 239-259 (1991).

17 Glenner, G. G. & Wong, C. W. Alzheimer's disease: initial report of the purification and characterization of a novel cerebrovascular amyloid protein. *Biochem Biophys Res Commun* **120**, 885-890 (1984).

18 Wong, C. W., Quaranta, V. & Glenner, G. G. Neuritic plaques and cerebrovascular amyloid in Alzheimer disease are antigenically related. *Proc Natl Acad Sci U S A* **82**, 8729-8732 (1985).

19 Allsop, D., Landon, M. & Kidd, M. The isolation and amino acid composition of senile plaque core protein. *Brain Res* **259**, 348-352 (1983).

20 Grundke-Iqbal, I. *et al.* Abnormal phosphorylation of the microtubule-associated protein tau (tau) in Alzheimer cytoskeletal pathology. *Proc Natl Acad Sci U S A* **83**, 4913-4917 (1986).

21 Kosik, K. S., Joachim, C. L. & Selkoe, D. J. Microtubule-associated protein tau (tau) is a major antigenic component of paired helical filaments in Alzheimer disease. *Proc Natl Acad Sci U S A* **83**, 4044-4048 (1986).

22 Wood, J. G., Mirra, S. S., Pollock, N. J. & Binder, L. I. Neurofibrillary tangles of Alzheimer disease share antigenic determinants with the axonal microtubule-associated protein tau (tau). *Proc Natl Acad Sci U S A* **83**, 4040-4043 (1986).

23 Kang, J. *et al.* The precursor of Alzheimer's disease amyloid A4 protein resembles a cell-surface receptor. *Nature* **325**, 733-736, doi:10.1038/325733a0 (1987).

24 Goldgaber, D., Lerman, M. I., McBride, O. W., Saffiotti, U. & Gajdusek, D. C. Characterization and chromosomal localization of a cDNA encoding brain amyloid of Alzheimer's disease. *Science* **235**, 877-880 (1987).

25 Robakis, N. K., Ramakrishna, N., Wolfe, G. & Wisniewski, H. M. Molecular cloning and characterization of a cDNA encoding the cerebrovascular and the neuritic plaque amyloid peptides. *Proc Natl Acad Sci U S A* **84**, 4190-4194 (1987).

26 Tanzi, R. E. *et al.* Amyloid beta protein gene: cDNA, mRNA distribution, and genetic linkage near the Alzheimer locus. *Science* **235**, 880-884 (1987).

27 Yoshikai, S., Sasaki, H., Doh-ura, K., Furuya, H. & Sakaki, Y. Genomic organization of the human-amyloid beta-protein precursor gene. *Gene* **102**, 291-292 (1991).

28 Dawkins, E. & Small, D. H. Insights into the physiological function of the beta-amyloid precursor protein: beyond Alzheimer's disease. *J Neurochem* **129**, 756-769, doi:10.1111/jnc.12675 (2014).

29 Rohan de Silva, H. A. *et al.* Cell-specific expression of beta-amyloid precursor protein isoform mRNAs and proteins in neurons and astrocytes. *Brain Res Mol Brain Res* **47**, 147-156 (1997).

30 LeBlanc, A. C. *et al.* Processing of amyloid precursor protein in human primary neuron and astrocyte cultures. *J Neurochem* **68**, 1183-1190 (1997).

31 Lindskog, C. The potential clinical impact of the tissue-based map of the human proteome. *Expert Rev Proteomics* **12**, 213-215, doi:10.1586/14789450.2015.1040771 (2015).

32 Ponte, P. *et al.* A new A4 amyloid mRNA contains a domain homologous to serine proteinase inhibitors. *Nature* **331**, 525-527, doi:10.1038/331525a0 (1988).

33 Tanaka, S. *et al.* Tissue-specific expression of three types of beta-protein precursor mRNA: enhancement of protease inhibitor-harboring types in Alzheimer's disease brain. *Biochem Biophys Res Commun* **165**, 1406-1414 (1989).

34 Muller, U. C. & Zheng, H. Physiological functions of APP family proteins. *Cold Spring Harb Perspect Med* **2**, a006288, doi:10.1101/cshperspect.a006288 (2012).

35 Chua, L. M., Lim, M. L. & Wong, B. S. The Kunitz-protease inhibitor domain in amyloid precursor protein reduces cellular mitochondrial enzymes expression and function. *Biochem Biophys Res Commun* **437**, 642-647, doi:10.1016/j.bbrc.2013.07.022 (2013).

36 Goodsell, D. Molecule of the Month- Amyloid-beta Precursor Protein. *PDB-101* (2006).

37 Haass, C., Kaether, C., Thinakaran, G. & Sisodia, S. Trafficking and proteolytic processing of APP. *Cold Spring Harb Perspect Med* **2**, a006270, doi:10.1101/cshperspect.a006270 (2012).

38 Zhang, Y. W., Thompson, R., Zhang, H. & Xu, H. APP processing in Alzheimer's disease. *Mol Brain* **4**, 3, doi:10.1186/1756-6606-4-3 (2011).

39 Haass, C. Take five--BACE and the gamma-secretase quartet conduct Alzheimer's amyloid beta-peptide generation. *EMBO J* **23**, 483-488, doi:10.1038/sj.emboj.7600061 (2004).

40 Chow, V. W., Mattson, M. P., Wong, P. C. & Gleichmann, M. An overview of APP processing enzymes and products. *Neuromolecular Med* **12**, 1-12, doi:10.1007/s12017-009-8104-z (2010).

41 Clarris, H. J. *et al.* Identification of heparin-binding domains in the amyloid precursor protein of Alzheimer's disease by deletion mutagenesis and peptide mapping. *J Neurochem* **68**, 1164-1172 (1997).

42 Mok, S. S. *et al.* Expression and analysis of heparin-binding regions of the amyloid precursor protein of Alzheimer's disease. *FEBS Lett* **415**, 303-307 (1997).

43 Small, D. H. *et al.* A heparin-binding domain in the amyloid protein precursor of Alzheimer's disease is involved in the regulation of neurite outgrowth. *J Neurosci* **14**, 2117-2127 (1994).

44 Beher, D., Hesse, L., Masters, C. L. & Multhaup, G. Regulation of amyloid protein precursor (APP) binding to collagen and mapping of the binding sites on APP and collagen type I. *J Biol Chem* **271**, 1613-1620 (1996).

45 Kibbey, M. C. *et al.* beta-Amyloid precursor protein binds to the neurite-promoting IKVAV site of laminin. *Proc Natl Acad Sci U S A* **90**, 10150-10153 (1993).

46 Yamazaki, T., Koo, E. H. & Selkoe, D. J. Cell surface amyloid beta-protein precursor colocalizes with beta 1 integrins at substrate contact sites in neural cells. *Journal of Neuroscience* **17**, 1004-1010 (1997).

47 Breen, K. C., Bruce, M. & Anderton, B. H. Beta amyloid precursor protein mediates neuronal cell-cell and cell-surface adhesion. *J Neurosci Res* **28**, 90-100, doi:10.1002/jnr.490280109 (1991).

48 Milward, E. A. *et al.* The Amyloid Protein-Precursor of Alzheimers-Disease Is a Mediator of the Effects of Nerve Growth-Factor on Neurite Outgrowth. *Neuron* **9**, 129-137, doi:Doi 10.1016/0896-6273(92)90228-6 (1992).

49 Qiu, W. Q., Ferreira, A., Miller, C., Koo, E. H. & Selkoe, D. J. Cell-Surface Beta-Amyloid Precursor Protein Stimulates Neurite Outgrowth of Hippocampal-Neurons in an Isoform-Dependent Manner. *Journal of Neuroscience* **15**, 2157-2167 (1995).

50 Young-Pearse, T. L., Chen, A. C., Chang, R., Marquez, C. & Selkoe, D. J. Secreted APP regulates the function of full-length APP in neurite outgrowth through interaction with integrin beta1. *Neural Dev* **3**, doi:Artn 1510.1186/1749-8104-3-15 (2008).

51 Soba, P. *et al.* Homo- and heterodimerization of APP family members promotes intercellular adhesion. *EMBO J* **24**, 3624-3634, doi:10.1038/sj.emboj.7600824 (2005).

52 Lee, S. *et al.* The E2 domains of APP and APLP1 share a conserved mode of dimerization. *Biochemistry* **50**, 5453-5464, doi:10.1021/bi101846x (2011).

53 Leblanc, A. C. *et al.* Role of Amyloid Precursor Protein (App) - Study with Antisense Transfection of Human Neuroblastoma-Cells. *Journal of Neuroscience Research* **31**, 635-645, doi:DOI 10.1002/jnr.490310407 (1992).

54 Majocha, R. E., Agrawal, S., Tang, J. Y., Humke, E. W. & Marotta, C. A. Modulation of the Pc12 Cell Response to Nerve Growth-Factor by Antisense Oligonucleotide to Amyloid Precursor Protein. *Cell Mol Neurobiol* **14**, 425-437, doi:Doi 10.1007/Bf02088829 (1994).

55 Allinquant, B. *et al.* Downregulation of amyloid precursor protein inhibits neurite outgrowth in vitro. *J Cell Biol* **128**, 919-927 (1995).

56 Young-Pearse, T. L. *et al.* A critical function for beta-amyloid precursor protein in neuronal migration revealed by In Utero RNA interference. *Journal of Neuroscience* **27**, 14459-14469, doi:10.1523/Jneurosci.4701-07.2007 (2007).

57 Perez, R. G., Zheng, H., Van der Ploeg, L. H. & Koo, E. H. The beta-amyloid precursor protein of Alzheimer's disease enhances neuron viability and modulates neuronal polarity. *J Neurosci* **17**, 9407-9414 (1997).

58 Clarris, H. J., Key, B., Beyreuther, K., Masters, C. L. & Small, D. H. Expression of the amyloid protein precursor of Alzheimer's disease in the developing rat olfactory system. *Brain Res Dev Brain Res* **88**, 87-95 (1995).

59 Loffler, J. & Huber, G. Beta-Amyloid Precursor Protein Isoforms in Various Rat-Brain Regions and during Brain-Development. *Journal of Neurochemistry* **59**, 1316-1324, doi:DOI 10.1111/j.1471-4159.1992.tb08443.x (1992).

60 Wang, Z. *et al.* Presynaptic and postsynaptic interaction of the amyloid precursor protein promotes peripheral and central synaptogenesis. *J Neurosci* **29**, 10788-10801, doi:10.1523/JNEUROSCI.2132-09.2009 (2009).

61 Bush, A. I. *et al.* A novel zinc(II) binding site modulates the function of the beta A4 amyloid protein precursor of Alzheimer's disease. *J Biol Chem* **268**, 16109-16112 (1993).

62 Hesse, L., Beher, D., Masters, C. L. & Multhaup, G. The beta A4 amyloid precursor protein binding to copper. *FEBS Lett* **349**, 109-116 (1994).

63 Acevedo, K. M. *et al.* Copper promotes the trafficking of the amyloid precursor protein. *J Biol Chem* **286**, 8252-8262, doi:10.1074/jbc.M110.128512 (2011).

64 Multhaup, G. *et al.* The amyloid precursor protein of Alzheimer's disease in the reduction of copper(II) to copper(I). *Science* **271**, 1406-1409 (1996).

65 White, A. R. *et al.* The Alzheimer's disease amyloid precursor protein modulates copper-induced toxicity and oxidative stress in primary neuronal cultures. *J Neurosci* **19**, 9170-9179 (1999).

66 Zheng, H. *et al.* Beta-Amyloid Precursor Protein-Deficient Mice Show Reactive Gliosis and Decreased Locomotor-Activity. *Cell* **81**, 525-531, doi:Doi 10.1016/0092-8674(95)90073-X (1995).

67 White, A. R. *et al.* Copper levels are increased in the cerebral cortex and liver of APP and APLP2 knockout mice. *Brain Research* **842**, 439-444, doi:Doi 10.1016/S0006-8993(99)01861-2 (1999).

68 Muller, U. *et al.* Behavioral and Anatomical Deficits in Mice Homozygous for a Modified Beta-Amyloid Precursor Protein Gene. *Cell* **79**, 755-765, doi:Doi 10.1016/0092-8674(94)90066-3 (1994).

69 Tremml, P., Lipp, H. P., Muller, U., Ricceri, L. & Wolfer, D. P. Neurobehavioral development, adult openfield exploration and swimming navigation learning in mice with a modified beta-amyloid precursor protein gene. *Behavioural Brain Research* **95**, 65-76, doi:Doi 10.1016/S0166-4328(97)00211-8 (1998).

70 Dawson, G. R. *et al.* Age-related cognitive deficits, impaired long-term potentiation and reduction in synaptic marker density in mice lacking the beta-amyloid precursor protein. *Neuroscience* **90**, 1-13, doi:Doi 10.1016/S0306-4522(98)00410-2 (1999).

71 Seabrook, G. R. *et al.* Mechanisms contributing to the deficits in hippocampal synaptic plasticity in mice lacking amyloid precursor protein. *Neuropharmacology* **38**, 349-359, doi:Doi 10.1016/S0028-3908(98)00204-4 (1999).

72 Ring, S. *et al.* The secreted beta-amyloid precursor protein ectodomain APPs alpha is sufficient to rescue the anatomical, behavioral, and electrophysiological abnormalities of APP-deficient mice. *J Neurosci* **27**, 7817-7826, doi:10.1523/JNEUROSCI.1026-07.2007 (2007).

73 Plant, L. D., Boyle, J. P., Smith, I. F., Peers, C. & Pearson, H. A. The production of amyloid beta peptide is a critical requirement for the viability of central neurons. *Journal of Neuroscience* **23**, 5531-5535 (2003).

74 Kamenetz, F. *et al.* APP processing and synaptic function. *Neuron* **37**, 925-937, doi:Doi 10.1016/S0896-6273(03)00124-7 (2003).

75 Garcia-Osta, A. & Alberini, C. M. Amyloid beta mediates memory formation. *Learn Memory* **16**, 267-272, doi:10.1101/lm.1310209 (2009).

76 Puzzo, D. *et al.* Picomolar Amyloid-beta Positively Modulates Synaptic Plasticity and Memory in Hippocampus. *Journal of Neuroscience* **28**, 14537-14545, doi:10.1523/Jneurosci.2692-08.2008 (2008).

77 Puzzo, D. *et al.* Endogenous Amyloid-beta is Necessary for Hippocampal Synaptic Plasticity and Memory. *Annals of Neurology* **69**, 819-830, doi:10.1002/ana.22313 (2011).

78 Bateman, R. J. *et al.* Human amyloid-beta synthesis and clearance rates as measured in cerebrospinal fluid in vivo. *Nat Med* **12**, 856-861, doi:10.1038/nm1438 (2006).

79 Deane, R., Bell, R. D., Sagare, A. & Zlokovic, B. V. Clearance of amyloid-beta peptide across the blood-brain barrier: implication for therapies in Alzheimer's disease. *CNS Neurol Disord Drug Targets* **8**, 16-30 (2009).

80 Rogers, J., Strohmeyer, R., Kovelowski, C. J. & Li, R. Microglia and inflammatory mechanisms in the clearance of amyloid beta peptide. *Glia* **40**, 260-269, doi:10.1002/glia.10153 (2002).

81 Shibata, M. *et al.* Clearance of Alzheimer's amyloid-beta(1-40) peptide from brain by LDL receptor-related protein-1 at the blood-brain barrier. *Journal of Clinical Investigation* **106**, 1489-1499, doi:Doi 10.1172/Jci10498 (2000).

82 Deane, R., Sagare, A. & Zlokovic, B. V. The role of the cell surface LRP and soluble LRP in blood-brain barrier Abeta clearance in Alzheimer's disease. *Curr Pharm Des* **14**, 1601-1605 (2008).

83 Miners, J. S., Barua, N., Kehoe, P. G., Gill, S. & Love, S. Abeta-degrading enzymes: potential for treatment of Alzheimer disease. *J Neuropathol Exp Neurol* **70**, 944-959, doi:10.1097/NEN.0b013e3182345e46 (2011).

84 Sadigh-Eteghad, S. *et al.* Amyloid-beta: a crucial factor in Alzheimer's disease. *Med Princ Pract* **24**, 1-10, doi:10.1159/000369101 (2015).

85 Andreadis, A. Misregulation of tau alternative splicing in neurodegeneration and dementia. *Prog Mol Subcell Biol* **44**, 89-107 (2006).

86 Wang, Y. & Mandelkow, E. Tau in physiology and pathology. *Nat Rev Neurosci* **17**, 5-21, doi:10.1038/nrn.2015.1 (2016).

87 Mandelkow, E. M. & Mandelkow, E. Biochemistry and cell biology of tau protein in neurofibrillary degeneration. *Cold Spring Harb Perspect Med* **2**, a006247, doi:10.1101/cshperspect.a006247 (2012).

88 Stamer, K., Vogel, R., Thies, E., Mandelkow, E. & Mandelkow, E. M. Tau blocks traffic of organelles, neurofilaments, and APP vesicles in neurons and enhances oxidative stress. *J Cell Biol* **156**, 1051-1063, doi:10.1083/jcb.200108057 (2002).

89 Dixit, R., Ross, J. L., Goldman, Y. E. & Holzbaur, E. L. Differential regulation of dynein and kinesin motor proteins by tau. *Science* **319**, 1086-1089, doi:10.1126/science.1152993 (2008).

90 Mukrasch, M. D. *et al.* Structural polymorphism of 441-residue tau at single residue resolution. *PLoS Biol* **7**, e34, doi:10.1371/journal.pbio.1000034 (2009).

91 Barghorn, S., Davies, P. & Mandelkow, E. Tau paired helical filaments from Alzheimer's disease brain and assembled in vitro are based on beta-structure in the core domain. *Biochemistry* **43**, 1694-1703, doi:10.1021/bi0357006 (2004).

92 Hanger, D. P., Anderton, B. H. & Noble, W. Tau phosphorylation: the therapeutic challenge for neurodegenerative disease. *Trends Mol Med* **15**, 112-119, doi:10.1016/j.molmed.2009.01.003 (2009).

93 Matsuo, E. S. *et al.* Biopsy-derived adult human brain tau is phosphorylated at many of the same sites as Alzheimer's disease paired helical filament tau. *Neuron* **13**, 989-1002 (1994).

94 Alonso, A., Zaidi, T., Novak, M., Grundke-Iqbal, I. & Iqbal, K. Hyperphosphorylation induces self-assembly of tau into tangles of paired helical filaments/straight filaments. *Proc Natl Acad Sci U S A* **98**, 6923-6928, doi:10.1073/pnas.121119298 (2001).

95 Schneider, A., Biernat, J., von Bergen, M., Mandelkow, E. & Mandelkow, E. M. Phosphorylation that detaches tau protein from microtubules (Ser262, Ser214) also protects it against aggregation into Alzheimer paired helical filaments. *Biochemistry* **38**, 3549-3558, doi:10.1021/bi981874p (1999).

96 Arendt, T. *et al.* Reversible paired helical filament-like phosphorylation of tau is an adaptive process associated with neuronal plasticity in hibernating animals. *J Neurosci* **23**, 6972-6981 (2003).

97 Andorfer, C. *et al.* Cell-cycle reentry and cell death in transgenic mice expressing nonmutant human tau isoforms. *J Neurosci* **25**, 5446-5454, doi:10.1523/JNEUROSCI.4637-04.2005 (2005).

98 Morsch, R., Simon, W. & Coleman, P. D. Neurons may live for decades with neurofibrillary tangles. *J Neuropathol Exp Neurol* **58**, 188-197 (1999).

99 Zhu, X. C. *et al.* Rate of early onset Alzheimer's disease: a systematic review and meta-analysis. *Ann Transl Med* **3**, 38, doi:10.3978/j.issn.2305-5839.2015.01.19 (2015).

100 Bateman, R. J. *et al.* Autosomal-dominant Alzheimer's disease: a review and proposal for the prevention of Alzheimer's disease. *Alzheimers Res Ther* **3**, 1, doi:10.1186/alzrt59 (2011).

101 St George-Hyslop, P. H. *et al.* The genetic defect causing familial Alzheimer's disease maps on chromosome 21. *Science* **235**, 885-890 (1987).

102 Goate, A. *et al.* Segregation of a missense mutation in the amyloid precursor protein gene with familial Alzheimer's disease. *Nature* **349**, 704-706, doi:10.1038/349704a0 (1991).

103 Schellenberg, G. D. *et al.* Genetic linkage evidence for a familial Alzheimer's disease locus on chromosome 14. *Science* **258**, 668-671 (1992).

104 Mullan, M. *et al.* A locus for familial early-onset Alzheimer's disease on the long arm of chromosome 14, proximal to the alpha 1-antichymotrypsin gene. *Nat Genet* **2**, 340-342, doi:10.1038/ng1292-340 (1992).

105 St George-Hyslop, P. *et al.* Genetic evidence for a novel familial Alzheimer's disease locus on chromosome 14. *Nat Genet* **2**, 330-334, doi:10.1038/ng1292-330 (1992).

106 Van Broeckhoven, C. *et al.* Mapping of a gene predisposing to early-onset Alzheimer's disease to chromosome 14q24.3. *Nat Genet* **2**, 335-339, doi:10.1038/ng1292-335 (1992).

107 Levy-Lahad, E. *et al.* A familial Alzheimer's disease locus on chromosome 1. *Science* **269**, 970-973 (1995).

108 Sherrington, R. *et al.* Cloning of a gene bearing missense mutations in early-onset familial Alzheimer's disease. *Nature* **375**, 754-760, doi:10.1038/375754a0 (1995).

109 Levy-Lahad, E. *et al.* Candidate gene for the chromosome 1 familial Alzheimer's disease locus. *Science* **269**, 973-977 (1995).

110 Rogaev, E. I. *et al.* Familial Alzheimer's disease in kindreds with missense mutations in a gene on chromosome 1 related to the Alzheimer's disease type 3 gene. *Nature* **376**, 775-778, doi:10.1038/376775a0 (1995).

111 Alzforum. *Mutations Database*, <www.alzforum.org/mutations> (2016).

112 Lin, X. *et al.* Human aspartic protease memapsin 2 cleaves the beta-secretase site of beta-amyloid precursor protein. *Proc Natl Acad Sci U S A* **97**, 1456-1460 (2000).

113 Vassar, R. *et al.* Beta-secretase cleavage of Alzheimer's amyloid precursor protein by the transmembrane aspartic protease BACE. *Science* **286**, 735-741 (1999).

114 Cai, X. D., Golde, T. E. & Younkin, S. G. Release of excess amyloid beta protein from a mutant amyloid beta protein precursor. *Science* **259**, 514-516 (1993).

115 Citron, M. *et al.* Mutation of the beta-amyloid precursor protein in familial Alzheimer's disease increases beta-protein production. *Nature* **360**, 672-674, doi:10.1038/360672a0 (1992).

116 Citron, M. *et al.* Excessive production of amyloid beta-protein by peripheral cells of symptomatic and presymptomatic patients carrying the Swedish familial Alzheimer disease mutation. *Proc Natl Acad Sci U S A* **91**, 11993-11997 (1994).

117 Hecimovic, S. *et al.* Mutations in APP have independent effects on Abeta and CTFgamma generation. *Neurobiol Dis* **17**, 205-218, doi:10.1016/j.nbd.2004.04.018 (2004).

118 Suzuki, N. *et al.* An increased percentage of long amyloid beta protein secreted by familial amyloid beta protein precursor (beta APP717) mutants. *Science* **264**, 1336-1340 (1994).

119 De Strooper, B. Aph-1, Pen-2, and Nicastrin with Presenilin generate an active gamma-Secretase complex. *Neuron* **38**, 9-12 (2003).

120 Li, N. *et al.* Effect of Presenilin Mutations on APP Cleavage; Insights into the Pathogenesis of FAD. *Front Aging Neurosci* **8**, 51, doi:10.3389/fnagi.2016.00051 (2016).

121 Bentahir, M. *et al.* Presenilin clinical mutations can affect gamma-secretase activity by different mechanisms. *Journal of Neurochemistry* **96**, 732-742, doi:10.1111/j.1471-4159.2005.03578.x (2006).

122 Walker, E. S., Martinez, M., Brunkan, A. L. & Goate, A. Presenilin 2 familial Alzheimer's disease mutations result in partial loss of function and dramatic changes in Abeta 42/40 ratios. *J Neurochem* **92**, 294-301, doi:10.1111/j.1471-4159.2004.02858.x (2005).

123 Wang, R., Wang, B., He, W. & Zheng, H. Wild-type presenilin 1 protects against Alzheimer disease mutation-induced amyloid pathology. *J Biol Chem* **281**, 15330-15336, doi:10.1074/jbc.M512574200 (2006).

124 Fluhrer, R. *et al.* Intramembrane Proteolysis of GXGD-type Aspartyl Proteases Is Slowed by a Familial Alzheimer Disease-like Mutation. *Journal of Biological Chemistry* **283**, 30121-30128, doi:10.1074/jbc.M806092200 (2008).

125 Qi, Y., Morishima-Kawashima, M., Sato, T., Mitsumori, R. & Ihara, Y. Distinct mechanisms by mutant presenilin 1 and 2 leading to increased intracellular levels of amyloid beta-protein 42 in Chinese hamster ovary cells. *Biochemistry* **42**, 1042-1052, doi:10.1021/bi0267590 (2003).

126 Shimojo, M. *et al.* Enzymatic characteristics of I213T mutant presenilin-1/gamma-secretase in cell models and knock-in mouse brains - Familial Alzheimer disease-linked mutation impairs gamma-site cleavage of amyloid precursor protein C-terminal fragment beta. *Journal of Biological Chemistry* **283**, 16488-16496, doi:10.1074/jbc.M801279200 (2008).

127 Peacock, M. L., Warren, J. T., Jr., Roses, A. D. & Fink, J. K. Novel polymorphism in the A4 region of the amyloid precursor protein gene in a patient without Alzheimer's disease. *Neurology* **43**, 1254-1256 (1993).

128 Jonsson, T. *et al.* A mutation in APP protects against Alzheimer's disease and age-related cognitive decline. *Nature* **488**, 96-99, doi:10.1038/nature11283 (2012).

129 Benilova, I. *et al.* The Alzheimer disease protective mutation A2T modulates kinetic and thermodynamic properties of amyloid-beta (Abeta) aggregation. *J Biol Chem* **289**, 30977-30989, doi:10.1074/jbc.M114.599027 (2014).

130 Maloney, J. A. *et al.* Molecular mechanisms of Alzheimer disease protection by the A673T allele of amyloid precursor protein. *J Biol Chem* **289**, 30990-31000, doi:10.1074/jbc.M114.589069 (2014).

131 Zheng, X., Liu, D., Roychaudhuri, R., Teplow, D. B. & Bowers, M. T. Amyloid beta-Protein Assembly: Differential Effects of the Protective A2T Mutation and Recessive A2V Familial Alzheimer's Disease Mutation. *ACS Chem Neurosci* **6**, 1732-1740, doi:10.1021/acschemneuro.5b00171 (2015).

132 Janssen, J. C. *et al.* Early onset familial Alzheimer's disease: Mutation frequency in 31 families. *Neurology* **60**, 235-239 (2003).

133 Mahley, R. W. Apolipoprotein E: cholesterol transport protein with expanding role in cell biology. *Science* **240**, 622-630 (1988).

134 Huang, Y. & Mahley, R. W. Apolipoprotein E: structure and function in lipid metabolism, neurobiology, and Alzheimer's diseases. *Neurobiol Dis* **72 Pt A**, 3-12, doi:10.1016/j.nbd.2014.08.025 (2014).

135 Pericak-Vance, M. A. *et al.* Linkage studies in familial Alzheimer disease: evidence for chromosome 19 linkage. *Am J Hum Genet* **48**, 1034-1050 (1991).

136 Strittmatter, W. J. *et al.* Apolipoprotein E: high-avidity binding to beta-amyloid and increased frequency of type 4 allele in late-onset familial Alzheimer disease. *Proc Natl Acad Sci U S A* **90**, 1977-1981 (1993).

137 Tsai, M. S. *et al.* Apolipoprotein E: risk factor for Alzheimer disease. *Am J Hum Genet* **54**, 643-649 (1994).

138 Harold, D. *et al.* Genome-wide association study identifies variants at CLU and PICALM associated with Alzheimer's disease. *Nat Genet* **41**, 1088-1093, doi:10.1038/ng.440 (2009).

139 Lambert, J. C. *et al.* Genome-wide association study identifies variants at CLU and CR1 associated with Alzheimer's disease. *Nat Genet* **41**, 1094-1099, doi:10.1038/ng.439 (2009).

140 Liu, C. C., Kanekiyo, T., Xu, H. & Bu, G. Apolipoprotein E and Alzheimer disease: risk, mechanisms and therapy. *Nat Rev Neurol* **9**, 106-118, doi:10.1038/nrneurol.2012.263 (2013).

141 Zannis, V. I. *et al.* Proposed nomenclature of apoE isoproteins, apoE genotypes, and phenotypes. *J Lipid Res* **23**, 911-914 (1982).

142 Farrer, L. A. *et al.* Effects of age, sex, and ethnicity on the association between apolipoprotein E genotype and Alzheimer disease. A meta-analysis. APOE and Alzheimer Disease Meta Analysis Consortium. *JAMA* **278**, 1349-1356 (1997).

143 Kok, E. *et al.* Apolipoprotein E-dependent accumulation of Alzheimer disease-related lesions begins in middle age. *Ann Neurol* **65**, 650-657, doi:10.1002/ana.21696 (2009).

144 Gomez-Isla, T. *et al.* Clinical and pathological correlates of apolipoprotein E epsilon 4 in Alzheimer's disease. *Ann Neurol* **39**, 62-70, doi:10.1002/ana.410390110 (1996).

145 Tiraboschi, P. *et al.* Impact of APOE genotype on neuropathologic and neurochemical markers of Alzheimer disease. *Neurology* **62**, 1977-1983 (2004).

146 Wisniewski, T. & Frangione, B. Apolipoprotein E: a pathological chaperone protein in patients with cerebral and systemic amyloid. *Neurosci Lett* **135**, 235-238 (1992).

147 Sanan, D. A. *et al.* Apolipoprotein E associates with beta amyloid peptide of Alzheimer's disease to form novel monofibrils. Isoform apoE4 associates more efficiently than apoE3. *J Clin Invest* **94**, 860-869, doi:10.1172/JCI117407 (1994).

148 Strittmatter, W. J. *et al.* Binding of human apolipoprotein E to synthetic amyloid beta peptide: isoform-specific effects and implications for late-onset Alzheimer disease. *Proc Natl Acad Sci U S A* **90**, 8098-8102 (1993).

149 Aleshkov, S., Abraham, C. R. & Zannis, V. I. Interaction of nascent ApoE2, ApoE3, and ApoE4 isoforms expressed in mammalian cells with amyloid peptide beta (1-40). Relevance to Alzheimer's disease. *Biochemistry* **36**, 10571-10580, doi:10.1021/bi9626362 (1997).

150 LaDu, M. J. *et al.* Isoform-specific binding of apolipoprotein E to beta-amyloid. *J Biol Chem* **269**, 23403-23406 (1994).

151 Yang, D. S., Smith, J. D., Zhou, Z., Gandy, S. E. & Martins, R. N. Characterization of the binding of amyloid-beta peptide to cell culture-derived native apolipoprotein E2, E3, and E4 isoforms and to isoforms from human plasma. *J Neurochem* **68**, 721-725 (1997).

152 Kim, J., Basak, J. M. & Holtzman, D. M. The role of apolipoprotein E in Alzheimer's disease. *Neuron* **63**, 287-303, doi:10.1016/j.neuron.2009.06.026 (2009).

153 Ma, J., Yee, A., Brewer, H. B., Jr., Das, S. & Potter, H. Amyloid-associated proteins alpha 1-antichymotrypsin and apolipoprotein E promote assembly of Alzheimer beta-protein into filaments. *Nature* **372**, 92-94, doi:10.1038/372092a0 (1994).

154 Hashimoto, T. *et al.* Apolipoprotein E, especially apolipoprotein E4, increases the oligomerization of amyloid beta peptide. *J Neurosci* **32**, 15181-15192, doi:10.1523/JNEUROSCI.1542-12.2012 (2012).

155 Bales, K. R. *et al.* Lack of apolipoprotein E dramatically reduces amyloid beta-peptide deposition. *Nat Genet* **17**, 263-264, doi:10.1038/ng1197-263 (1997).

156 Holtzman, D. M. *et al.* Apolipoprotein E isoform-dependent amyloid deposition and neuritic degeneration in a mouse model of Alzheimer's disease. *Proc Natl Acad Sci U S A* **97**, 2892-2897, doi:10.1073/pnas.050004797 (2000).

157 Raber, J. *et al.* Isoform-specific effects of human apolipoprotein E on brain function revealed in ApoE knockout mice: increased susceptibility of females. *Proc Natl Acad Sci U S A* **95**, 10914-10919 (1998).

158 Dolev, I. & Michaelson, D. M. A nontransgenic mouse model shows inducible amyloid-beta (Abeta) peptide deposition and elucidates the role of apolipoprotein E in the amyloid cascade. *Proc Natl Acad Sci U S A* **101**, 13909-13914, doi:10.1073/pnas.0404458101 (2004).

159 Youmans, K. L. *et al.* APOE4-specific changes in Abeta accumulation in a new transgenic mouse model of Alzheimer disease. *J Biol Chem* **287**, 41774-41786, doi:10.1074/jbc.M112.407957 (2012).

160 Fagan, A. M. *et al.* Cerebrospinal fluid tau/beta-amyloid(42) ratio as a prediction of cognitive decline in nondemented older adults. *Arch Neurol* **64**, 343-349, doi:10.1001/archneur.64.3.noc60123 (2007).

161 Tapiola, T. *et al.* Cerebrospinal fluid {beta}-amyloid 42 and tau proteins as biomarkers of Alzheimer-type pathologic changes in the brain. *Arch Neurol* **66**, 382-389, doi:10.1001/archneurol.2008.596 (2009).

162 Castellano, J. M. *et al.* Human apoE isoforms differentially regulate brain amyloid-beta peptide clearance. *Sci Transl Med* **3**, 89ra57, doi:10.1126/scitranslmed.3002156 (2011).

163 Karch, C. M. & Goate, A. M. Alzheimer's disease risk genes and mechanisms of disease pathogenesis. *Biol Psychiatry* **77**, 43-51, doi:10.1016/j.biopsych.2014.05.006 (2015).

164 Hardy, J. A. & Higgins, G. A. Alzheimer's disease: the amyloid cascade hypothesis. *Science* **256**, 184-185 (1992).

165 Hardy, J. & Allsop, D. Amyloid deposition as the central event in the aetiology of Alzheimer's disease. *Trends Pharmacol Sci* **12**, 383-388 (1991).

166 Selkoe, D. J. The molecular pathology of Alzheimer's disease. *Neuron* **6**, 487-498 (1991).

167 Mohandas, E., Rajmohan, V. & Raghunath, B. Neurobiology of Alzheimer's disease. *Indian J Psychiatry* **51**, 55-61, doi:10.4103/0019-5545.44908 (2009).

168 Folstein, M. F., Folstein, S. E. & McHugh, P. R. "Mini-mental state". A practical method for grading the cognitive state of patients for the clinician. *J Psychiatr Res* **12**, 189-198 (1975).

169 Rosen, W. G., Mohs, R. C. & Davis, K. L. A new rating scale for Alzheimer's disease. *Am J Psychiatry* **141**, 1356-1364, doi:10.1176/ajp.141.11.1356 (1984).

170 Galasko, D. *et al.* An inventory to assess activities of daily living for clinical trials in Alzheimer's disease. The Alzheimer's Disease Cooperative Study. *Alzheimer Dis Assoc Disord* **11 Suppl 2**, S33-39 (1997).

171 Saxton, J. M.-G., Karen L.; Swihart, Andrew A.; Miller, Vicki J.; Boller, Francois. Assessment of the severely impaired patient: Description and validation of a new neuropsychological test battery. *Psychological Assessment* **Vol 2**, 298-303 (1990).

172 Small, B. J., Viitanen, M. & Backman, L. Mini-Mental State Examination item scores as predictors of Alzheimer's disease: incidence data from the Kungsholmen Project, Stockholm. *J Gerontol A Biol Sci Med Sci* **52**, M299-304 (1997).

173 Tombaugh, T. N. & McIntyre, N. J. The mini-mental state examination: a comprehensive review. *J Am Geriatr Soc* **40**, 922-935 (1992).

174 Franco-Marina, F. *et al.* The Mini-mental State Examination revisited: ceiling and floor effects after score adjustment for educational level in an aging Mexican population. *Int Psychogeriatr* **22**, 72-81, doi:10.1017/S1041610209990822 (2010).

175 Robert, P. *et al.* Review of Alzheimer's disease scales: is there a need for a new multi-domain scale for therapy evaluation in medical practice? *Alzheimers Res Ther* **2**, 24, doi:10.1186/alzrt48 (2010).

176 Gerzon, K., Krumkalns, E. V., Brindle, R. L., Marshall, F. J. & Root, M. A. The Adamantyl Group in Medicinal Agents. I. Hypoglycemic N-Arylsulfonyl-N' -Adamantylureas. *J Med Chem* **6**, 760-763 (1963).

177 Parsons, C. G., Danysz, W. & Quack, G. Memantine is a clinically well tolerated N-methyl-D-aspartate (NMDA) receptor antagonist--a review of preclinical data. *Neuropharmacology* **38**, 735-767 (1999).

178 Blanpied, T. A., Boeckman, F. A., Aizenman, E. & Johnson, J. W. Trapping channel block of NMDA-activated responses by amantadine and memantine. *J Neurophysiol* **77**, 309-323 (1997).

179 Chen, H. S. & Lipton, S. A. Mechanism of memantine block of NMDA-activated channels in rat retinal ganglion cells: uncompetitive antagonism. *J Physiol* **499 (Pt 1)**, 27-46 (1997).

180 Paoletti, P., Bellone, C. & Zhou, Q. NMDA receptor subunit diversity: impact on receptor properties, synaptic plasticity and disease. *Nat Rev Neurosci* **14**, 383-400, doi:10.1038/nrn3504 (2013).

181 Sonkusare, S. K., Kaul, C. L. & Ramarao, P. Dementia of Alzheimer's disease and other neurodegenerative disorders - memantine, a new hope. *Pharmacol Res* **51**, 1-17, doi:10.1016/j.phrs.2004.05.005 (2005).

182 Bashir, Z. I., Alford, S., Davies, S. N., Randall, A. D. & Collingridge, G. L. Long-term potentiation of NMDA receptor-mediated synaptic transmission in the hippocampus. *Nature* **349**, 156-158, doi:10.1038/349156a0 (1991).

183 Berretta, N. *et al.* Long-term Potentiation of NMDA Receptor-mediated EPSP in Guinea-pig Hippocampal Slices. *Eur J Neurosci* **3**, 850-854 (1991).

184 O'Connor, J. J., Rowan, M. J. & Anwyl, R. Long-lasting enhancement of NMDA receptor-mediated synaptic transmission by metabotropic glutamate receptor activation. *Nature* **367**, 557-559, doi:10.1038/367557a0 (1994).

185 O'Connor, J. J., Rowan, M. J. & Anwyl, R. Tetanically induced LTP involves a similar increase in the AMPA and NMDA receptor components of the excitatory postsynaptic current: investigations of the involvement of mGlu receptors. *J Neurosci* **15**, 2013-2020 (1995).

186 Harnett, M. T., Bernier, B. E., Ahn, K. C. & Morikawa, H. Burst-timing-dependent plasticity of NMDA receptor-mediated transmission in midbrain dopamine neurons. *Neuron* **62**, 826-838, doi:10.1016/j.neuron.2009.05.011 (2009).

187 Xie, X., Berger, T. W. & Barrionuevo, G. Isolated NMDA receptor-mediated synaptic responses express both LTP and LTD. *J Neurophysiol* **67**, 1009-1013 (1992).

188 Selig, D. K., Hjelmstad, G. O., Herron, C., Nicoll, R. A. & Malenka, R. C. Independent mechanisms for long-term depression of AMPA and NMDA responses. *Neuron* **15**, 417-426 (1995).

189 Morishita, W., Marie, H. & Malenka, R. C. Distinct triggering and expression mechanisms underlie LTD of AMPA and NMDA synaptic responses. *Nat Neurosci* **8**, 1043-1050, doi:10.1038/nn1506 (2005).

190 Nowak, L., Bregestovski, P., Ascher, P., Herbet, A. & Prochiantz, A. Magnesium gates glutamate-activated channels in mouse central neurones. *Nature* **307**, 462-465 (1984).

191 Mayer, M. L., Westbrook, G. L. & Guthrie, P. B. Voltage-dependent block by Mg2+ of NMDA responses in spinal cord neurones. *Nature* **309**, 261-263 (1984).

192 Blanke, M. L. & VanDongen, A. M. J. in *Biology of the NMDA Receptor Frontiers in Neuroscience* (ed A. M. Van Dongen) (2009).

193 Dubinsky, J. M. Intracellular calcium levels during the period of delayed excitotoxicity. *J Neurosci* **13**, 623-631 (1993).

194 Gupta, K., Hardingham, G. E. & Chandran, S. NMDA receptor-dependent glutamate excitotoxicity in human embryonic stem cell-derived neurons. *Neurosci Lett* **543**, 95-100, doi:10.1016/j.neulet.2013.03.010 (2013).

195 Hynd, M. R., Scott, H. L. & Dodd, P. R. Glutamate-mediated excitotoxicity and neurodegeneration in Alzheimer's disease. *Neurochem Int* **45**, 583-595, doi:10.1016/j.neuint.2004.03.007 (2004).

196 Danysz, W. & Parsons, C. G. Alzheimer's disease, beta-amyloid, glutamate, NMDA receptors and memantine--searching for the connections. *Br J Pharmacol* **167**, 324-352, doi:10.1111/j.1476-5381.2012.02057.x (2012).

197 Parsons, C. G., Stoffler, A. & Danysz, W. Memantine: a NMDA receptor antagonist that improves memory by restoration of homeostasis in the glutamatergic system--too little activation is bad, too much is even worse. *Neuropharmacology* **53**, 699-723, doi:10.1016/j.neuropharm.2007.07.013 (2007).

198 Witt, A., Macdonald, N. & Kirkpatrick, P. Memantine hydrochloride. *Nat Rev Drug Discov* **3**, 109-110, doi:10.1038/nrd1311 (2004).

199 US Food and Drug Administration (FDA). *FDA Approved Drug Products: Memantine*, <http://www.accessdata.fda.gov/drugsatfda_docs/label/2003/021487lbl.pdf> (2003).

200 Picciotto, M. R., Higley, M. J. & Mineur, Y. S. Acetylcholine as a neuromodulator: cholinergic signaling shapes nervous system function and behavior. *Neuron* **76**, 116-129, doi:10.1016/j.neuron.2012.08.036 (2012).

201 Kawai, H., Lazar, R. & Metherate, R. Nicotinic control of axon excitability regulates thalamocortical transmission. *Nat Neurosci* **10**, 1168-1175, doi:10.1038/nn1956 (2007).

202 Douglas, C. L., Baghdoyan, H. A. & Lydic, R. Postsynaptic muscarinic M1 receptors activate prefrontal cortical EEG of C57BL/6J mouse. *J Neurophysiol* **88**, 3003-3009, doi:10.1152/jn.00318.2002 (2002).

203 McCormick, D. A. & Prince, D. A. Two types of muscarinic response to acetylcholine in mammalian cortical neurons. *Proc Natl Acad Sci U S A* **82**, 6344-6348 (1985).

204 Mansvelder, H. D., Keath, J. R. & McGehee, D. S. Synaptic mechanisms underlie nicotine-induced excitability of brain reward areas. *Neuron* **33**, 905-919 (2002).

205 Grady, S. R. *et al.* Nicotinic agonists stimulate acetylcholine release from mouse interpeduncular nucleus: a function mediated by a different nAChR than dopamine release from striatum. *J Neurochem* **76**, 258-268 (2001).

206 Parikh, V., Ji, J., Decker, M. W. & Sarter, M. Prefrontal beta2 subunit-containing and alpha7 nicotinic acetylcholine receptors differentially control glutamatergic and cholinergic signaling. *J Neurosci* **30**, 3518-3530, doi:10.1523/JNEUROSCI.5712-09.2010 (2010).

207 Raiteri, M., Leardi, R. & Marchi, M. Heterogeneity of presynaptic muscarinic receptors regulating neurotransmitter release in the rat brain. *J Pharmacol Exp Ther* **228**, 209-214 (1984).

208 Higley, M. J., Soler-Llavina, G. J. & Sabatini, B. L. Cholinergic modulation of multivesicular release regulates striatal synaptic potency and integration. *Nat Neurosci* **12**, 1121-1128, doi:10.1038/nn.2368 (2009).

209 Mansvelder, H. D. & McGehee, D. S. Long-term potentiation of excitatory inputs to brain reward areas by nicotine. *Neuron* **27**, 349-357 (2000).

210 Ge, S. & Dani, J. A. Nicotinic acetylcholine receptors at glutamate synapses facilitate long-term depression or potentiation. *J Neurosci* **25**, 6084-6091, doi:10.1523/JNEUROSCI.0542-05.2005 (2005).

211 Ji, D., Lape, R. & Dani, J. A. Timing and location of nicotinic activity enhances or depresses hippocampal synaptic plasticity. *Neuron* **31**, 131-141 (2001).

212 Colovic, M. B., Krstic, D. Z., Lazarevic-Pasti, T. D., Bondzic, A. M. & Vasic, V. M. Acetylcholinesterase inhibitors: pharmacology and toxicology. *Curr Neuropharmacol* **11**, 315-335, doi:10.2174/1570159X11311030006 (2013).

213 Whitehouse, P. J. *et al.* Alzheimer's disease and senile dementia: loss of neurons in the basal forebrain. *Science* **215**, 1237-1239 (1982).

214 Bowen, D. M., Smith, C. B., White, P. & Davison, A. N. Neurotransmitter-related enzymes and indices of hypoxia in senile dementia and other abiotrophies. *Brain* **99**, 459-496 (1976).

215 Perry, E. K., Gibson, P. H., Blessed, G., Perry, R. H. & Tomlinson, B. E. Neurotransmitter enzyme abnormalities in senile dementia. Choline acetyltransferase and glutamic acid decarboxylase activities in necropsy brain tissue. *J Neurol Sci* **34**, 247-265 (1977).

216 Nilsson, L., Nordberg, A., Hardy, J., Wester, P. & Winblad, B. Physostigmine restores 3H-acetylcholine efflux from Alzheimer brain slices to normal level. *J Neural Transm* **67**, 275-285 (1986).

217 Rylett, R. J., Ball, M. J. & Colhoun, E. H. Evidence for high affinity choline transport in synaptosomes prepared from hippocampus and neocortex of patients with Alzheimer's disease. *Brain Res* **289**, 169-175 (1983).

218 Contestabile, A. The history of the cholinergic hypothesis. *Behav Brain Res* **221**, 334-340, doi:10.1016/j.bbr.2009.12.044 (2011).

219 Lopez-Pousa, S. *et al.* Differential efficacy of treatment with acetylcholinesterase inhibitors in patients with mild and moderate Alzheimer's disease over a 6-month period. *Dement Geriatr Cogn Disord* **19**, 189-195, doi:10.1159/000083498 (2005).

220 Wilkinson, D. G. *et al.* A multinational, randomised, 12-week, comparative study of donepezil and rivastigmine in patients with mild to moderate Alzheimer's disease. *Int J Clin Pract* **56**, 441-446 (2002).

221 Wilcock, G. *et al.* A long-term comparison of galantamine and donepezil in the treatment of Alzheimer's disease. *Drugs Aging* **20**, 777-789 (2003).

222 Bullock, R. *et al.* Rivastigmine and donepezil treatment in moderate to moderately-severe Alzheimer's disease over a 2-year period. *Curr Med Res Opin* **21**, 1317-1327, doi:10.1185/030079905X56565 (2005).

223 Seltzer, B. *et al.* Efficacy of donepezil in early-stage Alzheimer disease: a randomized placebo-controlled trial. *Arch Neurol* **61**, 1852-1856, doi:10.1001/archneur.61.12.1852 (2004).

224 Folch, J. *et al.* Current Research Therapeutic Strategies for Alzheimer's Disease Treatment. *Neural Plast* **2016**, 8501693, doi:10.1155/2016/8501693 (2016).

225 Lai, R. *et al.* First-in-human study of E2609, a novel BACE1 inhibitor, demonstrates prolonged reductions in plasma beta-amyloid levels after single dosing. *Alzheimer's & Dementia: The Journal of the Alzheimer's Association* **8**, P96, doi:10.1016/j.jalz.2012.05.237.

226 Eisai Inc. *Dose-Finding Study To Evaluate Safety, Tolerability, and Efficacy of E2609 in Subjects With Mild Cognitive Impairment Due to Alzheimer's Disease (Prodromal Alzheimer's Disease) and Mild to Moderate Dementia Due to Alzheimer's Disease*, <https://clinicaltrials.gov/ct2/results?term=e2609&Search=Search> (2014).

227 Merck Sharp & Dohme Corp. *Efficacy and Safety Trial of Verubecestat (MK-8931) in Participants With Prodromal Alzheimer's Disease (MK-8931-019) (APECS)*, <https://clinicaltrials.gov/ct2/show/NCT01953601> (2013).

228 Merck Sharp & Dohme Corp. *An Efficacy and Safety Trial of Verubecestat (MK-8931) in Mild to Moderate Alzheimer's Disease (P07738) (EPOCH)*, <https://clinicaltrials.gov/ct2/show/NCT01739348> (2012).

229 May, P. C. *et al.* The potent BACE1 inhibitor LY2886721 elicits robust central Abeta pharmacodynamic responses in mice, dogs, and humans. *J Neurosci* **35**, 1199-1210, doi:10.1523/JNEUROSCI.4129-14.2015 (2015).

230 Eli Lilly and Company. *Study of LY2886721 in Mild Cognitive Impairment due to Alzheimer's Disease or Mild Alzheimer's Disease*, <https://clinicaltrials.gov/ct2/show/NCT01561430> (2012).

231 Bateman, R. J. *et al.* A gamma-secretase inhibitor decreases amyloid-beta production in the central nervous system. *Ann Neurol* **66**, 48-54, doi:10.1002/ana.21623 (2009).

232 Fleisher, A. S. *et al.* Phase 2 safety trial targeting amyloid beta production with a gamma-secretase inhibitor in Alzheimer disease. *Arch Neurol* **65**, 1031-1038, doi:10.1001/archneur.65.8.1031 (2008).

233 Siemers, E. R. *et al.* Safety, tolerability, and effects on plasma and cerebrospinal fluid amyloid-beta after inhibition of gamma-secretase. *Clin Neuropharmacol* **30**, 317-325, doi:10.1097/WNF.0b013e31805b7660 (2007).

234 Doody, R. S. *et al.* A phase 3 trial of semagacestat for treatment of Alzheimer's disease. *N Engl J Med* **369**, 341-350, doi:10.1056/NEJMoa1210951 (2013).

235 Chavez-Gutierrez, L. *et al.* The mechanism of gamma-Secretase dysfunction in familial Alzheimer disease. *EMBO J* **31**, 2261-2274, doi:10.1038/emboj.2012.79 (2012).

236 Gillman, K. W. *et al.* Discovery and Evaluation of BMS-708163, a Potent, Selective and Orally Bioavailable gamma-Secretase Inhibitor. *ACS Med Chem Lett* **1**, 120-124, doi:10.1021/ml1000239 (2010).

237 Crump, C. J. *et al.* BMS-708,163 targets presenilin and lacks notch-sparing activity. *Biochemistry* **51**, 7209-7211, doi:10.1021/bi301137h (2012).

238 Coric, V. *et al.* Safety and tolerability of the gamma-secretase inhibitor avagacestat in a phase 2 study of mild to moderate Alzheimer disease. *Arch Neurol* **69**, 1430-1440, doi:10.1001/archneurol.2012.2194 (2012).

239 Gervais, F. *et al.* Targeting soluble Abeta peptide with Tramiprosate for the treatment of brain amyloidosis. *Neurobiol Aging* **28**, 537-547, doi:10.1016/j.neurobiolaging.2006.02.015 (2007).

240 Aisen, P. S. *et al.* Alzhemed: a potential treatment for Alzheimer's disease. *Curr Alzheimer Res* **4**, 473-478 (2007).

241 Aisen, P. S. *et al.* Tramiprosate in mild-to-moderate Alzheimer's disease - a randomized, double-blind, placebo-controlled, multi-centre study (the Alphase Study). *Arch Med Sci* **7**, 102-111, doi:10.5114/aoms.2011.20612 (2011).

242 Bilikiewicz, A. & Gaus, W. Colostrinin (a naturally occurring, proline-rich, polypeptide mixture) in the treatment of Alzheimer's disease. *J Alzheimers Dis* **6**, 17-26 (2004).

243 Szaniszlo, P. *et al.* New insights into clinical trial for Colostrinin in Alzheimer's disease. *J Nutr Health Aging* **13**, 235-241 (2009).

244 Ma, K., Thomason, L. A. & McLaurin, J. scyllo-Inositol, preclinical, and clinical data for Alzheimer's disease. *Adv Pharmacol* **64**, 177-212, doi:10.1016/B978-0-12-394816-8.00006-4 (2012).

245 Sampson, E. L., Jenagaratnam, L. & McShane, R. Metal protein attenuating compounds for the treatment of Alzheimer's dementia. *Cochrane Database Syst Rev*, CD005380, doi:10.1002/14651858.CD005380.pub5 (2014).

246 Faux, N. G. *et al.* PBT2 rapidly improves cognition in Alzheimer's Disease: additional phase II analyses. *J Alzheimers Dis* **20**, 509-516, doi:10.3233/JAD-2010-1390 (2010).

247 Solomon, B., Koppel, R., Frankel, D. & Hanan-Aharon, E. Disaggregation of Alzheimer beta-amyloid by site-directed mAb. *Proc Natl Acad Sci U S A* **94**, 4109-4112 (1997).

248 Schenk, D. *et al.* Immunization with amyloid-beta attenuates Alzheimer-disease-like pathology in the PDAPP mouse. *Nature* **400**, 173-177, doi:10.1038/22124 (1999).

249 Morgan, D. *et al.* A beta peptide vaccination prevents memory loss in an animal model of Alzheimer's disease. *Nature* **408**, 982-985, doi:10.1038/35050116 (2000).

250 Janus, C. *et al.* A beta peptide immunization reduces behavioural impairment and plaques in a model of Alzheimer's disease. *Nature* **408**, 979-982, doi:10.1038/35050110 (2000).

251 Sigurdsson, E. M., Scholtzova, H., Mehta, P. D., Frangione, B. & Wisniewski, T. Immunization with a nontoxic/nonfibrillar amyloid-beta homologous peptide reduces Alzheimer's disease-associated pathology in transgenic mice. *Am J Pathol* **159**, 439-447 (2001).

252 Sigurdsson, E. M. *et al.* An attenuated immune response is sufficient to enhance cognition in an Alzheimer's disease mouse model immunized with amyloid-beta derivatives. *J Neurosci* **24**, 6277-6282, doi:10.1523/JNEUROSCI.1344-04.2004 (2004).

253 Bayer, A. J. *et al.* Evaluation of the safety and immunogenicity of synthetic Abeta42 (AN1792) in patients with AD. *Neurology* **64**, 94-101, doi:10.1212/01.WNL.0000148604.77591.67 (2005).

254 Wisniewski, T. & Frangione, B. Immunological and anti-chaperone therapeutic approaches for Alzheimer disease. *Brain Pathol* **15**, 72-77 (2005).

255 Bombois, S. *et al.* Absence of beta-amyloid deposits after immunization in Alzheimer disease with Lewy body dementia. *Arch Neurol* **64**, 583-587, doi:10.1001/archneur.64.4.583 (2007).

256 Masliah, E. *et al.* Abeta vaccination effects on plaque pathology in the absence of encephalitis in Alzheimer disease. *Neurology* **64**, 129-131, doi:10.1212/01.WNL.0000148590.39911.DF (2005).

257 Nicoll, J. A. *et al.* Neuropathology of human Alzheimer disease after immunization with amyloid-beta peptide: a case report. *Nat Med* **9**, 448-452, doi:10.1038/nm840 (2003).

258 Nicoll, J. A. *et al.* Abeta species removal after abeta42 immunization. *J Neuropathol Exp Neurol* **65**, 1040-1048, doi:10.1097/01.jnen.0000240466.10758.ce (2006).

259 Gilman, S. *et al.* Clinical effects of Abeta immunization (AN1792) in patients with AD in an interrupted trial. *Neurology* **64**, 1553-1562, doi:10.1212/01.WNL.0000159740.16984.3C (2005).

260 Holmes, C. *et al.* Long-term effects of Abeta42 immunisation in Alzheimer's disease: follow-up of a randomised, placebo-controlled phase I trial. *Lancet* **372**, 216-223, doi:10.1016/S0140-6736(08)61075-2 (2008).

261 Pride, M. *et al.* Progress in the active immunotherapeutic approach to Alzheimer's disease: clinical investigations into AN1792-associated meningoencephalitis. *Neurodegener Dis* **5**, 194-196, doi:10.1159/000113700 (2008).

262 Salloway, S. *et al.* A phase 2 multiple ascending dose trial of bapineuzumab in mild to moderate Alzheimer disease. *Neurology* **73**, 2061-2070, doi:10.1212/WNL.0b013e3181c67808 (2009).

263 Salloway, S. *et al.* Two phase 3 trials of bapineuzumab in mild-to-moderate Alzheimer's disease. *N Engl J Med* **370**, 322-333, doi:10.1056/NEJMoa1304839 (2014).

264 DeMattos, R. B. *et al.* Peripheral anti-A beta antibody alters CNS and plasma A beta clearance and decreases brain A beta burden in a mouse model of Alzheimer's disease. *Proc Natl Acad Sci U S A* **98**, 8850-8855, doi:10.1073/pnas.151261398 (2001).

265 DeMattos, R. B., Bales, K. R., Cummins, D. J., Paul, S. M. & Holtzman, D. M. Brain to plasma amyloid-beta efflux: a measure of brain amyloid burden in a mouse model of Alzheimer's disease. *Science* **295**, 2264-2267, doi:10.1126/science.1067568 (2002).

266 Siemers, E. R. *et al.* Safety and changes in plasma and cerebrospinal fluid amyloid beta after a single administration of an amyloid beta monoclonal antibody in subjects with Alzheimer disease. *Clin Neuropharmacol* **33**, 67-73, doi:10.1097/WNF.0b013e3181cb577a (2010).

267 Farlow, M. *et al.* Safety and biomarker effects of solanezumab in patients with Alzheimer's disease. *Alzheimers Dement* **8**, 261-271, doi:10.1016/j.jalz.2011.09.224 (2012).

268 Doody, R. S. *et al.* Phase 3 trials of solanezumab for mild-to-moderate Alzheimer's disease. *N Engl J Med* **370**, 311-321, doi:10.1056/NEJMoa1312889 (2014).

269 Siemers, E. R. *et al.* Phase 3 solanezumab trials: Secondary outcomes in mild Alzheimer's disease patients. *Alzheimers Dement* **12**, 110-120, doi:10.1016/j.jalz.2015.06.1893 (2016).

270 Hsia, A. Y. *et al.* Plaque-independent disruption of neural circuits in Alzheimer's disease mouse models. *Proc Natl Acad Sci U S A* **96**, 3228-3233 (1999).

271 Mucke, L. *et al.* High-level neuronal expression of abeta 1-42 in wild-type human amyloid protein precursor transgenic mice: synaptotoxicity without plaque formation. *J Neurosci* **20**, 4050-4058 (2000).

272 Westerman, M. A. *et al.* The relationship between Abeta and memory in the Tg2576 mouse model of Alzheimer's disease. *J Neurosci* **22**, 1858-1867 (2002).

273 Villemagne, V. L. *et al.* Longitudinal assessment of Abeta and cognition in aging and Alzheimer disease. *Ann Neurol* **69**, 181-192, doi:10.1002/ana.22248 (2011).

274 Terry, R. D. *et al.* Physical Basis of Cognitive Alterations in Alzheimers-Disease - Synapse Loss Is the Major Correlate of Cognitive Impairment. *Annals of Neurology* **30**, 572-580, doi:DOI 10.1002/ana.410300410 (1991).

275 Engler, H. *et al.* Two-year follow-up of amyloid deposition in patients with Alzheimer's disease. *Brain* **129**, 2856-2866, doi:10.1093/brain/awl178 (2006).

276 Crystal, H. *et al.* Clinico-pathologic studies in dementia: nondemented subjects with pathologically confirmed Alzheimer's disease. *Neurology* **38**, 1682-1687 (1988).

277 Katzman, R. *et al.* Clinical, pathological, and neurochemical changes in dementia: a subgroup with preserved mental status and numerous neocortical plaques. *Ann Neurol* **23**, 138-144, doi:10.1002/ana.410230206 (1988).

278 Dickson, D. W. *et al.* Identification of normal and pathological aging in prospectively studied nondemented elderly humans. *Neurobiol Aging* **13**, 179-189 (1992).

279 Arriagada, P. V., Marzloff, K. & Hyman, B. T. Distribution of Alzheimer-type pathologic changes in nondemented elderly individuals matches the pattern in Alzheimer's disease. *Neurology* **42**, 1681-1688 (1992).

280 Nelson, P. T., Braak, H. & Markesbery, W. R. Neuropathology and cognitive impairment in Alzheimer disease: a complex but coherent relationship. *J Neuropathol Exp Neurol* **68**, 1-14, doi:10.1097/NEN.0b013e3181919a48 (2009).

281 Lorenzo, A. & Yankner, B. A. Beta-amyloid neurotoxicity requires fibril formation and is inhibited by congo red. *Proc Natl Acad Sci U S A* **91**, 12243-12247 (1994).

282 Pike, C. J., Burdick, D., Walencewicz, A. J., Glabe, C. G. & Cotman, C. W. Neurodegeneration induced by beta-amyloid peptides in vitro: the role of peptide assembly state. *J Neurosci* **13**, 1676-1687 (1993).

283 Howlett, D. R. *et al.* Aggregation state and neurotoxic properties of Alzheimer beta-amyloid peptide. *Neurodegeneration* **4**, 23-32 (1995).

284 Lambert, M. P. *et al.* Diffusible, nonfibrillar ligands derived from Abeta1-42 are potent central nervous system neurotoxins. *Proc Natl Acad Sci U S A* **95**, 6448-6453 (1998).

285 Klein, W. L., Krafft, G. A. & Finch, C. E. Targeting small Abeta oligomers: the solution to an Alzheimer's disease conundrum? *Trends Neurosci* **24**, 219-224 (2001).

286 Podlisny, M. B. *et al.* Aggregation of secreted amyloid beta-protein into sodium dodecyl sulfate-stable oligomers in cell culture. *J Biol Chem* **270**, 9564-9570 (1995).

287 Xia, W. *et al.* Enhanced production and oligomerization of the 42-residue amyloid beta-protein by Chinese hamster ovary cells stably expressing mutant presenilins. *J Biol Chem* **272**, 7977-7982 (1997).

288 DaRocha-Souto, B. *et al.* Brain oligomeric beta-amyloid but not total amyloid plaque burden correlates with neuronal loss and astrocyte inflammatory response in amyloid precursor protein/tau transgenic mice. *J Neuropathol Exp Neurol* **70**, 360-376, doi:10.1097/NEN.0b013e318217a118 (2011).

289 Tomiyama, T. *et al.* A mouse model of amyloid beta oligomers: their contribution to synaptic alteration, abnormal tau phosphorylation, glial activation, and neuronal loss in vivo. *J Neurosci* **30**, 4845-4856, doi:10.1523/JNEUROSCI.5825-09.2010 (2010).

290 Tabaton, M., Nunzi, M. G., Xue, R., Autiliogambetti, L. & Gambetti, P. Soluble Amyloid-Beta Protein Is a Marker of Alzheimer Amyloid in the Brain but Plot in Cerebrospinal-Fluid. *Neurology* **44**, A371-A371 (1994).

291 Harigaya, Y. *et al.* Modified Amyloid-Beta Protein Ending at 42 or 40 with Different Solubility Accumulates in the Brain of Alzheimers-Disease. *Biochem Bioph Res Co* **211**, 1015-1022, doi:DOI 10.1006/bbrc.1995.1912 (1995).

292 Lue, L. F. *et al.* Soluble amyloid beta peptide concentration as a predictor of synaptic change in Alzheimer's disease. *American Journal of Pathology* **155**, 853-862, doi:Doi 10.1016/S0002-9440(10)65184-X (1999).

293 McLean, C. A. *et al.* Soluble pool of Abeta amyloid as a determinant of severity of neurodegeneration in Alzheimer's disease. *Ann Neurol* **46**, 860-866 (1999).

294 Hartmann, T. *et al.* Distinct sites of intracellular production for Alzheimer's disease A beta 40/42 amyloid peptides. *Nature Medicine* **3**, 1016-1020, doi:DOI 10.1038/nm0997-1016 (1997).

295 Cook, D. G. *et al.* Alzheimer's A beta(1-42) is generated in the endoplasmic reticulum/intermediate compartment of NT2N cells. *Nature Medicine* **3**, 1021-1023, doi:DOI 10.1038/nm0997-1021 (1997).

296 Greenfield, J. P. *et al.* Endoplasmic reticulum and trans-Golgi network generate distinct populations of Alzheimer beta-amyloid peptides. *P Natl Acad Sci USA* **96**, 742-747, doi:DOI 10.1073/pnas.96.2.742 (1999).

297 Xu, H. X. *et al.* Generation of Alzheimer beta-amyloid protein in the trans-Golgi network in the apparent absence of vesicle formation. *P Natl Acad Sci USA* **94**, 3748-3752, doi:DOI 10.1073/pnas.94.8.3748 (1997).

298 Youmans, K. L. *et al.* Intraneuronal Abeta detection in 5xFAD mice by a new Abeta-specific antibody. *Mol Neurodegener* **7**, 8, doi:10.1186/1750-1326-7-8 (2012).

299 Billings, L. M., Oddo, S., Green, K. N., McGaugh, J. L. & LaFerla, F. M. Intraneuronal A beta causes the onset of early Alzheimer's disease-related cognitive deficits in transgenic mice. *Neuron* **45**, 675-688, doi:10.1016/j.neuron.2005.01.040 (2005).

300 Lee, E. K., Park, Y. W., Shin, D. Y., Mook-Jung, I. & Yoo, Y. J. Cytosolic amyloid-beta peptide 42 escaping from degradation induces cell death. *Biochem Bioph Res Co* **344**, 471-477, doi:10.1016/j.bbrc.2006.03.166 (2006).

301 Zheng, L. *et al.* Intracellular distribution of amyloid beta peptide and its relationship to the lysosomal system. *Transl Neurodegener* **1**, 19, doi:10.1186/2047-9158-1-19 (2012).

302 Manczak, M. *et al.* Mitochondria are a direct site of A beta accumulation in Alzheimer's disease neurons: implications for free radical generation and oxidative damage in disease progression. *Hum Mol Genet* **15**, 1437-1449, doi:10.1093/hmg/ddl066 (2006).

303 Lustbader, J. W. *et al.* ABAD directly links Abeta to mitochondrial toxicity in Alzheimer's disease. *Science* **304**, 448-452, doi:10.1126/science.1091230 (2004).

304 Petersen, C. A. H. *et al.* The amyloid beta-peptide is imported into mitochondria via the TOM import machinery and localized to mitochondrial cristae. *P Natl Acad Sci USA* **105**, 13145-13150, doi:10.1073/pnas.0806192105 (2008).

305 Park, H. J. *et al.* beta-amyloid precursor protein is a direct cleavage target of HtrA2 serine protease - Implications for the physiological function of HtrA2 in the mitochondria. *Journal of Biological Chemistry* **281**, 34277-34287, doi:10.1074/jbc.M603443200 (2006).

306 Caspersen, C. *et al.* Mitochondrial Abeta: a potential focal point for neuronal metabolic dysfunction in Alzheimer's disease. *FASEB J* **19**, 2040-2041, doi:10.1096/fj.05-3735fje (2005).

307 Lin, M. T. & Beal, M. F. Alzheimer's APP mangles mitochondria. *Nat Med* **12**, 1241-1243, doi:10.1038/nm1106-1241 (2006).

308 Chen, J. X. & Yan, S. S. Role of mitochondrial amyloid-beta in Alzheimer's disease. *J Alzheimers Dis* **20 Suppl 2**, S569-578, doi:10.3233/JAD-2010-100357 (2010).

309 He, X. Y. *et al.* Characterization and localization of human type10 17beta-hydroxysteroid dehydrogenase. *Eur J Biochem* **268**, 4899-4907 (2001).

310 He, X. Y., Merz, G., Mehta, P., Schulz, H. & Yang, S. Y. Human brain short chain L-3-hydroxyacyl coenzyme A dehydrogenase is a single-domain multifunctional enzyme. Characterization of a novel 17beta-hydroxysteroid dehydrogenase. *J Biol Chem* **274**, 15014-15019 (1999).

311 Shafqat, N. *et al.* Expanded substrate screenings of human and Drosophila type 10 17beta-hydroxysteroid dehydrogenases (HSDs) reveal multiple specificities in bile acid and steroid hormone metabolism: characterization of multifunctional 3alpha/7alpha/7beta/17beta/20beta/21-HSD. *Biochem J* **376**, 49-60, doi:10.1042/BJ20030877 (2003).

312 He, X. Y. *et al.* Molecular cloning, modeling, and localization of rat type 10 17beta-hydroxysteroid dehydrogenase. *Mol Cell Endocrinol* **171**, 89-98 (2001).

313 Yang, S. Y. *et al.* Roles of 17beta-hydroxysteroid dehydrogenase type 10 in neurodegenerative disorders. *J Steroid Biochem Mol Biol* **143**, 460-472, doi:10.1016/j.jsbmb.2014.07.001 (2014).

314 Marques, A. T., Antunes, A., Fernandes, P. A. & Ramos, M. J. Comparative evolutionary genomics of the HADH2 gene encoding Abeta-binding alcohol dehydrogenase/17beta-hydroxysteroid dehydrogenase type 10 (ABAD/HSD10). *BMC Genomics* **7**, 202, doi:10.1186/1471-2164-7-202 (2006).

315 Torroja, L., Ortuno-Sahagun, D., Ferrus, A., Hammerle, B. & Barbas, J. A. scully, an essential gene of Drosophila, is homologous to mammalian mitochondrial type II L-3-hydroxyacyl-CoA dehydrogenase/amyloid-beta peptide-binding protein. *J Cell Biol* **141**, 1009-1017 (1998).

316 Zschocke, J. *et al.* Progressive infantile neurodegeneration caused by 2-methyl-3-hydroxybutyryl-CoA dehydrogenase deficiency: a novel inborn error of branched-chain fatty acid and isoleucine metabolism. *Pediatr Res* **48**, 852-855, doi:10.1203/00006450-200012000-00025 (2000).

317 Sosinsky, A., Bonin, C. P., Mann, R. S. & Honig, B. Target Explorer: An automated tool for the identification of new target genes for a specified set of transcription factors. *Nucleic Acids Res* **31**, 3589-3592 (2003).

318 Luo, M. J., Mao, L. F. & Schulz, H. Short-chain 3-hydroxy-2-methylacyl-CoA dehydrogenase from rat liver: purification and characterization of a novel enzyme of isoleucine metabolism. *Arch Biochem Biophys* **321**, 214-220, doi:10.1006/abbi.1995.1388 (1995).

319 Perez-Cerda, C. *et al.* 2-Methyl-3-hydroxybutyryl-CoA dehydrogenase (MHBD) deficiency: an X-linked inborn error of isoleucine metabolism that may mimic a mitochondrial disease. *Pediatr Res* **58**, 488-491, doi:10.1203/01.pdr.0000176916.94328.cd (2005).

320 Rauschenberger, K. *et al.* A non-enzymatic function of 17beta-hydroxysteroid dehydrogenase type 10 is required for mitochondrial integrity and cell survival. *EMBO Mol Med* **2**, 51-62, doi:10.1002/emmm.200900055 (2010).

321 Pasquali, M., Monsen, G., Richardson, L., Alston, M. & Longo, N. Biochemical findings in common inborn errors of metabolism. *Am J Med Genet C Semin Med Genet* **142C**, 64-76, doi:10.1002/ajmg.c.30086 (2006).

322 Fukao, T., Scriver, C. R., Kondo, N. & t2 Collaborative Working, G. The clinical phenotype and outcome of mitochondrial acetoacetyl-CoA thiolase deficiency (beta-ketothiolase or T2 deficiency) in 26 enzymatically proved and mutation-defined patients. *Mol Genet Metab* **72**, 109-114, doi:10.1006/mgme.2000.3113 (2001).

323 Korman, S. H. Inborn errors of isoleucine degradation: a review. *Mol Genet Metab* **89**, 289-299, doi:10.1016/j.ymgme.2006.07.010 (2006).

324 Zschocke, J. HSD10 disease: clinical consequences of mutations in the HSD17B10 gene. *J Inherit Metab Dis* **35**, 81-89, doi:10.1007/s10545-011-9415-4 (2012).

325 Poll-The, B. T. *et al.* Spastic diplegia and periventricular white matter abnormalities in 2-methyl-3-hydroxybutyryl-CoA dehydrogenase deficiency, a defect of isoleucine metabolism: differential diagnosis with hypoxic-ischemic brain diseases. *Mol Genet Metab* **81**, 295-299, doi:10.1016/j.ymgme.2003.11.013 (2004).

326 Ensenauer, R. *et al.* Clinical variability in 3-hydroxy-2-methylbutyryl-CoA dehydrogenase deficiency. *Ann Neurol* **51**, 656-659, doi:10.1002/ana.10169 (2002).

327 Olpin, S. E. *et al.* 2-methyl-3-hydroxybutyryl-CoA dehydrogenase deficiency in a 23-year-old man. *J Inherit Metab Dis* **25**, 477-482 (2002).

328 Sass, J. O., Forstner, R. & Sperl, W. 2-Methyl-3-hydroxybutyryl-CoA dehydrogenase deficiency: impaired catabolism of isoleucine presenting as neurodegenerative disease. *Brain Dev* **26**, 12-14 (2004).

329 Sutton, V. R., O'Brien, W. E., Clark, G. D., Kim, J. & Wanders, R. J. 3-Hydroxy-2-methylbutyryl-CoA dehydrogenase deficiency. *J Inherit Metab Dis* **26**, 69-71 (2003).

330 Deutschmann, A. J. *et al.* Mutation or knock-down of 17beta-hydroxysteroid dehydrogenase type 10 cause loss of MRPP1 and impaired processing of mitochondrial heavy strand transcripts. *Hum Mol Genet* **23**, 3618-3628, doi:10.1093/hmg/ddu072 (2014).

331 He, X. Y., Wegiel, J. & Yang, S. Y. Intracellular oxidation of allopregnanolone by human brain type 10 17beta-hydroxysteroid dehydrogenase. *Brain Res* **1040**, 29-35, doi:10.1016/j.brainres.2005.01.022 (2005).

332 Yang, S. Y. *et al.* Mental retardation linked to mutations in the HSD17B10 gene interfering with neurosteroid and isoleucine metabolism. *Proc Natl Acad Sci U S A* **106**, 14820-14824, doi:10.1073/pnas.0902377106 (2009).

333 Holzmann, J. *et al.* RNase P without RNA: identification and functional reconstitution of the human mitochondrial tRNA processing enzyme. *Cell* **135**, 462-474, doi:10.1016/j.cell.2008.09.013 (2008).

334 Powell, C. A., Nicholls, T. J. & Minczuk, M. Nuclear-encoded factors involved in post-transcriptional processing and modification of mitochondrial tRNAs in human disease. *Front Genet* **6**, 79, doi:10.3389/fgene.2015.00079 (2015).

335 Vilardo, E. *et al.* A subcomplex of human mitochondrial RNase P is a bifunctional methyltransferase--extensive moonlighting in mitochondrial tRNA biogenesis. *Nucleic Acids Res* **40**, 11583-11593, doi:10.1093/nar/gks910 (2012).

336 Chatfield, K. C. *et al.* Mitochondrial energy failure in HSD10 disease is due to defective mtDNA transcript processing. *Mitochondrion* **21**, 1-10, doi:10.1016/j.mito.2014.12.005 (2015).

337 Yan, S. D. *et al.* An intracellular protein that binds amyloid-beta peptide and mediates neurotoxicity in Alzheimer's disease. *Nature* **389**, 689-695 (1997).

338 Yan, S. D. *et al.* Role of ERAB/L-3-hydroxyacyl-coenzyme A dehydrogenase type II activity in Abeta-induced cytotoxicity. *J Biol Chem* **274**, 2145-2156 (1999).

339 Yao, J. *et al.* Inhibition of amyloid-beta (Abeta) peptide-binding alcohol dehydrogenase-Abeta interaction reduces Abeta accumulation and improves mitochondrial function in a mouse model of Alzheimer's disease. *J Neurosci* **31**, 2313-2320, doi:10.1523/JNEUROSCI.4717-10.2011 (2011).

340 Takuma, K. *et al.* ABAD enhances Abeta-induced cell stress via mitochondrial dysfunction. *FASEB J* **19**, 597-598, doi:10.1096/fj.04-2582fje (2005).

341 Kristofikova, Z. *et al.* Enhanced levels of mitochondrial enzyme 17beta-hydroxysteroid dehydrogenase type 10 in patients with Alzheimer disease and multiple sclerosis. *Mol Biosyst* **5**, 1174-1179, doi:10.1039/b904799a (2009).

342 Yao, J. *et al.* Interaction of amyloid binding alcohol dehydrogenase/Abeta mediates up-regulation of peroxiredoxin II in the brains of Alzheimer's disease patients and a transgenic Alzheimer's disease mouse model. *Mol Cell Neurosci* **35**, 377-382, doi:10.1016/j.mcn.2007.03.013 (2007).

343 Ren, Y. *et al.* Endophilin I expression is increased in the brains of Alzheimer disease patients. *J Biol Chem* **283**, 5685-5691, doi:10.1074/jbc.M707932200 (2008).

344 Xie, Y., Deng, S., Chen, Z., Yan, S. & Landry, D. W. Identification of small-molecule inhibitors of the Abeta-ABAD interaction. *Bioorg Med Chem Lett* **16**, 4657-4660, doi:10.1016/j.bmcl.2006.05.099 (2006).

345 Liu, H. & Naismith, J. H. An efficient one-step site-directed deletion, insertion, single and multiple-site plasmid mutagenesis protocol. *BMC Biotechnol* **8**, 91, doi:10.1186/1472-6750-8-91 (2008).

346 Liu, H. & Naismith, J. H. A simple and efficient expression and purification system using two newly constructed vectors. *Protein Expr Purif* **63**, 102-111, doi:10.1016/j.pep.2008.09.008 (2009).

347 Bolanos-Garcia, V. M. & Davies, O. R. Structural analysis and classification of native proteins from E. coli commonly co-purified by immobilised metal affinity chromatography. *Biochim Biophys Acta* **1760**, 1304-1313, doi:10.1016/j.bbagen.2006.03.027 (2006).

348 Kallinteri, P. & Antimisiaris, S. G. Solubility of drugs in the presence of gelatin: effect of drug lipophilicity and degree of ionization. *Int J Pharm* **221**, 219-226 (2001).

349 Yan, Y. *et al.* Surface plasmon resonance and nuclear magnetic resonance studies of ABAD-Abeta interaction. *Biochemistry* **46**, 1724-1731, doi:10.1021/bi061314n (2007).

350 Kissinger, C. R. *et al.* Crystal structure of human ABAD/HSD10 with a bound inhibitor: implications for design of Alzheimer's disease therapeutics. *J Mol Biol* **342**, 943-952, doi:10.1016/j.jmb.2004.07.071 (2004).

351 Zhang, J. H., Chung, T. D. & Oldenburg, K. R. A Simple Statistical Parameter for Use in Evaluation and Validation of High Throughput Screening Assays. *J Biomol Screen* **4**, 67-73 (1999).

352 Hanukoglu, I. Proteopedia: Rossmann fold: A beta-alpha-beta fold at dinucleotide binding sites. *Biochem Mol Biol Educ* **43**, 206-209, doi:10.1002/bmb.20849 (2015).

353 Cornish-Bowden, A. *Fundamentals of enzyme kinetics*. 4th, completely revised and greatly enlarged edition. edn, (Wiley-Blackwell, 2012).

354 Feng, B. Y. & Shoichet, B. K. A detergent-based assay for the detection of promiscuous inhibitors. *Nat Protoc* **1**, 550-553, doi:10.1038/nprot.2006.77 (2006).

355 Baell, J. B. & Holloway, G. A. New substructure filters for removal of pan assay interference compounds (PAINS) from screening libraries and for their exclusion in bioassays. *J Med Chem* **53**, 2719-2740, doi:10.1021/jm901137j (2010).

356 Pantoliano, M. W. *et al.* High-density miniaturized thermal shift assays as a general strategy for drug discovery. *J Biomol Screen* **6**, 429-440, doi:10.1089/108705701753364922 (2001).

357 Strelow, J. *et al.* in *Assay Guidance Manual* (eds G. S. Sittampalam *et al.*) (2004).

358 Ryan, T. M. *et al.* Ammonium hydroxide treatment of Abeta produces an aggregate free solution suitable for biophysical and cell culture characterization. *PeerJ* **1**, e73, doi:10.7717/peerj.73 (2013).

359 Peltoketo, H., Luu-The, V., Simard, J. & Adamski, J. 17beta-hydroxysteroid dehydrogenase (HSD)/17-ketosteroid reductase (KSR) family; nomenclature and main characteristics of the 17HSD/KSR enzymes. *J Mol Endocrinol* **23**, 1-11 (1999).

360 Yates, A. *et al.* Ensembl 2016. *Nucleic Acids Res* **44**, D710-716, doi:10.1093/nar/gkv1157 (2016).

361 Uhlen, M. *et al.* Proteomics. Tissue-based map of the human proteome. *Science* **347**, 1260419, doi:10.1126/science.1260419 (2015).

362 Shimomaye, E. & Salvato, M. Use of Avian-Myeloblastosis Virus Reverse-Transcriptase at High-Temperature for Sequence-Analysis of Highly Structured Rna. *Gene Anal Tech* **6**, 25-28, doi:Doi 10.1016/0735-0651(89)90022-8 (1989).

363 Vera, A., Gonzalez-Montalban, N., Aris, A. & Villaverde, A. The conformational quality of insoluble recombinant proteins is enhanced at low growth temperatures. *Biotechnol Bioeng* **96**, 1101-1106, doi:10.1002/bit.21218 (2007).

364 Wilkins, M. R. *et al.* Protein identification and analysis tools in the ExPASy server. *Methods Mol Biol* **112**, 531-552 (1999).

365 Fomitcheva, J., Baker, M. E., Anderson, E., Lee, G. Y. & Aziz, N. Characterization of Ke 6, a new 17beta-hydroxysteroid dehydrogenase, and its expression in gonadal tissues. *J Biol Chem* **273**, 22664-22671 (1998).

366 Bertoletti, N. *et al.* New Insights into Human 17 beta-Hydroxysteroid Dehydrogenase Type 14: First Crystal Structures in Complex with a Steroidal Ligand and with a Potent Nonsteroidal Inhibitor. *Journal of Medicinal Chemistry* **59**, 6961-6967, doi:10.1021/acs.jmedchem.6b00293 (2016).

367 Lukacik, P. *et al.* Structural and biochemical characterization of human orphan DHRS10 reveals a novel cytosolic enzyme with steroid dehydrogenase activity. *Biochem J* **402**, 419-427, doi:10.1042/BJ20061319 (2007).

368 Rosano, G. L. & Ceccarelli, E. A. Rare codon content affects the solubility of recombinant proteins in a codon bias-adjusted Escherichia coli strain. *Microb Cell Fact* **8**, 41, doi:10.1186/1475-2859-8-41 (2009).

369 Proteomics, N. M. L. f. S. G. a. *Rare Codon Calculator (RaCC)* <http://nihserver.mbi.ucla.edu/RACC/> (

370 Ferre, F. & Clote, P. DiANNA: a web server for disulfide connectivity prediction. *Nucleic Acids Res* **33**, W230-232, doi:10.1093/nar/gki412 (2005).

371 Baneyx, F. & Mujacic, M. Recombinant protein folding and misfolding in Escherichia coli. *Nat Biotechnol* **22**, 1399-1408, doi:10.1038/nbt1029 (2004).

372 Hammarstrom, M., Hellgren, N., van Den Berg, S., Berglund, H. & Hard, T. Rapid screening for improved solubility of small human proteins produced as fusion proteins in Escherichia coli. *Protein Sci* **11**, 313-321, doi:10.1110/ps.22102 (2002).

373 Dyson, M. R., Shadbolt, S. P., Vincent, K. J., Perera, R. L. & McCafferty, J. Production of soluble mammalian proteins in Escherichia coli: identification of protein features that correlate with successful expression. *BMC Biotechnol* **4**, 32, doi:10.1186/1472-6750-4-32 (2004).

374 Esposito, D. & Chatterjee, D. K. Enhancement of soluble protein expression through the use of fusion tags. *Curr Opin Biotechnol* **17**, 353-358, doi:10.1016/j.copbio.2006.06.003 (2006).

375 Raran-Kurussi, S. & Waugh, D. S. The ability to enhance the solubility of its fusion partners is an intrinsic property of maltose-binding protein but their folding is either spontaneous or chaperone-mediated. *PLoS One* **7**, e49589, doi:10.1371/journal.pone.0049589 (2012).

376 Chan, F. K., Moriwaki, K. & De Rosa, M. J. Detection of necrosis by release of lactate dehydrogenase activity. *Methods Mol Biol* **979**, 65-70, doi:10.1007/978-1-62703-290-2_7 (2013).

377 Vilardo, E. & Rossmanith, W. Molecular insights into HSD10 disease: impact of SDR5C1 mutations on the human mitochondrial RNase P complex. *Nucleic Acids Res* **43**, 6649, doi:10.1093/nar/gkv658 (2015).

378 He, X. Y. *et al.* Oxidative 3alpha-hydroxysteroid dehydrogenase activity of human type 10 17beta-hydroxysteroid dehydrogenase. *J Steroid Biochem Mol Biol* **87**, 191-198 (2003).

379 Carlson, E. A. *et al.* Overexpression of 17beta-hydroxysteroid dehydrogenase type 10 increases pheochromocytoma cell growth and resistance to cell death. *BMC Cancer* **15**, 166, doi:10.1186/s12885-015-1173-5 (2015).

380 Salas, S. *et al.* Molecular characterization of the response to chemotherapy in conventional osteosarcomas: predictive value of HSD17B10 and IFITM2. *Int J Cancer* **125**, 851-860, doi:10.1002/ijc.24457 (2009).

381 Jernberg, E. *et al.* Characterization of prostate cancer bone metastases according to expression levels of steroidogenic enzymes and androgen receptor splice variants. *PLoS One* **8**, e77407, doi:10.1371/journal.pone.0077407 (2013).

Appendix:

Appendix A: Protein Mass Spectrometry

17β-HSD10 Mass Spectrometry

MATRIX SCIENCE **Mascot Search Results**

```
User            : Patrick_Guest
Email           : pg34@st-andrews.ac.uk
Search title    : Project: Analysis\Sept16, Spot Set: Analysis\Sept16\13Sept16, Label: A6, Spot Id: 1708147, Peak List Id: 1747002, MS Job Run Id: 53794
MS data file    : \\cfs.st-andrews.ac.uk\Shared\Chem_PIs\BSRC_Mass_Spec\A MGF REPOSITORY\Data from 4800\Sept16\13Sept16\13Sept16_Patrick_17B_HSD10.mgf
Database 1      : BMS 160913 (3948 sequences; 1243416 residues)
Database 2      : contaminants 20120713 (247 sequences; 128130 residues)
Database 3      : cRAP 20120229 (115 sequences; 38188 residues)
Timestamp       : 13 Sep 2016 at 13:11:26 GMT
Protein hits    : 1::bms|BMS004871|HCD2_HUMAN HSD10 Q99714 [Homo sapiens] HSD10 Q99714 [Homo sapiens]
```

Mascot Score Histogram

Ions score is -10*Log(P), where P is the probability that the observed match is a random event.
Individual ions scores > 24 indicate identity or extensive homology (p<0.05).
Protein scores are derived from ions scores as a non-probabilistic basis for ranking protein hits.

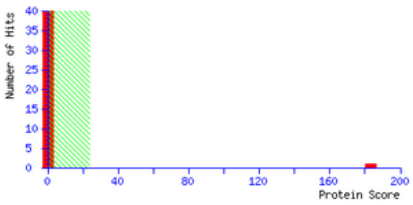

Peptide Summary Report

Format As: Peptide Summary — Help
Significance threshold p< 0.05 — Max. number of hits AUTO
Standard scoring / MudPIT scoring / Ions score or expect cut-off 0 — Show sub-sets 0
Show pop-ups / Suppress pop-ups — Sort unassigned: Decreasing Score — Require bold red
Preferred taxonomy: All entries

Select All | Select None | Search Selected | Error tolerant | Archive Report

1. 1::bms|BMS004871|HCD2_HUMAN HSD10 Q99714 [Homo sapiens] Mass: 27134 Score: 183 Matches: 6(6) Sequences: 6(6)
HSD10 Q99714 [Homo sapiens]
Check to include this hit in error tolerant search or archive report

Query	Observed	Mr(expt)	Mr(calc)	Delta	Miss	Score	Expect	Rank	Unique	Peptide
2	854.3988	853.3915	853.5021	-0.1106	0	36	0.0019	1	U	R.DLAPIGIR.V
10	1184.5240	1183.5167	1183.6747	-0.1580	0	40	0.0015	1	U	K.GGIVGMTLPIAR.D
16	1590.6460	1589.6387	1589.8600	-0.2212	0	88	3.4e-08	1	U	R.VLDVNLMGTFNVIR.L
20	1621.5841	1620.5768	1620.8083	-0.2314	0	47	0.0003	1	U	K.VCNFLASQVPFPSR.L
28	1812.7645	1811.7572	1812.0105	-0.2533	0	49	0.00016	1	U	K.GLVAVITGGASGLGLATAER.L
32	2084.8665	2083.8592	2084.1591	-0.2999	0	29	0.028	1	U	R.VMTIAPGLFGTPLLTSLPEK.V

17β-HSD8 Mass Spectrometry

MATRIX SCIENCE Mascot Search Results

```
User            : Patrick_Guest
Email           : pg34@st-andrews.ac.uk
Search title    : Project: Patrick HSD8
MS data file    : C:\Data from 4800\Mar16\15Mar16\Patrick HSD8.mgf
Database 1      : BMS 160311 (4826 sequences; 1543331 residues)
Database 2      : contaminants 20120713 (247 sequences; 128130 residues)
Database 3      : cRAP 20120229 (115 sequences; 38188 residues)
Timestamp       : 15 Mar 2016 at 12:29:04 GMT
Protein hits    : 1::bms|BMS004809|261aa PatrickG HSD8 [human] HSD8 [human]
```

Mascot Score Histogram

Ions score is -10*Log(P), where P is the probability that the observed match is a random event.
Individual ions scores > 24 indicate identity or extensive homology (p<0.05).
Protein scores are derived from ions scores as a non-probabilistic basis for ranking protein hits.

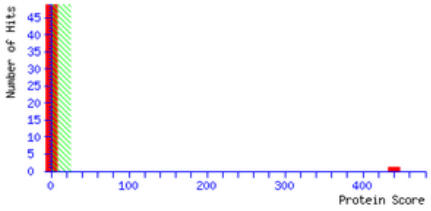

Peptide Summary Report

Format As: Peptide Summary — Help

Significance threshold p< 0.05 — Max. number of hits AUTO

Standard scoring / MudPIT scoring / Ions score or expect cut-off 0 — Show sub-sets 0

Show pop-ups / Suppress pop-ups — Sort unassigned: Decreasing Score — Require bold red

Preferred taxonomy: All entries

Select All | Select None | Search Selected | Error tolerant | Archive Report

1. 1::bms|BMS004809|261aa PatrickG HSD8 [human] Mass: 27299 Score: 439 Matches: 6(5) Sequences: 6(5)
HSD8 [human]

Check to include this hit in error tolerant search or archive report

Query	Observed	Mr(expt)	Mr(calc)	Delta	Miss	Score	Expect	Rank	Unique	Peptide
5	1157.6809	1156.6736	1156.6564	0.0172	0	82	1.1e-07	1	U	K.AGVIGLTQTAAR.E
12	1329.7657	1328.7584	1328.7412	0.0172	0	85	4.3e-08	1	U	R.SALALVTGAGSGIGR.A
16	1472.7024	1471.6951	1471.6804	0.0147	0	131	1.2e-12	1	U	R.GNHAAFQADVSEAR.A
25	1763.8818	1762.8745	1762.8746	-0.0001	0	97	3e-09	1	U	R.CNSVLPGFIATPMTQK.V
34	1964.0081	1963.0008	1962.9946	0.0063	0	142	1.1e-13	1	U	K.GTFLVTQAAAQALVSNGCR.G
45	2008.9602	2007.9529	2007.9511	0.0018	1	3	8.4	2	U	K.EGPPRGNHAAFQADVSEAR.A

17β-HSD14 Mass Spectrometry

Mascot Search Results

```
User            : Patrick_Guest
Email           : pg34@st-andrews.ac.uk
Search title    : patrick unknown ESI BMS, Patrick HSD14 unknown.mgf
MS data file    : \\cfs.st-andrews.ac.uk\Shared\Chem_PIs\BSRC_Mass_Spec\A MGF REPOSITORY\Data from 5600+\160513\Patrick HSD14 unknown.mgf
Database 1      : BMS 160516 (4836 sequences; 1549562 residues)
Database 2      : contaminants 20120713 (247 sequences; 128130 residues)
Database 3      : cRAP 20120229 (115 sequences; 38188 residues)
Timestamp       : 16 May 2016 at 10:36:30 GMT
Protein hits    : 1::bms|BMS004810|270aa_PatrickG HSD14 [human]          HSD14 [human]
                  3::sp|TRYP_PIG|                                        sp|TRYP_PIG|
                  1::SEQ0647 324 aa DE: 3-Hydroxyacyl-CoA dehydrogenase
                  2::P19001                                              SWISS-PROT:P19001 Tax_Id=10090 Gene_Symbol=Krt19 Keratin, type I cytoskeletal 19
```

Mascot Score Histogram

Ions score is -10*Log(P), where P is the probability that the observed match is a random event.
Individual ions scores > 15 indicate identity or extensive homology (p<0.05).
Protein scores are derived from ions scores as a non-probabilistic basis for ranking protein hits.

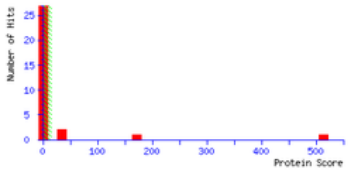

Peptide Summary Report

Format As: Peptide Summary — Help

Significance threshold p< 0.05 — Max. number of hits AUTO

Standard scoring / MudPIT scoring — Ions score or expect cut-off 0 — Show sub-sets 0

Show pop-ups / Suppress pop-ups — Sort unassigned: Decreasing Score — Require bold red

Preferred taxonomy: All entries

Select All | Select None | Search Selected | Error tolerant | Archive Report

1. 1::bms|BMS004810|270aa_PatrickG HSD14 [human] Mass: 28642 Score: 513 Matches: 14(14) Sequences: 10(10) emPAI: 6.89
HSD14 [human]

Check to include this hit in error tolerant search or archive report

Query	Observed	Mr(expt)	Mr(calc)	ppm	Miss	Score	Expect	Rank	Unique	Peptide
3	411.2178	820.4210	820.4191	2.32	0	48	4.8e-05	1	U	R.AFVNSGAR.V
12	422.2570	842.4995	842.4974	2.46	0	54	1.3e-05	1	U	K.VVVVTGGGR.G
13	423.2677	844.5209	844.5170	4.55	0	42	6.4e-05	1	U	K.LALPYLR.K
35	459.7676	917.5205	917.5182	2.57	0	52	1.4e-05	1	U	K.TLVSETIR.R
46	487.3140	972.6135	972.6120	1.53	1	18	0.016	1	U	K.LALPYLRK.S
54	536.2846	1070.5547	1070.5542	0.41	0	(65)	8.3e-07	1	U	R.EGMLAQPLGR.M
55	537.8181	1073.6216	1073.6193	2.14	1	19	0.019	1	U	K.TLVSETIRR.F
58	544.2819	1086.5492	1086.5492	0.08	0	(77)	4.3e-08	1	U	R.EGMLAQPLGR.M + Oxidation (M)
59	544.2823	1086.5500	1086.5492	0.78	0	85	5.9e-09	1	U	R.EGMLAQPLGR.M + Oxidation (M)
62	549.7694	1097.5242	1097.5241	0.15	0	(23)	0.0077	1	U	R.STPVDAPDIPS.-
63	549.7700	1097.5255	1097.5241	1.34	0	27	0.0038	1	U	R.STPVDAPDIPS.-
83	645.8379	1289.6613	1289.6615	-0.15	0	(82)	1.4e-08	1	U	K.ALALDESPYGVR.V
84	645.8383	1289.6620	1289.6615	0.39	0	97	4.5e-10	1	U	K.ALALDESPYGVR.V

Appendix B: DNA Construct Sequencing

pcDNA3-HSD10:

ATGTCCGTCCTGACGCCGCTGCTGCTGCGGGGCTTGACAGGCTCGGCCCGGCGGCTCCCAGTGCCGCGCGCCAAGATC
CATTCGTTGGGGGATCCACCGGTCGCCGAATTCACCATGGCAGCAGCGTGTCGGAGCGTGAAGGGCCTGGTGGCGGTA
ATAACCGGAGGAGCCTCGGGCCTGGGCCTGGCCACGGCGGAGCGACTTGTGGGGCAGGGAGCCTCTGCTGTGCTTCTG
GACCTGCCCAACTCGGGTGGGGAGGCCCAAGCCAAGAAGTTAGGAAACAACTGCGTTTTCGCCCCAGCCGACGTGACC
TCTGAGAAGGATGTGCAAACAGCTCTGGCTCTAGCAAAAGGAAAGTTTGGCCGTGTGGATGTAGCTGTCAACTGTGCA
GGCATCGCGGTGGCTAGCAAGACGTACAACTTAAAGAAGGGCCAGACCCATACCTTGGAAGACTTCCAGCGAGTTCTT
GATGTGAATCTCATGGGCACCTTCAATGTGATCCGCCTGGTGGCTGGTGAGATGGGCCAGAATGAACCAGACCAGGGA
GGCCAACGTGGGGTCATCATCAACACTGCCAGTGTGGCTGCCTTCGAGGGTCAGGTTGGACAAGCTGCATACTCTGCT
TCCAAGGGGGGAATAGTGGGCATGACACTGCCCATTGCTCGGGATCTGGCTCCCATAGGTATCCGGGTGATGACCATT
GCCCCAGGTCTGTTTGGCACCCCACTGCTGACCAGCCTCCCAGAGAAAGTGTGCAACTTCTTGGCCAGCCAAGTGCCC
TTCCCTAGCCGACTGGGTGACCCTGCTGAGTATGCTCACCTCGTACAGGCCATCATCGAGAACCCATTCCTCAATGGA
GAGGTCATCCGGCTGGATGGGGCCATTCGTATGCAGCCTTGA

Orange = MTS-Sequence

```
Alignment of Sequence_1:  [HSD10 cDNA Sequence] with  Sequence_2:
[Patrick_pcDNA3-HSD10_F-T7-150916-03-62(1).seq.xdna]

Similarity : 786/786 (100.00 %)

Seq_1  1     ATGGCAGCAGCGTGTCGGAGCGTGAAGGGCCTGGTGGCGGTAATAACCGGAGGAGCCTCG  60
             ||||||||||||||||||||||||||||||||||||||||||||||||||||||||||||
Seq_2  1     ATGGCAGCAGCGTGTCGGAGCGTGAAGGGCCTGGTGGCGGTAATAACCGGAGGAGCCTCG  60

Seq_1  61    GGCCTGGGCCTGGCCACGGCGGAGCGACTTGTGGGGCAGGGAGCCTCTGCTGTGCTTCTG  120
             ||||||||||||||||||||||||||||||||||||||||||||||||||||||||||||
Seq_2  61    GGCCTGGGCCTGGCCACGGCGGAGCGACTTGTGGGGCAGGGAGCCTCTGCTGTGCTTCTG  120

Seq_1  121   GACCTGCCCAACTCGGGTGGGGAGGCCCAAGCCAAGAAGTTAGGAAACAACTGCGTTTTC  180
             ||||||||||||||||||||||||||||||||||||||||||||||||||||||||||||
Seq_2  121   GACCTGCCCAACTCGGGTGGGGAGGCCCAAGCCAAGAAGTTAGGAAACAACTGCGTTTTC  180

Seq_1  181   GCCCCAGCCGACGTGACCTCTGAGAAGGATGTGCAAACAGCTCTGGCTCTAGCAAAAGGA  240
             ||||||||||||||||||||||||||||||||||||||||||||||||||||||||||||
Seq_2  181   GCCCCAGCCGACGTGACCTCTGAGAAGGATGTGCAAACAGCTCTGGCTCTAGCAAAAGGA  240

Seq_1  241   AAGTTTGGCCGTGTGGATGTAGCTGTCAACTGTGCAGGCATCGCGGTGGCTAGCAAGACG  300
             ||||||||||||||||||||||||||||||||||||||||||||||||||||||||||||
Seq_2  241   AAGTTTGGCCGTGTGGATGTAGCTGTCAACTGTGCAGGCATCGCGGTGGCTAGCAAGACG  300

Seq_1  301   TACAACTTAAAGAAGGGCCAGACCCATACCTTGGAAGACTTCCAGCGAGTTCTTGATGTG  360
             ||||||||||||||||||||||||||||||||||||||||||||||||||||||||||||
Seq_2  301   TACAACTTAAAGAAGGGCCAGACCCATACCTTGGAAGACTTCCAGCGAGTTCTTGATGTG  360

Seq_1  361   AATCTCATGGGCACCTTCAATGTGATCCGCCTGGTGGCTGGTGAGATGGGCCAGAATGAA  420
             ||||||||||||||||||||||||||||||||||||||||||||||||||||||||||||
Seq_2  361   AATCTCATGGGCACCTTCAATGTGATCCGCCTGGTGGCTGGTGAGATGGGCCAGAATGAA  420

Seq_1  421   CCAGACCAGGGAGGCCAACGTGGGGTCATCATCAACACTGCCAGTGTGGCTGCCTTCGAG  480
             ||||||||||||||||||||||||||||||||||||||||||||||||||||||||||||
Seq_2  421   CCAGACCAGGGAGGCCAACGTGGGGTCATCATCAACACTGCCAGTGTGGCTGCCTTCGAG  480

Seq_1  481   GGTCAGGTTGGACAAGCTGCATACTCTGCTTCCAAGGGGGGAATAGTGGGCATGACACTG  540
```

```
                ||||||||||||||||||||||||||||||||||||||||||||||||||||||||||||
Seq_2  481   GGTCAGGTTGGACAAGCTGCATACTCTGCTTCCAAGGGGGGAATAGTGGGCATGACACTG  540

Seq_1  541   CCCATTGCTCGGGATCTGGCTCCCATAGGTATCCGGGTGATGACCATTGCCCCAGGTCTG  600
                ||||||||||||||||||||||||||||||||||||||||||||||||||||||||||||
Seq_2  541   CCCATTGCTCGGGATCTGGCTCCCATAGGTATCCGGGTGATGACCATTGCCCCAGGTCTG  600

Seq_1  601   TTTGGCACCCCACTGCTGACCAGCCTCCCAGAGAAAGTGTGCAACTTCTTGGCCAGCCAA  660
                ||||||||||||||||||||||||||||||||||||||||||||||||||||||||||||
Seq_2  601   TTTGGCACCCCACTGCTGACCAGCCTCCCAGAGAAAGTGTGCAACTTCTTGGCCAGCCAA  660

Seq_1  661   GTGCCCTTCCCTAGCCGACTGGGTGACCCTGCTGAGTATGCTCACCTCGTACAGGCCATC  720
                ||||||||||||||||||||||||||||||||||||||||||||||||||||||||||||
Seq_2  661   GTGCCCTTCCCTAGCCGACTGGGTGACCCTGCTGAGTATGCTCACCTCGTACAGGCCATC  720

Seq_1  721   ATCGAGAACCCATTCCTCAATGGAGAGGTCATCCGGCTGGATGGGGCCATTCGTATGCAG  780
                ||||||||||||||||||||||||||||||||||||||||||||||||||||||||||||
Seq_2  721   ATCGAGAACCCATTCCTCAATGGAGAGGTCATCCGGCTGGATGGGGCCATTCGTATGCAG  780

Seq_1  781   CCTTGA  786
                ||||||
Seq_2  781   CCTTGA  786
```

pcDNA3-HSD10: Q165H Mutation

ATGGCAGCAGCGTGTCGGAGCGTGAAGGGCCTGGTGGCGGTAATAACCGGAGGAGCCTCGGGCCTGGGCCTGGCCACG
GCGGAGCGACTTGTGGGGCAGGGAGCCTCTGCTGTGCTTCTGGACCTGCCCAACTCGGGTGGGGAGGCCCAAGCCAAG
AAGTTAGGAAACAACTGCGTTTTCGCCCCAGCCGACGTGACCTCTGAGAAGGATGTGCAAACAGCTCTGGCTCTAGCA
AAAGGAAAGTTTGGCCGTGTGGATGTAGCTGTCAACTGTGCAGGCATCGCGGTGGCTAGCAAGACGTACAACTTAAAG
AAGGGCCAGACCCATACCTTGGAAGACTTCCAGCGAGTTCTTGATGTGAATCTCATGGGCACCTTCAATGTGATCCGC
CTGGTGGCTGGTGAGATGGGCCAGAATGAACCAGACCAGGGAGGCCAACGTGGGGTCATCATCAACACTGCCAGTGTG
GCTGCCTTCGAGGGTCAGGTTGGACAcGCTGCATACTCTGCTTCCAAGGGGGGAATAGTGGGCATGACACTGCCCATT
GCTCGGGATCTGGCTCCCATAGGTATCCGGGTGATGACCATTGCCCCAGGTCTGTTTGGCACCCCACTGCTGACCAGC
CTCCCAGAGAAAGTGTGCAACTTCTTGGCCAGCCAAGTGCCCTTCCCTAGCCGACTGGGTGACCCTGCTGAGTATGCT
CACCTCGTACAGGCCATCATCGAGAACCCATTCCTCAATGGAGAGGTCATCCGGCTGGATGGGGCCATTCGTATGCAG
CCTTGA

Red = Q165H mutation

```
Alignment of Sequence_1:  [Q165H_2_FW-T7-190815-09-72.seq.xdna] with
Sequence_2: [HSD10 cDNA Sequence]

Similarity : 785/786 (99.87 %)

            M  A  A  A  C  R  S  V  K  G  L  V  A  V  I  T  G  G  A  S
Seq_1  1     ATGGCAGCAGCGTGTCGGAGCGTGAAGGGCCTGGTGGCGGTAATAACCGGAGGAGCCTCG  60
            ||||||||||||||||||||||||||||||||||||||||||||||||||||||||||||
Seq_2  1     ATGGCAGCAGCGTGTCGGAGCGTGAAGGGCCTGGTGGCGGTAATAACCGGAGGAGCCTCG  60
            M  A  A  A  C  R  S  V  K  G  L  V  A  V  I  T  G  G  A  S


            G  L  G  L  A  T  A  E  R  L  V  G  Q  G  A  S  A  V  L  L
Seq_1  61    GGCCTGGGCCTGGCCACGGCGGAGCGACTTGTGGGGCAGGGAGCCTCTGCTGTGCTTCTG  120
            ||||||||||||||||||||||||||||||||||||||||||||||||||||||||||||
Seq_2  61    GGCCTGGGCCTGGCCACGGCGGAGCGACTTGTGGGGCAGGGAGCCTCTGCTGTGCTTCTG  120
            G  L  G  L  A  T  A  E  R  L  V  G  Q  G  A  S  A  V  L  L


            D  L  P  N  S  G  G  E  A  Q  A  K  K  L  G  N  N  C  V  F
Seq_1  121   GACCTGCCCAACTCGGGTGGGGAGGCCCAAGCCAAGAAGTTAGGAAACAACTGCGTTTTC  180
            ||||||||||||||||||||||||||||||||||||||||||||||||||||||||||||
Seq_2  121   GACCTGCCCAACTCGGGTGGGGAGGCCCAAGCCAAGAAGTTAGGAAACAACTGCGTTTTC  180
            D  L  P  N  S  G  G  E  A  Q  A  K  K  L  G  N  N  C  V  F


            A  P  A  D  V  T  S  E  K  D  V  Q  T  A  L  A  L  A  K  G
Seq_1  181   GCCCCAGCCGACGTGACCTCTGAGAAGGATGTGCAAACAGCTCTGGCTCTAGCAAAAGGA  240
            ||||||||||||||||||||||||||||||||||||||||||||||||||||||||||||
Seq_2  181   GCCCCAGCCGACGTGACCTCTGAGAAGGATGTGCAAACAGCTCTGGCTCTAGCAAAAGGA  240
            A  P  A  D  V  T  S  E  K  D  V  Q  T  A  L  A  L  A  K  G


            K  F  G  R  V  D  V  A  V  N  C  A  G  I  A  V  A  S  K  T
Seq_1  241   AAGTTTGGCCGTGTGGATGTAGCTGTCAACTGTGCAGGCATCGCGGTGGCTAGCAAGACG  300
            ||||||||||||||||||||||||||||||||||||||||||||||||||||||||||||
Seq_2  241   AAGTTTGGCCGTGTGGATGTAGCTGTCAACTGTGCAGGCATCGCGGTGGCTAGCAAGACG  300
            K  F  G  R  V  D  V  A  V  N  C  A  G  I  A  V  A  S  K  T


            Y  N  L  K  K  G  Q  T  H  T  L  E  D  F  Q  R  V  L  D  V
Seq_1  301   TACAACTTAAAGAAGGGCCAGACCCATACCTTGGAAGACTTCCAGCGAGTTCTTGATGTG  360
            ||||||||||||||||||||||||||||||||||||||||||||||||||||||||||||
Seq_2  301   TACAACTTAAAGAAGGGCCAGACCCATACCTTGGAAGACTTCCAGCGAGTTCTTGATGTG  360
            Y  N  L  K  K  G  Q  T  H  T  L  E  D  F  Q  R  V  L  D  V


            N  L  M  G  T  F  N  V  I  R  L  V  A  G  E  M  G  Q  N  E
Seq_1  361   AATCTCATGGGCACCTTCAATGTGATCCGCCTGGTGGCTGGTGAGATGGGCCAGAATGAA  420
            ||||||||||||||||||||||||||||||||||||||||||||||||||||||||||||
Seq_2  361   AATCTCATGGGCACCTTCAATGTGATCCGCCTGGTGGCTGGTGAGATGGGCCAGAATGAA  420
            N  L  M  G  T  F  N  V  I  R  L  V  A  G  E  M  G  Q  N  E
```

```
                P  D  Q  G  G  Q  R  G  V  I  I  N  T  A  S  V  A  A  F  E
Seq_1  421      CCAGACCAGGGAGGCCAACGTGGGGTCATCATCAACACTGCCAGTGTGGCTGCCTTCGAG  480
                ||||||||||||||||||||||||||||||||||||||||||||||||||||||||||||
Seq_2  421      CCAGACCAGGGAGGCCAACGTGGGGTCATCATCAACACTGCCAGTGTGGCTGCCTTCGAG  480
                P  D  Q  G  G  Q  R  G  V  I  I  N  T  A  S  V  A  A  F  E

                G  Q  V  G  H  A  A  Y  S  A  S  K  G  G  I  V  G  M  T  L
Seq_1  481      GGTCAGGTTGGACACGCTGCATACTCTGCTTCCAAGGGGGGAATAGTGGGCATGACACTG  540
                ||||||||||||||#||||||||||||||||||||||||||||||||||||||||||||||
Seq_2  481      GGTCAGGTTGGACAAGCTGCATACTCTGCTTCCAAGGGGGGAATAGTGGGCATGACACTG  540
                G  Q  V  G  Q  A  A  Y  S  A  S  K  G  G  I  V  G  M  T  L

                P  I  A  R  D  L  A  P  I  G  I  R  V  M  T  I  A  P  G  L
Seq_1  541      CCCATTGCTCGGGATCTGGCTCCCATAGGTATCCGGGTGATGACCATTGCCCCAGGTCTG  600
                ||||||||||||||||||||||||||||||||||||||||||||||||||||||||||||||
Seq_2  541      CCCATTGCTCGGGATCTGGCTCCCATAGGTATCCGGGTGATGACCATTGCCCCAGGTCTG  600
                P  I  A  R  D  L  A  P  I  G  I  R  V  M  T  I  A  P  G  L

                F  G  T  P  L  L  T  S  L  P  E  K  V  C  N  F  L  A  S  Q
Seq_1  601      TTTGGCACCCCACTGCTGACCAGCCTCCCAGAGAAAGTGTGCAACTTCTTGGCCAGCCAA  660
                ||||||||||||||||||||||||||||||||||||||||||||||||||||||||||||||
Seq_2  601      TTTGGCACCCCACTGCTGACCAGCCTCCCAGAGAAAGTGTGCAACTTCTTGGCCAGCCAA  660
                F  G  T  P  L  L  T  S  L  P  E  K  V  C  N  F  L  A  S  Q

                V  P  F  P  S  R  L  G  D  P  A  E  Y  A  H  L  V  Q  A  I
Seq_1  661      GTGCCCTTCCCTAGCCGACTGGGTGACCCTGCTGAGTATGCTCACCTCGTACAGGCCATC  720
                ||||||||||||||||||||||||||||||||||||||||||||||||||||||||||||||
Seq_2  661      GTGCCCTTCCCTAGCCGACTGGGTGACCCTGCTGAGTATGCTCACCTCGTACAGGCCATC  720
                V  P  F  P  S  R  L  G  D  P  A  E  Y  A  H  L  V  Q  A  I

                I  E  N  P  F  L  N  G  E  V  I  R  L  D  G  A  I  R  M  Q
Seq_1  721      ATCGAGAACCCATTCCTCAATGGAGAGGTCATCCGGCTGGATGGGGCCATTCGTATGCAG  780
                ||||||||||||||||||||||||||||||||||||||||||||||||||||||||||||||
Seq_2  721      ATCGAGAACCCATTCCTCAATGGAGAGGTCATCCGGCTGGATGGGGCCATTCGTATGCAG  780
                I  E  N  P  F  L  N  G  E  V  I  R  L  D  G  A  I  R  M  Q

                P  *
Seq_1  781      CCTTGA  786
                ||||||
Seq_2  781      CCTTGA  786
                P  *
```

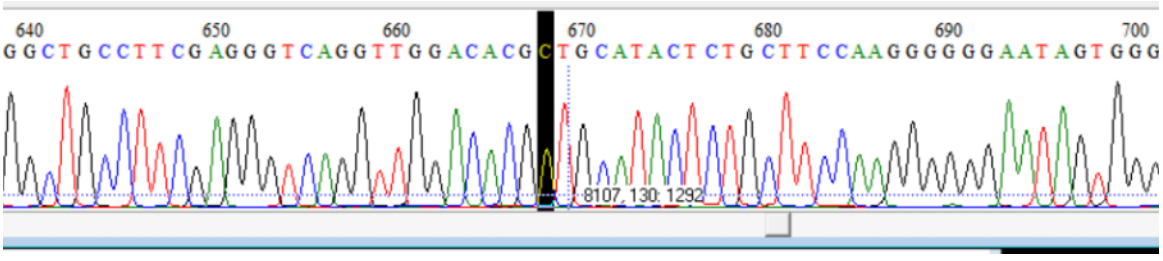

pcDNA3-HSD10: Y168G Mutation

```
ATGGCAGCAGCGTGTCGGAGCGTGAAGGGCCTGGTGGCGGTAATAACCGGAGGAGCCTCGGGCCTGGGCCTGGCCACG
GCGGAGCGACTTGTGGGGCAGGGAGCCTCTGCTGTGCTTCTGGACCTGCCCAACTCGGGTGGGGAGGCCCAAGCCAAG
AAGTTAGGAAACAACTGCGTTTTCGCCCCAGCCGACGTGACCTCTGAGAAGGATGTGCAAACAGCTCTGGCTCTAGCA
AAAGGAAAGTTTGGCCGTGTGGATGTAGCTGTCAACTGTGCAGGCATCGCGGTGGCTAGCAAGACGTACAACTTAAAG
AAGGGCCAGACCCATACCTTGGAAGACTTCCAGCGAGTTCTTGATGTGAATCTCATGGGCACCTTCAATGTGATCCGC
CTGGTGGCTGGTGAGATGGGCCAGAATGAACCAGACCAGGGAGGCCAACGTGGGGTCATCATCAACACTGCCAGTGTG
GCTGCCTTCGAGGGTCAGGTTGGACAAGCTGCAggCTCTGCTTCCAAGGGGGGAATAGTGGGCATGACACTGCCCATT
GCTCGGGATCTGGCTCCCATAGGTATCCGGGTGATGACCATTGCCCCAGGTCTGTTTGGCACCCCACTGCTGACCAGC
CTCCCAGAGAAAGTGTGCAACTTCTTGGCCAGCCAAGTGCCCTTCCCTAGCCGACTGGGTGACCCTGCTGAGTATGCT
CACCTCGTACAGGCCATCATCGAGAACCCATTCCTCAATGGAGAGGTCATCCGGCTGGATGGGGCCATTCGTATGCAG
CCTTGA
```

Red = Y168G mutation

```
Alignment of Sequence_1:  [Y168G _ Forward-T7-090916-01-26.seq.xdna] with
Sequence_2: [HSD10 cDNA Sequence]

Similarity : 784/786 (99.75 %)

            M  A  A  A  C  R  S  V  K  G  L  V  A  V  I  T  G  G  A  S
Seq_1  1     ATGGCAGCAGCGTGTCGGAGCGTGAAGGGCCTGGTGGCGGTAATAACCGGAGGAGCCTCG  60
            ||||||||||||||||||||||||||||||||||||||||||||||||||||||||||||
Seq_2  1     ATGGCAGCAGCGTGTCGGAGCGTGAAGGGCCTGGTGGCGGTAATAACCGGAGGAGCCTCG  60
            M  A  A  A  C  R  S  V  K  G  L  V  A  V  I  T  G  G  A  S

            G  L  G  L  A  T  A  E  R  L  V  G  Q  G  A  S  A  V  L  L
Seq_1  61    GGCCTGGGCCTGGCCACGGCGGAGCGACTTGTGGGGCAGGGAGCCTCTGCTGTGCTTCTG  120
            ||||||||||||||||||||||||||||||||||||||||||||||||||||||||||||
Seq_2  61    GGCCTGGGCCTGGCCACGGCGGAGCGACTTGTGGGGCAGGGAGCCTCTGCTGTGCTTCTG  120
            G  L  G  L  A  T  A  E  R  L  V  G  Q  G  A  S  A  V  L  L

            D  L  P  N  S  G  G  E  A  Q  A  K  K  L  G  N  N  C  V  F
Seq_1  121   GACCTGCCCAACTCGGGTGGGGAGGCCCAAGCCAAGAAGTTAGGAAACAACTGCGTTTTC  180
            ||||||||||||||||||||||||||||||||||||||||||||||||||||||||||||
Seq_2  121   GACCTGCCCAACTCGGGTGGGGAGGCCCAAGCCAAGAAGTTAGGAAACAACTGCGTTTTC  180
            D  L  P  N  S  G  G  E  A  Q  A  K  K  L  G  N  N  C  V  F

            A  P  A  D  V  T  S  E  K  D  V  Q  T  A  L  A  L  A  K  G
Seq_1  181   GCCCCAGCCGACGTGACCTCTGAGAAGGATGTGCAAACAGCTCTGGCTCTAGCAAAAGGA  240
            ||||||||||||||||||||||||||||||||||||||||||||||||||||||||||||
Seq_2  181   GCCCCAGCCGACGTGACCTCTGAGAAGGATGTGCAAACAGCTCTGGCTCTAGCAAAAGGA  240
            A  P  A  D  V  T  S  E  K  D  V  Q  T  A  L  A  L  A  K  G

            K  F  G  R  V  D  V  A  V  N  C  A  G  I  A  V  A  S  K  T
Seq_1  241   AAGTTTGGCCGTGTGGATGTAGCTGTCAACTGTGCAGGCATCGCGGTGGCTAGCAAGACG  300
            ||||||||||||||||||||||||||||||||||||||||||||||||||||||||||||
Seq_2  241   AAGTTTGGCCGTGTGGATGTAGCTGTCAACTGTGCAGGCATCGCGGTGGCTAGCAAGACG  300
            K  F  G  R  V  D  V  A  V  N  C  A  G  I  A  V  A  S  K  T

            Y  N  L  K  K  G  Q  T  H  T  L  E  D  F  Q  R  V  L  D  V
Seq_1  301   TACAACTTAAAGAAGGGCCAGACCCATACCTTGGAAGACTTCCAGCGAGTTCTTGATGTG  360
            ||||||||||||||||||||||||||||||||||||||||||||||||||||||||||||
Seq_2  301   TACAACTTAAAGAAGGGCCAGACCCATACCTTGGAAGACTTCCAGCGAGTTCTTGATGTG  360
            Y  N  L  K  K  G  Q  T  H  T  L  E  D  F  Q  R  V  L  D  V

            N  L  M  G  T  F  N  V  I  R  L  V  A  G  E  M  G  Q  N  E
Seq_1  361   AATCTCATGGGCACCTTCAATGTGATCCGCCTGGTGGCTGGTGAGATGGGCCAGAATGAA  420
            ||||||||||||||||||||||||||||||||||||||||||||||||||||||||||||
Seq_2  361   AATCTCATGGGCACCTTCAATGTGATCCGCCTGGTGGCTGGTGAGATGGGCCAGAATGAA  420
            N  L  M  G  T  F  N  V  I  R  L  V  A  G  E  M  G  Q  N  E
```

Appendix

```
                P  D  Q  G  G  Q  R  G  V  I  I  N  T  A  S  V  A  A  F  E
Seq_1  421      CCAGACCAGGGAGGCCAACGTGGGGTCATCATCAACACTGCCAGTGTGGCTGCCTTCGAG  480
                ||||||||||||||||||||||||||||||||||||||||||||||||||||||||||||
Seq_2  421      CCAGACCAGGGAGGCCAACGTGGGGTCATCATCAACACTGCCAGTGTGGCTGCCTTCGAG  480
                P  D  Q  G  G  Q  R  G  V  I  I  N  T  A  S  V  A  A  F  E

                G  Q  V  G  Q  A  A  G  S  A  S  K  G  G  I  V  G  M  T  L
Seq_1  481      GGTCAGGTTGGACAAGCTGCAGGCTCTGCTTCCAAGGGGGGAATAGTGGGCATGACACTG  540
                ||||||||||||||||||||##||||||||||||||||||||||||||||||||||||||
Seq_2  481      GGTCAGGTTGGACAAGCTGCATACTCTGCTTCCAAGGGGGGAATAGTGGGCATGACACTG  540
                G  Q  V  G  Q  A  A  Y  S  A  S  K  G  G  I  V  G  M  T  L

                P  I  A  R  D  L  A  P  I  G  I  R  V  M  T  I  A  P  G  L
Seq_1  541      CCCATTGCTCGGGATCTGGCTCCCATAGGTATCCGGGTGATGACCATTGCCCCAGGTCTG  600
                ||||||||||||||||||||||||||||||||||||||||||||||||||||||||||||
Seq_2  541      CCCATTGCTCGGGATCTGGCTCCCATAGGTATCCGGGTGATGACCATTGCCCCAGGTCTG  600
                P  I  A  R  D  L  A  P  I  G  I  R  V  M  T  I  A  P  G  L

                F  G  T  P  L  L  T  S  L  P  E  K  V  C  N  F  L  A  S  Q
Seq_1  601      TTTGGCACCCCACTGCTGACCAGCCTCCCAGAGAAAGTGTGCAACTTCTTGGCCAGCCAA  660
                ||||||||||||||||||||||||||||||||||||||||||||||||||||||||||||
Seq_2  601      TTTGGCACCCCACTGCTGACCAGCCTCCCAGAGAAAGTGTGCAACTTCTTGGCCAGCCAA  660
                F  G  T  P  L  L  T  S  L  P  E  K  V  C  N  F  L  A  S  Q

                V  P  F  P  S  R  L  G  D  P  A  E  Y  A  H  L  V  Q  A  I
Seq_1  661      GTGCCCTTCCCTAGCCGACTGGGTGACCCTGCTGAGTATGCTCACCTCGTACAGGCCATC  720
                ||||||||||||||||||||||||||||||||||||||||||||||||||||||||||||
Seq_2  661      GTGCCCTTCCCTAGCCGACTGGGTGACCCTGCTGAGTATGCTCACCTCGTACAGGCCATC  720
                V  P  F  P  S  R  L  G  D  P  A  E  Y  A  H  L  V  Q  A  I

                I  E  N  P  F  L  N  G  E  V  I  R  L  D  G  A  I  R  M  Q
Seq_1  721      ATCGAGAACCCATTCCTCAATGGAGAGGTCATCCGGCTGGATGGGGCCATTCGTATGCAG  780
                ||||||||||||||||||||||||||||||||||||||||||||||||||||||||||||
Seq_2  721      ATCGAGAACCCATTCCTCAATGGAGAGGTCATCCGGCTGGATGGGGCCATTCGTATGCAG  780
                I  E  N  P  F  L  N  G  E  V  I  R  L  D  G  A  I  R  M  Q

                P  *
Seq_1  781      CCTTGA  786
                ||||||
Seq_2  781      CCTTGA  786
                P  *
```

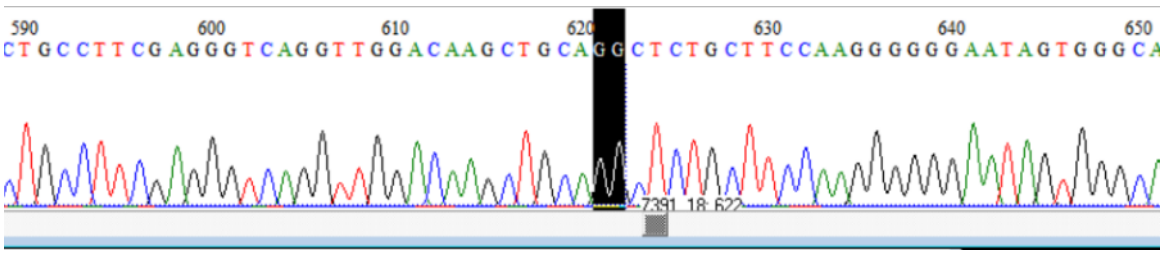

pcDNA4-APPswe

```
ATGCTGCCCGGTTTGGCACTGCTCCTGCTGGCCGCCTGGACGGCTCGGGCGCTGGAGGTACCCACTGATGGTAATGCT
GGCCTGCTGGCTGAACCCCAGATTGCCATGTTCTGTGGCAGACTGAACATGCACATGAATGTCCAGAATGGGAAGTGG
GATTCAGATCCATCAGGGACCAAAACCTGCATTGATACCAAGGAAGGCATCCTGCAGTATTGCCAAGAAGTCTACCCT
GAACTGCAGATCACCAATGTGGTAGAAGCCAACCAACCAGTGACCATCCAGAACTGGTGCAAGCGGGGCCGCAAGCAG
TGCAAGACCCATCCCCACTTTGTGATTCCCTACCGCTGCTTAGTTGGTGAGTTTGTAAGTGATGCCCTTCTCGTTCCT
GACAAGTGCAAATTCTTACACCAGGAGAGGATGGATGTTTGCGAAACTCATCTTCACTGGCACACCGTCGCCAAAGAG
ACATGCAGTGAGAAGAGTACCAACTTGCATGACTACGGCATGTTGCTGCCCTGCGGAATTGACAAGTTCCGAGGGGTA
GAGTTTGTGTGTTGCCCACTGGCTGAAGAAAGTGACAATGTGGATTCTGCTGATGCGGAGGAGGATGACTCGGATGTC
TGGTGGGGCGGAGCAGACACAGACTATGCAGATGGGAGTGAAGACAAAGTAGTAGAAGTAGCAGAGGAGGAAGAAGTG
GCTGAGGTGGAAGAAGAAGAAGCCGATGATGACGAGGACGATGAGGATGGTGATGAGGTAGAGGAAGAGGCTGAGGAA
CCCTACGAAGAAGCCACAGAGAGAACCACCAGCATTGCCACCACCACCACCACCACCACAGAGTCTGTGGAAGAGGTG
GTTCGAGTTCCTACAACAGCAGCCAGTACCCCTGATGCCGTTGACAAGTATCTCGAGACACCTGGGGATGAGAATGAA
CATGCCCATTTCCAGAAAGCCAAAGAGAGGCTTGAGGCCAAGCACCGAGAGAGAATGTCCCAGGTCATGAGAGAATGG
GAAGAGGCAGAACGTCAAGCAAAGAACTTGCCTAAAGCTGATAAGAAGGCAGTTATCCAGCATTTCCAGGAGAAAGTG
GAATCTTTGGAACAGGAAGCAGCCAACGAGAGACAGCAGCTGGTGGAGACACACATGGCCAGAGTGGAAGCCATGCTC
AATGACCGCCGCCGCCTGGCCCTGGAGAACTACATCACCGCTCTGCAGGCTGTTCCTCCTCGGCCTCGTCACGTGTTC
AATATGCTAAAGAAGTATGTCCGCGCAGAACAGAAGGACAGACAGCACACCCTAAAGCATTTCGAGCATGTGCGCATG
GTGGATCCCAAGAAAGCCGCTCAGATCCGGTCCCAGGTTATGACACACCTCCGTGTGATTTATGAGCGCATGAATCAG
TCTCTCTCCCTGCTCTACAACGTGCCTGCAGTGGCCGAGGAGATTCAGGATGAAGTTGATGAGCTGCTTCAGAAAGAG
CAAAACTATTCAGATGACGTCTTGGCCAACATGATTAGTGAACCAAGGATCAGTTACGGAAACGATGCTCTCATGCCA
TCTTTGACCGAAACGAAAACCACCGTGGAGCTCCTTCCCGTGAATGGAGAGTTCAGCCTGGACGATCTCCAGCCGTGG
CATTCTTTTGGGGCTGACTCTGTGCCAGCCAACACAGAAAACGAAGTTGAGCCTGTTGATGCCCGCCCTGCTGCCGAC
CGAGGACTGACCACTCGACCAGGTTCTGGGTTGACAAATATCAAGACGGAGGAGATCTCTGAAGTGAAtcTGGATGCA
GAATTCCGACATGACTCAGGATATGAAGTTCATCATCAAAAATTGGTGTTCTTTGCAGAAGATGTGGGTTCAAACAAA
GGTGCAATCATTGGACTCATGGTGGGCGGTGTTGTCATAGCGACATGATCGTCATCACCTTGGTGATGCTGAAGAAGA
AACAGTACACATCCATTCATCATGGTGTGGTGGAGGTTGACGCCGCTGTCACCCCAGAGGAGCGCCACCTGTCCAAGA
TGCAGCAGAACGGCTACGAAAATCCAACCTACAAGTTCTTTGAGCAGAGCAGAACTAG
```

Red = Swedish Mutation (KM670/671NL)

```
Alignment of Sequence_1:  [pcDNA4_APPswe_F-CMV Fwd-150916-03-64(2).seq.xdna]
with  Sequence_2: [APP695 cDNA Sequence]

Similarity : 2086/2088 (99.90 %)
             M  L  P  G  L  A  L  L  L  L  A  A  W  T  A  R  A  L  E  V
Seq_1  1     ATGCTGCCCGGTTTGGCACTGCTCCTGCTGGCCGCCTGGACGGCTCGGGCGCTGGAGGTA  60
             ||||||||||||||||||||||||||||||||||||||||||||||||||||||||||||
Seq_2  1     ATGCTGCCCGGTTTGGCACTGCTCCTGCTGGCCGCCTGGACGGCTCGGGCGCTGGAGGTA  60
             M  L  P  G  L  A  L  L  L  L  A  A  W  T  A  R  A  L  E  V


             P  T  D  G  N  A  G  L  L  A  E  P  Q  I  A  M  F  C  G  R
Seq_1  61    CCCACTGATGGTAATGCTGGCCTGCTGGCTGAACCCCAGATTGCCATGTTCTGTGGCAGA  120
             ||||||||||||||||||||||||||||||||||||||||||||||||||||||||||||
Seq_2  61    CCCACTGATGGTAATGCTGGCCTGCTGGCTGAACCCCAGATTGCCATGTTCTGTGGCAGA  120
             P  T  D  G  N  A  G  L  L  A  E  P  Q  I  A  M  F  C  G  R


             L  N  M  H  M  N  V  Q  N  G  K  W  D  S  D  P  S  G  T  K
Seq_1  121   CTGAACATGCACATGAATGTCCAGAATGGGAAGTGGGATTCAGATCCATCAGGGACCAAA  180
             ||||||||||||||||||||||||||||||||||||||||||||||||||||||||||||
Seq_2  121   CTGAACATGCACATGAATGTCCAGAATGGGAAGTGGGATTCAGATCCATCAGGGACCAAA  180
             L  N  M  H  M  N  V  Q  N  G  K  W  D  S  D  P  S  G  T  K


             T  C  I  D  T  K  E  G  I  L  Q  Y  C  Q  E  V  Y  P  E  L
Seq_1  181   ACCTGCATTGATACCAAGGAAGGCATCCTGCAGTATTGCCAAGAAGTCTACCCTGAACTG  240
             ||||||||||||||||||||||||||||||||||||||||||||||||||||||||||||
Seq_2  181   ACCTGCATTGATACCAAGGAAGGCATCCTGCAGTATTGCCAAGAAGTCTACCCTGAACTG  240
             T  C  I  D  T  K  E  G  I  L  Q  Y  C  Q  E  V  Y  P  E  L


             Q  I  T  N  V  V  E  A  N  Q  P  V  T  I  Q  N  W  C  K  R
Seq_1  241   CAGATCACCAATGTGGTAGAAGCCAACCAACCAGTGACCATCCAGAACTGGTGCAAGCGG  300
             ||||||||||||||||||||||||||||||||||||||||||||||||||||||||||||
Seq_2  241   CAGATCACCAATGTGGTAGAAGCCAACCAACCAGTGACCATCCAGAACTGGTGCAAGCGG  300
             Q  I  T  N  V  V  E  A  N  Q  P  V  T  I  Q  N  W  C  K  R
```

```
                G  R  K  Q  C  K  T  H  P  H  F  V  I  P  Y  R  C  L  V  G
Seq_1  301   GGCCGCAAGCAGTGCAAGACCCATCCCCACTTTGTGATTCCCTACCGCTGCTTAGTTGGT  360
              ||||||||||||||||||||||||||||||||||||||||||||||||||||||||||||
Seq_2  301   GGCCGCAAGCAGTGCAAGACCCATCCCCACTTTGTGATTCCCTACCGCTGCTTAGTTGGT  360
                G  R  K  Q  C  K  T  H  P  H  F  V  I  P  Y  R  C  L  V  G

                E  F  V  S  D  A  L  L  V  P  D  K  C  K  F  L  H  Q  E  R
Seq_1  361   GAGTTTGTAAGTGATGCCCTTCTCGTTCCTGACAAGTGCAAATTCTTACACCAGGAGAGG  420
              ||||||||||||||||||||||||||||||||||||||||||||||||||||||||||||
Seq_2  361   GAGTTTGTAAGTGATGCCCTTCTCGTTCCTGACAAGTGCAAATTCTTACACCAGGAGAGG  420
                E  F  V  S  D  A  L  L  V  P  D  K  C  K  F  L  H  Q  E  R

                M  D  V  C  E  T  H  L  H  W  H  T  V  A  K  E  T  C  S  E
Seq_1  421   ATGGATGTTTGCGAAACTCATCTTCACTGGCACACCGTCGCCAAAGAGACATGCAGTGAG  480
              ||||||||||||||||||||||||||||||||||||||||||||||||||||||||||||
Seq_2  421   ATGGATGTTTGCGAAACTCATCTTCACTGGCACACCGTCGCCAAAGAGACATGCAGTGAG  480
                M  D  V  C  E  T  H  L  H  W  H  T  V  A  K  E  T  C  S  E

                K  S  T  N  L  H  D  Y  G  M  L  L  P  C  G  I  D  K  F  R
Seq_1  481   AAGAGTACCAACTTGCATGACTACGGCATGTTGCTGCCCTGCGGAATTGACAAGTTCCGA  540
              ||||||||||||||||||||||||||||||||||||||||||||||||||||||||||||
Seq_2  481   AAGAGTACCAACTTGCATGACTACGGCATGTTGCTGCCCTGCGGAATTGACAAGTTCCGA  540
                K  S  T  N  L  H  D  Y  G  M  L  L  P  C  G  I  D  K  F  R

                G  V  E  F  V  C  C  P  L  A  E  E  S  D  N  V  D  S  A  D
Seq_1  541   GGGGTAGAGTTTGTGTGTTGCCCACTGGCTGAAGAAAGTGACAATGTGGATTCTGCTGAT  600
              ||||||||||||||||||||||||||||||||||||||||||||||||||||||||||||
Seq_2  541   GGGGTAGAGTTTGTGTGTTGCCCACTGGCTGAAGAAAGTGACAATGTGGATTCTGCTGAT  600
                G  V  E  F  V  C  C  P  L  A  E  E  S  D  N  V  D  S  A  D

                A  E  E  D  D  S  D  V  W  W  G  G  A  D  T  D  Y  A  D  G
Seq_1  601   GCGGAGGAGGATGACTCGGATGTCTGGTGGGGCGGAGCAGACACAGACTATGCAGATGGG  660
              ||||||||||||||||||||||||||||||||||||||||||||||||||||||||||||
Seq_2  601   GCGGAGGAGGATGACTCGGATGTCTGGTGGGGCGGAGCAGACACAGACTATGCAGATGGG  660
                A  E  E  D  D  S  D  V  W  W  G  G  A  D  T  D  Y  A  D  G

                S  E  D  K  V  V  E  V  A  E  E  E  E  V  A  E  V  E  E  E
Seq_1  661   AGTGAAGACAAAGTAGTAGAAGTAGCAGAGGAGGAAGAAGTGGCTGAGGTGGAAGAAGAA  720
              ||||||||||||||||||||||||||||||||||||||||||||||||||||||||||||
Seq_2  661   AGTGAAGACAAAGTAGTAGAAGTAGCAGAGGAGGAAGAAGTGGCTGAGGTGGAAGAAGAA  720
                S  E  D  K  V  V  E  V  A  E  E  E  E  V  A  E  V  E  E  E

                E  A  D  D  D  E  D  D  E  D  G  D  E  V  E  E  E  A  E  E
Seq_1  721   GAAGCCGATGATGACGAGGACGATGAGGATGGTGATGAGGTAGAGGAAGAGGCTGAGGAA  780
              ||||||||||||||||||||||||||||||||||||||||||||||||||||||||||||
Seq_2  721   GAAGCCGATGATGACGAGGACGATGAGGATGGTGATGAGGTAGAGGAAGAGGCTGAGGAA  780
                E  A  D  D  D  E  D  D  E  D  G  D  E  V  E  E  E  A  E  E

                P  Y  E  E  A  T  E  R  T  T  S  I  A  T  T  T  T  T  T  T
Seq_1  781   CCCTACGAAGAAGCCACAGAGAGAACCACCAGCATTGCCACCACCACCACCACCACCACA  840
              ||||||||||||||||||||||||||||||||||||||||||||||||||||||||||||
Seq_2  781   CCCTACGAAGAAGCCACAGAGAGAACCACCAGCATTGCCACCACCACCACCACCACCACA  840
                P  Y  E  E  A  T  E  R  T  T  S  I  A  T  T  T  T  T  T  T
```

```
E  S  V  E  E  V  V  R  V  P  T  T  A  A  S  T  P  D  A  V
Seq_1  841   GAGTCTGTGGAAGAGGTGGTTCGAGTTCCTACAACAGCAGCCAGTACCCCTGATGCCGTT  900
              ||||||||||||||||||||||||||||||||||||||||||||||||||||||||||||
Seq_2  841   GAGTCTGTGGAAGAGGTGGTTCGAGTTCCTACAACAGCAGCCAGTACCCCTGATGCCGTT  900
              E  S  V  E  E  V  V  R  V  P  T  T  A  A  S  T  P  D  A  V


              D  K  Y  L  E  T  P  G  D  E  N  E  H  A  H  F  Q  K  A  K
Seq_1  901   GACAAGTATCTCGAGACACCTGGGGATGAGAATGAACATGCCCATTTCCAGAAAGCCAAA  960
              ||||||||||||||||||||||||||||||||||||||||||||||||||||||||||||
Seq_2  901   GACAAGTATCTCGAGACACCTGGGGATGAGAATGAACATGCCCATTTCCAGAAAGCCAAA  960
              D  K  Y  L  E  T  P  G  D  E  N  E  H  A  H  F  Q  K  A  K


              E  R  L  E  A  K  H  R  E  R  M  S  Q  V  M  R  E  W  E  E
Seq_1  961   GAGAGGCTTGAGGCCAAGCACCGAGAGAGAATGTCCCAGGTCATGAGAGAATGGGAAGAG
1020
              ||||||||||||||||||||||||||||||||||||||||||||||||||||||||||||
Seq_2  961   GAGAGGCTTGAGGCCAAGCACCGAGAGAGAATGTCCCAGGTCATGAGAGAATGGGAAGAG
1020
              E  R  L  E  A  K  H  R  E  R  M  S  Q  V  M  R  E  W  E  E


              A  E  R  Q  A  K  N  L  P  K  A  D  K  K  A  V  I  Q  H  F
Seq_1  1021  GCAGAACGTCAAGCAAAGAACTTGCCTAAAGCTGATAAGAAGGCAGTTATCCAGCATTTC
1080
              ||||||||||||||||||||||||||||||||||||||||||||||||||||||||||||
Seq_2  1021  GCAGAACGTCAAGCAAAGAACTTGCCTAAAGCTGATAAGAAGGCAGTTATCCAGCATTTC
1080
              A  E  R  Q  A  K  N  L  P  K  A  D  K  K  A  V  I  Q  H  F


              Q  E  K  V  E  S  L  E  Q  E  A  A  N  E  R  Q  Q  L  V  E
Seq_1  1081  CAGGAGAAAGTGGAATCTTTGGAACAGGAAGCAGCCAACGAGAGACAGCAGCTGGTGGAG
1140
              ||||||||||||||||||||||||||||||||||||||||||||||||||||||||||||
Seq_2  1081  CAGGAGAAAGTGGAATCTTTGGAACAGGAAGCAGCCAACGAGAGACAGCAGCTGGTGGAG
1140
              Q  E  K  V  E  S  L  E  Q  E  A  A  N  E  R  Q  Q  L  V  E


              T  H  M  A  R  V  E  A  M  L  N  D  R  R  R  L  A  L  E  N
Seq_1  1141  ACACACATGGCCAGAGTGGAAGCCATGCTCAATGACCGCCGCCGCCTGGCCCTGGAGAAC
1200
              ||||||||||||||||||||||||||||||||||||||||||||||||||||||||||||
Seq_2  1141  ACACACATGGCCAGAGTGGAAGCCATGCTCAATGACCGCCGCCGCCTGGCCCTGGAGAAC
1200
              T  H  M  A  R  V  E  A  M  L  N  D  R  R  R  L  A  L  E  N


              Y  I  T  A  L  Q  A  V  P  P  R  P  R  H  V  F  N  M  L  K
Seq_1  1201  TACATCACCGCTCTGCAGGCTGTTCCTCCTCGGCCTCGTCACGTGTTCAATATGCTAAAG
1260
              ||||||||||||||||||||||||||||||||||||||||||||||||||||||||||||
Seq_2  1201  TACATCACCGCTCTGCAGGCTGTTCCTCCTCGGCCTCGTCACGTGTTCAATATGCTAAAG
1260
              Y  I  T  A  L  Q  A  V  P  P  R  P  R  H  V  F  N  M  L  K
```

Appendix

```
            K  Y  V  R  A  E  Q  K  D  R  Q  H  T  L  K  H  F  E  H  V
Seq_1  1261 AAGTATGTCCGCGCAGAACAGAAGGACAGACAGCACACCCTAAAGCATTTCGAGCATGTG
1320
            ||||||||||||||||||||||||||||||||||||||||||||||||||||||||||||
Seq_2  1261 AAGTATGTCCGCGCAGAACAGAAGGACAGACAGCACACCCTAAAGCATTTCGAGCATGTG
1320
            K  Y  V  R  A  E  Q  K  D  R  Q  H  T  L  K  H  F  E  H  V


            R  M  V  D  P  K  K  A  A  Q  I  R  S  Q  V  M  T  H  L  R
Seq_1  1321 CGCATGGTGGATCCCAAGAAAGCCGCTCAGATCCGGTCCCAGGTTATGACACACCTCCGT
1380
            ||||||||||||||||||||||||||||||||||||||||||||||||||||||||||||
Seq_2  1321 CGCATGGTGGATCCCAAGAAAGCCGCTCAGATCCGGTCCCAGGTTATGACACACCTCCGT
1380
            R  M  V  D  P  K  K  A  A  Q  I  R  S  Q  V  M  T  H  L  R


            V  I  Y  E  R  M  N  Q  S  L  S  L  L  Y  N  V  P  A  V  A
Seq_1  1381 GTGATTTATGAGCGCATGAATCAGTCTCTCTCCCTGCTCTACAACGTGCCTGCAGTGGCC
1440
            ||||||||||||||||||||||||||||||||||||||||||||||||||||||||||||
Seq_2  1381 GTGATTTATGAGCGCATGAATCAGTCTCTCTCCCTGCTCTACAACGTGCCTGCAGTGGCC
1440
            V  I  Y  E  R  M  N  Q  S  L  S  L  L  Y  N  V  P  A  V  A


            E  E  I  Q  D  E  V  D  E  L  L  Q  K  E  Q  N  Y  S  D  D
Seq_1  1441 GAGGAGATTCAGGATGAAGTTGATGAGCTGCTTCAGAAAGAGCAAAACTATTCAGATGAC
1500
            ||||||||||||||||||||||||||||||||||||||||||||||||||||||||||||
Seq_2  1441 GAGGAGATTCAGGATGAAGTTGATGAGCTGCTTCAGAAAGAGCAAAACTATTCAGATGAC
1500
            E  E  I  Q  D  E  V  D  E  L  L  Q  K  E  Q  N  Y  S  D  D


            V  L  A  N  M  I  S  E  P  R  I  S  Y  G  N  D  A  L  M  P
Seq_1  1501 GTCTTGGCCAACATGATTAGTGAACCAAGGATCAGTTACGGAAACGATGCTCTCATGCCA
1560
            ||||||||||||||||||||||||||||||||||||||||||||||||||||||||||||
Seq_2  1501 GTCTTGGCCAACATGATTAGTGAACCAAGGATCAGTTACGGAAACGATGCTCTCATGCCA
1560
            V  L  A  N  M  I  S  E  P  R  I  S  Y  G  N  D  A  L  M  P


            S  L  T  E  T  K  T  T  V  E  L  L  P  V  N  G  E  F  S  L
Seq_1  1561 TCTTTGACCGAAACGAAAACCACCGTGGAGCTCCTTCCCGTGAATGGAGAGTTCAGCCTG
1620
            ||||||||||||||||||||||||||||||||||||||||||||||||||||||||||||
Seq_2  1561 TCTTTGACCGAAACGAAAACCACCGTGGAGCTCCTTCCCGTGAATGGAGAGTTCAGCCTG
1620
            S  L  T  E  T  K  T  T  V  E  L  L  P  V  N  G  E  F  S  L


            D  D  L  Q  P  W  H  S  F  G  A  D  S  V  P  A  N  T  E  N
Seq_1  1621 GACGATCTCCAGCCGTGGCATTCTTTTGGGGCTGACTCTGTGCCAGCCAACACAGAAAAC
1680
            ||||||||||||||||||||||||||||||||||||||||||||||||||||||||||||
Seq_2  1621 GACGATCTCCAGCCGTGGCATTCTTTTGGGGCTGACTCTGTGCCAGCCAACACAGAAAAC
1680
            D  D  L  Q  P  W  H  S  F  G  A  D  S  V  P  A  N  T  E  N
```

```
            E  V  E  P  V  D  A  R  P  A  A  D  R  G  L  T  T  R  P  G
Seq_1  1681 GAAGTTGAGCCTGTTGATGCCCGCCCTGCTGCCGACCGAGGACTGACCACTCGACCAGGT
1740
            ||||||||||||||||||||||||||||||||||||||||||||||||||||||||||||
Seq_2  1681 GAAGTTGAGCCTGTTGATGCCCGCCCTGCTGCCGACCGAGGACTGACCACTCGACCAGGT
1740
            E  V  E  P  V  D  A  R  P  A  A  D  R  G  L  T  T  R  P  G


            S  G  L  T  N  I  K  T  E  E  I  S  E  V  N  L  D  A  E  F
Seq_1  1741 TCTGGGTTGACAAATATCAAGACGGAGGAGATCTCTGAAGTGAATCTGGATGCAGAATTC
1800
            ||||||||||||||||||||||||||||||||||||||||||||##|||||||||||||||
Seq_2  1741 TCTGGGTTGACAAATATCAAGACGGAGGAGATCTCTGAAGTGAAGATGGATGCAGAATTC
1800
            S  G  L  T  N  I  K  T  E  E  I  S  E  V  K  M  D  A  E  F


            R  H  D  S  G  Y  E  V  H  H  Q  K  L  V  F  F  A  E  D  V
Seq_1  1801 CGACATGACTCAGGATATGAAGTTCATCATCAAAAATTGGTGTTCTTTGCAGAAGATGTG
1860
            ||||||||||||||||||||||||||||||||||||||||||||||||||||||||||||
Seq_2  1801 CGACATGACTCAGGATATGAAGTTCATCATCAAAAATTGGTGTTCTTTGCAGAAGATGTG
1860
            R  H  D  S  G  Y  E  V  H  H  Q  K  L  V  F  F  A  E  D  V


            G  S  N  K  G  A  I  I  G  L  M  V  G  G  V  V  I  A  T  V
Seq_1  1861 GGTTCAAACAAAGGTGCAATCATTGGACTCATGGTGGGCGGTGTTGTCATAGCGACAGTG
1920
            ||||||||||||||||||||||||||||||||||||||||||||||||||||||||||||
Seq_2  1861 GGTTCAAACAAAGGTGCAATCATTGGACTCATGGTGGGCGGTGTTGTCATAGCGACAGTG
1920
            G  S  N  K  G  A  I  I  G  L  M  V  G  G  V  V  I  A  T  V


            I  V  I  T  L  V  M  L  K  K  K  Q  Y  T  S  I  H  H  G  V
Seq_1  1921 ATCGTCATCACCTTGGTGATGCTGAAGAAGAAACAGTACACATCCATTCATCATGGTGTG
1980
            ||||||||||||||||||||||||||||||||||||||||||||||||||||||||||||
Seq_2  1921 ATCGTCATCACCTTGGTGATGCTGAAGAAGAAACAGTACACATCCATTCATCATGGTGTG
1980
            I  V  I  T  L  V  M  L  K  K  K  Q  Y  T  S  I  H  H  G  V


            V  E  V  D  A  A  V  T  P  E  E  R  H  L  S  K  M  Q  Q  N
Seq_1  1981 GTGGAGGTTGACGCCGCTGTCACCCCAGAGGAGCGCCACCTGTCCAAGATGCAGCAGAAC
2040
            ||||||||||||||||||||||||||||||||||||||||||||||||||||||||||||
Seq_2  1981 GTGGAGGTTGACGCCGCTGTCACCCCAGAGGAGCGCCACCTGTCCAAGATGCAGCAGAAC
2040
            V  E  V  D  A  A  V  T  P  E  E  R  H  L  S  K  M  Q  Q  N


            G  Y  E  N  P  T  Y  K  F  F  E  Q  M  Q  N  *
Seq_1  2041 GGCTACGAAAATCCAACCTACAAGTTCTTTGAGCAGATGCAGAACTAG  2088
            ||||||||||||||||||||||||||||||||||||||||||||||
Seq_2  2041 GGCTACGAAAATCCAACCTACAAGTTCTTTGAGCAGATGCAGAACTAG  2088
            G  Y  E  N  P  T  Y  K  F  F  E  Q  M  Q  N  *
```

peHISTEV-HSD10

```
ATGGCAGCAGCGTGTCGGAGCGTGAAGGGCCTGGTGGCGGTAATAACCGGAGGAGCCTCGGGCCTGGGCCTGGCCACG
GCGGAGCGACTTGTGGGGCAGGGAGCCTCTGCTGTGCTTCTGGACCTGCCCAACTCGGGTGGGGAGGCCCAAGCCAAG
AAGTTAGGAAACAACTGCGTTTTCGCCCCAGCCGACGTGACCTCTGAGAAGGATGTGCAAACAGCTCTGGCTCTAGCA
AAAGGAAAGTTTGGCCGTGTGGATGTAGCTGTCAACTGTGCAGGCATCGCGGTGGCTAGCAAGACGTACAACTTAAAG
AAGGGCCAGACCCATACCTTGGAAGACTTCCAGCGAGTTCTTGATGTGAATCTCATGGGCACCTTCAATGTGATCCGC
CTGGTGGCTGGTGAGATGGGCCAGAATGAACCAGACCAGGGAGGCCAACGTGGGGTCATCATCAACACTGCCAGTGTG
GCTGCCTTCGAGGGTCAGGTTGGACAAGCTGCATACTCTGCTTCCAAGGGGGGAATAGTGGGCATGACACTGCCCATT
GCTCGGGATCTGGCTCCCATAGGTATCCGGGTGATGACCATTGCCCCAGGTCTGTTTGGCACCCCACTGCTGACCAGC
CTCCCAGAGAAAGTGTGCAACTTCTTGGCCAGCCAAGTGCCCTTCCCTAGCCGACTGGGTGACCCTGCTGAGTATGCT
CACCTCGTACAGGCCATCATCGAGAACCCATTCCTCAATGGAGAGGTCATCCGGCTGGATGGGGCCATTCGTATGCAG
CCTTGA
```

```
Alignment of Sequence_1:  [HSD10 cDNA Sequence] with  Sequence_2: [peHISTEV-
HSD10_F_aug-T7-190916-03-60.seq.xdna]

Similarity : 786/786 (100.00 %)

Seq_1  1     ATGGCAGCAGCGTGTCGGAGCGTGAAGGGCCTGGTGGCGGTAATAACCGGAGGAGCCTCG  60
             ||||||||||||||||||||||||||||||||||||||||||||||||||||||||||||
Seq_2  1     ATGGCAGCAGCGTGTCGGAGCGTGAAGGGCCTGGTGGCGGTAATAACCGGAGGAGCCTCG  60


Seq_1  61    GGCCTGGGCCTGGCCACGGCGGAGCGACTTGTGGGGCAGGGAGCCTCTGCTGTGCTTCTG  120
             ||||||||||||||||||||||||||||||||||||||||||||||||||||||||||||
Seq_2  61    GGCCTGGGCCTGGCCACGGCGGAGCGACTTGTGGGGCAGGGAGCCTCTGCTGTGCTTCTG  120


Seq_1  121   GACCTGCCCAACTCGGGTGGGGAGGCCCAAGCCAAGAAGTTAGGAAACAACTGCGTTTTC  180
             ||||||||||||||||||||||||||||||||||||||||||||||||||||||||||||
Seq_2  121   GACCTGCCCAACTCGGGTGGGGAGGCCCAAGCCAAGAAGTTAGGAAACAACTGCGTTTTC  180


Seq_1  181   GCCCCAGCCGACGTGACCTCTGAGAAGGATGTGCAAACAGCTCTGGCTCTAGCAAAAGGA  240
             ||||||||||||||||||||||||||||||||||||||||||||||||||||||||||||
Seq_2  181   GCCCCAGCCGACGTGACCTCTGAGAAGGATGTGCAAACAGCTCTGGCTCTAGCAAAAGGA  240


Seq_1  241   AAGTTTGGCCGTGTGGATGTAGCTGTCAACTGTGCAGGCATCGCGGTGGCTAGCAAGACG  300
             ||||||||||||||||||||||||||||||||||||||||||||||||||||||||||||
Seq_2  241   AAGTTTGGCCGTGTGGATGTAGCTGTCAACTGTGCAGGCATCGCGGTGGCTAGCAAGACG  300


Seq_1  301   TACAACTTAAAGAAGGGCCAGACCCATACCTTGGAAGACTTCCAGCGAGTTCTTGATGTG  360
             ||||||||||||||||||||||||||||||||||||||||||||||||||||||||||||
Seq_2  301   TACAACTTAAAGAAGGGCCAGACCCATACCTTGGAAGACTTCCAGCGAGTTCTTGATGTG  360


Seq_1  361   AATCTCATGGGCACCTTCAATGTGATCCGCCTGGTGGCTGGTGAGATGGGCCAGAATGAA  420
             ||||||||||||||||||||||||||||||||||||||||||||||||||||||||||||
Seq_2  361   AATCTCATGGGCACCTTCAATGTGATCCGCCTGGTGGCTGGTGAGATGGGCCAGAATGAA  420


Seq_1  421   CCAGACCAGGGAGGCCAACGTGGGGTCATCATCAACACTGCCAGTGTGGCTGCCTTCGAG  480
             ||||||||||||||||||||||||||||||||||||||||||||||||||||||||||||
Seq_2  421   CCAGACCAGGGAGGCCAACGTGGGGTCATCATCAACACTGCCAGTGTGGCTGCCTTCGAG  480


Seq_1  481   GGTCAGGTTGGACAAGCTGCATACTCTGCTTCCAAGGGGGGAATAGTGGGCATGACACTG  540
             ||||||||||||||||||||||||||||||||||||||||||||||||||||||||||||
Seq_2  481   GGTCAGGTTGGACAAGCTGCATACTCTGCTTCCAAGGGGGGAATAGTGGGCATGACACTG  540


Seq_1  541   CCCATTGCTCGGGATCTGGCTCCCATAGGTATCCGGGTGATGACCATTGCCCCAGGTCTG  600
             ||||||||||||||||||||||||||||||||||||||||||||||||||||||||||||
Seq_2  541   CCCATTGCTCGGGATCTGGCTCCCATAGGTATCCGGGTGATGACCATTGCCCCAGGTCTG  600
```

```
Seq_1  601   TTTGGCACCCCACTGCTGACCAGCCTCCCAGAGAAAGTGTGCAACTTCTTGGCCAGCCAA  660
             ||||||||||||||||||||||||||||||||||||||||||||||||||||||||||||
Seq_2  601   TTTGGCACCCCACTGCTGACCAGCCTCCCAGAGAAAGTGTGCAACTTCTTGGCCAGCCAA  660

Seq_1  661   GTGCCCTTCCCTAGCCGACTGGGTGACCCTGCTGAGTATGCTCACCTCGTACAGGCCATC  720
             ||||||||||||||||||||||||||||||||||||||||||||||||||||||||||||
Seq_2  661   GTGCCCTTCCCTAGCCGACTGGGTGACCCTGCTGAGTATGCTCACCTCGTACAGGCCATC  720

Seq_1  721   ATCGAGAACCCATTCCTCAATGGAGAGGTCATCCGGCTGGATGGGGCCATTCGTATGCAG  780
             ||||||||||||||||||||||||||||||||||||||||||||||||||||||||||||
Seq_2  721   ATCGAGAACCCATTCCTCAATGGAGAGGTCATCCGGCTGGATGGGGCCATTCGTATGCAG  780

Seq_1  781   CCTTGA  786
             ||||||
Seq_2  781   CCTTGA  786
```

peHISTEV-HSD14

```
ATGGCTACGGGAACGCGCTATGCCGGGAAGGTGGTGGTCGTGACCGGGGGCGGGCGCGGCATCGGAGCTGGGATCGTG
CGCGCCTTCGTGAACAGCGGGGCCCGAGTGGTTATCTGCGACAAGGATGAGTCTGGGGGCCGGGCCCTGGAGCAGGAG
CTCCCTGGAGCTGTCTTTATCCTCTGTGATGTGACTCAGGAAGATGATGTGAAGACCCTGGTTTCTGAGACCATCCGC
CGATTTGGCCGCCTGGATTGTGTTGTCAACAACGCTGGCCACCACCCACCCCCACAGAGGCCTGAGGAGACCTCTGCC
CAGGGATTCCGCCAGCTGCTGGAGCTGAACCTACTGGGGACGTACACCTTGACCAAGCTCGCCCTCCCCTACCTGCGG
AAGAGTCAAGGGAATGTCATCAACATCTCCAGCCTGGTGGGGGCAATCGGCCAGGCCCAGGCAGTTCCCTATGTGGCC
ACCAAGGGGGCAGTAACAGCCATGACCAAAGCTTTGGCCCTGGATGAAAGTCCATATGGTGTCCGAGTCAACTGTATC
TCCCCAGGAAACATCTGGACCCCGCTGTGGGAGGAGCTGGCAGCCTTAATGCCAGACCCTAGGGCCACAATCCGAGAG
GGCATGCTGGCCCAGCCACTGGGCCGCATGGGCCAGCCCGCTGAGGTCGGGGCTGCGGCAGTGTTCCTGGCCTCCGAA
GCCAACTTCTGCACGGGCATTGAACTGCTCGTGACGGGGGGGTGCAGAGCTGGGGTACGGGTGCAAGGCCAGTCGGAGC
ACCCCCGTGGACGCCCCCGATATCCCTTCCTGA
```

```
Alignment of Sequence_1:  [HSD14 cDNA Sequence] with  Sequence_2:
[HSD14_G228A_A440G_3_F-T7-020216-01-37(1).seq.xdna]

Similarity : 813/813 (100.00 %)

            M  A  T  G  T  R  Y  A  G  K  V  V  V  V  T  G  G  G  R  G
Seq_1  1     ATGGCTACGGGAACGCGCTATGCCGGGAAGGTGGTGGTCGTGACCGGGGGCGGGCGCGGC  60
            ||||||||||||||||||||||||||||||||||||||||||||||||||||||||||||
Seq_2  1     ATGGCTACGGGAACGCGCTATGCCGGGAAGGTGGTGGTCGTGACCGGGGGCGGGCGCGGC  60
            M  A  T  G  T  R  Y  A  G  K  V  V  V  V  T  G  G  G  R  G

            I  G  A  G  I  V  R  A  F  V  N  S  G  A  R  V  V  I  C  D
Seq_1  61    ATCGGAGCTGGGATCGTGCGCGCCTTCGTGAACAGCGGGGCCCGAGTGGTTATCTGCGAC  120
            ||||||||||||||||||||||||||||||||||||||||||||||||||||||||||||
Seq_2  61    ATCGGAGCTGGGATCGTGCGCGCCTTCGTGAACAGCGGGGCCCGAGTGGTTATCTGCGAC  120
            I  G  A  G  I  V  R  A  F  V  N  S  G  A  R  V  V  I  C  D

            K  D  E  S  G  G  R  A  L  E  Q  E  L  P  G  A  V  F  I  L
Seq_1  121   AAGGATGAGTCTGGGGGCCGGGCCCTGGAGCAGGAGCTCCCTGGAGCTGTCTTTATCCTC  180
            ||||||||||||||||||||||||||||||||||||||||||||||||||||||||||||
Seq_2  121   AAGGATGAGTCTGGGGGCCGGGCCCTGGAGCAGGAGCTCCCTGGAGCTGTCTTTATCCTC  180
            K  D  E  S  G  G  R  A  L  E  Q  E  L  P  G  A  V  F  I  L

            C  D  V  T  Q  E  D  D  V  K  T  L  V  S  E  T  I  R  R  F
Seq_1  181   TGTGATGTGACTCAGGAAGATGATGTGAAGACCCTGGTTTCTGAGACCATCCGCCGATTT  240
            ||||||||||||||||||||||||||||||||||||||||||||||||||||||||||||
Seq_2  181   TGTGATGTGACTCAGGAAGATGATGTGAAGACCCTGGTTTCTGAGACCATCCGCCGATTT  240
            C  D  V  T  Q  E  D  D  V  K  T  L  V  S  E  T  I  R  R  F

            G  R  L  D  C  V  V  N  N  A  G  H  H  P  P  P  Q  R  P  E
Seq_1  241   GGCCGCCTGGATTGTGTTGTCAACAACGCTGGCCACCACCCACCCCCACAGAGGCCTGAG  300
            ||||||||||||||||||||||||||||||||||||||||||||||||||||||||||||
Seq_2  241   GGCCGCCTGGATTGTGTTGTCAACAACGCTGGCCACCACCCACCCCCACAGAGGCCTGAG  300
            G  R  L  D  C  V  V  N  N  A  G  H  H  P  P  P  Q  R  P  E

            E  T  S  A  Q  G  F  R  Q  L  L  E  L  N  L  L  G  T  Y  T
Seq_1  301   GAGACCTCTGCCCAGGGATTCCGCCAGCTGCTGGAGCTGAACCTACTGGGGACGTACACC  360
            ||||||||||||||||||||||||||||||||||||||||||||||||||||||||||||
Seq_2  301   GAGACCTCTGCCCAGGGATTCCGCCAGCTGCTGGAGCTGAACCTACTGGGGACGTACACC  360
            E  T  S  A  Q  G  F  R  Q  L  L  E  L  N  L  L  G  T  Y  T

            L  T  K  L  A  L  P  Y  L  R  K  S  Q  G  N  V  I  N  I  S
Seq_1  361   TTGACCAAGCTCGCCCTCCCCTACCTGCGGAAGAGTCAAGGGAATGTCATCAACATCTCC  420
            ||||||||||||||||||||||||||||||||||||||||||||||||||||||||||||
Seq_2  361   TTGACCAAGCTCGCCCTCCCCTACCTGCGGAAGAGTCAAGGGAATGTCATCAACATCTCC  420
            L  T  K  L  A  L  P  Y  L  R  K  S  Q  G  N  V  I  N  I  S
```

```
            S  L  V  G  A  I  G  Q  A  Q  A  V  P  Y  V  A  T  K  G  A
Seq_1  421  AGCCTGGTGGGGGCAATCGGCCAGGCCCAGGCAGTTCCCTATGTGGCCACCAAGGGGGCA  480
            ||||||||||||||||||||||||||||||||||||||||||||||||||||||||||||
Seq_2  421  AGCCTGGTGGGGGCAATCGGCCAGGCCCAGGCAGTTCCCTATGTGGCCACCAAGGGGGCA  480
            S  L  V  G  A  I  G  Q  A  Q  A  V  P  Y  V  A  T  K  G  A

            V  T  A  M  T  K  A  L  A  L  D  E  S  P  Y  G  V  R  V  N
Seq_1  481  GTAACAGCCATGACCAAAGCTTTGGCCCTGGATGAAAGTCCATATGGTGTCCGAGTCAAC  540
            ||||||||||||||||||||||||||||||||||||||||||||||||||||||||||||
Seq_2  481  GTAACAGCCATGACCAAAGCTTTGGCCCTGGATGAAAGTCCATATGGTGTCCGAGTCAAC  540
            V  T  A  M  T  K  A  L  A  L  D  E  S  P  Y  G  V  R  V  N

            C  I  S  P  G  N  I  W  T  P  L  W  E  E  L  A  A  L  M  P
Seq_1  541  TGTATCTCCCCAGGAAACATCTGGACCCCGCTGTGGGAGGAGCTGGCAGCCTTAATGCCA  600
            ||||||||||||||||||||||||||||||||||||||||||||||||||||||||||||
Seq_2  541  TGTATCTCCCCAGGAAACATCTGGACCCCGCTGTGGGAGGAGCTGGCAGCCTTAATGCCA  600
            C  I  S  P  G  N  I  W  T  P  L  W  E  E  L  A  A  L  M  P

            D  P  R  A  T  I  R  E  G  M  L  A  Q  P  L  G  R  M  G  Q
Seq_1  601  GACCCTAGGGCCACAATCCGAGAGGGCATGCTGGCCCAGCCACTGGGCCGCATGGGCCAG  660
            ||||||||||||||||||||||||||||||||||||||||||||||||||||||||||||
Seq_2  601  GACCCTAGGGCCACAATCCGAGAGGGCATGCTGGCCCAGCCACTGGGCCGCATGGGCCAG  660
            D  P  R  A  T  I  R  E  G  M  L  A  Q  P  L  G  R  M  G  Q

            P  A  E  V  G  A  A  A  V  F  L  A  S  E  A  N  F  C  T  G
Seq_1  661  CCCGCTGAGGTCGGGGCTGCGGCAGTGTTCCTGGCCTCCGAAGCCAACTTCTGCACGGGC  720
            ||||||||||||||||||||||||||||||||||||||||||||||||||||||||||||
Seq_2  661  CCCGCTGAGGTCGGGGCTGCGGCAGTGTTCCTGGCCTCCGAAGCCAACTTCTGCACGGGC  720
            P  A  E  V  G  A  A  A  V  F  L  A  S  E  A  N  F  C  T  G

            I  E  L  L  V  T  G  G  A  E  L  G  Y  G  C  K  A  S  R  S
Seq_1  721  ATTGAACTGCTCGTGACGGGGGGTGCAGAGCTGGGGTACGGGTGCAAGGCCAGTCGGAGC  780
            ||||||||||||||||||||||||||||||||||||||||||||||||||||||||||||
Seq_2  721  ATTGAACTGCTCGTGACGGGGGGTGCAGAGCTGGGGTACGGGTGCAAGGCCAGTCGGAGC  780
            I  E  L  L  V  T  G  G  A  E  L  G  Y  G  C  K  A  S  R  S

            T  P  V  D  A  P  D  I  P  S  *
Seq_1  781  ACCCCCGTGGACGCCCCCGATATCCCTTCCTGA  813
            |||||||||||||||||||||||||||||||
Seq_2  781  ACCCCCGTGGACGCCCCCGATATCCCTTCCTGA  813
            T  P  V  D  A  P  D  I  P  S  *
```

pET-MBP-HSD8 (Codon Optimised)

```
ATGGCGAGCCAGCTGCAGAATCGTCTGCGTAGCGCACTGGCACTGGTTACCGGTGCAGGTAGCGGTATTGGTCGTGCA
GTTAGCGTTCGTCTGGCAGGCGAAGGTGCAACCGTTGCAGCATGTGATCTGGATCGTGCAGCAGCACAAGAAACCGTG
CGTCTGCTGGGTGGTCCGGGTAGCAAAGAAGGTCCGCCTCGCGGTAATCATGCAGCATTTCAGGCAGATGTTAGCGAA
GCACGTGCAGCACGTTGTCTGCTGGAACAGGTTCAGGCATGTTTTAGCCGTCCGCCTAGCGTTGTTGTTAGCTGTGCA
GGTATTACCCAGGATGAATTTCTGCTGCATATGAGCGAAGATGATTGGGATAAAGTTATTGCCGTTAATCTGAAAGGC
ACCTTTCTGGTTACCCAGGCAGCAGCCCAGGCCCTGGTTAGCAATGGTTGTCGTGGTAGCATTATTAACATTAGCAGC
ATTGTTGGCAAAGTGGGTAATGTTGGTCAGACCAATTATGCAGCAAGCAAAGCCGGTGTTATTGGCCTGACCCAGACC
GCAGCACGTGAACTGGGTCGTCATGGTATTCGTTGTAATAGCGTTCTGCCTGGTTTTATTGCAACCCCGATGACCCAG
AAAGTTCCGCAGAAAGTTGTTGATAAAATCACCGAAATGATTCCGATGGGTCATCTGGGCGATCCGGAAGATGTTGCA
GATGTTGTTGCATTTCTGGCCAGCGAAGATAGCGGTTATATCACCGGCACCAGCGTTGAAGTGACCGGTGGTCTGTTT
ATGTAA
```

```
Alignment of Sequence_1:  [HSD8_MBP_Rev-T7 Term-260416-09-65(1).seq.xdna] with
Sequence_2: [HSD8_CodonOptimised.fas]

Similarity : 786/786 (100.00 %)

            M  A  S  Q  L  Q  N  R  L  R  S  A  L  A  L  V  T  G  A  G
Seq_1  1     ATGGCGAGCCAGCTGCAGAATCGTCTGCGTAGCGCACTGGCACTGGTTACCGGTGCAGGT  60
            ||||||||||||||||||||||||||||||||||||||||||||||||||||||||||||
Seq_2  1     ATGGCGAGCCAGCTGCAGAATCGTCTGCGTAGCGCACTGGCACTGGTTACCGGTGCAGGT  60
            M  A  S  Q  L  Q  N  R  L  R  S  A  L  A  L  V  T  G  A  G


            S  G  I  G  R  A  V  S  V  R  L  A  G  E  G  A  T  V  A  A
Seq_1  61    AGCGGTATTGGTCGTGCAGTTAGCGTTCGTCTGGCAGGCGAAGGTGCAACCGTTGCAGCA  120
            ||||||||||||||||||||||||||||||||||||||||||||||||||||||||||||
Seq_2  61    AGCGGTATTGGTCGTGCAGTTAGCGTTCGTCTGGCAGGCGAAGGTGCAACCGTTGCAGCA  120
            S  G  I  G  R  A  V  S  V  R  L  A  G  E  G  A  T  V  A  A


            C  D  L  D  R  A  A  A  Q  E  T  V  R  L  L  G  G  P  G  S
Seq_1  121   TGTGATCTGGATCGTGCAGCAGCACAAGAAACCGTGCGTCTGCTGGGTGGTCCGGGTAGC  180
            ||||||||||||||||||||||||||||||||||||||||||||||||||||||||||||
Seq_2  121   TGTGATCTGGATCGTGCAGCAGCACAAGAAACCGTGCGTCTGCTGGGTGGTCCGGGTAGC  180
            C  D  L  D  R  A  A  A  Q  E  T  V  R  L  L  G  G  P  G  S


            K  E  G  P  P  R  G  N  H  A  A  F  Q  A  D  V  S  E  A  R
Seq_1  181   AAAGAAGGTCCGCCTCGCGGTAATCATGCAGCATTTCAGGCAGATGTTAGCGAAGCACGT  240
            ||||||||||||||||||||||||||||||||||||||||||||||||||||||||||||
Seq_2  181   AAAGAAGGTCCGCCTCGCGGTAATCATGCAGCATTTCAGGCAGATGTTAGCGAAGCACGT  240
            K  E  G  P  P  R  G  N  H  A  A  F  Q  A  D  V  S  E  A  R


            A  A  R  C  L  L  E  Q  V  Q  A  C  F  S  R  P  P  S  V  V
Seq_1  241   GCAGCACGTTGTCTGCTGGAACAGGTTCAGGCATGTTTTAGCCGTCCGCCTAGCGTTGTT  300
            ||||||||||||||||||||||||||||||||||||||||||||||||||||||||||||
Seq_2  241   GCAGCACGTTGTCTGCTGGAACAGGTTCAGGCATGTTTTAGCCGTCCGCCTAGCGTTGTT  300
            A  A  R  C  L  L  E  Q  V  Q  A  C  F  S  R  P  P  S  V  V


            V  S  C  A  G  I  T  Q  D  E  F  L  L  H  M  S  E  D  D  W
Seq_1  301   GTTAGCTGTGCAGGTATTACCCAGGATGAATTTCTGCTGCATATGAGCGAAGATGATTGG  360
            ||||||||||||||||||||||||||||||||||||||||||||||||||||||||||||
Seq_2  301   GTTAGCTGTGCAGGTATTACCCAGGATGAATTTCTGCTGCATATGAGCGAAGATGATTGG  360
            V  S  C  A  G  I  T  Q  D  E  F  L  L  H  M  S  E  D  D  W


            D  K  V  I  A  V  N  L  K  G  T  F  L  V  T  Q  A  A  A  Q
Seq_1  361   GATAAAGTTATTGCCGTTAATCTGAAAGGCACCTTTCTGGTTACCCAGGCAGCAGCCCAG  420
            ||||||||||||||||||||||||||||||||||||||||||||||||||||||||||||
Seq_2  361   GATAAAGTTATTGCCGTTAATCTGAAAGGCACCTTTCTGGTTACCCAGGCAGCAGCCCAG  420
            D  K  V  I  A  V  N  L  K  G  T  F  L  V  T  Q  A  A  A  Q
```

```
                A  L  V  S  N  G  C  R  G  S  I  I  N  I  S  S  I  V  G  K
Seq_1  421      GCCCTGGTTAGCAATGGTTGTCGTGGTAGCATTATTAACATTAGCAGCATTGTTGGCAAA  480
                ||||||||||||||||||||||||||||||||||||||||||||||||||||||||||||
Seq_2  421      GCCCTGGTTAGCAATGGTTGTCGTGGTAGCATTATTAACATTAGCAGCATTGTTGGCAAA  480
                A  L  V  S  N  G  C  R  G  S  I  I  N  I  S  S  I  V  G  K

                V  G  N  V  G  Q  T  N  Y  A  A  S  K  A  G  V  I  G  L  T
Seq_1  481      GTGGGTAATGTTGGTCAGACCAATTATGCAGCAAGCAAAGCCGGTGTTATTGGCCTGACC  540
                ||||||||||||||||||||||||||||||||||||||||||||||||||||||||||||
Seq_2  481      GTGGGTAATGTTGGTCAGACCAATTATGCAGCAAGCAAAGCCGGTGTTATTGGCCTGACC  540
                V  G  N  V  G  Q  T  N  Y  A  A  S  K  A  G  V  I  G  L  T

                Q  T  A  A  R  E  L  G  R  H  G  I  R  C  N  S  V  L  P  G
Seq_1  541      CAGACCGCAGCACGTGAACTGGGTCGTCATGGTATTCGTTGTAATAGCGTTCTGCCTGGT  600
                ||||||||||||||||||||||||||||||||||||||||||||||||||||||||||||
Seq_2  541      CAGACCGCAGCACGTGAACTGGGTCGTCATGGTATTCGTTGTAATAGCGTTCTGCCTGGT  600
                Q  T  A  A  R  E  L  G  R  H  G  I  R  C  N  S  V  L  P  G

                F  I  A  T  P  M  T  Q  K  V  P  Q  K  V  V  D  K  I  T  E
Seq_1  601      TTTATTGCAACCCCGATGACCCAGAAAGTTCCGCAGAAAGTTGTTGATAAAATCACCGAA  660
                ||||||||||||||||||||||||||||||||||||||||||||||||||||||||||||
Seq_2  601      TTTATTGCAACCCCGATGACCCAGAAAGTTCCGCAGAAAGTTGTTGATAAAATCACCGAA  660
                F  I  A  T  P  M  T  Q  K  V  P  Q  K  V  V  D  K  I  T  E

                M  I  P  M  G  H  L  G  D  P  E  D  V  A  D  V  V  A  F  L
Seq_1  661      ATGATTCCGATGGGTCATCTGGGCGATCCGGAAGATGTTGCAGATGTTGTTGCATTTCTG  720
                ||||||||||||||||||||||||||||||||||||||||||||||||||||||||||||
Seq_2  661      ATGATTCCGATGGGTCATCTGGGCGATCCGGAAGATGTTGCAGATGTTGTTGCATTTCTG  720
                M  I  P  M  G  H  L  G  D  P  E  D  V  A  D  V  V  A  F  L

                A  S  E  D  S  G  Y  I  T  G  T  S  V  E  V  T  G  G  L  F
Seq_1  721      GCCAGCGAAGATAGCGGTTATATCACCGGCACCAGCGTTGAAGTGACCGGTGGTCTGTTT  780
                ||||||||||||||||||||||||||||||||||||||||||||||||||||||||||||
Seq_2  721      GCCAGCGAAGATAGCGGTTATATCACCGGCACCAGCGTTGAAGTGACCGGTGGTCTGTTT  780
                A  S  E  D  S  G  Y  I  T  G  T  S  V  E  V  T  G  G  L  F

                M  *
Seq_1  781      ATGTAA  786
                ||||||
Seq_2  781      ATGTAA  786
                M  *
```

Appendix C: Compound Synthesis and NMR

Synthesis Methodology

Solvents and reagents were purchased from Fluka and Sigma-Aldrich (Czech Republic) and used without further purification. Reactions were monitored by thin layer chromatography (TLC) performed on aluminium sheets pre-coated with silica gel 60 F_{254} (Merck, Czech Republic), using a mobile phase of ethyl acetate/methanol (EtOAc/MeOH; 0-50%) and detected under 254 nm UV light. Melting points were measured on a micro heating stage PHMK 05 (VEB KombinatNagema, Radebeul, Germany) and are uncorrected. Yields were calculated for the two-step synthesis.

NMR spectra were generally recorded at Varian Gemini 300 (^{1}H 300 MHz, ^{13}C 75 MHz, Palo Alto CA, USA) or Varian S500 (^{1}H 500 MHz, ^{13}C 126 MHz, Palo Alto CA, USA). In all cases, the chemical shift values for ^{1}H spectra are reported in ppm (δ) relative to residual $CHD_2SO_2CD_3$ (δ 2.50), shift values for ^{13}C spectra are reported in ppm (δ) relative to solvent peak dimethylsulfoxide-d_6 (δ 39.52).

Mass spectra (MS, respectively, multiple stage MS) were recorded on a LTQ XL linear ion trap mass spectrometer and evaluated using Xcalibur v 2.5.0 software (both Thermo Fisher Scientific, San Jose, CA, USA). The samples were dissolved in methanol (HPLC grade; Sigma-Aldrich, Prague, Czech Republic) and injected continuously (10 µl/min) using a Hamilton syringe into the electrospray ion source. The parameters of the electrospray were set up as follows: sheath gas flow rate 20 arbitrary units, aux gas flow rate 10 arbitrary units, sweep gas flow rate 0 arbitrary units, spray voltage 4.5 kV, capillary temperature 275 °C, capillary voltage 13 V, tube lens 100 V.

Elemental analysis (EA) was measured at Perkin-Elmer CHN Analyser 2,400 Series II apparatus.

Initially, 2-amino-6-fluorobenzo[*d*]thiazole (1 g, 5.95 mmol) was dissolved in a mixture of anhydrous dichloromethane (DCM; 60 ml) and anhydrous dimethylformamide (DMF, 10 ml). 1,1'-carbonyldiimidazole (CDI; 1.16 g, 7.13 mmol) was added and the reaction mixture was vigorously stirred at reflux for 16 hours under nitrogen. The resulting precipitate was collected by filtration, washed with DCM (30 ml) and dried under reduced pressure to obtain *N*-(6-fluorobenzo[*d*]thiazol-2-yl)-1*H*-imidazole-1-carboxamide as a white solid (95 % yield).
In the second step, *N*-(6-fluorobenzo[*d*]thiazol-2-yl)-1*H*-imidazole-1-carboxamide (0.3g, 1.14 mmol) was dissolved in a mixture of anhydrous DMF (10 ml) and triethylamine (Et_3N; 0.35 ml, 2.51 mmol). 4-hydroxyaniline (0.14 g, 1.26 mmol) was added and the reaction mixture was stirred at room temperature for 16 hours under nitrogen. The reaction mixture was portioned with water (40 ml) or 10 % HCl (40 ml; compounds with free carboxylic moiety), solid product was collected by filtration, washed with water (30 ml), cold MeOH (5 ml) and dried under reduced pressure at 60°C to obtain *N*-(4-hydroxyphenyl)-*N*'-(6-fluorobenzo[*d*]thiazol-2-yl)urea as a beige solid (95 % yield)

Series 1: K684-K711

K684

N-(4-hydroxyphenyl)-*N*'-(6-fluorobenzo[d]thiazol-2-yl)urea

M.p. 250 °C decomp. Yield 90 %.^{1}H NMR (500 MHz, DMSO-d_6): δ (ppm) 8.85 (br s, 1H), 7.81 (dd, *J* = 8.7, 2.7 Hz, 1H), 7.67 – 7.60 (m, 1H), 7.30 – 7.25 (m, 2H), 7.21 (td, *J* = 9.1, 2.7 Hz, 1H), 6.76 – 6.71 (m, 2H). ^{13}C NMR (126 MHz, DMSO-d_6): δ (ppm) 159.64, 158.26 (d, *J* = 238.9 Hz), 153.51, 151.97, 145.48, 132.62 (d, *J* = 11.0 Hz), 129.65, 121.22, 120.52, 115.37, 113.72 (d, *J* = 24.3 Hz), 108.03 (d, *J* = 26.9 Hz). ESI-MS: *m/z* 304 [M+H$^+$] (calc. for $C_{14}H_{10}FN_3O_2S$: 303.05). EA: calc. C 55.44; H 3.32; N 13.85; S 10.57. Found: C 55.22; H 3.50; N 13.55; S 10.48.

K685

N-(4-hydroxyphenyl)-*N*'-(6-chlorobenzo[d]thiazol-2-yl)urea

M.p. 285 °C decomp. Yield 58 %.^{1}H NMR (300 MHz, DMSO-d_6): δ (ppm) 9.25 (br s, 1H), 8.83 (br s, 1H), 8.03 (d, *J* = 2.1 Hz, 1H), 7.63 (d, *J* = 8.6 Hz, 1H), 7.39 (dd, *J* = 8.6, 2.2 Hz, 1H), 7.33 – 7.22 (m, 2H), 6.80 – 6.68 (m, 2H). ^{13}C NMR (75 MHz, DMSO-d_6): δ (ppm) 160.33, 153.55, 151.77, 147.74, 133.15, 129.57, 126.81, 126.16, 121.21, 120.81, 115.37. ESI-MS: *m/z* 320 [M+H$^+$] (calc. for $C_{14}H_{10}ClN_3O_2S$: 319.02). EA: calc. C 52.59; H 3.15; N 13.14; S 10.03. Found: C 52.34; H 3.45; N 12.90; S 9.81.

K686

N-(3-hydroxyphenyl)-*N*'-(6-fluorobenzo[d]thiazol-2-yl)urea

M.p. 298–300 °C.Yield 49 %.^{1}H NMR (500 MHz, DMSO-d_6): δ (ppm) 9.45 (br s, 1H), 9.02 (br s, 1H), 7.83 (dd, *J* = 8.7, 2.5 Hz, 1H), 7.71 – 7.60 (m, 1H), 7.23 (td, *J* = 9.1, 2.7 Hz, 1H), 7.14 – 7.06 (m, 2H), 6.84 (d, *J* = 8.0 Hz, 1H), 6.47 (dd, *J* = 8.1, 1.7 Hz, 1H). ^{13}C NMR (126 MHz, DMSO-d_6): δ (ppm) 158.29 (d, *J* = 239.0 Hz), 157.85, 151.41, 145.58, 139.33, 132.60, 129.66, 120.80, 113.80 (d, *J* = 24.3 Hz), 110.19, 109.45, 108.06 (d, *J* = 26.9 Hz), 105.80. ESI-MS: *m/z* 304 [M+H$^+$] (calc. for $C_{14}H_{10}FN_3O_2S$: 303.05). EA: calc. C 55.44; H 3.32; N 13.85; S 10.57. Found: C 55.15; H 3.66; N 13.59; S 10.27.

K687

N-(3-hydroxyphenyl)-*N*'-(6-chlorobenzo[d]thiazol-2-yl)urea

M.p. 294–296 °C.Yield 36 %.^{1}H NMR (300 MHz, DMSO-d_6): δ (ppm) 9.47 (br s, 1H), 9.05 (br s, 1H), 8.05 (d, *J* = 2.1 Hz, 1H), 7.64 (d, *J* = 8.7 Hz, 1H), 7.40 (dd, *J* = 8.7, 2.2 Hz, 1H), 7.18 – 7.03 (m, 2H), 6.85 (d, *J* = 8.4 Hz, 1H), 6.47 (dd, *J* = 8.0, 1.9 Hz, 1H). ^{13}C NMR (75 MHz, DMSO-d_6): δ (ppm) 160.21, 157.89, 151.59, 139.33, 133.09, 129.72, 126.93, 126.24, 121.26, 120.81, 110.26, 109.48, 105.82. ESI-MS: *m/z* 320 [M+H$^+$] (calc. for $C_{14}H_{10}ClN_3O_2S$: 319.02). EA: calc. C 52.59; H 3.15; N 13.14; S 10.03. Found: C 52.30; H 3.38; N 12.88; S 10.32.

K688

N-(2-hydroxyphenyl)-*N*'-(6-fluorobenzo[d]thiazol-2-yl)urea

M.p. 228–230 °C.Yield 80 %.^{1}H NMR (500 MHz, DMSO-d_6): δ (ppm) 8.82 (br s, 1H), 8.04 (d, *J* = 8.0 Hz, 1H), 7.83 (dd, *J* = 8.7, 2.4 Hz, 1H), 7.69 – 7.63 (m, 1H), 7.23 (td, *J* = 9.0, 2.4 Hz, 1H), 6.88 (d, *J* = 4.3 Hz, 2H), 6.83 – 6.77 (m, 1H). ^{13}C NMR (126 MHz, DMSO-d_6): δ (ppm) 159.12, 158.28 (d, *J* = 238.9 Hz), 151.41, 146.17, 145.81, 132.74 (d, *J* = 11.1 Hz), 126.47, 123.11, 120.83, 119.21, 119.05, 114.63, 113.76 (d, *J* = 24.3 Hz), 108.04 (d, *J* = 27.0 Hz). ESI-MS: *m/z* 304 [M+H$^+$] (calc. for $C_{14}H_{10}FN_3O_2S$: 303.05). EA: calc. C 55.44; H 3.32; N 13.85; S 10.57. Found: C 55.21; H 3.69; N 13.47; S 10.23.

K689

N-(2-hydroxyphenyl)-*N*'-(6-chlorobenzo[d]thiazol-2-yl)urea

M.p. 216–218 °C.Yield 42 %.^{1}H NMR (500 MHz, DMSO-d_6): δ (ppm) 11.30 (br s, 1H), 10.12 (br s, 1H), 8.84 (br s, 1H), 8.04 (d, *J* = 1.8 Hz, 1H), 7.99 (d, *J* = 6.5 Hz, 1H), 7.64 (d, *J* = 8.6 Hz, 1H), 7.40 (dd, *J* = 8.6, 2.1 Hz, 1H), 6.93 – 6.88 (m, 2H), 6.85 – 6.77 (m, 1H). ^{13}C NMR (126 MHz, DMSO-d_6): δ (ppm) 160.77, 152.24, 148.09, 146.47, 133.35, 126.67, 126.54, 125.97, 123.13, 121.01, 120.77, 119.28, 119.06, 114.91. ESI-MS: *m/z* 320 [M+H$^+$] (calc. for $C_{14}H_{10}ClN_3O_2S$: 319.02). EA: calc. C 52.59; H, 3.15; N 13.14; S 10.03. Found: C 52.72; H 3.27; N 13.09; S 10.07.

K690

N-(3-chloro-4-hydroxyphenyl)-*N*'-(6-fluorobenzo[d]thiazol-2-yl)urea

M.p. 298–299.5 °C.Yield 74 %.^{1}H NMR (500 MHz, DMSO-d_6): δ (ppm) 9.94 (br s, 1H), 8.98 (br s, 1H), 7.82 (dd, *J* = 8.6, 2.6 Hz, 1H), 7.69 – 7.61 (m, 1H), 7.59 (d, *J* = 2.5 Hz, 1H), 7.22 (td, *J* = 9.1, 2.7 Hz, 1H), 7.18 (dd, *J* = 8.7, 2.5 Hz, 1H), 6.94 (d, *J* = 8.7 Hz, 1H). ^{13}C NMR (126 MHz, DMSO-d_6): δ (ppm) 159.42, 158.29 (d, *J* = 239.1 Hz), 151.83, 149.05, 145.57, 132.52, 130.60, 120.92, 120.57, 119.59, 119.36, 116.67, 113.80 (d, *J* = 24.4 Hz), 108.11 (d, *J* = 27.0 Hz). ESI-MS: *m/z* 338 [M+H$^+$] (calc. for $C_{14}H_9ClFN_3O_2S$: 337.01). EA: calc. C 49.78; H 2.69; N 12.44; S 9.49. Found: C 47.39; H 2.89; N 12.12; S 9.15.

K691

N-(3-chloro-4-hydroxyphenyl)-*N*'-(6-chlorobenzo[d]thiazol-2-yl)urea

M.p. 283.5–285 °C.Yield 30 %.^{1}H NMR (300 MHz, DMSO-d_6): δ (ppm) 9.95 (br s, 1H), 9.01 (br s, 1H), 8.04 (d, *J* = 2.1 Hz, 1H), 7.70 – 7.56 (m, 2H), 7.40 (dd, *J* = 8.6, 2.2 Hz, 1H), 7.19 (dd, *J* = 8.8, 2.5 Hz, 1H), 6.94 (d, *J* = 8.7 Hz, 1H). ^{13}C NMR (75 MHz, DMSO-d_6): δ (ppm) 160.40, 151.93, 149.07, 132.94, 130.55, 126.88, 126.20, 121.24, 120.93, 119.60, 119.34, 116.66. ESI-MS: *m/z* 354 [M+H$^+$] (calc. for $C_{14}H_9Cl_2N_3O_2S$: 352.98). EA: calc. C 47.47; H 2.56; N 11.86; S 9.05. Found: C 47.12; H 2.96; N 11.49; S 9.33.

K692

2-hydroxy-5-[3-(6-fluorobenzo[d]thiazol-2-yl)ureido]benzoic acid

M.p. 304–305 °C.Yield 70 %.^{1}H NMR (500 MHz, DMSO-d_6): δ (ppm) 9.13 (br s, 1H), 8.01 (d, *J* = 2.7 Hz, 1H), 7.82 (dd, *J* = 8.7, 2.7 Hz, 1H), 7.69 – 7.61 (m, 1H), 7.58 (dd, *J* = 8.8, 2.7 Hz, 1H), 7.22 (td, *J* = 9.1, 2.7 Hz, 1H), 6.95 (d, *J* = 8.9 Hz, 1H). ^{13}C NMR (126 MHz, DMSO-d_6): δ (ppm) 171.60, 159.58, 158.29 (d, *J* = 239.1 Hz),

157.09, 152.26, 144.93, 132.45 (d, *J* = 11.3 Hz), 129.97, 127.69, 120.52, 120.42, 117.45, 113.79 (d, *J* = 24.2 Hz), 112.65, 108.09 (d, *J* = 26.9 Hz). ESI-MS: *m/z* 348 [M+H$^+$] (calc. for $C_{15}H_{10}FN_3O_4S$: 347.04). EA: calc. C 51.87; H 2.90; N 12.10; S 9.23. Found: C 51.52; H 2.66; N 12.02; S 8.99.

K693

2-hydroxy-5-[3-(6-chlorobenzo[d]thiazol-2-yl)ureido]benzoic acid

M.p. 285–287 °C.Yield 61 %.^{1}H NMR (300 MHz, DMSO-*d*$_6$): δ (ppm) 9.10 (br s, 1H), 8.05 (d, *J* = 2.1 Hz, 1H), 8.01 (d, *J* = 2.7 Hz, 1H), 7.63 (d, *J* = 8.6 Hz, 1H), 7.57 (dd, *J* = 8.8, 2.5 Hz, 1H), 7.40 (ddd, *J* = 8.6, 2.2, 0.7 Hz, 1H), 6.95 (d, *J* = 8.9 Hz, 1H). ^{13}C NMR (75 MHz, DMSO-*d*$_6$): δ (ppm) 189.75, 171.62, 160.45, 157.14, 152.28, 147.04 132.94, 129.93, 127.74, 126.90, 126.22, 121.24, 120.58, 117.47, 112.66. ESI-MS: *m/z* 364 [M+H$^+$] (calc. for $C_{15}H_{10}ClN_3O_4S$: 363.01). EA: calc. C 49.53; H 2.77; N 11.55; S 8.81. Found: C 49.39; H 2.89; N 11.40; S 8.78.

K694

N-(4-methoxyphenyl)-N'-(6-fluorobenzo[d]thiazol-2-yl)urea

M.p. 331–333 °C.Yield 70 %.^{1}H NMR (500 MHz, DMSO-*d*$_6$): δ (ppm) 8.95 (br s, 1H), 7.82 (dd, *J* = 8.6, 2.4 Hz, 1H), 7.69 – 7.61 (m, 1H), 7.41 (d, *J* = 8.9 Hz, 2H), 7.22 (td, *J* = 9.1, 2.7 Hz, 1H), 6.91 (d, *J* = 9.0 Hz, 2H), 3.73 (s, 3H). ^{13}C NMR (126 MHz, DMSO-*d*$_6$): δ (ppm) 159.44, 158.26 (d, *J* = 239.0 Hz), 155.30, 151.85, 145.47, 132.62, 131.22, 120.82, 120.70, 114.11, 113.75 (d, *J* = 24.3 Hz), 108.05 (d, *J* = 26.8 Hz), 55.21. ESI-MS: *m/z* 318 [M+H$^+$] (calc. for $C_{15}H_{12}FN_3O_2S$: 317.06). EA: calc. C 56.77; H 3.81; N 13.24; S 10.10. Found: C 56.59; H 3.41; N 12.92; S 9.87.

K695

N-(4-methoxyphenyl)-*N*'-(6-chlorobenzo[d]thiazol-2-yl)urea

M.p. 280–282 °C.Yield 92 %.^{1}H NMR (300 MHz, DMSO-*d*$_6$): δ (ppm) 8.96 (br s, 1H), 8.04 (d, *J* = 2.1 Hz, 1H), 7.63 (d, *J* = 8.6 Hz, 1H), 7.45 – 7.36 (m, 3H), 6.95 – 6.88 (m, 2H), 3.73 (s, 3H). ^{13}C NMR (75 MHz, DMSO-*d*$_6$): δ (ppm) 160.31, 155.33, 151.83, 147.59, 133.08, 131.18, 126.83, 126.16, 121.19, 120.83, 114.11, 55.21. ESI-MS: *m/z* 334 [M+H$^+$] (calc. for $C_{15}H_{12}ClN_3O_2S$: 333.03). EA: calc. C 53.97; H 3.62; N 12.59; S 9.61. Found: C 53.71; H3.95; N 12.21; S 9.30.

K696

N-(3,4-dimethoxyphenyl)-*N*'-(6-fluorobenzo[d]thiazol-2-yl)urea

M.p. 280–282 °C.Yield 84 %.^{1}H NMR (300 MHz, DMSO-*d*$_6$): δ (ppm) 8.97 (br s, 1H), 7.82 (dd, *J* = 8.7, 2.7 Hz, 1H), 7.73 – 7.59 (m, 1H), 7.28 – 7.17 (m, 2H), 6.97 (dd, *J* = 8.6, 2.3 Hz, 1H), 6.91 (d, *J* = 8.7 Hz, 1H), 3.76 (s, 3H), 3.73 (s, 3H). ^{13}C NMR (75 MHz, DMSO-*d*$_6$): δ (ppm) 159.47, 158.29 (d, *J* = 239.0 Hz), 148.81, 144.91, 132.53, 131.72, 120.54, 113.79 (d, *J* = 24.3 Hz), 112.28, 111.11, 108.07 (d, *J* = 26.9 Hz), 104.46, 55.78, 55.47. ESI-MS: *m/z* 348 [M+H$^+$] (calc. for $C_{16}H_{14}FN_3O_3S$: 347.07). EA: calc. C 55.32; H 4.06; N 12.10; S 9.23. Found: C 54.97; H 4.00; N 11.94; S 8.86.

K697

N-(3,4-dimethoxyphenyl)-*N*'-(6-chlorobenzo[d]thiazol-2-yl)urea

M.p. 280–282 °C.Yield 87 %.^{1}H NMR (500 MHz, DMSO-d_6): δ (ppm) 8.98 (br s, 1H), 8.03 (d, *J* = 2.1 Hz, 1H), 7.64 (d, *J* = 8.6 Hz, 1H), 7.40 (dd, *J* = 8.6, 2.2 Hz, 1H), 7.20 (d, *J* = 2.1 Hz, 1H), 6.97 (dd, *J* = 8.6, 2.3 Hz, 1H), 6.91 (d, *J* = 8.7 Hz, 1H), 3.76 (s, 3H), 3.73 (s, 3H). ^{13}C NMR (126 MHz, DMSO-d_6): δ (ppm) 160.27, 151.78, 148.80, 147.81, 144.94, 133.06, 131.66, 126.85, 126.18, 121.19, 120.76, 112.28, 111.12, 104.47, 55.78, 55.47. ESI-MS: *m/z* 364 [M+H$^+$] (calc. for $C_{16}H_{14}ClN_3O_3S$: 363.04). EA: calc. C 52.82; H 3.88; N 11.55; S 8.81. Found: C 52.38; H 4.26; N 10.97; S 8.37.

K698

2-methoxy-5-[3-(6-fluorobenzo[d]thiazol-2-yl)ureido]benzoic acid

M.p. 278–279 °C.Yield 47 %.^{1}H NMR (500 MHz, DMSO-d_6): δ (ppm) 9.13 (br s, 1H), 7.85 – 7.80 (m, 2H), 7.68 – 7.62 (m, 1H), 7.60 (dd, *J* = 8.9, 2.8 Hz, 1H), 7.23 (td, *J* = 9.1, 2.7 Hz, 1H), 7.11 (d, *J* = 9.0 Hz, 1H), 3.80 (s, 3H). ^{13}C NMR (126 MHz, DMSO-d_6): δ (ppm) 166.97, 159.56, 158.30 (d, *J* = 239.0 Hz), 154.11, 152.22, 144.87, 132.44 (d, *J* = 12.1 Hz), 130.95, 124.02, 121.71, 121.27, 120.41, 113.80 (d, *J* = 24.3 Hz), 113.17, 108.10 (d, *J* = 26.9 Hz), 56.05. ESI-MS: *m/z* 362 [M+H$^+$] (calc. for $C_{16}H_{12}FN_3O_4S$: 361.05). EA: calc. C 53.18; H 3.35; N 11.63; S 8.87. Found: C 52.83; H 2.96; N 11.59; S 8.48.

K699

2-methoxy-5-[3-(6-chlorobenzo[d]thiazol-2-yl)ureido]benzoic acid

M.p. 268.5–270.5 °C.Yield 56 %.^{1}H NMR (500 MHz, DMSO-d_6): δ (ppm) 9.12 (br s, 1H), 8.05 (d, *J* = 1.9 Hz, 1H), 7.82 (d, *J* = 2.7 Hz, 1H), 7.63 (d, *J* = 8.6 Hz, 1H), 7.60 (dd, *J* = 9.0, 2.7 Hz, 1H), 7.40 (dd, *J* = 8.6, 2.1 Hz, 1H), 7.11 (d, *J* = 9.0 Hz, 1H), 3.80 (s, 3H). ^{13}C NMR (126 MHz, DMSO-d_6): δ (ppm) 166.95, 160.44, 154.13, 152.22, 132.92, 130.89, 126.89, 126.20, 124.04, 121.74, 121.26, 121.23, 120.49, 113.16, 56.05. ESI-MS: *m/z* 378 [M+H$^+$] (calc. for $C_{16}H_{12}ClN_3O_4S$: 377.02). EA: calc. C 50.87; H 3.20; N 11.12; S 8.49. Found: C 50.37; H 3.31; N 10.79; S 8.97.

K700

N-(4-phenoxyphenyl)-*N*'-(6-fluorobenzo[d]thiazol-2-yl)urea

M.p. 305–307 °C.Yield 83 %.^{1}H NMR (500 MHz, DMSO-d_6): δ (ppm) 9.15 (br s, 1H), 7.82 (dd, *J* = 8.6, 2.2 Hz, 1H), 7.69 – 7.62 (m, 1H), 7.53 (d, *J* = 8.7 Hz, 2H), 7.37 (t, *J* = 7.8 Hz, 2H), 7.23 (td, *J* = 9.1, 2.5 Hz, 1H), 7.10 (t, *J* = 7.4 Hz, 1H), 7.02 (d, *J* = 8.8 Hz, 2H), 6.98 (d, *J* = 8.0 Hz, 2H). ^{13}C NMR (126 MHz, DMSO-d_6): δ (ppm) 158.29 (d, *J* = 238.4 Hz), 151.74, 134.16, 132.54, 129.96, 122.99, 120.79, 120.67, 119.67, 117.87, 113.80 (d, *J* = 24.3 Hz), 108.09 (d, *J* = 27.1 Hz). ESI-MS: *m/z* 380 [M+H$^+$] (calc. for $C_{20}H_{14}FN_3O_2S$: 379.08). EA: calc. C 63.31; H 3.72; N 11.08; S 8.45. Found: C 62.89; H 3.40; N 10.70; S 8.05.

K701

N-(4-phenoxyphenyl)-*N*'-(6-chlorobenzo[d]thiazol-2-yl)urea

M.p. 295–297 °C.Yield 88 %.^{1}H NMR (500 MHz, DMSO-d_6): δ (ppm) 9.15 (br s, 1H), 8.05 (d, *J* = 2.0 Hz, 1H), 7.64 (d, *J* = 8.9 Hz, 1H), 7.53 (d, *J* = 9.2 Hz, 2H), 7.41 (dd, *J* = 8.6, 2.2 Hz, 1H), 7.40 – 7.35 (m, 2H), 7.11 (t, *J* = 7.4 Hz, 1H), 7.03 (d, *J* = 8.9 Hz, 2H), 6.98 (d, *J* = 7.7 Hz, 2H). ^{13}C NMR (126 MHz, DMSO-d_6): δ (ppm) 160.31, 157.66, 157.33, 151.78, 150.59, 135.75, 134.12, 133.01, 129.97, 126.90, 126.21, 123.01, 122.73, 121.24, 120.81, 119.92, 119.79, 119.66, 117.89, 117.57. ESI-MS: *m/z* 396 [M+H$^+$] (calc. for $C_{20}H_{14}ClN_3O_2S$: 395.05). EA: calc. C 60.68; H 3.56; N 10.61; S 8.10. Found: C 60.33; H 3.94; N 10.30; S 7.85.

K702

4-[3-(6-fluorobenzo[d]thiazol-2-yl)ureido]benzoic acid

M.p. 300 °C decomp. Yield 67 %.^{1}H NMR (500 MHz, DMSO-d_6): δ (ppm) 10.38 (br s, 1H), 7.91 (d, *J* = 8.7 Hz, 2H), 7.84 (dd, *J* = 8.7, 2.6 Hz, 1H), 7.69 – 7.65 (m, 1H), 7.63 (d, *J* = 8.8 Hz, 2H), 7.24 (td, *J* = 9.1, 2.7 Hz, 1H). ^{13}C NMR (126 MHz, DMSO-d_6): δ (ppm) 166.92, 162.31, 159.07, 158.36 (d, *J* = 239.1 Hz), 152.10, 144.90, 142.80, 132.50 (d, *J* = 11.0 Hz), 130.63, 120.57 (d, *J* = 9.0 Hz), 117.68, 113.89 (d, *J* = 24.2 Hz), 108.12 (d, *J* = 27.0 Hz). ESI-MS: *m/z* 332 [M+H$^+$] (calc. for $C_{15}H_{10}FN_3O_3S$: 331.04). EA: calc. C 54.38; H 3.04; N 12.68; S 9.68. Found: C 54.04; H 3.33; N 12.39; S 9.35.

K703

4-[3-(6-chlorobenzo[d]thiazol-2-yl)ureido]benzoic acid

M.p. 300 °C decomp. Yield 35 %.^{1}H NMR (500 MHz, DMSO-d_6): δ (ppm) 9.76 (br s, 1H), 8.06 (d, *J* = 2.0 Hz, 1H), 7.92 (d, *J* = 8.6 Hz, 2H), 7.70 – 7.59 (m, 3H), 7.41 (dd, *J* = 8.6, 2.1 Hz, 1H). ^{13}C NMR (126 MHz, DMSO-d_6): δ (ppm) 166.90, 160.24, 152.21, 142.67, 132.81, 130.59, 127.04, 126.30, 124.82, 121.31, 120.48, 117.90. ESI-MS: *m/z* 348 [M+H$^+$] (calc. for $C_{15}H_{10}ClN_3O_3S$: 347.01). EA: calc. C 51.80; H 2.90; N 12.08; S 9.22. Found: C 51.41; H 3.13; N 11.80; S 8.91.

K704

ethyl-[3-(6-fluorobenzo[d]thiazol-2-yl)ureido]benzoate

M.p. 333–335 °C.Yield 32 %.^{1}H NMR (500 MHz, DMSO-d_6): δ (ppm) 9.53 (br s, 1H), 7.99 – 7.79 (m, 3H), 7.72 – 7.56 (m, 3H), 7.29 – 7.20 (m, 1H), 4.33 – 4.25 (m, 2H), 1.31 (t, *J* = 6.5 Hz, 3H). ^{13}C NMR (126 MHz, DMSO-d_6): δ (ppm) 165.30, 158.36 (d, *J* = 237.5 Hz), 142.93, 130.39, 123.85, 118.02, 117.49, 113.94 (d, *J* = 23.6 Hz), 108.21 (d, *J* = 26.9 Hz), 60.44, 14.24. ESI-MS: *m/z* 360 [M+H$^+$] (calc. for $C_{17}H_{14}FN_3O_3S$: 359.07). EA: calc. C 56.82; H 3.93; N 11.69; S 8.92. Found: C 56.37; H 3.77; N 11.92; S 9.24.

K705

ethyl-4-[3-(6-chlorobenzo[d]thiazol-2-yl)ureido]benzoate

M.p. 326–328 °C.Yield 45 %.^{1}H NMR (500 MHz, DMSO-d_6): δ (ppm) 9.19 (br s, 1H), 8.08 (s, 1H), 7.97 – 7.86 (m, 2H), 7.72 – 7.55 (m, 3H), 7.48 – 7.39 (m, 1H), 4.34 – 4.25 (m, 2H), 1.32 (t, *J* = 6.9 Hz, 3H). ^{13}C NMR (126 MHz, DMSO-d_6): δ (ppm) 165.27, 160.41, 151.78, 142.91, 132.73, 130.37, 127.04, 126.31, 123.86, 121.33,

118.03, 117.45, 60.45, 14.24.ESI-MS: *m/z* 376 [M+H$^+$] (calc. for $C_{17}H_{14}ClN_3O_3S$: 375.04). EA: calc. C 54.33; H 3.75; N 11.18; S 8.53. Found: C 54.01; H 3.89; N 11.50; S 8.82.

K706

N-(4-acetylphenyl)-*N*'-(6-fluorobenzo[d]thiazol-2-yl)urea

M.p. 308–310 °C.Yield 48 %.^{1}H NMR (500 MHz, DMSO-d_6): δ (ppm) 9.53 (br s, 1H), 8.00 – 7.80 (m, 3H), 7.71 – 7.55 (m, 3H), 7.25 (t, *J* = 7.8 Hz, 1H), 2.53 (s, 3H). ^{13}C NMR (126 MHz, DMSO-d_6): δ (ppm) 196.41, 158.37 (d, *J* = 235.7 Hz), 151.85, 143.91, 143.02, 132.24, 131.36, 129.67, 120.45, 117.89, 117.38, 113.96 (d, *J* = 23.8 Hz), 108.26 (d, *J* = 27.9 Hz), 26.45. ESI-MS: *m/z* 330 [M+H$^+$] (calc. for $C_{16}H_{12}FN_3O_2S$: 329.06). EA: calc. C 58.35; H 3.67; N 12.76; S 9.74. Found: C 57.97; H 3.46; N 13.18; S 10.19.

K707

N-(4-acetylphenyl)-*N*'-(6-chlorobenzo[d]thiazol-2-yl)urea

M.p. 288–290 °C.Yield 38 %.^{1}H NMR (300 MHz, DMSO-d_6): δ (ppm) 9.62 (br s, 1H), 8.20 – 7.80 (m, 3H), 7.66 (d, *J* = 13.9 Hz, 3H), 7.42 (d, *J* = 13.3 Hz, 1H), 2.53 (s, 3H). ^{13}C NMR (75 MHz, DMSO-d_6): δ (ppm) 196.40, 160.77, 152.56, 143.05, 132.72, 131.37, 129.63, 126.99, 126.29, 121.32, 120.32, 117.93, 117.38, 26.43. ESI-MS: *m/z* 346 [M+H$^+$] (calc. for $C_{16}H_{12}ClN_3O_2S$: 345.03). EA: calc. C 55.57; H 3.50; N 12.15; S 9.27. Found: C 55.29; H 3.88; N 12.22; S 9.49.

K708

N-{4-[3-(6-fluorobenzo[d]thiazol-2-yl)ureido]phenyl}acetamide

M.p. 335–337 °C.Yield 85 %.^{1}H NMR (500 MHz, DMSO-d_6): δ (ppm) 9.88 (br s, 1H), 9.03 (br s, 1H), 7.82 (dd, *J* = 8.6, 2.5 Hz, 1H), 7.69 – 7.62 (m, 1H), 7.54 (d, *J* = 8.9 Hz, 2H), 7.42 (d, *J* = 8.9 Hz, 2H), 7.23 (td, *J* = 9.1, 2.7 Hz, 1H), 2.03 (s, 3H). ^{13}C NMR (126 MHz, DMSO-d_6): δ (ppm) 167.94, 158.27 (d, *J* = 239.0 Hz), 151.64, 145.50, 134.84, 133.37, 132.52, 120.66, 119.60, 119.41, 118.52, 113.76 (d, *J* = 24.2 Hz), 108.05 (d, *J* = 26.8 Hz), 23.88. ESI-MS: *m/z* 345 [M+H$^+$] (calc. for $C_{16}H_{13}FN_4O_2S$: 344.07). EA: calc. C 55.80; H 3.81; N 16.27; S 9.31. Found: C 55.53; H 3.77; N 16.71; S 8.95.

K709

N-{4-[3-(6-chlorobenzo[d]thiazol-2-yl)ureido]phenyl}acetamide

M.p. 335–337 °C.Yield 89 %.^{1}H NMR (500 MHz, DMSO-d_6): δ (ppm) 9.89 (br s, 1H), 9.06 (br s, 1H), 8.04 (d, *J* = 1.9 Hz, 1H), 7.64 (d, *J* = 8.7 Hz, 1H), 7.54 (d, *J* = 9.2 Hz, 2H), 7.45 – 7.36 (m, 3H), 2.03 (s, 3H). ^{13}C NMR (126 MHz, DMSO-d_6): δ (ppm) 167.98, 160.25, 151.69, 134.89, 133.34, 126.87, 126.19, 121.21, 120.80, 119.60, 119.46, 23.90. ESI-MS: *m/z* 361 [M+H$^+$] (calc. for $C_{16}H_{13}ClN_4O_2S$: 360.04). EA: calc. C 53.26; H 3.63; N 15.53; S 8.89. Found: C 52.95; H, 3.95; N 15.22; S 8.48.

K710

methyl-2-hydroxy-5-[3-(6-fluorobenzo[d]thiazol-2-yl)ureido]benzoate

M.p. 277–279 °C.Yield 81 %.^{1}H NMR (500 MHz, DMSO-d_6): δ (ppm) 10.28 (br s, 1H), 9.09 (br s, 1H), 8.04 (d, *J* = 2.6 Hz, 1H), 7.82 (dd, *J* = 8.7, 2.6 Hz, 1H), 7.68 – 7.60 (m, 1H), 7.55 (dd, *J* = 8.9, 2.7 Hz, 1H), 7.23 (td, *J* = 9.1, 2.7 Hz, 1H), 6.98 (d, *J* = 9.0 Hz, 1H), 3.92 (s, 3H). ^{13}C NMR (126 MHz, DMSO-d_6): δ (ppm) 168.94, 159.54, 158.29 (d, *J* = 239.0 Hz), 155.98, 152.11, 132.43, 130.19, 127.59, 120.38, 120.13, 117.80, 113.80 (d, *J* = 24.4 Hz), 112.71, 108.09 (d, *J* = 26.9 Hz), 52.55. ESI-MS: *m/z* 362 [M+H$^+$] (calc. for $C_{16}H_{12}FN_3O_4S$: 361.05). EA: calc. C 53.18; H 3.35; N 11.63; S 8.87. Found: C 52.90; H 2.96; N 11.28; S 9.15.

K711

methyl-2-hydroxy-5-[3-(6-chlorobenzo[d]thiazol-2-yl)ureido]benzoate

M.p. 278–280 °C.Yield 80 %.^{1}H NMR (500 MHz, DMSO-d_6): δ (ppm) 10.29 (br s, 1H), 9.11 (br s, 1H), 8.08 – 8.00 (m, 2H), 7.62 (d, *J* = 9.0 Hz, 1H), 7.55 (dd, *J* = 9.6, 2.3 Hz, 1H), 7.39 (dd, *J* = 9.0, 2.1 Hz, 1H), 6.98 (d, *J* = 9.7 Hz, 1H), 3.92 (s, 3H). ^{13}C NMR (126 MHz, DMSO-d_6): δ (ppm) 168.94, 160.46, 156.00, 152.24, 147.04, 132.88, 130.15, 127.59, 126.89, 126.20, 121.21, 120.13, 117.80, 112.69, 52.55. ESI-MS: *m/z* 378 [M+H$^+$] (calc. for $C_{16}H_{12}ClN_3O_4S$: 377.02). EA: calc. C 50.87; H 3.20; N 11.12; S 8.49. Found: C 50.57; H 3.47; N 10.88; S, 8.52.

Series 2: K795-K805

K795

1-(6-chlorobenzo[d]thiazol-2-yl)-3-(3-chlorophenyl)urea

M.p. 351–353 °C; Yield 83 %; ^{1}H NMR (500 MHz, DMSO-d_6): δ (ppm) 11.07 (br s, 1H), 9.36 (br s, 1H), 8.04 (s, 1H), 7.73 (s, 1H), 7.63 (d, *J* = 8.4 Hz, 1H), 7.47 – 7.27 (m, 3H), 7.10 (d, *J* = 7.3 Hz, 1H); ^{13}C NMR (126 MHz, DMSO-d_6): δ (ppm) 160.42, 152.17, 146.76, 139.99, 133.28, 132.77, 130.54, 127.04, 126.30, 122.69, 121.32, 120.54, 118.29, 117.40; ESI-MS: *m/z* 338 [M+H$^+$] (calc. for $C_{14}H_9Cl_2N_3OS$: 336.98); EA: calc. C 49.72; H 2.68; N12.42; S 9.48. Found: C 49.29; H 2.76; N 12.53; S 9.81.

K796

1-(6-chlorobenzo[d]thiazol-2-yl)-3-(4-chlorophenyl)urea

M.p. 335–337 °C; Yield 86 %; ^{1}H NMR (500 MHz, DMSO-d_6): δ (ppm) 10.98 (br s, 1H), 9.29 (br s, 1H), 8.04 (s, 1H), 7.63 (d, *J* = 8.3 Hz, 1H), 7.55 (d, *J* = 8.6 Hz, 2H), 7.47 – 7.27 (m, 3H); ^{13}C NMR (126 MHz, DMSO-d_6): δ (ppm) 160.24, 152.01, 147.33, 137.40, 132.83, 128.79, 126.99, 126.68, 126.26, 121.28, 120.48; ESI-MS: *m/z* 338 [M+H$^+$] (calc. for $C_{14}H_9Cl_2N_3OS$: 336.98); EA: calc. C 49.72; H 2.68; N 12.42; S 9.48. Found: C 49.67; H 2.72; N 12.54; S 9.78.

K797

1-(6-chlorobenzo[d]thiazol-2-yl)-3-(3,4-dichlorophenyl)urea

M.p. 334–336 °C; Yield 85 %; ^{1}H NMR (300 MHz, DMSO-d_6): δ (ppm) 11.25 (br s, 1H), 9.47 (br s, 1H), 8.03 (s, 1H), 7.90 (s, 1H), 7.77 – 7.19 (m, 4H); ^{13}C NMR (75 MHz, DMSO-d_6): δ (ppm) 160.70, 152.89, 145.92, 138.79, 132.47, 131.13, 130.66, 127.05, 126.31, 124.36, 121.35, 120.01, 119.01; ESI-MS: *m/z* 372 [M+H$^+$] (calc. for $C_{14}H_8Cl_3N_3OS$: 370.95); EA: calc. C 45.12; H 2.16; N 11.28; S 8.60. Found: C 44.91; H 2.20; N 11.39; S 9.01.

K798

1-(2-chloro-4-hydroxyphenyl)-3-(6-chlorobenzo[d]thiazol-2-yl)urea

M.p. 283–285 °C; Yield 71 %; ^{1}H NMR (500 MHz, DMSO-d_6): δ (ppm) 11.29 (br s, 1H), 9.77 (br s, 1H), 8.74 (br s, 1H), 8.05 (d, *J* = 2.4 Hz, 1H), 7.73 (d, *J* = 8.9 Hz, 1H), 7.65 (d, *J* = 8.6 Hz, 1H), 7.40 (dd, *J* = 8.6, 2.4 Hz, 1H), 6.90 (d, *J* = 2.6 Hz, 1H), 6.77 (dd, *J* = 8.9, 2.5 Hz, 1H); ^{13}C NMR (126 MHz, DMSO-d_6): δ (ppm) 160.16, 154.72, 151.80, 147.81, 133.14, 126.94, 126.19, 125.94, 125.42, 125.04, 121.19, 121.00, 115.61, 114.65; ESI-MS: *m/z* 354 [M+H$^+$] (calc. for $C_{14}H_9Cl_2N_3O_2S$: 352.98); EA: calc. C 47.47; H 2.56; N 11.86; S 9.05. Found: C 47.10; H 2.74; N 11.90; S 9.17.

K799

1-(3-chloro-4-methoxyphenyl)-3-(6-chlorobenzo[d]thiazol-2-yl)urea

M.p. 307–309 °C; Yield 93 %; ^{1}H NMR (500 MHz, DMSO-*d*$_6$): δ (ppm) 11.00 (br s, 1H), 9.12 (br s, 1H), 8.03 (d, *J* = 2.2 Hz, 1H), 7.68 (d, *J* = 2.4 Hz, 1H), 7.62 (d, *J* = 8.5 Hz, 1H), 7.39 (dd, *J* = 8.6, 2.2 Hz, 1H), 7.36 (dd, *J* = 8.9, 2.3 Hz, 1H), 7.11 (d, *J* = 9.0 Hz, 1H), 3.83 (s, 3H); ^{13}C NMR (126 MHz, DMSO-*d*$_6$): δ (ppm) 160.39, 152.14, 150.50, 147.12, 132.84, 131.96, 126.90, 126.20, 121.23, 120.86, 120.82, 119.16, 113.04, 56.20; ESI-MS: *m/z* 368 [M+H$^+$] (calc. for $C_{15}H_{11}Cl_2N_3O_2S$: 366.99); EA: calc. C 48.93; H 3.01; N 11.41; S 8.71. Found: C 48.84; H 3.13; N 11.89; S 8.65.

K800

2-chloro-4-(3-(6-chlorobenzo[d]thiazol-2-yl)ureido)benzoic acid

M.p. 324–326 °C; Yield 83 %; ^{1}H NMR (300 MHz, DMSO-*d*$_6$): δ (ppm) 12.27 (br s, 1H), 9.69 (br s, 1H), 8.05 (d, *J* = 1.9 Hz, 1H), 7.92 – 7.77 (m, 2H), 7.62 (d, *J* = 8.6 Hz, 1H), 7.50 (dd, *J* = 8.6, 1.6 Hz, 1H), 7.41 (dd, *J* = 8.6, 2.0 Hz, 1H); ^{13}C NMR (75 MHz, DMSO-*d*$_6$): δ (ppm) 166.00, 160.99, 152.98, 145.64, 142.54, 133.30, 132.53, 132.40, 127.13, 126.40, 124.12, 121.43, 119.90, 119.74, 116.74; ESI-MS: *m/z* 382 [M+H$^+$] (calc. for $C_{15}H_9Cl_2N_3O_3S$: 380.97); EA: calc. C 47.14; H 2.37; N 10.99; S 8.39. Found: C 47.05; H 2.49; N 11.12; S 8.66.

K801

1-(6-chlorobenzo[d]thiazol-2-yl)-3-(3,5-dichloro-4-hydroxyphenyl)urea

M.p. 300 °C decomp.; Yield 69 %; ^{1}H NMR (300 MHz, DMSO-*d*$_6$): δ (ppm) 10.61 (br s, 1H), 9.19 (br s, 1H), 8.03 (d, *J* = 2.1 Hz, 1H), 7.61 (d, *J* = 8.6 Hz, 1H), 7.55 (s, 2H), 7.39 (dd, *J* = 8.6, 2.2 Hz, 1H); ^{13}C NMR (75 MHz, DMSO-*d*$_6$): δ (ppm) 160.83, 152.82, 146.07, 144.82, 132.58, 131.55, 126.97, 126.28, 122.42, 121.33, 120.06, 119.41; ESI-MS: *m/z* 388 [M+H$^+$] (calc. for $C_{14}H_8Cl_3N_3O_2S$: 386.94); EA: calc. C 43.27; H 2.07; N 10.81; S 8.25. Found: C 42.92; H 2.32; N 10.60; S 8.09.

K802

1-(6-chlorobenzo[d]thiazol-2-yl)-3-(3,5-dichloro-4-methoxyphenyl)urea

M.p. 290 °C decomp.; Yield 90 %; ^{1}H NMR (500 MHz, DMSO-*d*$_6$): δ (ppm) 11.26 (br s, 1H), 9.39 (br s, 1H), 8.02 (d, *J* = 2.0 Hz, 1H), 7.65 (s, 2H), 7.60 (d, *J* = 8.6 Hz, 1H), 7.40 (dd, *J* = 8.7, 2.0 Hz, 1H), 3.79 (s, 3H); ^{13}C NMR (126 MHz, DMSO-*d*$_6$): δ (ppm) 146.74, 135.97, 132.25, 128.14, 127.03, 126.31, 121.36, 119.07, 60.64; ESI-MS: *m/z* 402 [M+H$^+$] (calc. for $C_{15}H_{10}Cl_3N_3O_2S$: 400.96); EA: calc. C 44.74; H 2.50; N 10.44; S 7.96. Found: C 45.10; H 2.58; N 10.90; S 8.26.

K803

3-chloro-5-(3-(6-chlorobenzo[d]thiazol-2-yl)ureido)-2-hydroxybenzoic acid

M.p. 268–270 °C; Yield 68 %; ^{1}H NMR (300 MHz, DMSO-d_6): δ (ppm) 11.34 (br s, 1H), 9.23 (br s, 1H), 8.03 (d, *J* = 2.1 Hz, 1H), 7.93 (d, *J* = 2.6 Hz, 1H), 7.87 (d, *J* = 2.7 Hz, 1H), 7.61 (d, *J* = 8.6 Hz, 1H), 7.39 (dd, *J* = 8.6, 2.2 Hz, 1H); ^{13}C NMR (75 MHz, DMSO-d_6): δ (ppm) 171.37, 160.76, 152.64, 146.45, 132.67, 130.24, 126.97, 126.73, 126.28, 121.30, 120.47, 119.53, 114.20; ESI-MS: *m/z* 398 [M+H$^+$] (calc. for $C_{15}H_9Cl_2N_3O_4S$: 396.97); EA: calc. C 45.24; H 2.28; N 10.55; S 8.05. Found: C 44.83; H 2.69; N 10.19; S 7.89.

K804

3-chloro-5-(3-(6-chlorobenzo[d]thiazol-2-yl)ureido)-2-methoxybenzoic acid

M.p. 263.6–265 °C; Yield 60%; ^{1}H NMR (500 MHz, DMSO-d_6): δ (ppm) 12.10 (br s, 1H), 9.41 (br s, 1H), 8.04 (d, *J* = 2.1 Hz, 1H), 7.89 (d, *J* = 2.7 Hz, 1H), 7.79 (d, *J* = 2.7 Hz, 1H), 7.61 (d, *J* = 8.6 Hz, 1H), 7.40 (dd, *J* = 8.6, 2.2 Hz, 1H), 3.80 (s, 3H); ^{13}C NMR (126 MHz, DMSO-d_6): δ (ppm) 166.11, 160.84, 152.95, 149.82, 145.83, 135.06, 132.50, 128.18, 128.02, 127.04, 126.31, 123.23, 121.34, 119.79, 61.67; ESI-MS: *m/z* 412 [M+H$^+$] (calc. for $C_{16}H_{11}Cl_2N_3O_4S$: 410.98); EA: calc. C 46.62; H 2.69; N 10.19; S 7.78. Found: C 46.12; H 3.08; N 9.72; S 7.68.

K805

1-(6-chlorobenzo[d]thiazol-2-yl)-3-(2,4-dihydroxyphenyl)urea

M.p. 241–243 °C; Yield 81 %; ^{1}H NMR (500 MHz, DMSO-d_6): δ (ppm) 8.60 (br s, 1H), 8.03 (d, *J* = 2.1 Hz, 1H), 7.72 – 7.53 (m, 2H), 7.38 (dd, *J* = 8.6, 2.1 Hz, 1H), 6.42 (d, *J* = 2.6 Hz, 1H), 6.21 (dd, *J* = 8.7, 2.5 Hz, 1H); ^{13}C NMR (126 MHz, DMSO-d_6): δ (ppm) 160.33, 153.99, 151.53, 148.23, 147.76, 133.19, 126.78, 126.16, 121.37, 121.15, 120.81, 117.75, 105.63, 102.57; ESI-MS: *m/z* 336 [M+H$^+$] (calc. for $C_{14}H_{10}ClN_3O_3S$: 335.01); EA: calc. C 50.08; H 3.00; N 12.52; S 9.55. Found: C 49.77; H 3.48; N 12.30; S 9.22.

Appendix D: NCI Diversity IV Hits

NCI Diversity IV hit compounds, ranked on the basis of residual enzyme activity (Top 100 compounds).

Plate	Well	NSC	Percentage Activity
	Control	Control	100.00
4784104	G03	120622	0.70
4774104	D09	63001	2.99
4787104	C07	339161	3.77
4774104	F02	33005	4.27
4786104	C07	50650	4.54
4785104	B05	328111	5.54
4770104	C07	17796	6.28
4787104	E08	106231	6.67
4779104	E03	55453	9.00
4788104	A11	73735	9.37
4773104	E08	19063	10.33
4789104	E08	378719	10.54
4788104	F09	8675	10.95
4772104	F08	246415	11.01
4786104	F02	622608	11.80
4771104	E05	67307	12.04
4785104	E09	105827	12.30
4770104	H10	43013	13.22
4779104	C07	88402	13.34
4779104	C08	93945	13.83
4781104	F07	327444	14.53
4783104	D05	69359	14.97
4776104	D03	148170	15.79
4775104	D04	98857	16.22
4782104	A06	9037	16.26
4772104	G03	128068	16.38
4780104	H10	201634	16.70
4775104	G05	106461	16.94
4778104	B08	34875	17.00
4788104	A03	622689	17.14
4781104	D08	343526	17.44
4783104	F07	90749	21.08
4784104	C08	191441	21.80
4787104	F03	191454	22.52
4777104	C02	311727	22.67
4786104	C10	99925	23.60
4785104	H07	371765	24.19
4787104	D03	164991	24.28
4774104	H05	45291	25.18
4779104	C10	108783	25.72

4784104	D10	217913	26.72
4774104	H03	38042	26.88
4776104	A02	129260	26.92
4787104	D08	88600	28.68
4782104	H04	661221	29.61
4788104	H10	70931	30.00
4782104	B04	637827	30.62
4777104	A02	309971	30.80
4775104	E04	99796	31.35
4783104	A02	44750	31.98
4787104	E06	319435	32.08
4787104	A03	159566	32.33
4787104	H02	156565	32.58
4778104	C09	38007	32.78
4775104	A04	93817	33.69
4779104	A08	92937	35.37
4779104	H08	98938	35.69
4774104	E06	49652	35.85
4775104	H02	88962	35.86
4783104	C09	637359	36.48
4778104	B04	17055	37.03
4788104	E10	55691	37.46
4781104	A11	177866	37.65
4770104	A03	65248	37.69
4773104	G08	19108	37.99
4774104	C08	58907	38.12
4772104	E10	311723	38.55
4783104	A09	99657	39.53
4779104	G05	73753	41.16
4784104	D08	194308	41.91
4783104	H02	48617	43.90
4777104	F10	11624	44.33
4788104	D07	215718	45.40
4782104	E09	33570	45.43
4774104	A03	35676	45.52
4785104	B09	339316	45.54
4775104	G10	42212	46.13
4779104	D08	95909	46.30
4785104	H02	299119	46.49
4773104	G07	15372	46.58

4775104	H09	126405	46.67
4776104	G09	277806	46.92
4783104	G02	48443	46.95
4782104	C06	12262	47.02
4789104	D03	371178	47.29
4775104	H03	92794	47.39
4777104	F05	379639	47.72
4783104	H06	83497	47.97
4787104	A04	204665	48.18
4782104	H02	400770	48.19
4780104	B07	151262	48.70
4786104	C02	379697	48.87
4772104	G09	288686	49.13
4772104	B07	169566	49.57
4776104	A10	282187	50.53
4770104	F08	29193	50.58
4777104	E09	9782	50.76
4786104	A09	84126	50.98
4789104	F07	645987	51.00
4786104	G04	11668	51.44

Appendix E: 17β-HSD14 Rare-Codons

RaCC results:

Red = rare Arg codons **AGG, AGA, CGA**
Green = rare Leu codon **CTA**
Blue = rare Ile codon **ATA**
Orange = rare Pro codon **CCC**

for the following input sequence:

```
atg gct acg gga acg cgc tat gcc ggg aag gtg gtg gtc gtg acc ggg ggc ggg cgc ggc atc gga gct ggg atc gtg cgc gcc ttc gtg aac agc ggg gcc CGA gtg gtt atc tgc gac aag gat gag tct ggg ggc cgg gcc
ctg gag cag gag ctc cct gga gct gtc ttt atc ctc tgt gat gtg act cag gaa gat gat gtg aag acc ctg gtt tct gag acc atc cgc CGA ttt ggc cgc ctg gat tgt gtt gtc aac aac gct ggc cac cac cca CCC cca
cag AGG cct gag gag acc tct gcc cag gga ttc cgc cag ctg ctg gag ctg aac CTA ctg ggg acg tac acc ttg acc aag ctc gcc ctc CCC tac ctg cgg aag agt caa ggg aat gtc atc aac atc tcc agc ctg gtg ggg
gca atc ggc cag gcc cag gca gtt CCC tat gtg gcc acc aag ggg gca gta aca gcc atg acc aaa gct ttg gcc ctg gat gaa agt cca tat ggt gtc CGA gtc aac tgt atc tcc cca gga aac atc tgg acc ccg ctg tgg
gag gag ctg gca gcc tta atg cca gac cct AGG gcc aca atc CGA gag ggc atg ctg gcc cag cca ctg ggc cgc atg ggc cag CCC gct gag gtc ggg gct gcg gca gtg ttc ctg gcc tcc gaa gcc aac ttc tgc acg ggc
att gaa ctg ctc gtg acg ggg ggt gca gag ctg ggg tac ggg tgc aag gcc agt cgg agc acc CCC gtg gac gcc CCC gat atc cct tcc tga
```

The length is: 813 nucleotides

Number of total single rare Arg codons: 6
occurring at codons:
35, 79, 98, 178, 203, 207

Number of tandem rare Arg codon double repeats: 0
Number of tandem rare Arg codon triple repeats: 0

Too lazy to beautify this new part right now...Results are in order for Arginine, Leucine, Isoleucine, and Proline, respectively (delimited by numbers 1.1, 2.1, 3.1, 4.1 for singles; 1.2, 2.2, 3.2, 4.2 for doubles; etc.).
Single rare codons at positions:
35 79 98 178 203 207 (agg)|(aga)|(cga)1.1 115 cta2.1 ata3.1 95 127 153 221 262 266 ccc4.1

Double rare codons at positions:
(agg)|(aga)|(cga)1.2 cta2.2 ata3.2 ccc4.2

Triple rare codons at positions:
(agg)|(aga)|(cga)1.3 cta2.3 ata3.3 ccc4.3

Appendix F: Publications

Lukas Hroch*, Ondrej Benek*, **Patrick Guest*,** Laura Aitken* *et al.,* Design, synthesis and in vitro evaluation of benzothiazole-based ureas as potential ABAD/17b-HSD10 modulators for Alzheimer's disease treatment (2016). *Bioorganic & Medicinal Chemistry Letters* (*Co-First Authors).